QUANTITATIVE ^{1}H NMR ANALYSES OF IMMUNOMETABOLIC MODULATION IN HUMAN MACROPHAGES

by

Amanda Lee Fuchs

A dissertation submitted in partial fulfillment
of the requirements for the degree

of

Doctor of Philosophy

in

Biochemistry

MONTANA STATE UNIVERSITY
Bozeman, Montana

November 2019

DEDICATION

To my parents William and Sandra Fuchs. Thank you for always being there for me. I would not be the person I am today without the guidance, encouragement, support, and love you have provided throughout my entire life. I doubt I could have gotten to where I am today, nor accomplished this work, without you.

To ALL my family and friends. Thank you for all of your love and unwavering support over the years.

ACKNOWLEDGEMENTS

First and foremost, I would like to thank my thesis advisor, Dr. Valérie Copié, for everything she has done for me and her mentorship throughout my graduate career. Your guidance and support have been instrumental in my success and have made me into the strong, independent scientist that I am today. Although we have had disagreements at times, I am so grateful for the relationship that we now share. I would also like to thank Dr. Brian Tripet for his advice throughout my endeavors and for encouraging me to critically think about my research and what exactly I needed to accomplish.

I would like to thank the past and present members of the Copié lab for all of their support over the years. Thank you to all of the undergraduate and graduate students that I have had the great pleasure of working with, particularly Sage Schiller, Wyatt Keegan, Cole Davidson, Isaac Miller, Rosalyn Huard, Alexia Kosea, and Demetri Stoumbos. Your research efforts and support were greatly appreciated and will never be forgotten.

Thank you to the Voyich, Teintze, Pincus, and Bimczok lab members for all of their guidance and assistance with my research projects. Lastly, I would like to thank all of my colleagues and friends whom I may not have mentioned specifically, but who have been a part of my graduate career.

TABLE OF CONTENTS

TABLE OF CONTENTS CONTINUED

TABLE OF CONTENTS CONTINUED

LIST OF TABLES

Table Page

LIST OF TABLES CONTINUED

Table Page

LIST OF FIGURES

LIST OF FIGURES CONTINUED

Figure Page

LIST OF FIGURES CONTINUED

Figure Page

LIST OF FIGURES CONTINUED

Figure Page

ABSTRACT

Macrophages are innate immune cells that are found ubiquitously in nearly all human tissues, where they support host innate and adaptive immune responses in an effort to maintain systemic homeostasis. They are inherently plastic in nature and can dramatically modulate their functional phenotype according to pathogen and microenvironmental stimuli. Previous studies have shown that macrophages are particularly important for the resolution of inflammation in acute wound healing, which is marked by a phenotypic transition of wound macrophages from pro-inflammatory to anti-inflammatory. Chronic, or non-healing, wounds, such as diabetic, pressure, and venous leg ulcers, feature a prolonged host inflammatory response due in part to aberrant wound macrophage behavior. Non-healing in chronic wounds has also been shown to be dependent upon the establishment of pathogenic biofilms, which are more resistant to host defense mechanisms than planktonic, or free-floating, bacteria. Therefore, investigating macrophage dysregulation in the presence of bacterial biofilms has gained considerable interest.

Here, 1D ^{1}H NMR-based metabolomics was utilized to identify metabolic pathways that are differentially modulated following primary human monocyte-derived macrophage activation with pro-inflammatory or anti-inflammatory stimuli relative to resting macrophages. Metabolic profiling of inflammatory macrophages indicated a substantial increase in oxidative stress as well as a decrease in mitochondrial respiration. These metabolic profiles also provided evidence that inflammatory macrophages divert metabolites from *de novo* glycerophospholipid synthesis to inhibit oxidative phosphorylation. In addition, we investigated which metabolic pathways are differentially modulated following primary human monocyte-derived macrophage exposure to *Pseudomonas aeruginosa* planktonic- and biofilm-conditioned media. Metabolic profiling of PCM- and BCM-exposed macrophages indicated a significant depletion of intracellular glucose without elevation of downstream glycolytic products. These metabolic patterns suggest that PCM- and BCM-exposed macrophages potentially divert glycolytic intermediates towards inositol phosphate metabolism. Overall, our studies provide additional support to previous findings, generate novel results regarding metabolic modulation of human MΦs following activation and exposure to planktonic- vs. biofilm-conditioned media, and contribute new insight to the field of immunometabolism.

CHAPTER ONE

INTRODUCTION

Metabolomics

Metabolomics is the global analysis of the metabolic profiles of organisms and the identification and quantitation of intra- and extracellular metabolite levels, i.e. small molecules derived from host, microbial, dietary, or other exogenous sources, within complex biological samples, such as biofluids, tissues, and cells, to better understand and establish how biochemical pathways are modulated in organisms as responses to changes in their environment, which allows us to gain mechanistic insights into pathological, physiological, and aberrant conditions, including diseased states [1-4]. Metabolites are substrates and products of metabolism that drive and support cellular functions, including the production and storage of energy, signal transduction, regulation of gene expression, and apoptosis [5]. Rather than examining single compounds, reactions, cycles, and kinetic properties, metabolomics entails the collection, processing, and quantitation of the widest range of metabolites possible, aiming for comprehensive metabolome coverage, to elucidate the metabolic dynamics underlying conditions of interest [6]. This methodology allows for the investigation of the metabolic functional state of an organism, tissue, cell, or biofluid at a specific point in time following exposure to stimuli [6]. Furthermore, metabolic information nicely complements data derived from other -omics fields, such as genomics, transcriptomics, and proteomics, by providing another level/perspective to the systems biology approach employed to better understand disease pathophysiology and

treatment outcomes [6]. Several disease states already have reported characteristic metabolic signatures associated with Alzheimer's disease [7], depression [8], schizophrenia [9-11], breast cancer [12], hypertension [13], type 2 diabetes [14,15], and pre-eclampsia [16]. Overall, metabolomics has a potentially broad range of applications in biomedical research and practice due to its capability to yield vital information concerning drug action, disease mechanisms, and organisms' responses to pathogen exposure or other environmental stressors.

NMR-Based Metabolomics

The two most common and powerful approaches utilized in metabolomics studies are mass spectrometry (MS) [17,18] and nuclear magnetic resonance (NMR) spectroscopy [19,20], and although each of these methods present their own advantages and disadvantages [21,22], this section will solely focus on NMR-based metabolomics as it has been the method employed for the dissertation work described herein.

While NMR suffers from more limited sensitivity, it possesses several advantages over MS-based metabolomics, yet complements the MS approach nicely. For example, NMR allows for the observation and quantification of the more abundant metabolites present in cell/tissue extracts and biofluids without requiring complex sample pre-processing, such as fractionation or derivatization. In addition, NMR can identify compounds that may be difficult to ionize or those that exhibit identical masses. NMR can also be used to investigate dynamic metabolite reactions, transformations, and compartmentalization by way of stable isotope labeling [23,24]. In addition to its quantitative power, NMR spectra are highly reproducible and data acquired on one

spectrometer can be easily reproduced on another instrument of the same magnetic field strength, facilitating inter-laboratory experimental replication.

One-dimensional (1D) ^{1}H NMR is used most frequently in NMR-based metabolomics studies, particularly for the metabolic comparison of healthy subjects to patients presenting with disease [24,25]. However, the limited spectral width, approximately 10 ppm, of ^{1}H NMR spectroscopy may lead to resonance crowding and overlapping ^{1}H signals, which contributes to metabolite assignment and identification uncertainty. Conversely, 1D ^{13}C NMR spectroscopy affords a much wider sweep width, approximately 200 ppm; however, the analysis of ^{13}C is challenging due to the intrinsic lower sensitivity and natural abundance of ^{13}C spins [21]. Nonetheless, ^{13}C NMR sensitivity for metabolites, such as amino acids, can be enhanced using derivatization methods as demonstrated by Shanaiah *et al.*, who were able to improve quantitation of amino acids from ^{13}C NMR spectra acquired from inborn error in metabolism patients' serum and urine samples using metabolite acetylation via the addition of ^{13}C-acetic anhydride [26]. 1D ^{31}P, which is 100% naturally abundant, NMR has been employed in studies investigating the metabolite profiles and phospholipids modulating energy metabolism [27,28]; however, this approach is fairly limited due to lower sensitivity, compared to ^{1}H NMR spectroscopy, and the fact that ^{31}P is not present in many metabolites.

Whereas 1D ^{1}H NMR is a common approach in untargeted metabolomics, which is a global metabolome quantitative analysis, due in part to its high throughput nature, its capacity to verify metabolite identity is limited due to NMR resonance overlap and

crowding as mentioned previously. In the absence of instrumental and data acquisition time restrictions, two-dimensional (2D) NMR spectroscopy can be utilized to identify, confirm, and validate metabolite annotation and identification [21]. Several 2D NMR experiments have been employed in metabolomics studies, including heteronuclear single quantum coherence (HSQC) [29], heteronuclear multiple bond correlation (HMBC) [30], and homonuclear correlation spectroscopy methods, such as total correlation spectroscopy (TOCSY) [31], correlation spectroscopy (COSY) [32], diffusion ordered spectroscopy (DOSY) [33], and 2D J-resolved NMR spectroscopy (J-Res) [34]. If NMR time is limited, 2D ^{1}H-^{13}C NMR methods have been developed for high throughput quantitation of biologically abundant metabolites [35]. Using this technique, Lewis *et al.* were able to demonstrate enhanced metabolite molar concentration accuracy, compared to 1D methods, in the analysis of mixtures of synthetic compounds and extracts from *Arabidopsis thaliana*, *Saccharomyces cerevisiae*, and *Medicago sativa*, which required experimental ^{1}H-^{13}C NMR data acquisition times of only 12 minutes. Methods such as this could be used as a practical alternative to 1D ^{1}H NMR metabolomics studies when substantial extract dry weights, $\geq$ 50 mg, are available.

Applications of NMR in Metabolomics

The majority of NMR metabolomics studies are based upon metabolite profiling without the use of isotope tracers, which are molecules that are labeled with a radioactive or stable isotope yet functionally and chemically identical to naturally occurring molecules [36]; the application of which has been utilized in the diagnosis of diseases, drug monitoring and risk assessment, and the investigation of metabolic perturbations

resulting from a wide range of experimental conditions, such as diet, exercise, aging, and mutation [24]. One of the first applications of NMR spectroscopy in metabolomics involved the profiling of metabolites in tumor tissues and cells, because this technique was notably effective for examining metabolic phenomenon such as the Warburg effect and glycerophospholipid metabolism [37,38]. For example, Sitter *et al.* identified glycerophosphocholine, phosphocholine, and choline as discriminatory metabolites in malignant versus benign tumor tissues using high-resolution magic angle spinning (HR-MAS) ^{1}H NMR spectroscopy; in addition, they determined that taurine, glycine, glutamine, and glutamate are particularly important in differentiation of tumor types [39]. Furthermore, NMR-based metabolomics has been used to distinguish between different types of inflammatory bowel diseases, such as ulcerative colitis (UC) and Crohn's disease (CD) [40]. Marchesi *et al.* established that diminished levels of methylamine, trimethylamine, butyrate, and acetate were observed in UC and CD patients' fecal extracts relative to healthy controls; however, elevated glycerol, relative to UC patients and healthy controls, was determined to be a specific biomarker of CD patients' pathology [25].

Although metabolism and metabolic networks are often thought of and depicted in a linear manner, this is not biologically realistic. For instance, glycolysis is defined as the oxidation of glucose to form pyruvate; yet, glycolytic intermediates can be directed towards and utilized in other metabolic and regulatory pathways, including the tricarboxylic acid (TCA) cycle, the pentose phosphate pathway (PPP), glycolytic regulatory networks, the synthesis of hexosamines and lipids, and many more [41,42].

While metabolic profiling by NMR and/or MS yield information regarding the metabolic state of a biological sample, these methods remain incomplete for the deconvolution of metabolic perturbations, regulation, and dynamics that govern steady-state systems, given the redundancy and complexity of metabolic networks and the cross talk between metabolism, cell signaling, gene expression and regulation, and cells' immune responses [43].

The utilization of isotope tracers is crucial for the investigation and resolution of metabolic pathway dynamics. Even though radiotracers have been widely used in research since the 1950s [44,45], stable isotope tracers, such as ^{13}C and ^{15}N, are currently preferred due to advancements in biological NMR [46-48], coupled with the fact that, unlike radionuclides, biologically relevant stable isotopes are NMR active and non-hazardous [23]. Using uniformly ^{13}C-labeled glucose (U-$^{13}C_6$-glucose), $^{13}C_1$-3-lactate, and $^{13}C_2$-2,3-alanine tracers, $^{1}H\{^{13}C\}$- HSQC NMR, and gas chromatography (GC)-MS, Fan *et al.* were able to establish the impact of lithium chloride, a bipolar disorder therapeutic, on glial and neuronal cell metabolism; furthermore, the trafficking of metabolites between these two cells types was also elucidated. Their findings indicate that the therapeutic efficacy of lithium treatment may be due to enhanced support of the glutamine/glutamate cycle between neurons and astrocytes [49]. Gaining novel insights regarding the metabolic flux and interactions occurring within complex biological systems would not be possible without the use of isotope tracer labeling and subsequent isotopomer analysis by NMR.

Current Challenges

Although the metabolomics field has advanced substantially over the past few decades [50], some major challenges, such as metabolite identification, validation, and the ability for the scientific community to translate their metabolic findings into biologically relevant stress- and disease-induced mechanisms, persist.

A considerable amount of effort, focus, and importance in metabolomics research has been given to the identification of biomarkers that can be correlated to environmental and disease factors. However, metabolite identification and validation are vital in order to associate a particular metabolic biomarker (metabotypes) with a biological phenotype [5]. Most metabolomic profiling studies utilize an untargeted approach, with only a minor subset of the metabolites detected being definitively identified. Validation of metabolite identification has been improved with the expansion of metabolite databases [51], such as the Human Metabolome Database (HMDB) [52], development of *in silico* tools [53], and synthesis of novel metabolite standards [54]. Nevertheless, researchers need to be more cognizant of the challenges regarding unambiguous validation of biomarkers and follow-up their initial untargeted approaches with more targeted experiments; in addition, studies must have some way to account for inter-patient variability due to genetic and environmental factors, which confound clinical biomarker identification [55,56].

Translating experimental biomarkers and metabolic signatures into biological mechanisms is conceivably the greatest hurdle currently facing metabolomics research. To obtain a thorough understanding of systematic biological disease-induced perturbations correlated with specific metabolites or biomarkers, their function and

interconnectivity within metabolic pathways must be determined using follow-up *in vitro* patient-derived primary cell mechanistic studies where environmental factors can be controlled [57]. Yet, comprehensive elucidation of metabolite interactions is quite challenging; current maps detailing metabolic networks contain thousands of metabolites and are often incomplete as novel, previously unknown metabolites are frequently discovered [58]. Integration of multi-omics datasets acquired from the same biological samples allows for a deeper systems-level analysis of metabolic networks, changes in metabolite pools, and molecular interactions during disease [59]. Furthermore, additional metabolomics approaches, such as stable isotope analysis, which yields important information concerning metabolite utilization and metabolic flux should be employed more regularly [60].

Macrophages

Macrophages (MΦs) are a vital cellular component of the innate immune system. They perform countless immunological roles ranging from host defense to the maintenance and regulation of tissue homeostasis [61]. MΦs express a wide array of cell surface markers, including phagocytic, scavenger, and pattern recognition receptors, that enable them to be particularly adept at perceiving and responding to pathogenic invasion and infection [62,63]. In addition, their inherent phagocytic system can serve multiple homeostatic functions, including the clearance of apoptotic cells, foreign debris, and lipoproteins [64,65]. Therefore, MΦs are innate immune cells which are critical for the coordination and support of immune responses under both pathological and homeostatic

conditions.

The classical understanding of MΦ ontogeny and function suggests that MΦs are derived from the hematopoietic system, lack any further proliferative potential, and demonstrate either pro-inflammatory (M1) or anti-inflammatory (M2) phenotypes [66,67]. Consequently, MΦ characterization has been restricted by this discrete M1/M2 MΦ model, and it has been assumed that MΦs undergo continuous replenishment from monocytes originating from bone marrow-derived myeloid progenitor cells [66]. However, recent studies have demonstrated that tissue-resident MΦs are generated and maintained by unique precursor populations, which are supplied from either bone-marrow derived myeloid cells or embryonic hematopoietic cells [68]. Aside from this ontogenic diversity, recent evidence has also indicated that MΦs display remarkable plasticity, which resembles a spectrum of functional MΦ phenotypes beyond the traditional bimodal dogma traditionally utilized in immunological research [67].

MΦ Functions and Plasticity

One of the pivotal characteristics of MΦs is their exceptional functional diversity [69]. These functions include, but are not limited to, phagocytosis, remodeling of tissues, metabolism, inflammation, and immunoregulation, which are very briefly discussed below. Phagocytosis is perhaps one of the most well-known MΦ functions concerning host defense, which involves the engulfment and elimination of bacterial pathogens, apoptotic cells, and cellular debris [70]. These processes also support immunoregulation in that MΦ phagocytosis of dead cells has been demonstrated to shift MΦs to an anti-inflammatory phenotype [71]. MΦs are also known to produce multiple factors, including

colony stimulating factor 1 (CSF1), vascular endothelial growth factor (VEGF), matrix metalloproteinase 9 (MMP9), and interleukin 8 (IL-8), which stimulate tissue remodeling and repair mechanisms, such as fibrosis and angiogenesis [72]. Metabolic regulation is another essential function demonstrated by MΦs. For example, foamy MΦs in atherosclerosis have been shown to regulate cholesterol efflux and fatty acid uptake [73]. MΦs also initiate the activation and infiltration of other immune cells during inflammation by way of pro-inflammatory cytokine expression in response to bacterial stimuli [69]. However, MΦs can also assist in dampening an inflammatory immune response as a result of their immunoregulatory functions [74]. For instance, anti-inflammatory MΦs express lipid mediators, including resolvins and lipoxin, which promote the resolution of inflammation [74,75]. Collectively, these examples emphasize the significance of MΦ functional plasticity to biological system maintenance and homeostasis.

Although the phenotypic malleability of MΦs is invaluable for enabling balanced innate immune responses to variable microenvironmental stimuli, MΦ plasticity has been identified as a particularly influential element in disease progression. Pathologies linked to obesity, including diabetes, metabolic syndrome, and insulin resistance, are known to be in part driven by chronic inflammation [76]. Adipose tissue contains multiple types of cells, including endothelial cells, adipocytes, lymphocytes, and adipose-tissue MΦs (ATMs). Under normal conditions, ATMs support homeostasis in adipose tissue; however, obese conditions prime ATMs to promote inflammation, which contributes to the development of metabolic disease [77, 78]. Previous studies have established that IL-

4 secreted by adipocytes in lean murine models shifts MΦs to an anti-inflammatory (M2) phenotype to inhibit inflammation. Yet obese adipose tissue demonstrates elevated MΦ infiltration, and obese ATMs exhibit multiple pro-inflammatory (M1) characteristics, including increased expression of tumor necrosis factor (TNF) and inducible nitric oxide synthase (iNOS) [79,80]. Notably, ATMs also display plasticity and functional heterogeneity. For example, influx of anti-inflammatory (M2) MΦs into adipose tissue is associated with increased lipolysis and chronic weight loss in murine models [81].

MΦ Immunometabolism

Immunometabolism is a growing field of study that examines how metabolic reactions and pathways modulate effector function in immune cells, including MΦs. A brief review of the current literature concerning the utilization of glycolysis, the PPP, the TCA cycle, oxidative phosphorylation, fatty acid synthesis and oxidation, and amino acid metabolism is detailed herein. M1 MΦs are known to heavily rely upon aerobic glycolysis as their primary source of energy, whereas M2 MΦs utilize oxidative phosphorylation for adenosine triphosphate (ATP) production [82-84]. In fact, several studies have shown that hallmarks of M1 MΦ activation, including pro-inflammatory cytokine production, phagocytosis, and ROS generation, are inhibited upon administration of 2-deoxyglucose, a glucose derivative [85-87]. In addition, M1 MΦs exhibit upregulation of glucose transporter 1 (GLUT1) expression to facilitate rapid glucose consumption in support of their elevated glycolytic flux [85,88]. Regulation of the PPP in MΦs is governed by carbohydrate kinase-like protein (CARKL). MΦs upregulate CARKL expression in response to IL-4, which then suppresses PPP flux in

M2 MΦs [89]. However, CARKL expression is reduced in LPS-stimulated, or M1, MΦs, with subsequent upregulation of the PPP, reduced oxygen consumption, and increased extracellular acidification [89-91]. Therefore, CARKL downregulation is a critical metabolic switch for the diversion of glucose from glycolysis to the PPP in M1 MΦs. Disruption of the TCA cycle at distinct enzymatic steps has been well-established in M1 MΦs; consequently, the accumulation of particular TCA cycle intermediates, including succinate, citrate, and itaconate, occurs in M1 MΦs [91,92]. On the other hand, resting (M0) and M2 MΦs utilize an intact TCA cycle for the production of ATP using oxidative phosphorylation [91]. Notably, previous studies have also shown that fumarate accumulation in M1 MΦs leads to epigenetic alterations and is important for the induction of trained innate immunity in MΦs [93]. While the electron transport chain (ETC) and oxidative phosphorylation is dysregulated in M1 MΦs, which are known to generate the majority of their ATP from glycolysis, M2 MΦs maintain their ETC and oxidative phosphorylation mechanisms in order to produce ATP using ATP synthase [91]. Overexpression of PPARγ coactivator-1β (PGC-1β), which has been shown to induce the upregulation of oxidative phosphorylation in IL-4 treated MΦs, suppresses pro-inflammatory cytokine production. Furthermore, inhibition of PGC-1β impairs metabolic characteristics of M2 MΦ activation, including arginase activity and fatty acid oxidation [94]. Increased fatty acid synthesis has been linked to M1 MΦ effector functions. Feingold *et al*. determined that elevation of glycolysis and resultant glucose-derived carbons were favorably assimilated into sterols and fatty acids [95]. In addition, foam MΦs, which are associated with the pathogenesis of atherosclerosis and other

chronic inflammatory disorders, are known to accumulate cholesterol esters and triglycerides [96,97]. To the contrary, M2 MΦs rely upon lysosomal acid lipase (LAL)-mediated lipolysis for the liberation of fatty acids to fuel mitochondrial oxidative phosphorylation [94,98]. Branched chain amino acid transaminase 1 (BCAT1), the enzyme that catalyzes the initial step of branched-chain amino acid (BCAA) metabolism, inhibition in human MΦs has been shown to reduce O_2 consumption, immune-responsive gene 1 (IRG1) protein expression, intracellular itaconate levels, and glycolytic flux [99]. Previous studies have also shown that branched-chain ketoacids (BCKAs), which are a product of BCAA catabolism, can suppress phagocytosis in tumor-associated MΦs (TAMs) [100]. Moreover, arginine consumption by MΦs, for nitric oxide (NO) production, has been demonstrated to inhibit tumor growth [101,102]. The rapidly expanding field of immunometabolism has established novel roles for metabolic intermediates and pathways in the modulation of immune cell effector functions. Many inquiries have yet to be investigated and answered, but further immunometabolic studies will contribute new knowledge towards the discovery and development of future therapeutics for immunometabolic-related pathologies.

MΦs in Acute Wound Healing

The three overlapping phases of acute wound healing consist of inflammation, proliferation, and tissue remodeling [103-105]. Upon tissue injury, activated platelets induce clot formation to prevent additional blood loss. In addition, platelets secrete chemokines that promote the migration of circulatory immune cells to the site of injury, which initiates the inflammatory phase. Neutrophils are the first innate immune cells to

infiltrate the wound, where they secrete proteases, pro-inflammatory cytokines, and reactive oxygen species (ROS) to disinfect the site. Following neutrophil arrival, blood monocytes migrate into the wound and differentiate into MΦs [106]. After neutrophils have sanitized the wound, they undergo apoptosis and are phagocytosed by MΦs, which will also engulf other debris and bacteria to further cleanse the wound bed in preparation for proliferation [104,107]. During this phase, fibroblasts, endothelial cells, and keratinocytes proliferate and begin to repair damaged tissues by generating granular tissue (GT), which is a vascularized extracellular matrix. Keratinocytes then migrate across the wound until it is closed in a process known as re-epithelialization. The final phase of tissue remodeling includes GT and collagen maturation in an effort to reclaim tissue tensile strength [108]. Once tissue remodeling is complete, vascular cells and myofibroblasts within the collagen-rich scarred region undergo apoptosis [109].

MΦs are essential regulators in wound healing processes, where they serve distinct roles to ensure that healing occurs in a timely and orderly manner. MΦ phenotype is known to evolve throughout the progressive phases of wound healing [110,111]. During the inflammatory phase, M1 MΦs clear the wound of apoptotic cells, foreign or cellular debris, and bacteria. However, upon the resolution of inflammation, these MΦs shift to an M2 phenotype, and as a result they promote the proliferation and infiltration of cells that repair and regenerate the epidermis, vasculature, and dermis, including keratinocytes, endothelial cells, and fibroblasts, respectively. In addition, MΦs aid in re-vascularization by supporting the fusion and stabilization of new blood vessels [112,113]. MΦs also secrete MMPs, which are crucial for the maturation and remodeling of

transitional GT in order to increase tensile strength in wounded tissues [114]. Although it is well-established that MΦ phenotype changes during wound healing, several MΦ subtypes have since been defined based upon their functions, cell surface marker expression, and cytokine production, which are beyond the discrete M1/M2 model [67].

Chronic Wounds

The majority of tissue lacerations, injuries, and surgical incisions are classified as acute wounds, which generally heal with little to no complications. Venous, diabetic, and pressure ulcers are the most common types of chronic, or non-healing, wounds that fail to progress through the normal stages of wound healing in a timely manner [109,115]. Prolonged inflammation is a shared characteristic across all chronic wound types, which prevents the wound from progressing into the proliferative and remodeling stages of wound healing [107,109]. Concurrent with the steady growth of obese, elderly, and diabetic populations, the incidence of chronic wounds is rising at rates of 6-9% annually [115]. Recent studies have reported the global number of venous, diabetic, and pressure ulcer wound patients to be upwards of 24 million [115]. Unfortunately, the development and implementation of novel effective therapies for chronic wounds is not occurring at a complementary accelerated rate.

Chronic wounds are an enormous burden, not only upon the patients whom are afflicted but also the health care staff and systems tasked with their treatment. Annual costs associated with chronic wound care in the U.S. alone are in excess of $25 billion [116]. Average chronic wound treatment patient costs in the U.S. and England for

pressure ulcers were reported as $4000 and $8000, respectively [117,118]. In the event that tissue damage and bacterial infection within chronic wounds is not responsive to standard care and treatment options, limb amputation is performed [116]. These surgical amputation procedures are quite expensive, often costing more than $35,000, and can be devastating to the patient [116,119,120]. Understanding chronic wound pathophysiology and progression is critical for the informed development and advancement of treatments and interventions to resolve inflammation and restore healing in chronic wounds.

MΦ Dysregulation in Chronic Wounds

As previously mentioned, MΦs are critical innate immune cells in the regulation of wound healing progression, particularly in the transition from inflammation to proliferation [111,113]. Notably, chronic wounds feature an excessive and prolonged inflammatory response, which prevents them from progressing to the proliferative phase of wound healing where tissue repair and regeneration occurs [107,109]. Chronic diabetic and venous ulcers have been shown to contain significantly higher numbers of MΦs at wound edges and in the dermis than acute wounds [121,122]. Correspondingly, previous studies have also found that chronic wound exudate exhibits 100-fold increased levels of interleukin-1β (IL-1β) and TNF-α, both of which are pro-inflammatory cytokines [123,124]. Elevation of MMP levels, especially MMP2 and MMP9, have also been demonstrated in chronic wound fluids [125]. Since MΦs and blood monocytes are known to produce MMPs, which degrade proteins, extracellular matrices, and reduce growth factor bioactivity, upon pro-inflammatory stimulation, MΦs have been further implicated as potential culprits that contribute to the exorbitant inflammation seen in non-healing,

chronic wounds [123,126,127].

Diabetic murine models are often used in the investigation of chronic wound development and progression, because they display deferred healing and characteristics similar to human chronic wounds [128,129]. Mirza and Koh demonstrated that M1 MΦs persist longer in diabetic murine wounds; therefore, these findings suggest that diabetic wound MΦs are inefficient at transitioning to the pro-resolving, M2 MΦ, phenotype compared to wild-type controls [130]. Moreover, this study determined that diabetic murine wound MΦs retained pro-inflammatory features, including elevated IL-1β and MMP-9 gene expression and suppressed growth factor production, even after transitioning to an anti-inflammatory, or M2, phenotype [130]. M1 MΦs in chronic wounds have also been shown to contain elevated levels of intracellular iron, which is derived from erythrocytes in wound tissues [131]. Furthermore, administration of intravenous iron in murine wound models leads to the production of hydroxyl radicals and TNF by wound MΦs, fibroblast senescence, and consequent delayed wound closure [131]. Previous studies have demonstrated differential iron regulation in the context of MΦ activation, where M1 MΦs store intracellular iron as ferritin, and M2 MΦs secrete iron into the extracellular microenvironment using ferroportin transmembrane channels [131,132]. Overall, these examples indicate that aberrant MΦ behavior in chronic wounds contributes to complications observed during the wound healing process.

Biofilm Formation in Chronic Wounds

Biofilms are immobile, structured bacterial communities that adhere to biotic and abiotic surfaces [133,134]. Bacteria growing in biofilms are more resistant to host

defense mechanisms and antibiotics than planktonic bacteria [135,136]. Chronic wounds have been shown to be inherently vulnerable to microbial infection due to delayed re-epithelialization [137], hypoxia [138], reduced blood flow, and attenuated host immune responses [121,114]. Previous studies have determined that bacteria residing in chronic wounds are primarily in the biofilm mode of growth [139]. In fact, porcine model wounds inoculated with bacteria exhibit biofilm formation within 48 hours [140]. Furthermore, colonization of wounds by biofilms has been implicated as a major contributor to chronicity and delayed healing [141]. Since the contribution of biofilm formation to chronic wound pathogenesis has been well-established, their interaction and cross talk with host innate immune cells must be investigated further.

Although biofilms in chronic wounds are composed of a diverse flora of microbial species, the most prominent bacteria in pressure, diabetic, and venous ulcers include *Staphylococcus*, *Pseudomonas, Peptoniphilus*, *Enterobacter*, *Stenotrophomonas*, *Finegoldia*, and *Serratia* spp [142]. Notably, the chronic wound microbiome fluctuates significantly between individuals and wound types, with most chronic wounds demonstrating microbial colonization by multiple species [142]. This underlying complexity confounds the elucidation of specific innate immune responses and corresponding culpable bacterial secretory products. Therefore, to gain insight and further our understanding of the role of biofilms in chronic wound pathogenesis, a single opportunistic human pathogen, *Pseudomonas aeruginosa*, was investigated in the dissertation work described herein. While *P. aeruginosa* is only found predominantly in chronic venous leg ulcers, it is quite a virulent pathogen [142]. Chronic *P. aeruginosa*

infections have been correlated with worsened disease progression and prognosis, and increased mortality and morbidity [143,144]. Previous studies conducted in the Center for Biofilm Engineering (CBE) here at Montana State University (MSU) have established that biofilm-conditioned media (BCM), containing soluble, secretory bacterial products, induces distinct changes in fibroblasts and keratinocytes, including altered cytokine production, decreased viability, and the promotion of apoptosis, relative to planktonic-conditioned medium (PCM) [145,146].

Innate Immune Responses to *P. aeruginosa* Biofilms

P. aeruginosa is a Gram-negative, rod-shaped bacterium that is typically found in aqueous and soil environments. However, *P. aeruginosa* is also known to cause diverse opportunistic human infections, particularly in immunocompromised individuals [147]. *P. aeruginosa* biofilm formation has also been previously demonstrated in chronic wound infections [142]. Over the past few decades, the increasing prevalence of drug-resistant strains of *P. aeruginosa* has made antibiotic control and treatment of acute and chronic infections quite challenging [148]. Consequently, studies investigating host innate immune responses to *P. aeruginosa* infections have garnered considerable interest.

Recent evidence has shown that innate immune cells are essential for host response to *P. aeruginosa* biofilms [149,150]. Previous studies using murine and human models have established that activated host neutrophils surround and significantly accumulate in close proximity to *P. aeruginosa* biofilms [151,152]. Furthermore, exposure of isolated primary human neutrophils and MΦs to *P. aeruginosa* biofilms

induces strong inflammatory responses in both innate immune cells types, including respiratory burst, degranulation, and phagocytosis [153,154]. However, prior studies have found that the antimicrobial function of neutrophils and MΦs is greatly attenuated in the presence of *P. aeruginosa* biofilms. Neutrophils exposed to *P. aeruginosa* biofilms generate a significantly reduced respiratory burst, -4-fold, compared to that detected upon exposure to planktonic bacteria [155]. Moreover, *P. aeruginosa* upregulates rhamnolipid expression in the presence of neutrophils as a defense mechanism, in order to impair neutrophil chemotaxis and induce necrotic cell death [156,157]. Specific MΦ responses to *P. aeruginosa* biofilms are not as well-characterized. Yet, Leid *et al.* determined that alginate, an extracellular polysaccharide component of *P. aeruginosa* biofilm matrices, contributes to biofilm protection from killing by MΦs [154]. In addition, compared to their equivalent planktonic counterparts, *P. aeruginosa* biofilms induce a more robust inflammatory response in MΦs. Presence of human MΦs or MΦ-associated secretion products has been found to surprisingly enhance *P. aeruginosa* biofilm growth, maturation, and virulence factor production [149,158].These examples indicate that cross talk between bacterial biofilms and host cells is essential for *P. aeruginosa* biofilm evasion of host defense mechanisms and warrants further investigation.

Research Questions, Hypotheses, and Aims

The two main research questions addressed in the dissertation work described herein were, (1) “does human MΦ metabolism change during activation and/or exposure to bacterial secretory products?” and (2) “which metabolic pathways are modulated in

human MΦs during activation and/or exposure to bacterial secretory products?" Several hypotheses were established prior to the commencement of and over the course of this dissertation project. These included, (1) differentially-activated MΦs (M1 vs. M2) will exhibit disparate metabolic strategies, (2) M1 MΦs will preferentially utilize glycolysis, whereas M2 MΦs will rely on the TCA cycle for energy production, (3) MΦs exposed to *P. aeruginosa* BCM will display a unique metabolic signature when compared to MΦs exposed to *P. aeruginosa* PCM, and (4) MΦs exposed to *P. aeruginosa* BCM will fail to exhibit metabolic hallmarks and characteristics which are reflective of M1 MΦ activation.

The aims of this dissertation research included the detailed metabolic characterization of distinct primary human monocyte-derived MΦ activation states using established cytokine stimuli and the metabolic shift of human M0 MΦs upon exposure to *P. aeruginosa* PCM versus BCM. Preceding the onset of these aims, a considerable amount of optimization regarding metabolite extraction, 1D ^{1}H NMR data acquisition, and validation of human MΦ phenotypes by flow cytometry was conducted. Optimization of metabolite extraction from primary human MΦs was performed in order to achieve sufficient signal-to-noise ratios in resulting 1D ^{1}H NMR spectra; in addition, Dr. Brian Tripet, MSU NMR facility manager, determined that shimming problems, which can greatly affect downstream metabolite quantitation in NMR metabolomics, encountered while using the 'noesypr1d' pulse sequence could be alleviated by switching to the excitation sculpting (ES)-based 'zgesgp' pulse sequence [159,160]. Furthermore, our *in vitro* generated human M0, M1, and M2a MΦs were evaluated by flow cytometry

to confirm and compare our MΦ phenotypes, which were found to be consistent with previously established MΦ phenotypic and cell surface marker expression profiles reported in the literature [161]. These various optimization steps enabled for the detailed investigation and interpretation of differential modulation of metabolic pathways within several human MΦ activation states, including M0, M1, and M2a MΦs.

Once the initial metabolic characterization of discrete cytokine-induced primary human monocyte-derived MΦ activation states had been accomplished, the subsequent aim of this dissertation research was to characterize the temporal metabolic impact of exposure to *P. aeruginosa* PCM versus BCM on primary human monocyte-derived M0 MΦs. Although *in vivo* research is prominent in studies concerning host-pathogen models, the simplicity and validation of network interactions offered by *in vitro* models has been acknowledged. *In vitro* studies often provide complementary information to gain molecular insights into observation made in *in vivo* infectious disease models [162,163]. ^{1}H NMR metabolic profiling with subsequent multivariate statistical analysis, modeling, and correlation analysis has been demonstrated as a valuable approach to investigate host-pathogen interactions at the molecular level. This approach enables the assessment of host-pathogen metabolic communication networks and allows for unique insights into pathogen specific effects and systemic metabolic modulation in the host [164,165]. Further knowledge and understanding of immunometabolic processes and host-pathogen interactions can thus be achieved using NMR metabolomics methods.

While utilization of metabolomics in immune cell characterization is becomingly increasingly more common with the recent emergence of immunometabolism, the use of

physiologically relevant cells, such as primary human monocyte-derived MΦs, is limited [166]. Previous studies have reported metabolic distinctions between M1 and M2 MΦs; however, the majority of these findings have been derived from bone marrow-derived murine MΦs and immortalized human and murine cell lines [167], which minimize their human health relevance. Murine MΦs display notable metabolic distinctions from human MΦs, including expression of proteins involved in arginine metabolism, including arginase 1 (Arg1) and iNOS, which are not comparably expressed in human M1 or M2 MΦs [168,169]. Furthermore, metabolic data derived from immortalized human cell lines may be confounded by the prevalence of the Warburg effect in tumor cells [37]. Using metabolomics to elucidate the metabolic signatures of primary human immune cells, crucial information regarding the functional and biochemical discrepancies between murine and human MΦs and the modulation of metabolic pathways upon human immune challenge can be accurately established.

References

1. van der Greef J, Martin S, Juhasz P, Adourian A, Plasterer T, Verheji ER, et al. The art and practice of systems biology in medicine: mapping patterns of relationships. J Proteome Res. 2007; 6(4): 1540-59.

2. Lindon JC, Holmes E, Bollard ME, Stanley EG, Nicholson JK. Metabonomics technologies and their applications in physiological monitoring, drug safety assessment and disease diagnosis. Biomarkers. 2004; 9(1): 1-31.

3. Schmidt C. Metabolomics takes its place as latest up-and-coming "omic" science. J Natl Cancer Inst. 2004; 96(10): 732-4.

4. Schmidt CW. Metabolomics: what's happening downstream of DNA. Environ Health Perspect. 2004; 112(7): A410-A415.

5. Johnson CH, Ivanisevic J, Siuzdak G. Metabolomics: beyond biomarkers and towards mechanisms. Nat Rev Mol Cell Biol. 2016; 17(7): 451-9.

6. Kaddurah-Daouk R, Kristal BS, Weinshilboum RM. Metabolomics: a global biochemical approach to drug response and disease. Annu Rev Pharmacol Toxicol. 2008; 48: 653-83.

7. Han X, Holtzman DM, McKeel DW Jr, Kelley J, Morris JC. Substantial sulfatide deficiency and ceramide elevation in very early Alzheimer's disease: potential role in disease pathogenesis. J Neurochem. 2002; 82(4): 809-18.

8. Paige LA, Mitchell MW, Krishnan KR, Kaddurah-Daouk R, Steffens DC. A preliminary metabolomics analysis of older adults with and without depression. Int J Geriatr Psychiatry. 2007; 22(5): 418-23.

9. Holmes E, Tsang TM, Huang JT, Leweke FM, Koethe D, Gerth CW, et al. Metabolic profiling of CSF: evidence that early intervention may impact on disease progression and outcome in schizophrenia. PLoS Med. 2006; 3(8): e327.

10. Kaddurah-Daouk R. Metabolic profiling of patients with schizophrenia. PLoS Med. 2006; 3(8): e363.

11. Kaddurah-Daouk R, McEvoy J, Baillie RA, Lee D, Yao JK, Doraiswamy PM, et al. Metabolomic mapping of atypical antipsychotic effects in schizophrenia. Mol Psychiatry. 2007; 12(10): 934-45.

12. Fan X, Bai J, Shen P. Diagnosis of breast cancer using HPLC metabonomics fingerprints coupled with computational methods. Conf Proc IEEE Eng Med Biol Soc. 2005; 6: 6081-4.

13. Brindle JT, Nicholson JK, Schofield PM, Grainger DJ, Holmes E. Application of chemometrics to ^{1}H NMR spectroscopic data to investigate a relationship between human serum metabolic profiles and hypertension. Analyst. 2003; 128(1): 32-6.

14. Wang C, Kong H, Guan Y, Yang J, Gu J, Yang S, et al. Plasma phospholipid metabolic profiling and biomarkers of type 2 diabetes mellitus based on high-performance liquid chromatography/electrospray mass spectrometry and multivariate statistical analysis. Anal Chem. 2005; 77(13): 4108-16.

15. Yuan K, Kong H, Guan Y, Yang J, Xu G. A GC-based metabonomics investigation of type 2 diabetes by organic acids metabolic profile. J Chromatogr B Analyt Technol Biomed Life Sci. 2007; 850(1-2): 236-40.

16. Kenny LC, Dunn WB, Ellis DI, Myers J, Baker PN, Consortium GOPEC, et al. Novel biomarkers for pre-eclampsia detected using metabolomics and machine learning. Metabolomics. 2005; 1: 227-34.

17. Dettmer K, Aronov PA, Hammock BD. Mass spectrometry-based metabolomics. Mass Spectrom Rev. 2007; 26(1): 51-78.

18. Gika HG, Theodoridis GA, Plumb RS, Wilson ID. Current practice of liquid chromatography-mass spectrometry in metabolomics and metabonomics. J Pharm Biomed Anal. 2014; 87: 12-25.

19. Smolinska A, Blanchet L, Buydens LM, Wijmenga SS. NMR and pattern recognition methods in metabolomics: from data acquisition to biomarker discovery: a review. Anal Chim Acta. 2012; 750: 82-97.

20. Bingol K, Brüschweiler R. Multidimensional approaches to NMR-based metabolomics. Anal Chem. 2014; 86(1): 47-57.

21. Emwas AHM, Salek RM, Griffin JL, Merzaban J. NMR-based metabolomics in human disease diagnosis: applications, limitations, and recommendations. Metabolomics. 2013; 9(5): 1048-1072.

22. Scalbert A, Brennan L, Fiehn O, Hankemeier T, Kristal BS, van Ommen B, et al. Mass-spectrometry-based metabolomics: limitations and recommendations for future progress with particular focus on nutrition research. Metabolomics. 2009; 5(4): 435-458.

23. Fan TW, Lane AN. Applications of NMR spectroscopy to systems biochemistry. Prog Nucl Magn Reson Spectrosc. 2016; 92-93: 18-53.

24. Markley JL, Brüschweiler R, Edison AS, Eghbalnia HR, Powers R, Raftery D, et al. The future of NMR-based metabolomics. Curr Opin Biotechnol. 2017; 43: 34-40.

25. Marchesi JR, Holmes E, Khan F, Kochhar S, Scanlan P, Shanahan F, et al. Rapid and noninvasive metabonomic characterization of inflammatory bowel disease. J Proteome Res. 2007; 6(2): 546-51.

26. Shanaiah N, Desilva MA, Nagana Gowda GA, Raftery MA, Hainline BE, Raftery D. Class selection of amino acid metabolites in body fluids using chemical derivatization and their enhanced ^{13}C NMR. Proc Natl Acad Sci USA. 2007; 104(28): 11540-4.

27. Kaplan O, van Zijl PC, Cohen JS. Information from combined ^{1}H and ^{31}P NMR studies of cell extracts: differences in metabolism between drug-sensitive and drug-resistant MCF-7 human breast cancer cells. Biochem Biophys Res Commun. 1990; 169(2): 383-90.

28. Ruiz-Cabello J, Cohen JS. Phospholipid metabolites as indicators of cancer cell function. NMR Biomed. 1992; 5(5): 226-33.

29. Hyberts SG, Heffron GJ, Tarragona NG, Solanky K, Edmonds KA, Luithardt H, et al. Ultrahigh-resolution ^{1}H-^{13}C HSQC spectra of metabolite mixtures using nonlinear sampling and forward maximum entropy reconstruction. J Am Chem Soc. 2007; 129(16): 5108-16.

30. Dumas ME, Canlet C, André F, Vercauteren J, Paris A. Metabonomic assessment of physiological disruptions using ^{1}H-^{13}C HMBC-NMR spectroscopy combined with pattern recognition procedures performed on filtered variables. Anal Chem. 2002; 74(10): 2261-73.

31. Sandusky P, Raftery D. Use of selective TOCSY NMR experiments for quantifying minor components in complex mixtures: application to the metabonomics of amino acids in honey. Anal Chem. 2005; 77(8): 2455-63.

32. Xi Y, de Ropp JS, Viant MR, Woodruff DL, Yu P. Automated screening for metabolites in complex mixtures using 2D COSY NMR spectroscopy. Metabolomics. 2006; 2(4): 221-233.

33. Mannina L, Sobolev AP, Capitani D, Iaffaldano N, Rosato MP, Ragni P, et al. NMR metabolic profiling of organic and aqueous sea bass extracts: implications in the discrimination of wild and cultured sea bass. Talanta. 2008; 77(1): 433-44.

34. Fonville JM, Maher AD, Coen M, Holmes E, Lindon JC, Nicholson JK. Evaluation of full-resolution J-resolved ^{1}H NMR projections of biofluids for metabonomics information retrieval and biomarker identification. Anal Chem. 2010; 82(5): 1811-21.

35. Lewis IA, Schommer SC, Hodis B, Robb KA, Tonelli M, Westler WM, et al. Method for determining molar concentrations of metabolites in complex solutions from two-dimensional ^{1}H-^{13}C NMR spectra. Anal Chem. 2007; 79(24): 9385-90.

36. Kim IY, Suh SH, Lee IK, Wolfe RR. Applications of stable, nonradioactive isotope tracers in *in vivo* human metabolic research. Exp Mol Med. 2016; 48(1): e203.

37. Gebregiworgis T, Powers R. Application of NMR metabolomics to search for human disease biomarkers. Comb Chem High Throughput Screen. 2012; 15(8): 595-610.

38. Huang Z, Chen Y, Hang W, Gao Y, Lin L, Li DY, et al. Holistic metabonomic profiling of urine affords potential early diagnosis for bladder and kidney cancers. Metabolomics. 2013; 9(1): 119-129.

39. Sitter B, Sonnewald U, Spraul M, Fjösne HE, Gribbestad IS. High-resolution magic angle spinning MRS of breast cancer tissue. NMR Biomed. 2002; 15(5): 327-37.

40. Beckonert O, Keun HC, Ebbels TM, Bundy J, Holmes E, Lindon JC, et al. Metabolic profiling, metabolomic and metabonomic procedures for NMR spectroscopy of urine, plasma, serum and tissue extracts. Nat Protoc. 2007; 2(11): 2692-703.

41. Fan TW, Lane AN, Higashi RM, Farag MA, Gao H, Bousamra M, et al. Altered regulation of metabolic pathways in human lung cancer discerned by (13)C stable isotope-resolved metabolomics (SIRM). Mol Cancer. 2009; 8: 41.

42. Lane AN, Fan TW. Regulation of mammalian nucleotide metabolism and biosynthesis. Nucleic Acids Res. 2015; 43(4): 2466-85.

43. Fan TW, Lorkiewicz PK, Sellers K, Moseley HN, Higashi RM, Lane AN. Stable isotope-resolved metabolomics and applications for drug development. Pharmacol Ther. 2012; 133(3): 366-91.

44. Weinman EO, Strisower EH, Chaikoff IL. Conversion of fatty acids to carbohydrate; application of isotopes to this problem and role of the Krebs cycle as a synthetic pathway. Physiol Rev. 1957; 37(2): 252-72.

45. Strisower EH, Kohler GD, Chaikoff IL. Incorporation of acetate carbon into glucose by liver slices from normal and alloxan-diabetic rats. J Biol Chem. 1952; 198(1): 115-26.

46. Clore M, Potts J. Recent developments in biomolecular NMR. RSC Publishing. 2012.

47. Bax A. Multidimensional nuclear magnetic resonance methods for protein studies. Curr Opin Struct Biol. 1994; 4(5): 738-744.

48. Fesik SW, Zuiderweg ER. Heteronuclear three-dimensional NMR spectroscopy of isotopically labelled biological macromolecules. Q Rev Biophys. 1990; 23(2): 97-131.

49. Fan TW, Yuan P, Lane AN, Higashi RM, Wang Y, Hamidi AB, et al. Stable isotope-resolved metabolomic analysis of lithium effects on glial-neuronal metabolism and interactions. Metabolomics. 2010; 6(2): 165-179.

50. Johnson CH, Gonzalez FJ. Challenges and opportunities of metabolomics. J Cell Physiol. 2012; 227(8): 2975-81.

51. Vinaixa M, Schymanski EL, Neumann S, Navarro M, Salek RM, Yanes O. Mass spectral databases for LC/MS- and GC/MS-based metabolomics: state of the field and future prospects. Trends Analyt Chem. 2016; 78: 23-35.

52. Wishart DS, Jewison T, Guo AC, Wilson M, Knox C, Liu Y, et al. HMDB 3.0--the human metabolome database in 2013. Nucleic Acids Res. 2013; 41(Database issue): D801-7.

53. Wolf S, Schmidt S, Müller-Hannemann M, Neumann S. *In silico* fragmentation for computer assisted identification of metabolite mass spectra. BMC Bioinformatics. 2010; 11: 148.

54. Rocca-Serra P, Salek RM, Arita M, Correa E, Dayalan S, Gonzalez-Beltran A, et al. Data standards can boost metabolomics research, and if there is a will, there is a way. Metabolomics. 2016; 12: 14.

55. Ellis JK, Athersuch TJ, Thomas LD, Teichert F, Pérez-Trujillo M, Svendsen C, et al. Metabolic profiling detects early effects of environmental and lifestyle exposure to cadmium in a human population. BMC Med. 2012; 10: 61.

56. Scalbert A, Brennan L, Manach C, Andres-Lacueva C, Dragsted LO, Draper J, et al. The food metabolome: a window over dietary exposure. Am J Clin Nutr. 2014; 99(6): 1286-308.

57. Sreekumar A, Poisson LM, Rajendiran TM, Khan AP, Cao Q, Yu J, et al. Metabolomic profiles delineate potential role for sarcosine in prostate cancer progression. Nature. 2009; 457(7231): 910-4.

58. Mathé EA, Patterson AD, Haznadar M, Manna SK, Krausz KW, Bowman ED, et al. Noninvasive urinary metabolomic profiling identifies diagnostic and prognostic markers in lung cancer. Cancer Res. 2014; 74(12): 3259-70.

59. Wu Y, Williams EG, Dubuis S, Mottis A, Jovaisaite V, Houten SM, et al. Multilayered genetic and omics dissection of mitochondrial activity in a mouse reference population. Cell. 2014; 158(6): 1415-1430.

60. Buescher JM, Antoniewicz MR, Boros LG, Burgess SC, Brunengraber H, Clish CB, et al. A roadmap for interpreting ^{13}C metabolite labeling patterns from cells. Curr Opin Biotechnol. 2015; 34: 189-201.

61. Lavin Y, Mortha A, Rahman A, Merad M. Regulation of macrophage development and function in peripheral tissues. Nat Rev Immunol. 2015; 15(12): 731-44.

62. Canton J, Neculai D, Grinstein S. Scavenger receptors in homeostasis and immunity. Nat Rev Immunol. 2013; 13(9): 621-34.

63. Kawai T, Akira S. The role of pattern-recognition receptors in innate immunity: update on Toll-like receptors. Nat Immunol. 2010; 11(5): 373-84.

64. Hussell T, Bell TJ. Alveolar macrophages: plasticity in a tissue-specific context. Nat Rev Immunol. 2014; 14(2): 81-93.

65. Kohyama M, Ise W, Edelson BT, Wilker PR, Hildner K, Mejia C, et al. Nature. 2009; 457(7227): 318-21.

66. van Furth R, Cohn ZA. The origin and kinetics of mononuclear phagocytes. J Exp Med. 1968; 128(3): 415-35.

67. Martinez FO, Gordon S. The M1 and M2 paradigm of macrophage activation: time for reassessment. F1000Prime Rep. 2014; 6:13.

68. Ginhoux F, Jung S. Monocytes and macrophages: developmental pathways and tissue homeostasis. Nat Rev Immunol. 2014; 14(6): 392-404.

69. Gordon S, Taylor PR. Monocyte and macrophage heterogeneity. Nat Rev Immunol. 2005; 5(12): 259-70.

70. Biswas SK, Chittezhath M, Shalova IN, Lim JY. Macrophage polarization and plasticity in health and disease. Immunol Res. 2012; 53(1-3): 11-24.

71. Weigert A, Johann AM, von Knethen A, Schmidt H, Geisslinger G, Brune B. Apoptotic cells promote macrophage survival by releasing the antiapoptotic mediator sphingosine-1-phosphate. Blood. 2006; 108(5): 1635-42.

72. Biswas SK, Mantovani A. Macrophage plasticity and interaction with lymphocyte subsets: cancer as a paradigm. Nat Immunol. 2010; 11(10): 889-96.

73. Moore KJ, Tabas I. Macrophages in the pathogenesis of atherosclerosis. Cell. 2011; 145(3): 341-55.

74. Serhan CN, Yang R, Martinod K, Kasuga K, Pillai PS, Porter TF, et al. Maresins: novel macrophage mediators with potent anti-inflammatory and proresolving actions. J Exp Med. 2009; 206(1): 15-23.

75. Serhan CN, Brain SD, Buckley CD, Gilroy DW, Haslett C, O'Neill LA, et al. Resolution of inflammation: state of the art, definitions and terms. Faseb J. 2007; 21(2): 325-32.

76. Hotamisligil GS. Inflammation and metabolic disorders. Nature. 2006; 444(7121): 860-7.

77. Olefsky JM, Glass CK. Macrophages, inflammation, and insulin resistance. Annu Rev Physiol. 2010; 72: 219-46.

78. Odegaard JI, Chawla A. Alternative macrophage activation and metabolism. Annu Rev Pathol. 2011; 6: 275-97.

79. Lumeng CN, Bodzin JL, Saltiel AR. Obesity induces a phenotypic switch in adipose tissue macrophage polarization. J Clin Invest. 2007; 117(1): 175-84.

80. Nguyen MT, Favelyukis S, Nguyen AK, Reichart D, Scott PA, Jenn A, et al. A subpopulation of macrophages infiltrates hypertrophic adipose tissue and is activated by free fatty acids via Toll-like receptors 2 and 4 and JNK-dependent pathways. J Biol Chem. 2007; 282(48): 35279-92.

81. Kosteli A, Sugaru E, Haemmerle G, Martin JF, Lei J, Zechner R, et al. Weight loss and lipolysis promote a dynamic immune response in murine adipose tissue. J Clin Invest. 2010; 120(10): 3466-79.

82. Oren R, Farnham AE, Saito K, Milofsky E, Karnovsky ML. Metabolic patterns in three types of phagocytizing cells. J Cell Biol. 1963; 17(3): 487-501.

83. Nagy C, Haschemi A. Time and demand are two critical dimensions of immunometabolism: the process of macrophage activation and the pentose phosphate pathway. Front Immunol. 2015; 6: 164.

84. O'Neill LA, Kishton RJ, Rathmell J. A guide to immunometabolism for immunologists. Nat Rev Immunol. 2016; 16(9): 553-65.

85. Freemerman AJ, Johnson AR, Sacks GN, Milner JJ, Kirk EL, Troester MA, et al. Metabolic reprogramming of macrophages: glucose transporter 1 (GLUT1)-mediated glucose metabolism drives a proinflammatory phenotype. J Biol Chem. 2014; 289(11): 7884-96.

86. Michl J, Ohlbaum DJ, Silverstein SC. 2-deoxyglucose selectively inhibits Fc and complement receptor-mediated phagocytosis in mouse peritoneal macrophages II. Dissociation of the inhibitory effects of 2-deoxyglucose on phagocytosis and ATP generation. J Exp Med. 1976; 144(6): 1484-93.

87. Pavlou S, Wang L, Xu H, Chen M. Higher phagocytic activity of thioglycollate-elicited peritoneal macrophages is related to metabolic status of the cells. J Inflamm (Lond). 2017; 14: 4.

88. Fukuzumi M, Shinomiya H, Shimizu Y, Ohishi K, Utsumi S. Endotoxin-induced enhancement of glucose influx into murine peritoneal macrophages via GLUT1. Infect Immun. 1996; 64(1): 108-12.

89. Haschemi A, Kosma P, Gille L, Evans CR, Burant CF, Starkl P, et al. The sedoheptulose kinase CARKL directs macrophage polarization through control of glucose metabolism. Cell Metab. 2012; 15(6): 813-26.

90. Tannahill GM, Curtis AM, Adamik J, Palsson-McDermott EM, McGettrick AF, Goel G, et al. Succinate is an inflammatory signal that induces IL-1β through HIF-1α. Nature. 2013; 496(7444): 238-42.

91. Jha AK, Huang SC, Sergushichev A, Lampropoulou V, Ivanova Y, Loginicheva E, et al. Network integration of parallel metabolic and transcriptional data reveals metabolic modules that regulate macrophage polarization. Immunity. 2015; 42(3): 419-30.

92. Ryan DG, O'Neill LAJ. Krebs cycle rewired for macrophage and dendritic cell effector functions. FEBS Lett. 2017; 591(19): 2992-3006.

93. Arts RJ, Novakovic B, Ter Horst R, Carvalho A, Bekkering S, Lachmandas E, et al. Glutaminolysis and fumarate accumulation integrate immunometabolic and epigenetic programs in trained immunity. Cell Metab. 2016; 24(6): 807-819.

94. Vats D, Mukundan L, Odegaard JI, Zhang L, Smith KL, Morel CR, et al. Oxidative metabolism and PGC-1β attenuate macrophage-mediated inflammation. Cell Metab. 2006; 4(1): 13-24.

95. Feingold KR, Shigenaga JK, Kazemi MR, McDonald CM, Patzek SM, Cross AS, et al. Mechanisms of triglyceride accumulation in activated macrophages. J Leukoc Biol. 2012; 92(4): 829-39.

96. Funk JL, Feingold KR, Moser AH, Grunfeld C. Lipopolysaccharide stimulation of RAW 264.7 macrophages induces lipid accumulation and foam cell formation. Atherosclerosis. 1993; 98(1): 67-82.

97. Oiknine J, Aviram M. Increased susceptibility to activation and increased uptake of low density lipoprotein by cholesterol-loaded macrophages. Arterioscler Thromb. 1992; 12(6): 745-53.

98. Huang SC, Everts B, Ivanova Y, O'Sullivan D, Nascimento M, Smith AM, et al. Cell-intrinsic lysosomal lipolysis is essential for alternative activation of macrophages. Nat Immunol. 2014; 15(9): 846-55.

99. Papathanassiu AE, Ko JH, Imprialou M, Bagnati M, Srivastava PK, Vu HA, et al. BCAT1 controls metabolic reprogramming in activated human macrophages and is associated with inflammatory diseases. Nat Commun. 2017; 8: 16040.

100. Silva LS, Poschet G, Nonnenmacher Y, Becker HM, Sapcariu S, Gaupel AC, et al. Branched-chain ketoacids secreted by glioblastoma cells via MCT1 modulate macrophage phenotype. EMBO Rep. 2017; 18(12): 2172-2185.

101. Currie GA, Gyure L, Cifuentes L. Microenvironmental arginine depletion by macrophages in vivo. Br J Cancer. 1979; 39(6): 613-20.

102. Keller R, Geiges M, Keist R. L-arginine-dependent reactive nitrogen intermediates as mediators of tumor cell killing by activated macrophages. Cancer Res. 1990; 50(5): 1421-5.

103. Singer AJ, Clark RA. Cutaneous wound healing. N Engl J Med. 1999; 341(10): 738-46.

104. Baum CL, Arpey CJ. Normal cutaneous would healing: clinical correction with cellular and molecular events. Dermatol Surg. 2005; 31(6): 674-86; discussion 686.

105. Liu ZJ, Velazquez OC. Hyperoxia, endothelial progenitor cell mobilization, and diabetic wound healing. Antioxid Redox Signal. 2008; 10(11): 1869-82.

106. Sindrilaru A, Scharffetter-Kochanek K. Disclosure of the culprits: macrophages-versatile regulators of wound healing. Adv Wound Care (New Rochelle). 2013; 2(7): 357-368.

107. Frykberg RG, Banks J. Challenges in the treatment of chronic wounds. Adv Wound Care (New Rochelle). 2015; 4(9): 560-582.

108. Falanga V. Wound healing and its impairment in the diabetic foot. Lancet. 2005; 366(9498): 1736-43.

109. Zhao R, Liang H, Clarke E, Jackson C, Xue M. Inflammation in chronic wounds. Int J Mol Sci. 2016; 17(12): 2085.

110. Mosser DM, Edwards JP. Exploring the full spectrum of macrophage activation. Nat Rev Immunol. 2008; 8(12): 958-69.

111. Ferrante CJ, Leibovich SJ. Regulation of macrophage polarization and wound healing. Adv Wound Care (New Rochelle). 2012; 1(1): 10-16.

112. Fantin A, Vieira JM, Gestri G, Denti L, Schwarz Q, Prykhozhij S, et al. Tissue macrophages act as cellular chaperones for vascular anastomosis downstream of VEGF-mediated endothelial tip cell induction. Blood. 2010; 116(5): 829-40.

113. Ogle ME, Segar CE, Sridhar S, Botchwey EA. Monocytes and macrophages in tissue repair: implications for immunoregenerative biomaterial design. Exp Biol Med (Maywood). 2016; 241(10): 1084-97.

114. Vannella KM, Wynn TA. Mechanisms of organ injury and repair by macrophages. Annu Rev Physiol. 2017; 79: 593-617.

115. Krzyszczyk P, Schloss R, Palmer A, Berthiaume F. The role of macrophages in acute and chronic wound healing and interventions to promote pro-wound healing phenotypes. Front Physiol. 2018; 9: 419.

116. Sen CK, Gordillo GM, Roy S, Kirsner R, Lambert L, Hunt TK, et al. Human skin wounds: a major and snowballing threat to public health and the economy. Wound Repair Regen. 2009; 17(6): 763-71.

117. Nussbaum SR, Carter MJ, Fife CE, DaVanzo J, Haught R, Nusgart M, et al. An economic evaluation of the impact, cost, and medicare policy implications of chronic nonhealing wounds. Value Health. 2018; 21(1): 27-32.

118. Posnett J, Franks PJ. The burden of chronic wounds in the UK. Nurs Times. 2008; 104(3): 44-5.

119. Gordois A, Scuffham P, Shearer A, Oglesby A, Tobian JA. The health care costs of diabetic peripheral neuropathy in the US. Diabetes Care. 2003; 26(6): 1790-5.

120. Carls GS, Gibson TB, Driver VR, Wrobel JS, Garoufalis MG, Defrancis RR, et al. The economic value of specialized lower-extremity medical care by podiatric physicians in the treatment of diabetic foot ulcers. J Am Podiatr Med Assoc. 2011; 101(2): 93-115.

121. Loots MA, Lamme EN, Zeegelaar J, Mekkes JR, Bos JD, Middelkoop E. Differences in cellular infiltrate and extracellular matrix of chronic diabetic and venous ulcers versus acute wounds. J Invest Dermatol. 1998; 111(5): 850-7.

122. Moore K, Ruge F, Harding KG. T lymphocytes and the lack of activated macrophages in wound margin biopsies from chronic leg ulcers. Br J Dermatol. 1997; 137(2): 188-94.

123. Tarnuzzer RW, Schultz GS. Biochemical analysis of acute and chronic wound environments. Wound Repair Regen. 1996; 4(3): 321-5.

124. Wallace HJ, Stacey MC. Levels of tumor necrosis factor-α (TNF-α) and soluble TNF receptors in chronic venous leg ulcers—correlations to healing status. J Invest Dermatol. 1998; 110(3): 292-6.

125. Wysocki AB, Staiano-Coico L, Grinnell F. Wound fluid from chronic leg ulcers contains elevated levels of metalloproteinases MMP-2 and MMP-9. J Invest Dermatol. 1993; 101(1): 64-8.

126. Newby AC. Metalloproteinase expression in monocytes and macrophages and its relationship to atherosclerotic plaque instability. Arterioscler Thromb Vasc Biol. 2008; 28(12): 2108-14.

127. Zhou M, Zhang Y, Ardans JA, Wahl LM. Interferon-γ differentially regulates monocyte matrix metalloproteinase-1 and -9 through tumor necrosis factor-α and caspase 8. J Biol Chem. 2003; 278(46): 45406-13.

128. Blakytny R, Jude E. The molecular biology of chronic wounds and delayed healing in diabetes. Diabet Med. 2006; 23(6): 594-608.

129. Nunan R, Harding KG, Martin P. Clinical challenges of chronic wounds: searching for an optimal animal model to recapitulate their complexity. Dis Model Mech. 2014; 7(11): 1205-13.

130. Mirza R, Koh TJ. Dysregulation of monocyte/macrophage phenotype in wounds of diabetic mice. Cytokine. 2011; 56(2): 256-64.

131. Sindrilaru A, Peters T, Wieschalka S, Baican C, Baican A, Peter H, et al. An unrestrained proinflammatory M1 macrophage population induced by iron impairs wound healing in humans and mice. J Clin Invest. 2011; 121(3): 985-97.

132. Cairo G, Recalcati S, Mantovani A, Locati M. Iron trafficking and metabolism in macrophages: contribution to the polarized phenotype. Trends Immunol. 2011; 32(6): 241-7.

133. Costerton JW, Stewart PS, Greenberg EP. Bacterial biofilms: a common cause of persistent infections. Science. 1999; 284(5418): 1318-22.

134. Mann EE, Wozniak DJ. *Pseudomonas* biofilm matrix composition and niche biology. FEMS Microbiol Rev. 2012; 36(4): 893-916.

135. Lebeaux D, Ghigo JM, Beloin C. Biofilm-related infections: bridging the gap between clinical management and fundamental aspects of recalcitrance toward antibiotics. Microbiol Mol Biol Rev. 2014; 78(3): 510-43.

136. Lewis K. Multidrug tolerance of biofilms and persister cells. Curr Top Microbiol Immunol. 2008; 322: 107-31.

137. Goren I, Müller E, Schiefelbein D, Christen U, Pfeilschifter J, Mühl H, et al. Systematic anti-TNFalpha treatment restores diabetes-impaired skin repair in ob/ob mice by inactivation of macrophages. J Invest Dermatol. 2007; 127(9): 2259-67.

138. Sen CK. Wound healing essentials: let there be oxygen. Wound Repair Regen. 2009; 17(1): 1-18.

139. James GA, Swogger E, Wolcott R, Pulcini Ed, Secor P, Sestrich J, et al. Biofilms in chronic wounds. Wound Repair Regen. 2008; 16(1): 37-44.

140. Davis SC, Ricotti C, Cazzaniga A, Welsh E, Eaglstein WH, Mertz PM. Microscopic and physiologic evidence for biofilm-associated wound colonization *in vivo*. Wound Repair Regen. 2008; 16(1): 23-9.

141. Zhao G, Hochwalt PC, Usui ML, Underwood RA, Singh PK, James GA, et al. Delayed wound healing in diabetic (db/db) mice with *Pseudomonas aeruginosa* biofilm challenge: a model for the study of chronic wounds. Wound Repair Regen. 2010; 18(5): 467-77.

142. Dowd SE, Sun Y, Secor PR, Rhoads DD, Wolcott BM, James GA, et al. Survey of bacterial diversity in chronic wounds using pyrosequencing, DGGE, and full ribosome shotgun sequencing. BMC Microbiol. 2008; 8: 43.

143. Maurice NM, Bedi B, Sadikot RT. *Pseudomonas aeruginosa* biofilms: host response and clinical implication in lung infections. Am J Respir Cell Mol Biol. 2018; 58(4): 428-439.

144. Nixon GM, Armstrong DS, Carzino R, Carlin JB, Olinsky A, Robertson CF, et al. Clinical outcome after early *Pseudomonas aeruginosa* infection in cystic fibrosis. J Pediatr. 2001; 138(5): 699-704.

145. Kirker KR, Secor PR, James GA, Fleckman P, Olerud JE, Stewart PS. Loss of viability and induction of apoptosis in human keratinocytes exposed to *Staphylococcus aureus* biofilms in vitro. Wound Repair Regen. 2009; 17(5): 690-699.

146. Kirker KR, James GA, Fleckman P, Olerud JE, Stewart PS. Differential effects of planktonic and biofilm MRSA on human fibroblasts. Wound Repair Regen. 2012; 20(2): 253-261.

147. Iwańska A, Nowak J, Skorupa W, Augustynowicz-Kopeć E. Analysis of the frequency of isolation and drug resistance of microorganisms isolated from the airways of adult CF patients treated in the Institute of Tuberculosis and Lung Disease during 2008-2011. Pneumonol Alergol Pol. 2013; 81(2): 105-13.

148. Chastre J, Fagon JY. Ventilator-associated pneumonia. Am J Respir Crit Care Med. 2002; 165(7): 867-903.

149. Moser C, Pedersen HT, Lerche CJ, Kolpen M, Line L, Thomsen K, et al. Biofilms and host response – helpful or harmful. APMIS. 2017; 125(4): 320-338.

150. Alhede M, Bjarnsholt T, Givskov M, Alhede M. *Pseudomonas aeruginosa* biofilms: mechanisms of immune evasion. Adv Appl Microbiol. 2014; 86: 1-40.

151. Jensen PØ, Moser C, Kobayashi O, Hougen HP, Kharazmi A, Høiby N. Faster activation of polymorphonuclear neutrophils in resistant mice during early innate response to *Pseudomonas aeruginosa* lung infection. Clin Exp Immunol. 2004; 137(3): 478-85.

152. Bjarnsholt T, Jensen PØ, Fiandaca MJ, Pedersen J, Hansen CR, Andersen CB, et al. *Pseudomonas aeruginosa* biofilms in the respiratory tract of cystic fibrosis patients. Pediatr Pulmonol. 2009; 44(6): 547-58.

153. Jesaitis AJ, Franklin MJ, Berglund D, Sasaki M, Lord CI, Bleazard JB, et al. Compromised host defense on *Pseudomonas aeruginosa* biofilms: characterization of neutrophil and biofilm interactions. J Immunol. 2003; 171(8): 4329-39.

154. Leid JG, Willson CJ, Shirtliff ME, Hassett DJ, Parsek MR, Jeffers AK. The exopolysaccharide alginate protects *Pseudomonas aeruginosa* biofilm bacteria from IFN-γ-mediated macrophage killing. J Immunol. 2005; 175(11): 7512-8.

155. Jensen ET, Kharazmi A, Lam K, Costerton JW, Høiby N. Human polymorphonuclear leukocyte response to *Pseudomonas aeruginosa* grown in biofilms. Infect Immun. 1990; 58(7): 2383-5.

156. Jensen PØ, Bjarnsholt T, Phipps R, Rasmussen TB, Calum H, Christoffersen L, et al. Rapid necrotic killing of polymorphonuclear leukocytes is caused by quorum-sensing-controlled production of rhamnolipid by *Pseudomonas aeruginosa*. Microbiology. 2007; 153(Pt 5): 1329-38.

157. Alhede M, Bjarnsholt T, Jensen PØ, Phipps RK, Moser C, Christophersen L, et al. *Pseudomonas aeruginosa* recognizes and responds aggressively to the presence of polymorphonuclear leukocytes. Microbiology. 2009; 155(Pt 11): 3500-8.

158. Mittal R, Sharma S, Chhibber S, Harjai K. Effect of macrophage secretory products on elaboration of virulence factors by planktonic and biofilm cells of *Pseudomonas aeruginosa*. Comp Immunol Microbiol Infect Dis. 2006; 29(1): 12-26.

159. Fathi F, Brun A, Rott KH, Falco Cobra P, Tonelli M, Eghbalnia HR, et al. NMR-based identification of metabolites in polar and non-polar extracts of avian liver. Metabolites. 2017; 7: 61.

160. Ramm Sander P, Peer M, Grandl M, Bogdahn U, Schmitz G, Robert Kalbitzer H. NMR spectroscopy of macrophages loaded with native, oxidized or enzymatically degraded lipoproteins. PLoS One. 2013; 8: e56360.

161. Rőszer T. Understanding the mysterious M2 macrophage through activation markers and effector mechanisms. Mediators Inflamm. 2015; 2015: 816460.

162. Birungi G, Chen SM, Loy BP, Ng ML, Li SF. Metabolomics approach for investigation of effects of dengue virus infection using the EA.hy926 cell line. J Proteome Res. 2010; 9(12): 6523-34.

163. Ellis JK, Athersuch TJ, Cavill R, Radford R, Slattery C, Jennings P, et al. Metabolic response to low-level toxicant exposure in novel renal tubule epithelial cell system. Mol Biosyst. 2011; 7(1): 247-57.

164. Saric J, Li JV, Wang Y, Keiser J, Veselkov K, Dirnhofer S, et al. Panorganismal metabolic response modeling of an experimental *Echinostoma caproni* infection in the mouse. J Proteome Res. 2009; 8(8): 3899-3911.

165. Wang Y, Utzinger J, Saric J, Li JV, Burckhardt J, Dirnhofer S, et al. Global metabolic responses of mice to *Trypanosoma brucei brucei* infection. Proc Natl Acad Sci USA. 2008; 105(16): 6127-32.

166. León Z, García-Cañaveras JC, Donato MT, Lahoz A. Mammalian cell metabolomics: experimental design and sample preparation. Electrophoresis. 2013; 34: 2762-2775.

167. Diskin C, Pålsson-McDermott EM. Metabolic modulation in macrophage effector function. Front Immunol. 2018; 9: 270.

168. Murray PJ, Wynn TA. Protective and pathogenic functions of macrophage subsets. Nat Rev Immunol. 2011; 11: 723-737.

169. Thomas AC, Mattila JT. "Of mice and men": arginine metabolism in macrophages. Front Immunol. 2014; 5: 479.

CHAPTER TWO

QUANTITATIVE ^{1}H NMR METABOLOMICS REVEALS DISTINCT METABOLIC ADAPTATIONS IN HUMAN MACROPHAGES FOLLOWING DIFFERENTIAL ACTIVATION

Contribution of Authors and Co-Authors

Manuscript in Chapter 2

Author: Amanda L. Fuchs

Contributions: Conceptualized the study, developed methodology, provided software, validated and visualized the data, conducted formal analysis and investigation, curated the data, wrote the original manuscript draft, reviewed and edited the manuscript, supervised and administered the project, and acquired funding.

Author: Sage M. Schiller

Contributions: Validated the data, conducted investigation, and reviewed and edited the manuscript.

Co-Author: Wyatt J. Keegan

Contributions: Validated the data, conducted investigation, and reviewed and edited the manuscript.

Co-Author: Mary Cloud B. Ammons

Contributions: Conceptualized the study, developed methodology, provided resources, administered the project, and acquired funding.

Co-Author: Brian Eilers

Contributions: Developed methodology, provided resources, reviewed and edited the manuscript, and supervised the project.

Contribution of Authors and Co-Authors – Continued

Co-Author: Brian Tripet

Contributions: Developed methodology, provided resources, reviewed and edited the manuscript, and supervised the project.

Co-Author: Valérie Copié

Contributions: Conceptualized the study, developed methodology, provided software and resources, wrote the original manuscript draft, reviewed and edited the manuscript, visualized the data, supervised the project, administered the project, and acquired funding.

Manuscript Information Page

Amanda L. Fuchs, Sage M. Schiller, Wyatt J. Keegan, Mary Cloud B. Ammons, Brian Eilers, Brian Tripet, Valérie Copié

Journal Name: Metabolites

Status of Manuscript:
_____ Prepared for submission to a peer-reviewed journal
_____ Officially submitted to a peer-reviewed journal
_____ Accepted by a peer-reviewed journal
__x__ Published in a peer-reviewed journal

Publisher: Multidisciplinary Digital Publishing Institute (MDPI)
Issue in which manuscript appears: Volume 9, Issue 11, 2019

QUANTITATIVE ^{1}H NMR METABOLOMICS REVEALS DISTINCT METABOLIC ADAPTATIONS IN HUMAN MACROPHAGES FOLLOWING DIFFERENTIAL ACTIVATION

Amanda L. Fuchs[*], Sage M. Schiller, Wyatt J. Keegan, Mary Cloud B. Ammons[†], Brian Eilers, Brian Tripet, Valérie Copié[*]

Department of Chemistry and Biochemistry, Montana State University, Bozeman, Montana, 59717, United States of America
[†]Current Address: Boise Veterans Medical Center, Idaho Veterans Research and Education Foundation, Boise, Idaho, 83702, United States of America

[*]Correspondence: vcopie@montana.edu; Tel.: (406) 994-7244 (V.C.); afuchs03143@gmail.com; Tel.: (406) 946-2073 (A.L.F.)

Abstract

Macrophages (MΦs) are phagocytic immune cells that are found in nearly all human tissues, where they modulate innate and adaptive immune responses, thereby maintaining cellular homeostasis. MΦs display a spectrum of functional phenotypes as a result of microenvironmental and stress-induced stimuli. Evidence has emerged demonstrating that metabolism is not only crucial for the generation of energy and biomolecular precursors, but also contributes to the function and plasticity of MΦs. Here, 1D ^{1}H NMR-based metabolomics was employed to identify metabolic pathways that are differentially modulated following primary human monocyte-derived MΦ activation with pro-inflammatory (M1) or anti-inflammatory (M2a) stimuli relative to resting (M0) MΦs. The metabolic profiling of M1 MΦs indicated a substantial increase in oxidative stress as well as a decrease in mitochondrial respiration. These metabolic profiles also provide

compelling evidence that M1 MΦs divert metabolites from *de novo* glycerophospholipid synthesis to inhibit oxidative phosphorylation. Furthermore, glycolysis and lactic acid fermentation were significantly increased in both M1 and M2a MΦs. These metabolic patterns highlight robust metabolic activation markers of MΦ phenotypes. Overall, our study generates additional support to previous observations, presents novel findings regarding metabolic modulation of human MΦs following activation, and contributes new knowledge to the rapidly evolving field of immunometabolism.

Introduction

The rapidly expanding field of immunometabolism converges on the cross-talk between metabolism and immune cell function, with recent findings bringing this area of research to the forefront of immunology [1,2]. Metabolomics research aims to elucidate cellular and/or systemic perturbations in biochemical pathways by identifying and quantifying changes in small molecule metabolite profiles within complex biological systems [3,4]. Notably, metabolites, such as succinate and itaconate, have been shown to function as signaling molecules and to mediate macrophage (MΦ) cellular phenotypes, in addition to providing metabolic precursors [5,6]. Studies have indicated that pro- and anti-inflammatory MΦs employ markedly different metabolic strategies with regard to central carbon metabolic pathways, including glycolysis, oxidative phosphorylation, and fatty acid metabolism, reinforcing the concept that immunometabolism is critical to immune cell functions [7-9].

Pro-inflammatory, or classically activated, (M1) MΦs play a vital role in host

defense through clearance of bacteria, foreign particles, and cellular debris [10,11]. However, aberrant M1 MΦ function has been implicated in several pathologies, including type 2 diabetes, atherosclerosis, colitis, and Crohn's disease [12-15]. Succinate has been discovered to be an inflammatory regulator and metabolic marker of M1 MΦs, due in part to its concentration-dependent effect on the inhibition of prolyl hydroxylases, the stabilization of hypoxia-inducible factor 1α (HIF-1α), the upregulation of pro-inflammatory cytokines, such as interleukin-1β (IL-1β), and the upregulation of pro-inflammatory gene expression [5,6]. Furthermore, stabilized HIF-1α has been shown to bind HIF-1β, which is a constitutively expressed protein subunit that initiates the expression of additional target genes, including those encoding glycolytic enzymes and glucose transporters [16,17]. An increased flow of intermediates through glycolysis has been reported to be a characteristic metabolic signature of M1 MΦ activation, and previous studies have demonstrated that a decreased flow of metabolites through glycolysis downregulates M1 MΦ effector functions, including phagocytosis, the capacity to generate reactive oxygen species (ROS), and the ability to generate pro-inflammatory cytokines [18-20].

Anti-inflammatory, or alternatively activated, (M2) MΦs clear apoptotic cells, promote and regulate wound healing, and alleviate inflammatory responses [10,21]. Although M2 MΦs are more favorably viewed than their M1 MΦ counterparts due to their anti-inflammatory characteristics, they have been implicated in several pathologies, including tumorigenesis, T_H2-driven allergic inflammation, and idiopathic pulmonary fibrosis [10]. Numerous M2 MΦ subtypes, associated with distinct functional

phenotypes, have also been identified, including M2a, M2b, M2c, and M2d [21]. However, M2a MΦs, activated using interleukin-4 (IL-4) stimuli, are presently the best characterized M2 phenotype [21]. Disparate from M1 MΦs, M2a MΦ activation leads to a metabolic switch from glycolysis to oxidative phosphorylation and fatty acid beta oxidation for adenosine triphosphate (ATP) production and energetic homeostasis [1,7]. Using ^{14}C-labeled glucose and oleic acid stimulation, Vats *et al.* demonstrated that M2 MΦs lower their glucose consumption, and increase fatty acid uptake and beta oxidation to fuel mitochondrial oxidative phosphorylation, in addition to enhancing the expression of fatty acid oxidation genes, relative to M1 MΦs [7]. Moreover, Huang *et al.* determined that lysosomal acid lipase (LAL)-mediated lipolysis is crucial for the generation of M2 MΦ activation hallmarks, including the promotion of oxidative phosphorylation and increased respiratory capacity [22].

While previous studies have identified significant metabolic differences between M1 and M2 MΦs, the overwhelming majority of these studies have been conducted using bone marrow-derived murine MΦs and immortalized murine and human cell lines [17], which limit their relevance to human health. Several inquiries have indeed highlighted notable distinctions between human and murine MΦs, including significant differences in cell surface markers, nitric oxide (NO) production, NO synthase transcript expression, arginine metabolism, and transcriptomic and proteomic profiles [10,23-25]. In particular, metabolic enzymes involved in arginine metabolism, such as arginase 1 (Arg1) and inducible NO synthase (iNOS), are expressed in murine MΦs; however, comparable expression has not been observed in *in vitro* cultures of M1 or M2a human MΦs [10,24].

In addition, although primary human cells present more physiologically accurate phenotypic and metabolic characteristics relevant to *in vivo* cellular environments, the usage of such cell cultures in metabolomics studies is currently limited [26]. To further understand and appreciate the potential biochemical discrepancies and functional differences between murine and human MΦ responses, additional research is needed to clearly establish the extent of human MΦ phenotypic heterogeneity, with a particular emphasis on primary human MΦs.

In this study, we sought to elucidate the metabolic consequences of pro-inflammatory and anti-inflammatory stimuli on primary human monocyte-derived MΦs, using $CD14^+$ magnetic-activated cell sorting (MACS) technology, *in vitro* MΦ differentiation and activation schemes, 1D ^{1}H NMR metabolomics, metabolite profiling using Chenomx NMR Suite software, and multivariate statistical analysis. To generate M1 and M2a MΦs, naïve cells were stimulated with MΦ colony-stimulating factor (M-CSF) and a combination of lipopolysaccharide (LPS) and interferon-γ (IFN-γ) or IL-4, respectively, for 72 hrs, whereas resting M0 MΦs were generated using M-CSF with no additional stimuli. Subsequently, intra- and extracellular metabolites were extracted, followed by 1D ^{1}H NMR acquisition and spectral profiling of resulting metabolite mixtures. Results from this study highlight major metabolic pathways that are differentially modulated in activated human MΦs, including glycolysis, lactic acid fermentation, the tricarboxylic acid (TCA) cycle, glutathione metabolism, oxidative stress, and *de novo* glycerophospholipid synthesis within the Kennedy pathway. The functional significance of the observed metabotypes (i.e., resulting metabolite profiles)

found to be associated with M1 and M2a MΦ cellular phenotypes is also discussed.

Results

Quantitative Metabolic Profiles Differentiate Between MΦ Activation States

To identify characteristic metabolic patterns associated with MΦ activation phenotypes, metabolite profiles of M0, M1, and M2a MΦs cultured *in vitro* were characterized using an untargeted ^{1}H NMR metabolomics approach. One-dimensional (1D) ^{1}H NMR spectra of intra- and extracellular MΦ metabolite extracts (Figure S1) were recorded on Montana State University (MSU)'s 600 MHz (^{1}H Larmor frequency) solution NMR spectrometer. This approach facilitated the deconvolution of complex NMR spectral patterns [27] and the identification and quantitation of 51 metabolites in these cell cultures.

Two-dimensional principal component analysis (2D-PCA) scores plots of intra- and extracellular metabolite profiles (Figure 1A, B, respectively; see Figure S2 for corresponding PCA loadings plots; see File S1 and File S2 for corresponding PCA loadings) demonstrated that M0, M1, and M2a MΦs are metabolically distinct from one another, with the most striking separation observed between M0 and M1 MΦs along the principal component 1 (PC1) dimension of the 2D-PCA scores plot (Figure 1A) of the intracellular metabolite profiles. The intra- and extracellular metabolite datasets were subjected to hierarchical clustering analysis (HCA) and heatmap generation to visually assess which metabolites contributed most significantly to the discrimination between MΦ activation states (Figure 1C, D, respectively). The intracellular metabolite profiles of

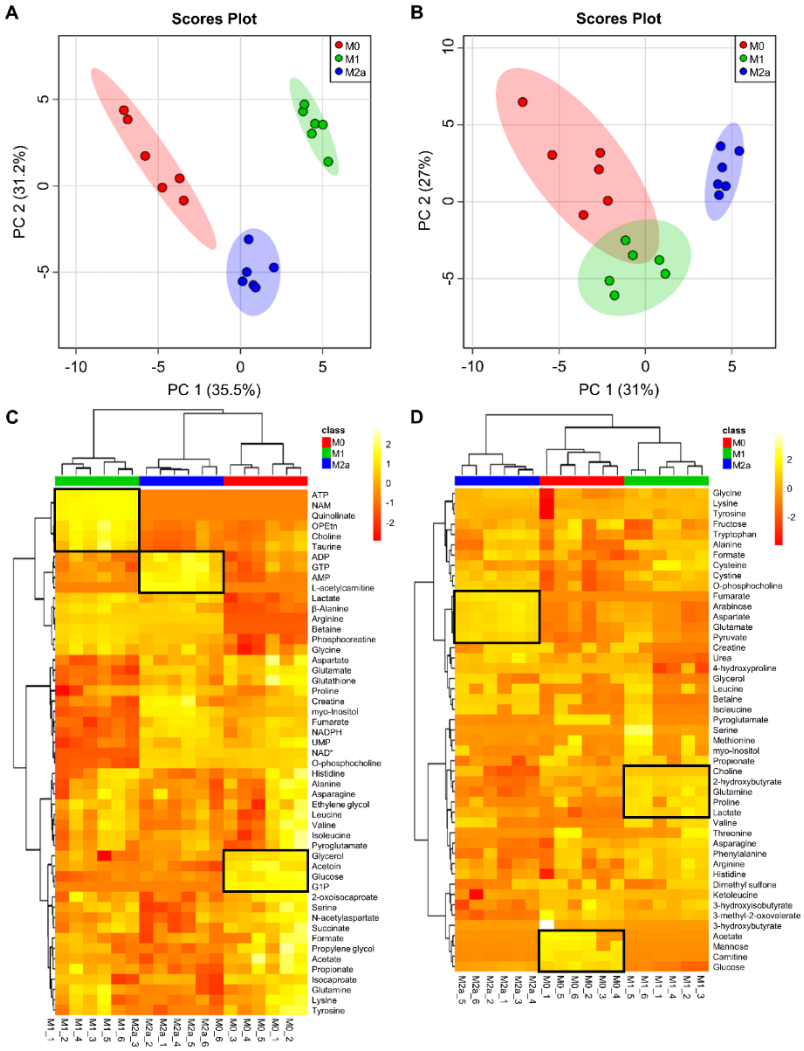

Figure 1. Multivariate statistical analysis reveals metabolic differences between MΦ activation states. Two-dimensional principal component analysis (2D-PCA) scores plots generated by analysis of metabolic profiles from intra- (A) and extracellular (B) MΦ metabolite extracts (M0, red; M1, green; M2a, blue), with shaded regions illustrating respective 95% confidence intervals. Hierarchical clustering analysis (HCA) and heatmap visualization of metabolic profiles from intra- (C) and extracellular (D) MΦ metabolite extracts was performed using a Euclidean distance calculated from metabolite abundance and a Ward clustering algorithm. The upmost column bar is colored according to MΦ activation state (M0, red; M1, green; M2a, blue), and the color scale represents the scaled abundance of each metabolite, with yellow indicating high abundance and red indicating low abundance. Particular sets of discriminatory metabolites are highlighted in boxed regions on the heatmaps. Abbreviations denote: ADP, adenosine diphosphate; AMP, adenosine monophosphate; ATP, adenosine triphosphate; G1P, glucose-1-phosphate; GTP, guanosine triphosphate; NAD^+, nicotinamide adenine dinucleotide; NADPH, reduced nicotinamide adenine dinucleotide phosphate; NAM, niacinamide; OPEtn, o-phosphoethanolamine; UMP, uridine monophosphate.

each MΦ activation state presented a unique metabolic signature that was not observed in the other activation states. These included increased concentrations of metabolites such as ATP, niacinamide, quinolinate, phosphoethanolamine, choline, and taurine in M1 MΦs, adenosine diphosphate (ADP), guanosine triphosphate (GTP), adenosine monophosphate (AMP), and L-acetylcarnitine in M2a MΦs, and glycerol, acetoin, glucose, and glucose-1-phosphate in M0 MΦs as indicated in Figure 1C. MΦ activation states were also distinguishable based upon their extracellular metabolite profiles, with increased concentrations of metabolites such as choline, 2-hydroxybutyrate, glutamine, proline, and lactate in the extracellular milieu of M1 MΦs, fumarate, arabinose, aspartate, glutamate, and pyruvate in M2a MΦs, and acetate, mannose, carnitine, and glucose in M0 MΦs as indicated in Figure 1D.

Glycolytic Activity and Lactic Acid Fermentation are Universal Markers of Activation

The metabolic profiling of intra- and extracellular MΦ metabolite extracts revealed that M1 and M2a MΦ activation states induced significant metabolic changes, especially with regard to glycolytic and lactic acid fermentation pathways (Figure 2A), when compared to the metabolite profiles of M0 MΦs. M1 and M2a MΦs exhibited intracellular glucose levels that were -9.85 and -6.68-fold lower, respectively, and intracellular lactate levels that were 1.79 and 1.66-fold higher, respectively, relative to those found in M0 MΦs (Figure 2B and Table 1). These patterns were also reflected in the extracellular metabolite profiles, where M0, M1, and M2a MΦs displayed an average deficit of -21.04, -42.21, and -30.55 μmol glucose/mg protein, and an average surplus of

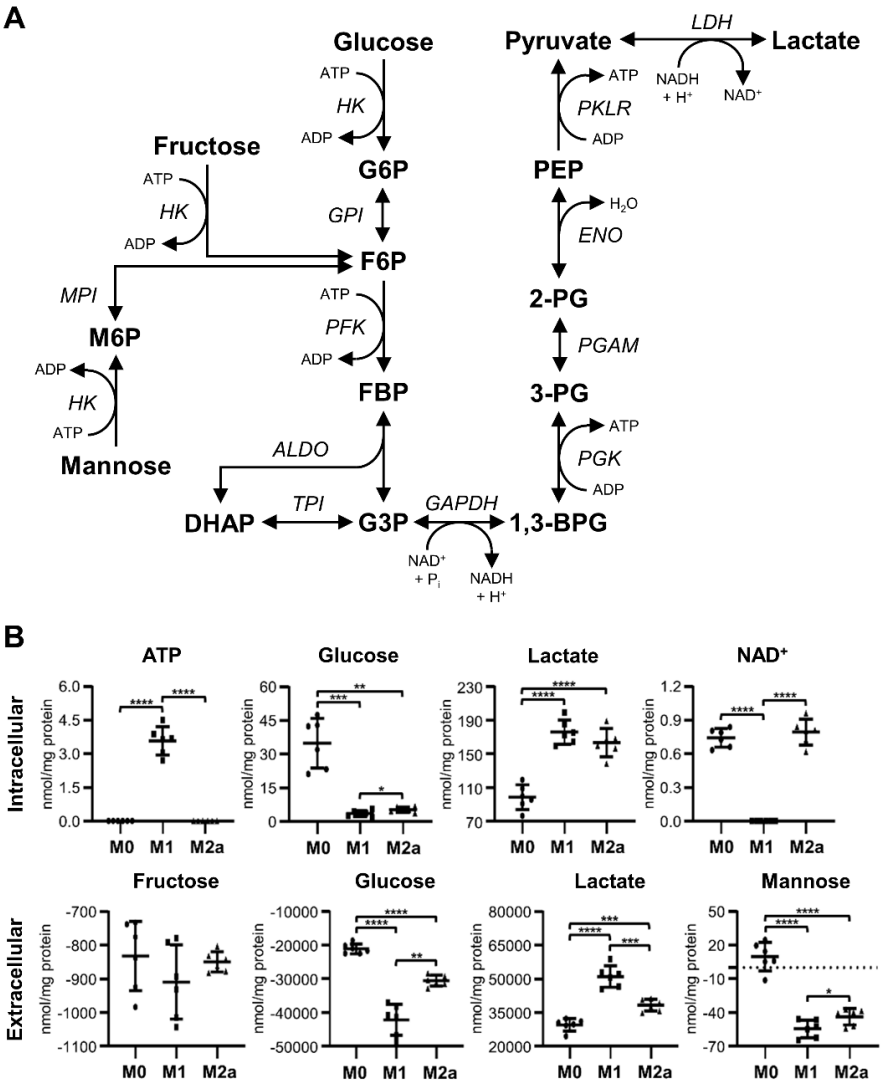

Figure 2. Increased glycolytic activity and lactate production are universal markers of MΦ activation. Schematic diagram of glycolysis and lactic acid fermentation pathways (A), and quantitative levels of corresponding metabolites (B) detected in intra- and extracellular MΦ metabolite extracts (mean ± SD). Unpaired parametric *t*-tests with Welch's correction (two-tailed; **p* < 0.05; ***p* < 0.01; ****p* < 0.001; *****p* < 0.0001). Abbreviations denote: 2-PG, 2-phosphoglycerate; 3-PG, 3-phosphoglycerate; ADP, adenosine diphosphate; *ALDO*, aldolase; ATP, adenosine triphosphate; BPG, bisphosphoglycerate; DHAP, dihydroxyacetone phosphate; *ENO*, enolase; F6P, fructose 6-phosphate; FBP, fructose bisphosphate; G3P, glyceraldehyde 3-phosphate; G6P, glucose 6-phosphate; *GAPDH*, glyceraldehyde-3-phosphate dehydrogenase; *GPI*, glucose-6-phosphate isomerase; *HK*, hexokinase; *LDH*, lactate dehydrogenase; M6P, mannose 6-phosphate; NAD^+, nicotinamide adenine dinucleotide; NADH, reduced nicotinamide adenine dinucleotide; PEP, phosphoenolpyruvate; *PFK*, phosphofructokinase; *PGAM*, phosphoglycerate mutase; *PGK*, phosphoglycerate kinase; *PKLR*, pyruvate kinase L/R; *TPI*, triosephosphate isomerase.

Table 1. Discriminatory metabolites in intracellular extracts associated with activation.

Metabolite	M1 MΦs		M2a MΦs	
	FC	*p*-value	FC	*p*-value
2-oxoisocaproate	-1.28	NS	-1.88	**
Acetate	-1.66	*	-2.11	**
ADP	1.05	NS	1.42	***
AMP	1.33	**	2.43	****
Arginine	7.54	****	7.44	****
Aspartate	-1.60	**	-1.21	NS
ATP	9.14	****	ND	N/A
β-alanine	3.01	****	2.53	***
Betaine	6.38	****	2.95	****
Choline	1.63	***	-1.18	NS
Creatine	-1.24	**	1.18	NS
Creatine phosphate	2.81	****	2.13	***
Fumarate	-1.68	***	1.11	NS
Glucose	-9.85	***	-6.68	**
Glucose-1-phosphate	-5.10	****	-5.10	****
Glutamate	-2.67	***	-1.22	NS
Glutamine	1.02	NS	-1.33	*
Glutathione	-1.81	**	-1.34	*
Glycerol	-3.10	***	-2.53	***
Glycine	1.27	**	1.21	*
GTP	-1.01	NS	1.48	***
Lactate	1.79	****	1.66	****
Lysine	-1.11	NS	-1.25	*
myo-Inositol	-2.43	****	1.88	***
NAD^+	-3.79	****	1.07	NS
NADPH	-2.40	**	1.34	*
Niacinamide	5.19	****	ND	N/A
O-phosphocholine	-9.23	****	1.03	NS
O-phosphoethanolamine	2.00	***	-1.02	NS
Propionate	-1.13	NS	-1.57	*
Quinolinate	25.90	****	ND	N/A
Serine	-1.12	NS	-1.67	*
Succinate	-1.23	NS	-1.82	**
Taurine	1.23	*	-1.18	*
Tyrosine	-1.20	NS	-1.50	*
UMP	-1.67	***	-1.04	NS

Metabolites were selected based upon fold change (FC) of intracellular metabolite concentrations, and statistical significance between activated MΦ subsets (M1 and M2a MΦs; nmol/mg protein; calculated from metabolite spectral fitting using the Chenomx NMR Suite software and the standard Chenomx 600-MHz metabolite library; ND, not detected) relative to M0 MΦs. Fold changes were calculated relative to M0 MΦs, whereby increases are shown as positive values and decreases are shown as negative values. Statistical significance (*p*) was measured using two-tailed unpaired parametric *t*-tests with Welch's correction, whereby *, $p < 0.05$; **, $p < 0.01$; ***, $p < 0.001$; ****, $p < 0.0001$. Abbreviations denote: NS, not statistically significant; N/A, not applicable; ADP, adenosine diphosphate; AMP, adenosine monophosphate; ATP, adenosine triphosphate; GTP, guanosine triphosphate; NAD^+, nicotinamide adenine dinucleotide; NADPH, reduced nicotinamide adenine dinucleotide phosphate; UMP, uridine monophosphate. Fold change (FC) values for arginine, ATP, betaine, glucose-1 phosphate, NAD^+, niacinamide, and quinolinate in M1 MΦs and arginine, betaine, and glucose-1 phosphate in M2a MΦs were calculated using limit of detection (LOD) values (see Table S1) determined from M0 MΦ intracellular metabolite extract 1D ^{1}H NMR spectra.

29.47, 51.05, and 38.15 µmol lactate/mg protein, respectively (Figure 2B and Table 2), relative to sham extracellular metabolite extract controls. Distinct metabolic characteristics of M1 MΦs included a significant, 9.14-fold, increase in intracellular ATP levels, and a significant -3.79-fold decrease in intracellular nicotinamide adenine dinucleotide (NAD^+) levels (Figure 2B and Table 1), relative to M0 MΦs. No significant changes were observed with respect to extracellular fructose concentrations. However, extracellular mannose concentrations were found to be significantly decreased in M1 and M2a MΦs, with M0, M1, and M2a MΦs exhibiting average concentrations of 9.84, -54.62, and -43.79 nmol mannose/mg protein, respectively (Figure 2B and Table 2), relative to sham extracellular extract controls.

Significant differences in metabolite profile patterns were also established for M1 relative to M2a MΦs. These included a 9.14-fold increase in intracellular ATP, and -1.47 and -4.06-fold decreases in intracellular glucose and NAD^+ levels, respectively (Figure 2B and Table S2). In addition, the extracellular metabolite profiles of M1 MΦs exhibited significant increases in lactate and decreases in glucose and mannose, relative to the extracellular metabolite profiles of M2a MΦs (Figure 2B and Table 2). These results support the notion that elevated glycolytic and lactic acid fermentation activities are robust markers of MΦ activation, with M1 MΦs displaying significantly greater metabolic activity with respect to these specific pathways compared to M2a MΦs.

M1 and M2a MΦs Exhibit Distinct Anaplerotic Trends Corresponding to the TCA Cycle

M1 and M2a MΦs presented significantly different metabolic trends with respect

Table 2. Discriminatory metabolites in extracellular extracts associated with activation.

Metabolite	Concentration (mean ± SD)			*p*-value		
	M0 MΦs	M1 MΦs	M2a MΦs	M1	M2a	M1 vs. M2a
2-hydroxybutyrate	48.65 ± 13.52	132.89 ± 17.24	23.43 ± 7.29	****	**	****
2-oxoisocaproate	60.64 ± 10.85	26.96 ± 5.31	2.81 ± 2.92	***	****	****
3-hydroxybutyrate	-20.75 ± 13.78	-116.64 ± 8.81	-96.50 ± 3.85	****	****	**
3-hydroisobutyrate	18.01 ± 3.36	16.87 ± 2.38	12.49 ± 2.03	NS	**	**
3-methyl-2-oxovalerate	108.34 ± 49.08	61.13 ± 9.68	21.34 ± 3.60	NS	**	****
Acetate	39.73 ± 73.93	-150.67 ± 13.89	-213.14 ± 27.60	**	***	**
Alanine	-60.54 ± 73.40	98.11 ± 67.21	20.73 ± 35.65	**	*	*
Arabinose	-107.36 ± 12.28	-109.08 ± 12.55	-75.83 ± 4.50	NS	***	***
Arginine	852.67 ± 399.21	1349.61 ± 290.20	788.70 ± 198.71	*	NS	**
Aspartate	-791.19 ± 90.54	-797.31 ± 93.74	-573.21 ± 22.03	NS	**	**
Carnitine	37.60 ± 39.79	-10.46 ± 1.09	-9.89 ± 0.39	*	*	NS
Choline	13.83 ± 12.57	52.20 ± 9.38	6.41 ± 14.85	***	NS	***
Creatine	1.50 ± 4.85	-5.73 ± 5.69	3.80 ± 3.65	*	NS	**
Cysteine	-147.54 ± 22.37	-103.71 ± 24.21	-125.00 ± 11.15	**	NS	NS
Cystine	183.44 ± 50.04	419.86 ± 62.88	468.59 ± 62.40	****	****	NS
Formate	140.60 ± 46.15	195.50 ± 61.22	228.89 ± 66.43	NS	*	NS
Fumarate	ND	ND	9.51 ± 1.67	N/A	****	****
Glucose	-21044.40 ± 1478.98	-42208.15 ± 4621.45	-30552.65 ± 1595.13	****	****	**
Glutamate	-674.75 ± 78.82	-595.54 ± 116.43	-363.96 ± 18.48	NS	***	**
Glutamine	1235.12 ± 211.97	1976.33 ± 320.59	731.62 ± 127.38	**	***	****
Glycine	179.01 ± 122.04	404.88 ± 106.51	501.91 ± 115.32	**	***	NS
Histidine	41.76 ± 24.39	98.44 ± 23.25	56.36 ± 17.82	**	NS	**
Isoleucine	-78.84 ± 63.44	-13.97 ± 166.32	60.25 ± 54.71	NS	**	NS
Lactate	29467.61 ± 2714.66	51046.16 ± 4806.45	38150.09 ± 2610.21	****	***	***
Leucine	-141.51 ± 88.78	28.65 ± 126.92	19.93 ± 35.22	*	**	NS
Lysine	25.26 ± 51.14	325.04 ± 43.60	209.60 ± 20.31	****	***	***
Mannose	9.84 ± 12.78	-54.62 ± 7.85	-43.79 ± 7.40	****	****	*
O-phosphocholine	-81.15 ± 20.78	-50.46 ± 7.86	-42.20 ± 2.26	*	**	*
Phenylalanine	2.21 ± 11.13	26.02 ± 18.03	-9.66 ± 9.85	*	NS	**
Proline	-51.72 ± 53.94	60.38 ± 54.56	-27.75 ± 21.10	**	NS	**
Pyroglutamate	121.33 ± 345.73	-564.30 ± 551.92	-386.27 ± 161.22	*	*	NS
Pyruvate	-642.79 ± 67.35	-489.93 ± 121.02	-336.50 ± 17.62	*	****	*
Serine	-179.15 ± 49.58	-45.09 ± 75.77	-284.36 ± 89.47	**	*	***
Urea	-1521.10 ± 205.87	-2142.83 ± 454.07	-1152.24 ± 159.89	*	**	**
Valine	-25.75 ± 27.43	89.95 ± 97.95	10.00 ± 50.05	*	NS	NS

Metabolites were selected based upon the statistical significance of extracellular metabolite concentrations between activated MΦ subsets (M1 and M2a MΦs; nmol/mg protein; calculated from metabolite spectral fitting using the Chenomx NMR Suite software and the standard Chenomx 600 MHz metabolite library; ND, not detected) relative to M0 MΦs. Metabolite concentrations were normalized to sham media controls, whereby increases are shown as positive values and decreases are shown as negative values. Statistical significance (*p*) was measured using two-tailed unpaired parametric *t*-tests with Welch's correction, whereby *, $p < 0.05$; **, $p < 0.01$; ***, $p < 0.001$; ****, $p < 0.0001$; NS, not statistically significant; N/A, not applicable. Limit of detection (LOD) values for fumarate in M0 and M1 MΦ extracellular metabolite extract 1D ^{1}H NMR spectra have been provided for reference (see Table S1).

to TCA cycle intermediates and substrates (Figure 3A), relative to M0 MΦs. Initial analyses focused on metabolites that can enter the TCA cycle at the acetyl-coenzyme A (acetyl-CoA) entry point, including acetate, alanine, 3-hydroxybutyrate, and pyruvate (Figure 3A). Intracellular acetate was significantly decreased in M1 and M2a MΦs, -1.66 and -2.11-fold, respectively, relative to M0 MΦs (Figure 3B and Table 1). This trend was also reflected in the extracellular metabolite profiles, where the spent medium of M0,

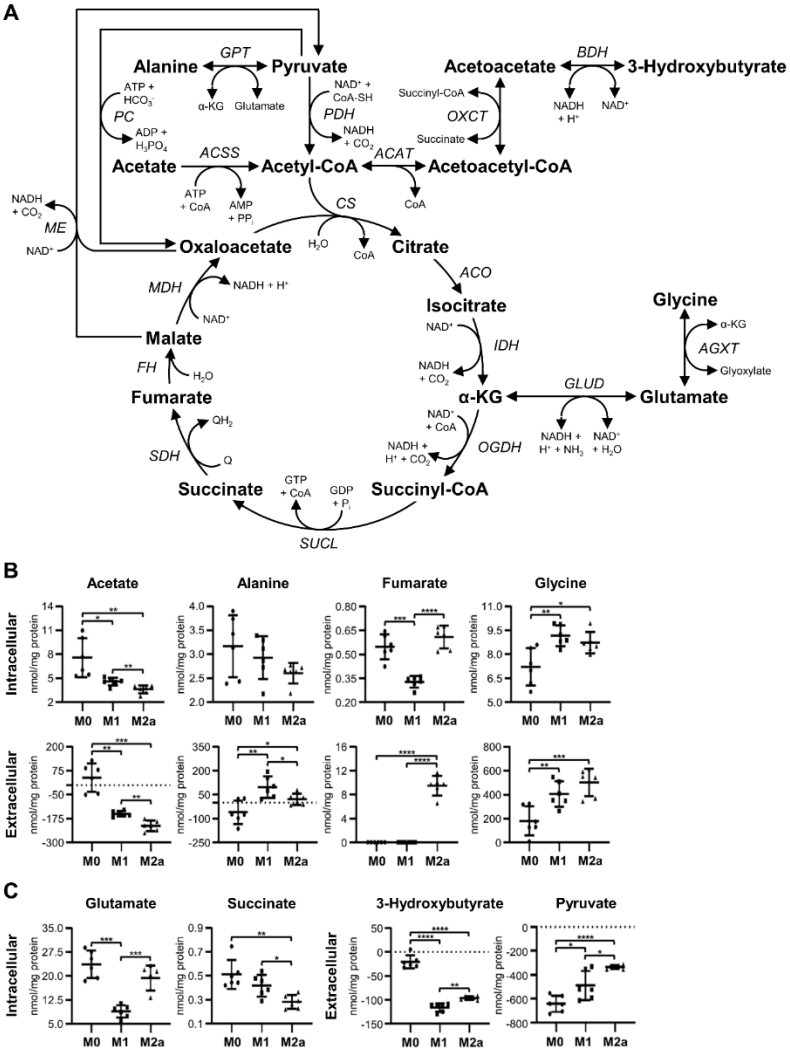

Figure 3. M1 and M2a MΦs exhibit contrasting substrate utilization strategies regarding the tricarboxylic acid (TCA) cycle. Schematic diagram of metabolite flow through the TCA cycle (A), and quantitative levels of corresponding metabolites (B,C) detected in intra- and extracellular MΦ metabolite extracts (mean ± SD). Unpaired parametric *t*-tests with Welch's correction (two-tailed; **p* < 0.05; ***p* < 0.01; ****p* < 0.001; *****p* < 0.0001). Abbreviations denote: *ACAT*, acetyl-CoA acetyltransferase; *ACO*, aconitase; *ACSS*, acetyl-CoA synthetase; *AGXT*, alanine-glyoxylate transaminase; AMP, adenosine monophosphate; ATP, adenosine triphosphate; *BDH*, 3-hydroxybutyrate dehydrogenase; CoA, coenzyme A; *CS*, citrate synthase; *FH*, fumarate hydratase; GABA, γ-aminobutyrate; GDP, guanosine diphosphate; *GLUD*, glutamate dehydrogenase; *GPT*, glutamate pyruvate transaminase; GTP, guanosine triphosphate; *IDH*, isocitrate dehydrogenase; *MDH*, malate dehydrogenase; *ME*, malic enzyme; NAD^+, nicotinamide adenine dinucleotide; NADH, reduced nicotinamide adenine dinucleotide; *OGDH*, oxoglutarate dehydrogenase; *OXCT*, 3-oxoacid CoA-transferase; *PC*, pyruvate carboxylase; *PDH*, pyruvate dehydrogenase; Q, quinone; QH_2, quinol; *SDH*, succinate dehydrogenase; *SUCL*, succinate-CoA ligase; α-KG, α-ketoglutarate.

M1, and M2a MΦs contained average concentrations of 39.73, -150.67, and -213.14 nmol acetate/mg protein, respectively (Figure 3B and Table 2), relative to sham extracellular extract controls. In addition, M1 MΦs displayed a 1.27-fold increase in intracellular acetate and significantly elevated concentrations of extracellular acetate relative to M2a MΦs (Figure 3B, Table 2, and Table S2). No significant changes were observed with respect to intracellular alanine levels. However, extracellular alanine levels were significantly increased in M1 and M2a MΦs compared to M0 MΦs, with spent culture medium of M0, M1, and M2a MΦs possessing average concentrations of -60.54, 98.11, and 20.73 nmol alanine/mg protein, respectively (Figure 3B and Table 2), relative to sham extracellular extract controls. Furthermore, M1 MΦs secreted a significantly greater amount of alanine into the media relative to M2a MΦs (Figure 3B and Table 2). Extracellular 3-hydroxybutyrate levels were significantly decreased in M1 and M2a MΦs relative to M0 MΦs, with M0, M1, and M2a MΦs exhibiting average deficits of -20.75, -116.64, and -96.50 nmol 3-hydroxybutyrate/mg protein, respectively (Figure 3C and Table 2), relative to sham extracellular extract controls. M1 and M2a MΦs also had significantly increased levels of extracellular pyruvate relative to M0 MΦs, with M0, M1, and M2a MΦs displaying average deficits of -642.79, -489.93, and -336.50 nmol pyruvate/mg protein, respectively (Figure 3C and Table 2), relative to sham extracellular extract controls. However, M1 MΦs consumed significantly greater amounts of 3-hydroxybutyrate and pyruvate from the media compared to M2a MΦs (Figure 3B and Table 2). Altogether, these results suggest that M1 and M2a MΦs preferentially utilize acetate and 3-hydroxybutyrate as their extracellular carbon sources, compared to utilizing

pyruvate, relative to M0 MΦs. Moreover, M1 MΦs utilize 3-hydroxybutyrate to a significantly greater extent than M2a MΦs, and secrete greater amounts of alanine into the cell culture medium than M0 and M2a MΦs, potentially due to preferred conversion of pyruvate to alanine.

These data are consistent with published reports on the differential O_2 consumption of MΦ subtypes. For example, O_2 consumption has been shown to decrease in M1-activated MΦs [5,6], which is consistent with our MΦ metabolic profiling data that suggest that our M1 MΦs are consuming 3-hydroxybutyrate from the extracellular cell culture media without the need to invoke the *de novo* synthesis of 3-hydroxybutyrate from ketogenic pathways.

Subsequent analyses were performed on metabolites that serve as TCA cycle intermediates and which can participate in anaplerotic reactions to replenish critical intermediates of the TCA cycle. Such metabolites included fumarate, glycine, glutamate, and succinate (Figure 3A). M1 MΦs demonstrated significantly decreased levels of intracellular fumarate, -1.68 and -1.86-fold, relative to M0 and M2a MΦs, respectively (Figure 3B, Table 1, and Table S2), whereas extracellular fumarate was only detected in M2a MΦs, at a level of 9.51 nmol fumarate/mg protein (Figure 3B and Table 2). M1 and M2a MΦ metabolite profiles revealed significantly increased levels of intracellular glycine, 1.27 and 1.21-fold, relative to M0 MΦs, respectively (Figure 3B and Table 1). This trend is also distinct from the one observed for extracellular glycine levels, whereby M0, M1, and M2a MΦ cultures contained average concentrations of 179.01, 404.88, and 501.91 nmol glycine/mg protein in their spent media, respectively (Figure 3B and Table

2), relative to sham extracellular extract controls. Intracellular levels of glutamate were significantly decreased in M1 MΦs, amounting to -2.67 and -2.19-fold decreases, relative to M0 and M2a MΦs, respectively (Figure 3C, Table 1, and Table S2). In addition, M2a MΦs displayed -1.82 and -1.48-fold decreased levels of intracellular succinate relative to M0 and M1 MΦs, respectively (Figure 3C, Table 1, and Table S2). These findings support the notion that M1 MΦ activation leads to impaired conversion of succinate to fumarate and to an increased requirement for metabolic reactions associated with the generation of α-ketoglutarate (α-KG), such as those catalyzed by glutamate dehydrogenase (GLUD), glutamate-pyruvate transaminase (GPT), or alanine--glyoxylate transaminase (AGXT; Figure 3A) enzymes.

Activated MΦs Undergo Significant Oxidative Stress

MΦ activation resulted in intracellular metabolic adaptations associated with glutathione metabolism and pathways involved in mitigating oxidative stress (Figure 4A), which were significantly different from the metabolic pathways used preferentially by M0 MΦs. The intracellular metabolite profiles of M1 and M2a MΦs featured significantly decreased levels of reduced glutathione (GSH), -1.81 and -1.34-fold, respectively, relative to M0 MΦs (Figure 4B and Table 1). In addition, M1 MΦs contained significantly less intracellular GSH, -1.34-fold, compared to M2a MΦs (Figure 4B and Table S2). Reduced nicotinamide adenine dinucleotide phosphate (NADPH) was depleted in M1 MΦs relative to M0 and M2a MΦs, amounting to -2.40 and -3.20-fold decreases, respectively (Figure 4B, Table 1, and Table S2). On the other hand, M2a MΦs

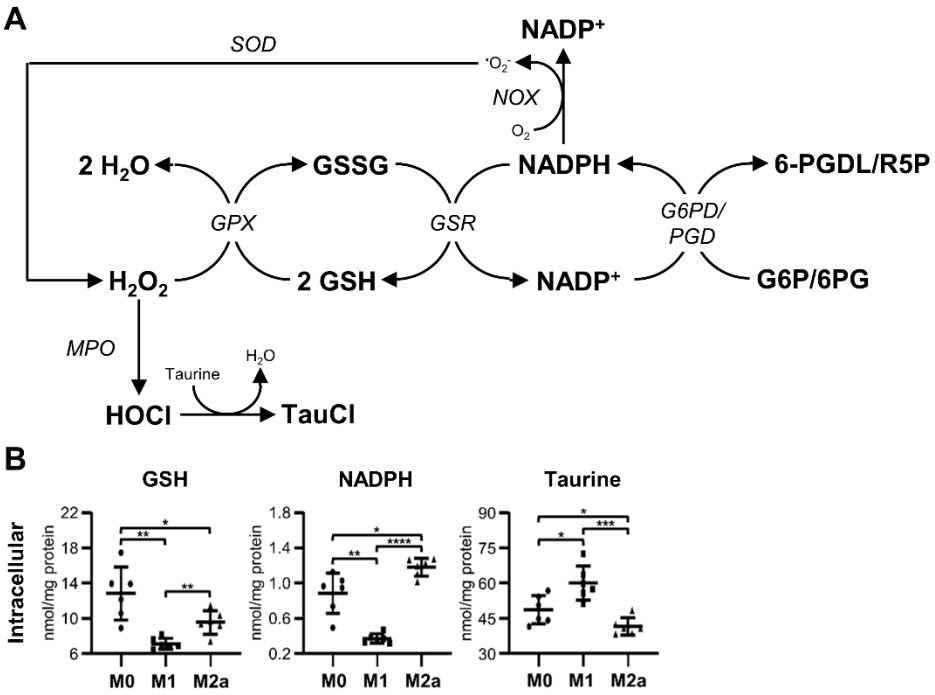

Figure 4. Activation induces significant oxidative stress in MΦs. Schematic diagram of glutathione metabolism and oxidative stress pathways (A), and quantitative levels of corresponding metabolites (B) detected in intracellular MΦ metabolite extracts (mean ± SD). Unpaired parametric *t*-tests with Welch's correction (two-tailed; **p* < 0.05; ***p* < 0.01; ****p* < 0.001; *****p* < 0.0001). Abbreviations denote: GSH, reduced glutathione; GSSG, oxidized glutathione; $NADP^+$, nicotinamide adenine dinucleotide phosphate; NADPH, reduced nicotinamide adenine dinucleotide phosphate; G6P, glucose 6-phosphate; *G6PD*, glucose-6-phosphate dehydrogenase; *GPX*, glutathione peroxidase; *GSR*, glutathione-disulfide reductase; *MPO*, myeloperoxidase; *NOX*, NADPH oxidase; 6PG, 6-phosphogluconate; *PGD*, phosphogluconate dehydrogenase; 6-PGDL, 6-phosphoglucono-1,5-lactone; R5P, ribulose 5-phosphate; *SOD*, superoxide dismutase; TauCl, taurine chloramine.

contained significantly more NADPH, 1.34-fold, compared to M0 MΦs (Figure 4B and Table 1). M1 MΦs also contained significantly increased levels of intracellular taurine relative to M0 and M2a MΦs, amounting to 1.23 and 1.45-fold increases, respectively (Figure 4B, Table 1, and Table S2), while M2a MΦs had significantly less intracellular taurine, -1.18-fold decrease, compared to M0 MΦs (Figure 4B and Table 1). Collectively, these results demonstrate that MΦ activation induces oxidative stress in both M1 and

M2a MΦs. Furthermore, M1 MΦs appear to consume NADPH to a greater extent than M0 or M2a MΦs, possibly to generate substantial levels of reactive oxygen species (ROS) as part of the M1 MΦ immune phenotype. Increased levels of taurine in M1 MΦs may also be used to compensate for or neutralize excessive or harmful ROS production.

M1 MΦs Manipulate the Kennedy Pathway

Unexpectedly, M1 MΦs exhibited distinct metabolic changes associated with the choline and ethanolamine branches of the Kennedy pathway (Figure 5A), when compared to M0 and M2a MΦs. The profiling of MΦ intracellular metabolite extracts revealed a significant accumulation of choline and phosphoethanolamine in M1 MΦs (Figure 5B), where choline levels were increased 1.63 and 1.91-fold, and phosphoethanolamine levels were increased 2.00 and 2.03-fold relative to M0 and M2a MΦs, respectively (Table 1 and Table S2). Furthermore, intracellular phosphocholine levels were significantly decreased, -9.23 and -9.51-fold, in M1 MΦs relative to M0 and M2a MΦs, respectively (Figure 5B, Table 1, and Table S2). The profiling of MΦ extracellular metabolite extracts revealed similar trends with respect to choline levels (Figure 5B), with M0, M1, and M2a MΦ spent media containing an average surplus of 13.83, 52.20, and 6.41 nmol choline/mg protein, respectively (Table 2), relative to sham extracellular metabolite extract controls. Conversely, extracellular phosphocholine levels were significantly higher in M1 and M2a MΦs relative to M0 MΦs, and M2a MΦs had significantly higher levels of extracellular phosphocholine compared to M1 MΦs (Figure 5B); this amounted to average deficits of -81.15, -50.46, and -42.20 nmol phosphocholine/mg protein in the spent media of M0, M1, and M2a MΦs, respectively (Table 2), compared to sham

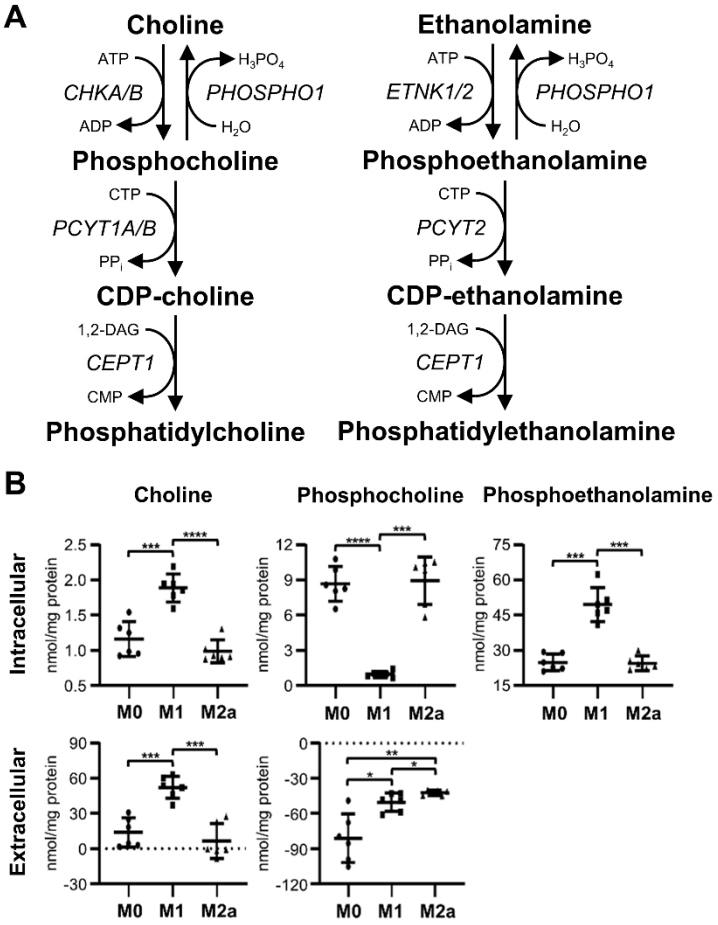

Figure 5. M1 MΦs have a distinct metabolic signature characterized by alterations of metabolite flow within the Kennedy pathway. Schematic diagram of metabolite flow through the Kennedy pathway (A), and quantitative levels of corresponding metabolites (B) detected in intra- and extracellular MΦ metabolite extracts (mean ± SD). Unpaired parametric *t*-tests with Welch's correction (two-tailed; **p* < 0.05; ***p* < 0.01; ****p* < 0.001; *****p* < 0.0001). Abbreviations denote: ADP, adenosine diphosphate; ATP, adenosine triphosphate; CDP, cytidine diphosphate; *CEPT1*, choline/ethanolamine phosphotransferase 1; *CHKA/B*, choline kinase α/β; CMP, cytidine monophosphate; CTP, cytidine triphosphate; DAG, diacylglycerol; *ETNK1/2*, ethanolamine kinase 1/2; *PHOSPHO1*, phosphoethanolamine/phosphocholine phosphatase; *PCYT1A/B*, phosphate cytidylyltransferase 1α/β; *PCYT2*, phosphate cytidylyltransferase 2.

extracellular metabolite extract controls. These data suggest that M1 MΦs repurpose the Kennedy pathway by diverting phosphocholine to choline, secreting excess choline into the media, and allowing for the accumulation of intracellular phosphoethanolamine.

Discussion

Several studies have highlighted the metabolic differences between M1 and M2 MΦs. While M1 MΦs appear to rely substantially on glycolysis for ATP production, M2 MΦs display greater dependence on mitochondrial ATP biogenesis and oxidative phosphorylation [9,17,18,28,29]. In addition, fatty acid synthesis predominates in M1 MΦs, whereas fatty acid beta oxidation seems to be preferentially associated with M2 MΦ phenotypes [17,22,30]. Thus, these studies thus explicitly suggest that the modulation of metabolism is vital to MΦ activation. However, most previous studies employed *in vitro* cell culture models using immortalized murine and human cell lines, and bone marrow-derived murine MΦs [17]. Comparable metabolomics studies of physiologically relevant human MΦ populations, such as primary human monocyte-derived MΦs, upon activation have been lacking. Although donor-dependent variation has been reported for human peripheral-blood cells, this donor heterogeneity has been demonstrated to be both stimulus- and cell subset-specific, with monocytes and B cells presenting lower inter-donor immune response variation compared to cytotoxic and helper T cells [31-33]. Our results from this study do not indicate any significant inter-donor variation; however, we have observed substantial inter-donor variability in primary human neutrophil metabolic adaptations upon stimulation, the data from which is currently being analyzed and assembled into another manuscript to be considered for publication, and have developed and implemented control and normalization methods to mitigate this issue. In the present study, we found that characteristic metabolic profiles clearly differentiate between human monocyte-derived M0, M1, and M2a MΦs.

Diagnostic pathways include significant perturbation of glycolysis, lactate fermentation, the TCA cycle, oxidative stress, and *de novo* glycerophospholipid synthesis, which is also referred to as the Kennedy pathway [34].

The upregulation of glycolysis (Figure 2A) is viewed as a metabolic hallmark of M1 MΦ activation, which is critical for the modulation of M1 MΦ effector functions, including phagocytosis, pro-inflammatory cytokine secretion, and ROS production [18-20]. In our study, we established that M1 MΦs consume significantly greater amounts of carbohydrate substrates, such as fructose, glucose, and mannose, while concurrently secreting significantly greater amounts of lactate into the cell culture medium relative to M0 MΦs. These findings are consistent with previously reported results, and provide further evidence that pro-inflammatory MΦ activation induces Warburg-like metabolic traits [9,18,28]. Notably, we discovered that M2a MΦs exhibit similar glycolytic trends relative to M0 MΦs, albeit to a lesser extent than M1 MΦs. Although predominantly demonstrated in inflammatory, M1, MΦs, our study demonstrates that glycolysis is also significantly upregulated in anti-inflammatory M2a MΦs. Previous studies had reported that M-CSF enhances the expression of genes encoding glucose transporters and glycolytic enzymes, in addition to promoting greater lactate production in M2 MΦs [35,36]. The addition of M-CSF in our *in vitro* differentiation model of primary human monocyte-derived MΦs may account for the differences observed between our study and other published reports with respect to M2 MΦ metabolism [28,37]. Our metabolomics results also indicate that increased glycolytic activity and lactate production may be universal markers of MΦ activation in primary human monocyte-derived M1 and M2a

MΦs.

In addition to supporting the generation of the glycolytic intermediate fructose 6-phosphate (F6P), mannose can be used for the synthesis of N-glycans (Figure S3), which are important elements of protein glycosylation. Although N-glycosylation is well-established as a critical upregulated pathway in M2 MΦs [38], other studies have demonstrated that the inhibition of N-glycosylation also leads to the slight inhibition of M1 MΦ polarization [9]. Since our M1 and M2a MΦs both displayed a significant consumption of extracellular mannose relative to M0 MΦs, we examined these trends in the context of N-glycan biosynthesis, using microarray transcriptomics information that has been reported in Zhang et al. (Figure S3, Table S3) [39]. Bone marrow-derived murine MΦs stimulated with IFN-γ or LPS exhibit reduced gene expression of phosphomannomutase 1 (*Pmm1*), whereas IL-4-stimulated murine MΦs exhibit elevated gene expression of *Pmm1* relative to unstimulated control MΦs (Figure S3, Table S3) [39]. No consistent trend concerning guanosine diphosphate (GDP)-mannose pyrophosphorylase A (*Gmppa*) gene expression was reported in the Zhang et al. microarray data. However, IFN-γ, IL-4, and LPS-stimulated murine MΦs all exhibited elevated transcript expression of *Pmm2* and *Gmppb*, with the exception of the 2 and 4-hr time points following IL-4 stimulation, relative to unstimulated control MΦs (Figure S3, Table S3) [39]. These published transcriptomics data, combined with our metabolic observations regarding extracellular mannose consumption, thus suggest that M1 and M2a MΦs may utilize mannose for N-glycan biosynthesis and protein glycosylation, in addition to being used to provide substrates for glycolysis.

The utilization of a fully functional TCA cycle (Figure 3A) and concomitant oxidative phosphorylation is recognized as a metabolic characteristic of M0 and M2 MΦs [8,9,17], whereas M1 MΦs have been shown to reprogram this pathway to permit the accumulation of TCA cycle intermediates, including citrate and succinate, which are crucial for M1 MΦ effector functions [17,40]. Although previous studies have focused on TCA cycle intermediate-associated metabolic differences between M1 and M2a MΦs [40,41], investigations with respect to additional carbon sources that can enter the TCA cycle at the acetyl-CoA entry point are lacking. The metabolic data generated in this study suggest that M1 and M2a MΦs display distinct catabolic trends with respect to TCA cycle utilization. Both M1 and M2a MΦs exhibited preferential consumption of extracellular 3-hydroxybutyrate and acetate over pyruvate, relative to M0 MΦs. However, M1 MΦs utilized 3-hydroxybutyrate to a greater extent than M2a MΦs, and M2a MΦs utilized acetate to a greater extent than M1 MΦs. In addition, M1 and M2a MΦs secreted significant amounts of alanine and glycine into their spent culture medium, relative to M0 MΦs. These findings suggest that while M0 MΦs favor pyruvate as a carbon source for ATP energy production, M1 and M2a MΦs appear to prefer 3-hydroxybutyrate and acetate, respectively. This may be due, in part, to the fact that acetyl-CoA derived from 3-hydroxybutyrate coincidentally generates succinate, a known metabolic marker of M1 MΦs. Furthermore, acetyl-CoA derived from acetate utilizes ATP and not NAD^+, the latter being needed to keep glycolysis going, an observation which is also supported by our glycolytic metabolic data for M1 and M2a MΦs (Figure 2). Previous studies have shown that bone marrow murine-derived MΦs stimulated with

LPS exhibit elevated transcript expression of genes coding for 3-hydroxybutyrate dehydrogenase 1 (*Bdh1*) and 3-oxoacid-Co-A transferase 2 (*Oxct2*) enzymes at 24 hrs post-stimulation (Figure S4, Table S3) [39]. Although our intracellular succinate data for M1 MΦs do not reflect that expected from increased OXCT activity, it is important to note that our MΦs were stimulated for 72 hrs; therefore, without conducting additional temporal MΦ activation studies at time points shorter than 72 hrs, it is difficult to make any firm conclusions regarding differential 3-hydroxybutyrate consumption in our MΦ activation subtypes. The secretion of alanine and glycine, which takes place to a greater extent in M1 than M2a MΦs, may be a reflection of enhanced GPT and AGXT activity, with the concurrent generation of α-KG (Figure 3A), which is an important TCA cycle intermediate that has also been implicated in MΦ activation [17,40,42]. Altogether, these results suggest that M0, M1, and M2a MΦs preferentially utilize different carbon and amino acid sources that connect to the TCA cycle.

Additional enzymes that are critical for the flow of intermediates through the TCA cycle include pyruvate carboxylase (PC) and the malic enzyme (ME), which catalyze the conversion of pyruvate to oxaloacetate and malate to pyruvate, respectively (Figure 3A). The upregulation of these metabolic enzymes can occur when the flow of metabolites through the enzymatic reaction of pyruvate dehydrogenase (PDH; Figure 3A) is diminished, and when lactate fermentation is employed as a primary means to generate energy (ATP), a process referred to as the Warburg effect and which has been demonstrated in previous studies to take place in proliferating cancer cells (i.e., occurrence of aerobic glycolysis) [43–45]. Furthermore, increased activity of PC under

glutamine-limited conditions has been previously shown to take place in glioblastoma and T cells [46,47]. Although our M1 and M2a MΦs display characteristics of Warburg metabolism (Figure 2), previous work by Meiser et al. has shown that PDH activity is unaffected in M1 MΦs [41]. Although our studies did not detect oxaloacetate or malate in our MΦ intracellular metabolite profiles, extracellular glutamine in our M0, M1, and M2a MΦ cultures was not found to be limiting upon MΦ harvest, remaining at extracellular concentrations of 0.92 ± 0.12, 1.37 ± 0.08, and 0.94 ± 0.05 mM, respectively, in the three MΦ subtypes. Our data leads us to conclude that replenishment of TCA cycle intermediates via the pyruvate carboxylase or malic enzyme reactions does not take place to a significant degree under the experimental conditions tested in our study.

Succinate is a key metabolic marker of M1 MΦ activation, and previous studies have established that its accumulation leads to the induction of Warburg-like metabolism in MΦs due to the stabilization of HIF-1α, which has also been shown to promote the upregulation of pro-inflammatory cytokine and gene expression [5,6]. Our M1 MΦ metabolic data are inconsistent with that shown by others in that we observed no significant difference between intracellular succinate levels in M1 MΦs relative to M0 MΦs; however, M2a MΦs do exhibit significantly decreased levels of intracellular succinate compared to M1 MΦs. Furthermore, we did not detect itaconate, which has been demonstrated to be an inflammatory regulator in murine and human MΦs [6,48], in any of our intra- or extracellular MΦ activation state metabolite extracts. These discrepancies may be due to the fact that our MΦs were activated for 72 hrs prior to metabolite extraction, while other studies typically employ shorter incubation periods,

such as less than or up to 24 hrs. Notably, we also found that M1 MΦs display significantly decreased intracellular levels of fumarate. This suggests that our M1 MΦs may experience some level of succinate dehydrogenase (SDH) inhibition, as previously determined by others [5,40,49], since M1 MΦs exhibit a higher intracellular succinate to fumarate ratio than either M0 or M2a MΦs. Thus, these data would indicate that M1 MΦs attenuate their inflammatory response following 72 hrs stimulation with LPS and IFN-γ. However, our results are consistent and in agreement with our other findings, as discussed below.

In addition to being derived from glutamate as a result of AGXT enzyme activity, glycine can also be produced from choline, serine, or alanine conversion (Figure S5). Unfortunately, the only available transcript data from Zhang et al. relevant to these metabolic pathways is that of *Agxt2*, which can catalyze the conversion of both alanine and glutamate to glycine [39]. Examining the microarray data, we found that *Agxt2* gene transcription is upregulated at 24 hrs in IFN-γ and LPS-stimulated murine MΦs, and is downregulated at 24 hrs in IL-4-stimulated murine MΦs, relative to unstimulated control murine MΦs (Figure S5, Table S3) [39]. A further investigation of our relevant metabolic data revealed that M2a MΦs consume significantly less extracellular serine than M0 or M1 MΦs. In addition, M2a MΦs displayed significantly decreased levels of intracellular serine (Figure S5). Furthermore, M2a MΦs consumed significantly less extracellular glutamate than M0 or M1 MΦs (Figure S5). Overall, these metabolic findings, combined with the microarray data of Zhang et al., thus suggest that glycine is derived primarily from glutamate as a result of AGXT2 enzyme activity in M1 MΦs, while M2a MΦs may

be producing glycine primarily from serine using serine hydroxymethyltransferase (SHMT), although further studies are needed to validate the interpretations of these data.

Extracellular secreted fumarate, at a concentration of 3.95 ± 0.73 μM, was only found in our M2a MΦ cultures (Figure 3B). These findings are consistent with studies that have shown that fumarate is a key metabolite for memory induction in innate immune cells, which is also known as trained immunity [50]. Arts et al. determined that the training of primary human monocyte-derived MΦs using 100 μM of fumarate induced changes >2.5-fold relative to non-trained MΦs, in 456 dynamic epigenetic regions as a result of histone modifications, such as H3K4me3 and H3K27ac [50]. Many of these dynamic fumarate-induced epigenetic alterations were found to be associated with cellular pathways involved in leukocyte migration and the innate immune response, including pro-inflammatory cytokine expression [50]. Findings by Arts et al. are also consistent with previous trained immunity studies, which used β-glucan-trained monocytes [51,52]. Additional studies have shown that fumarate treatment induces IL-4 production and T_H2 responses in human type II dendritic cells and $CD4^+$ T cells [53]. Therefore, these published data, together with our observation of significant levels of extracellular fumarate in our human M2a MΦ cell cultures, would suggest that our M2a MΦs may be undergoing local immunological memory and T_H2-like cell responses.

Microbicidal ROS production is a well-characterized phenomenon of MΦ function and immune responses. Nevertheless, excessive ROS production can lead to impaired intracellular redox balance, a depletion of intracellular pools of GSH due to excessive conversion of GSH to its oxidized form (GSSG), NADPH depletion, lipid

and protein peroxidation, and oxidative DNA damage (Figure 4A), which, if left unchecked, can lead to significant cellular damage and apoptosis [54,55]. Our study indicates that M1 and M2a MΦs experience significant oxidative stress, as revealed by significantly decreased levels of intracellular GSH relative to M0 MΦs. Furthermore, M1 MΦs have significantly lower intracellular levels of NADPH relative to M0 MΦs. These results are consistent with other published works, which have reported that NADPH oxidase (NOX) produces superoxide ($^{\bullet}O_2^-$) from molecular oxygen (O_2) using NADPH produced during the oxidative phase of the pentose phosphate pathway (PPP), which is upregulated in M1 MΦs [9,17,54]. In addition, NADPH provides a source of reducing power to regenerate GSH from GSSG, thereby indirectly contributing to ROS neutralization [17,56]. Such a process seems to account for the significantly decreased intracellular levels of GSH that we have observed in M1 MΦs relative to M2a MΦs. Although ROS production is associated predominantly with M1 MΦ phenotypes, another published report demonstrated that Cu,Zn-superoxide dismutase (SOD)-mediated hydrogen peroxide (H_2O_2) production supports M2 MΦ activation via redox-dependent STAT6 nuclear translocation, which results in reduced TNF-α expression and elevated profibrotic factor gene expression [57]. These reports are consistent with our metabolomics findings, which indicate that primary human monocyte-derived M2a MΦs experience an oxidative stress response, which may be due to low-level ROS production in these MΦs. We also found that M1 MΦs contain a significantly greater intracellular amount of taurine compared to M0 and M2a MΦs. Similar to reduced glutathione (GSH), taurine exhibits cytoprotective effects by neutralizing toxic oxidative species and

attenuating excessive oxidative stress responses [55,58]. Collectively, our findings indicate that MΦ activation results in significant oxidative stress and suggest that M1 MΦs deplete intracellular NADPH for ROS production and GSH regeneration, in addition to accumulating intracellular taurine to mitigate ROS-mediated M1 MΦ cell damage.

Previous studies have shown that M1 and M2 MΦs have disparate metabolic preferences concerning lipid metabolism, with fatty acid synthesis being associated with M1 MΦ activation and fatty acid beta oxidation being preferentially associated with M2 MΦ activation [1,7,17,22]. In this study, we found that M1 MΦs display unique metabolic markers related to *de novo* glycerophospholipid synthesis, which is also known as the Kennedy pathway (Figure 5A). M1 MΦs exhibited significantly increased levels of intra- and extracellular choline and significantly decreased levels of intracellular phosphocholine, relative to M0 and M2a MΦs. Snider et al. showed that M1 MΦs consume greater amounts of choline, promote phosphatidylcholine biosynthesis, and that antibody-mediated inhibition of choline uptake altered M1 MΦ secretion of pro-inflammatory cytokines [59]. While our results differ from this published work, our M1 MΦs were stimulated for 72 hrs prior to metabolic analysis, whereas Snider et al. used much shorter LPS incubation times, ranging from 10 min to 16 hrs [59], which may account for the different observations. In addition, other studies have determined that choline reduces inflammation, IL-1β release from innate immune cells, pro-inflammatory gene expression, such as *TLR4*, *NFKB1*, and *TNFA*, and increases lymphocyte proliferation [60-62]. Thus, our M1 MΦ data thus suggest that at 72 hrs post-activation,

these cells display metabolic trends that are associated with inflammatory mitigation. We also found that M1 MΦs accumulate significant amounts of intracellular phosphoethanolamine, which was not observed in M0 or M2a MΦs. Gohil et al. demonstrated that mammalian cells elevate intracellular phosphoethanolamine levels following meclizine treatment due to dose-dependent, non-competitive inhibition of phosphate cytidylyltransferase 2 (PCYT2) enzymatic activity [63]. Furthermore, it was also determined that phosphoethanolamine reduces mitochondria membrane potential, increases flavin adenine dinucleotide (FAD^+), and decreases reduced nicotinamide adenine dinucleotide (NADH) levels, as a result of mitochondrial respiration inhibition [63]. Examining supplementary microarray transcriptomics data included in Zhang et al., we discovered that bone marrow-derived murine MΦs stimulated with IFN-γ or LPS have reduced expression of *Chkα*, *Chkβ*, *Pcyt1a*, and *Pcyt2* transcripts and elevated expression of *Etnk1*, whereas bone marrow-derived murine MΦs stimulated with IL-4 exhibit reduced expression of *Chkα* and *Chkβ* transcripts and elevated gene expression of *Etnk1*, *Pcyt1a*, and *Pcyt2* relative to unstimulated control MΦs (Figure 5A, Figure S6, and Table S3) [39]. These transcriptomics profiles are consistent with our metabolomics findings, and together suggest that M1 MΦs distinctly manipulate the Kennedy pathway to downregulate mitochondrial respiration and to attenuate their inflammatory response, at least at the 72-hr stimulation time point used in this study.

Quinolinate, an N-methyl-D-aspartate (NMDA) receptor agonist and neurotoxin, is a metabolite derived from tryptophan within the kynurenine pathway (KP) [64]. Our results indicate that intracellular metabolite extracts from M1 MΦs contain significantly

greater amounts, 25.90-fold compared to M0 MΦs, of quinolinate (Table 1). This is consistent with previous studies that have demonstrated substantial quinolinate production by macrophages following IFN-γ stimulation [64,65]. At concentrations less than 50 nM, quinolinate serves as a substrate for NAD^+ synthesis by the KP; however, at concentrations above 150 nM, quinolinate can induce excitotoxicity in astrocytes and neurons, induce NOS, and oxidative stress [66]. Quinolinate is able to form complexes with Fe(II), which promotes the formation of ROS, such as hydroxyl ($^{\bullet}OH$) radicals, and subsequent DNA degradation and lipid peroxidation [67]. More recent evidence has emerged indicating that KP activation is triggered upon innate immune challenge in MΦs; yet, the conversion of quinolinate to NAD^+ is oddly inhibited [68]. This particular study also found that oxidative phosphorylation in activated MΦs can be restored by increasing *de novo* NAD^+ synthesis by the KP, which implies that this process is a metabolic switch for MΦ effector function [68]. Our M1 MΦs also displayed significantly depleted levels, -3.79-fold compared to M0 MΦs, of intracellular NAD^+; therefore, we believe these findings suggest that M1 MΦs may accumulate intracellular quinolinate as another means to inhibit oxidative phosphorylation and/or generate ROS.

While O_2 consumption was not directly measured in our MΦ subtype NMR metabolomics experiments, the metabolome profiles of M0, M1, and M2a primary MΦs that we have characterized in this study are consistent with published reports on this subject. An interesting future direction for this work would be to track the metabolome changes of our different MΦ subtypes as a function of time, i.e., 24, 36, and 48 hrs, rather than at the single 72 hr time point that was employed in this current study. We would

expect to detect interesting metabolic adaptations as the MΦs activate over time in this *in vitro* cell culture model. In the future, we aim to conduct these O_2 consumption measurements in parallel with longitudinal metabolomics analyses, as well as to report on the metabolic adaptations of MΦs when co-cultured with bacterial pathogens.

Materials and Methods

Primary Human Monocyte Isolation

Heparinized whole blood was obtained in accordance with proper guidelines, local Institutional Review Board (IRB) approval (ID# 00000799; Protocol #VC100118), and informed consent from healthy, adult donors in Bozeman, Montana, USA. A total of 6 donors, in the age range of 19 to 27 were included in this study, 50% of whom were female. Peripheral blood mononuclear cells (PBMCs) were isolated by centrifugation in lymphocyte separation media (Corning) at 800 x g for 25 min at room temperature. $CD14^+$ monocytes were isolated from PBMCs by MACS using CD14 human microbeads (Miltenyi Biotec, San Diego, CA, USA), which resulted in an average purity of 97.1 ± 1.3% (Figure S7) when subjected to sorting on an LSR Fortessa cell analyzer (BD Biosciences, San Jose, CA, USA).

Culture of Primary Human Monocyte-Derived MΦs

To generate primary human monocyte-derived MΦs, $CD14^+$ monocytes were cultured in 25 cm^2 tissue culture flasks (1 x 10^6 cells per mL; Falcon/Corning) in Roswell Park Memorial Institute (RPMI) 1640, w/L-glutamine (Lonza, Bend, OR, USA) media,

supplemented with 1 mM sodium pyruvate (Lonza), 1X MEM non-essential amino acids (NEAAs; Gibco, ThermoFisher Scientific, USA), 10% (v/v) fetal bovine serum (FBS; ATCC, Manassas, VA, USA), and 50 ng/mL recombinant human M-CSF (rHU-MCSF; PeproTech, Rocky Hill, NJ, USA) for 6 d. Media and cytokines were replenished every 3 d.

Activation of Primary Human Monocyte-Derived MΦs

Mature (6 d) monocyte-derived MΦs were prepared in 3 replicates using 25 cm^2 tissue culture flasks (Falcon/Corning) containing RPMI 1640, w/L-glutamine (Lonza) media, supplemented with 1 mM sodium pyruvate (Lonza), 1X MEM NEAAs (Gibco), 10% (v/v) FBS (ATCC), and 50 ng/mL rHU-MCSF (PeproTech). Three different MΦ activation groups were assessed and compared, including M0, M1, and M2a MΦs. Cell cultures corresponding to each MΦ activation state, and parallel sham media controls, corresponding to macrophage activation and cell culture media added to 25 cm^2 tissue culture flasks that did not contain mature monocyte-derived MΦs, were set up and incubated for 72 hrs at 37 °C, 5% CO_2. MΦ activation stimuli included 100 ng/mL LPS and 50 ng/mL recombinant human IFN-γ (rHU-IFNγ) for M1 MΦs (Sigma Aldrich and PeproTech, respectively) whereas no additional stimuli were added to the M0 MΦs. Then, 20 ng/mL recombinant human IL-4 (rHU-IL4; PeproTech) was utilized to generate M2a MΦs. Following culture and activation, the characterization of primary human monocyte-derived MΦs (MoMΦs) was conducted using flow cytometry (Figure S8).

Antibodies and Flow Cytometry

Primary human monocytes were stained using anti-human antibodies directed against CD14 (BD Biosciences) and appropriate isotype controls. M0, M1, and M2a MoMΦs using anti-human antibodies directed against CD68, CD80, and CD163 (BD Biosciences) and appropriate isotype controls. Permeabilization of a cell subset was conducted using Cytofix/Cytoperm (BD Biosciences) for the intracellular staining of CD68. Following staining, cells were resuspended in fluorescence-activated cell sorting (FACS) buffer for analysis on an LSR Fortessa Flow Cytometer (BD Biosciences). FACS data were analyzed using FCSalyzer software (version 0.9.14-alpha) with monocytes and MoMΦs gated based upon size and single cells. Since baseline fluorescence levels differed between MΦ activation states, mean fluorescence intensity (MFI) values were normalized by subtracting the appropriate isotype control MFI from the sample MFI (normalized MFI; Figure S8).

Intra- and Extracellular
Metabolite Extraction

Following MΦ activation, spent cell culture medium was transferred from 25 cm^2 tissue culture flasks into sterile 15-mL conical tubes and centrifuged at 2000 x g for 1 min at room temperature (RT) to pellet any cellular debris. Two 1.5-mL aliquots of sham and spent cell culture medium were transferred to sterile 1.5-mL tubes and stored at -80 °C prior to extracellular metabolite extraction. Cell monolayers were washed with 1 mL of cold (4 °C) sterile 1X phosphate-buffered saline (PBS). Wash solutions were pipetted into a 15-mL conical tube, centrifuged at 2000 x g to pellet any remaining non-adherent

cells, decanted, and then resuspended in 500 µL of -20 °C 50% aqueous methanol. Then, 1.5-mL of -20 °C 50% aqueous methanol was added to 25 cm^2 tissue culture flasks to simultaneously quench, extract, and detach cells from flask surface with the aid of a cell scraper. Cell suspensions were removed from 25 cm^2 tissue culture flasks, transferred to 15-mL conical tubes containing non-adherent cell suspensions, and thoroughly mixed.

Two aliquots of 1-mL cell suspensions were transferred to two separate 2-mL lysis B matrix tubes (MP Biomedicals) and lysed using a FastPrep-24 5^G homogenizer (MP Biomedicals) at a speed of 6.0 m/s for 2 cycles of 40 s each, with lysis tubes placed on ice between cycles. Then, 50 µL of cell lysate was stored at -80 °C for protein determination, and then 500 µL of chloroform ($CHCl_3$) was added to each lysis tube. Tubes were vortexed for 3 cycles of 10 s each, and then placed at -20 °C for 20 min, prior to centrifugation at 10,000 x g for 10 min to separate aqueous and nonpolar phases [69]. The aqueous phase, containing the intracellular metabolite mixture, was transferred to a 1.5-mL tube, dried using a Speedvac vacuum centrifuge with no heat overnight, and stored at -80 °C until NMR metabolite sample preparation.

Sham and spent cell culture medium samples were filtered through 3-kDa molecular weight cutoff (MWCO) centrifuge filters (Millipore Amicon), which were prewashed extensively [70], prior to being dried using a Speedvac vacuum centrifuge with no heat overnight and stored at -80 °C until NMR sample preparation.

Determination of Protein Content

Protein concentrations were measured using the Pierce BCA Protein Assay Kit (ThermoFisher Scientific; Cat. No. 23225) for normalization of intra- and extracellular

metabolite extracts.

NMR Sample Preparation

Dried intra- and extracellular metabolite extracts were resuspended in 600 µL of NMR buffer [consisting of 25 mM NaH_2PO_4/Na_2HPO_4, 0.4 mM imidazole, 0.25 mM 4,4-dimethyl-4-silapentane-1-sulfonic acid (DSS) in 90% H_2O/10% D_2O, pH 7.0]. Following resuspension, samples were centrifuged at 21,000 rpm for 1 min to pellet insoluble debris, and then transferred to 5-mm NMR tubes for NMR metabolomics analysis.

NMR Spectra Acquisition
and Preprocessing

All NMR spectra were collected at 298 K (25 °C) using a Bruker 600 MHz (^{1}H Larmor frequency) AVANCE III solution NMR spectrometer, equipped with a SampleJet automatic sample loading system, a 5-mm triple resonance (^{1}H, ^{15}N, ^{13}C), liquid-helium-cooled three channel inverse (TCI) NMR cryoprobe, and Topspin software (Bruker version 3.2). Then, 1D ^{1}H NMR spectra acquisition was performed using the Bruker-supplied excitation sculpting (ES)-based 'zgesgp' pulse sequence [71,72], and NMR spectra were recorded with 256 scans and a ^{1}H spectral window of 9615.38 Hz. Free induction decays (FIDs) were collected with 32K data points and a dwell time interval of 52 µsec, amounting to a data acquisition time of 1.7 s. Recovery delay (D1) times between acquisitions were set to 1 s, resulting in an overall 2.7 s relaxation recovery delay between scans [73,74]. DSS chemical shift referencing and phase correction of 1D ^{1}H NMR spectra were conducted using Topspin software (Bruker version 3.2).

For verification of select metabolite identifications, 2D ^{1}H-^{1}H total correlation

spectroscopy (TOCSY) spectra were acquired for representative samples using the Bruker-supplied ‘mlevphpr.2/mlevgpph19’ pulse sequences (256 × 2048 data points, 2 s relaxation delay, 32 transients per FID, ^{1}H spectral window of 6602.11 Hz, 80 ms TOCSY spin lock mixing period). Then, 2D ^{1}H-^{1}H TOCSY spectra were processed using Topspin software (Bruker version 3.2).

NMR Data Analysis

Further processing of 1D ^{1}H NMR spectra and metabolite profiling analyses were conducted using Chenomx NMR Suite software (version 8.1; Chenomx Inc., Edmonton, Alberta, Canada). The baseline correction of NMR spectra following an import of preprocessed ‘1r’ NMR spectral files into Chenomx software was performed using the automatic cubic spline function in Chenomx, and subsequent manual breakpoint adjustment to obtain a flat, well-defined baseline, following recommendations from Chenomx application notes and previously reported methods [75,76]. ^{1}H chemical shifts were referenced to the 0.0 ppm DSS signal, and the ^{1}H NMR signals arising from imidazole were used to correct for small chemical shift changes due to slight variations in sample pH. Metabolite identification and quantification were performed by fitting the 1D ^{1}H spectral patterns, chemical shifts, and spectral intensities to reference spectral patterns of small molecules, using the Chenomx small molecule spectral database for 600 MHz (^{1}H Larmor frequency) magnetic field strength NMR, and a manually peak-based fit style, where adjustments were made to achieve optimal fits for compound peak cluster location and intensity [77]. An internal (0.25 mM DSS) standard was used for metabolite quantitation.

Although pulse programs utilizing ES suppress proton signals around the water region to a greater extent than NOEPR (1D NOESY with presaturation during relaxation and mixing time), the relative intensities observed between these particular ^{1}H signals have been demonstrated to be identical to those seen in NOEPR [78]. To evaluate differences between 1D ^{1}H spectra acquired using 'zgesgp' versus 'noesypr1d' pulse sequences, we have conducted comparative analyses by constructing our own in-house 'zgesgp'-acquired 600 MHz metabolite library using pure standards. If our in-house metabolite standard 1D ^{1}H NMR spectra presented significant deviations from the 600 MHz Chenomx small molecule spectral database, we added these 'zgesgp' metabolite standard spectra to a custom library using the 'Compound Builder' module of Chenomx NMR Suite program (version 8.0), as described previously [74].

Statistical Analysis

Quantitative intra- and extracellular metabolic profiles were exported from Chenomx software, as mM concentrations, with metabolic profiles generated in parallel from blank NMR buffer control samples subtracted from our experimental MΦ extract profiles. In addition, metabolite profiles generated from parallel sham media controls were subtracted from our extracellular MΦ extract metabolite profiles. Intra- and extracellular metabolite concentrations were converted from mM to nmol by accounting for NMR buffer volume, and resulting metabolic profiles were normalized to protein content prior to multivariate statistical analysis using MetaboAnalyst 4.0 [79,80]. Normalized metabolite concentrations were further log-transformed to ensure a Gaussian distribution of the data and auto-scaled (i.e., mean centered and divided by standard

deviation) prior to statistical analysis, including 2D-PCA and HCA. The false discovery rate (FDR) was evaluated using the 'ANOVA' module of MetaboAnalyst, an adjusted *p*-value (FDR) cutoff of 0.05, and Tukey's HSD post-hoc analysis. Metabolites with FDR values ≥0.05 were excluded from further statistical analysis in GraphPad Prism. HCA was conducted in MetaboAnalyst using a Euclidean distance measure and Ward clustering algorithm. Statistical significance was assessed by unpaired parametric *t*-test with Welch's correction using the GraphPad Prism program version 8.0.2 (GraphPad Software, La Jolla, CA).

Conclusions

In conclusion, our metabolite profiling data generated using *in vitro* MΦs derived from primary human monocytes indicate that M1 and M2a MΦs both utilize glycolysis and exhibit significant oxidative stress. Furthermore, the M1 MΦs generated in this study reveal a previously unknown and unique repurposing of the *de novo* glycerophospholipid metabolic pathway associated with the inhibition of oxidative phosphorylation and inflammatory mitigation. Moreover, we identified unique metabolite expression patterns relevant to metabolite flow through the TCA cycle, including the preferential utilization of 3-hydroxybutyrate and acetate in M1 and M2a MΦs, respectively, rather than pyruvate. The results from our study emphasize the importance of investigating the biochemical properties of physiologically relevant innate immune cell populations, such as primary human monocyte-derived MΦs. Our work also highlights the usefulness of NMR metabolomics to define characteristic metabolic phenotypes (i.e., metabotypes)

associated with specific cellular phenotypes, and to better understand how functionally relevant metabolic adaptations correspond to distinct, physiologically relevant activation states of primary human immune cells cultured *in vitro*.

Supplementary Materials

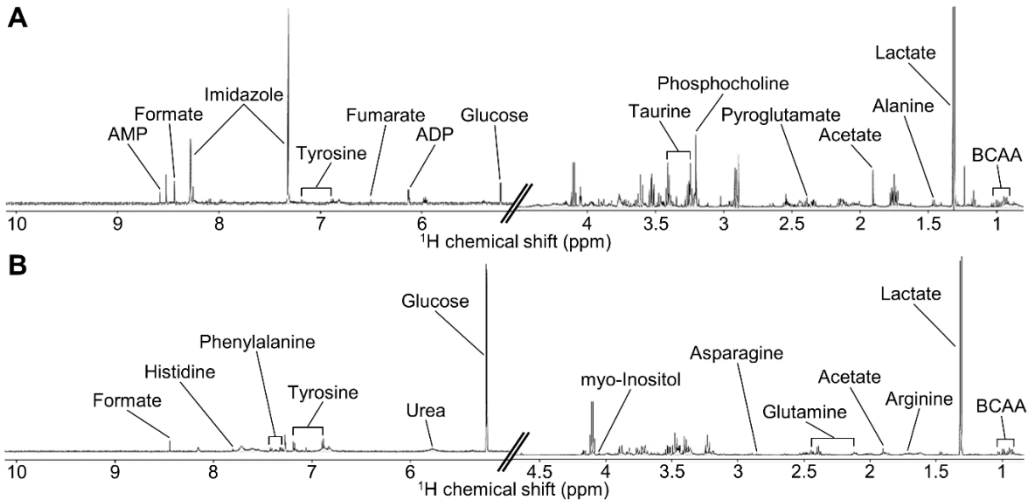

Figure S1. 1D ^{1}H NMR spectra acquired on MSU's Bruker 600 MHz (^{1}H Larmor frequency) NMR spectrometer on intra- (A) and extracellular (B) metabolite extracts from M0 MΦs. Abbreviations denote: AMP, adenosine monophosphate; ADP, adenosine diphosphate; BCAA, branched chain amino acids.

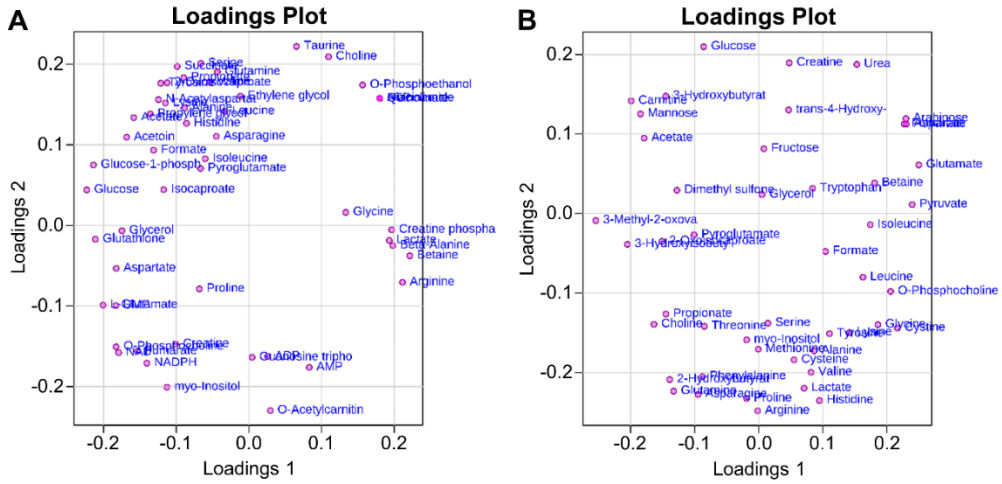

Figure S2. PCA loadings plots for intra- (A) and extracellular (B) MΦ metabolite extracts.

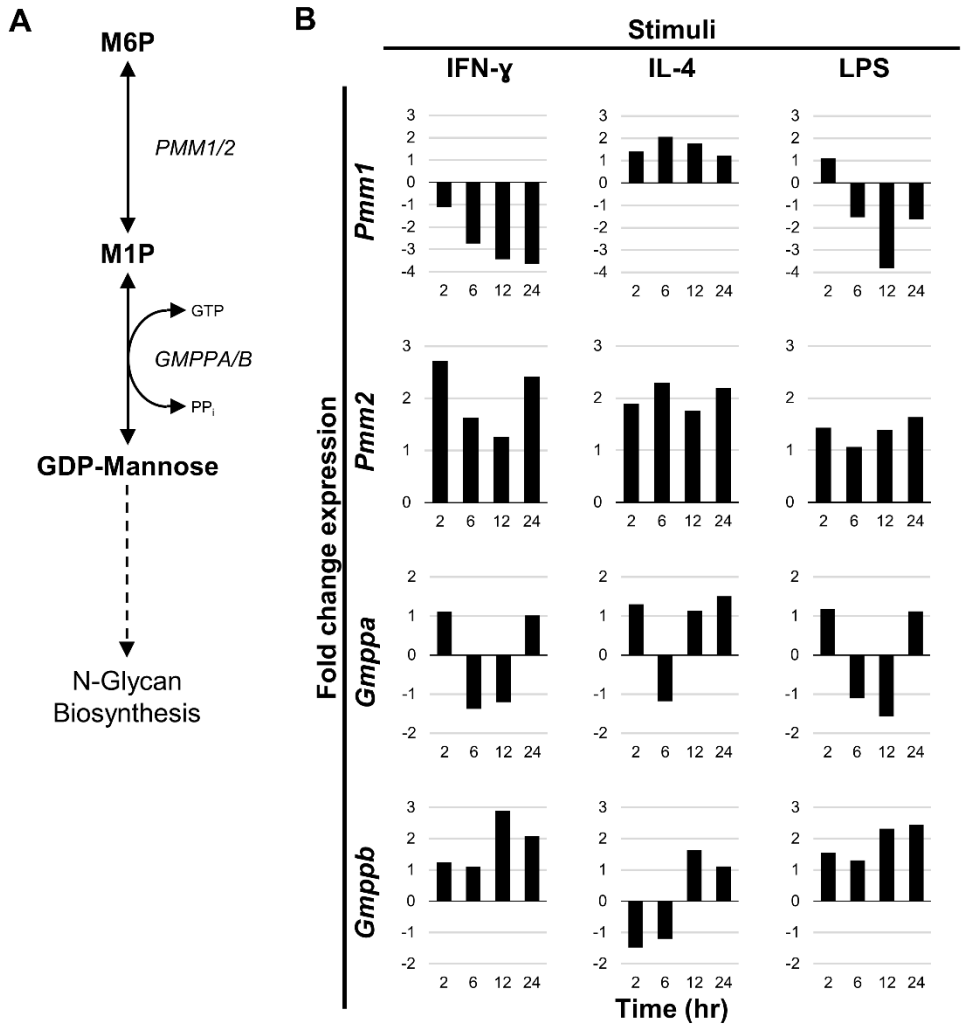

Figure S3. Metabolism of mannose for N-glycan biosynthesis (A) and fold change expression of *Gmppa*, *Gmppb*, *Pmm1*, and *Pmm2* in bone marrow-derived murine MΦs upon differential stimuli (B). Data has been derived from Zhang *et al.* to generate these plots [39]. Abbreviations denote: GDP, guanosine diphosphate; *Gmppa*, GDP-mannose pyrophosphorylase A; *Gmppb*, GDP-mannose pyrophosphorylase B; GTP, guanosine triphosphate; IFN-γ, interferon-γ; IL-4, interleukin-4; LPS, lipopolysaccharide; M1P, mannose 1-phosphate; M6P, mannose 6-phosphate; *Pmm1*, phosphomannomutase 1; *Pmm2*, phosphomannomutase 2.

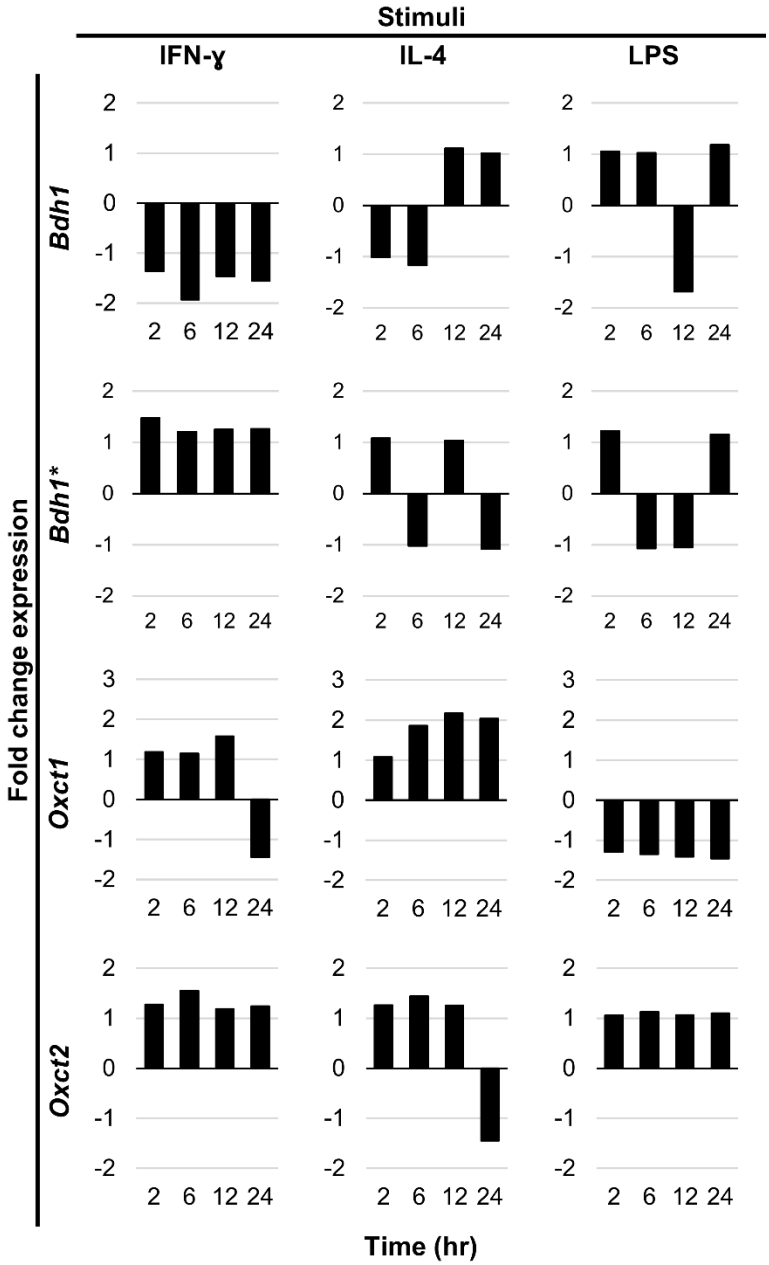

Figure S4. Fold change expression of *Bdh1* (mMR028403), *Bdh1** (mMC011803), *Oxct1*, and *Oxct2* in bone marrow-derived murine MΦs upon differential stimuli. Data has been derived from Zhang *et al.* to generate these plots [39]. Abbreviations denote: *Bdh1*, 3-hydroxybutyrate dehydrogenase 1; IFN-γ, interferon-γ; IL-4, interleukin-4; LPS, lipopolysaccharide; *Oxct1/2*, 3-oxoacid Co-A transferase 1/2.

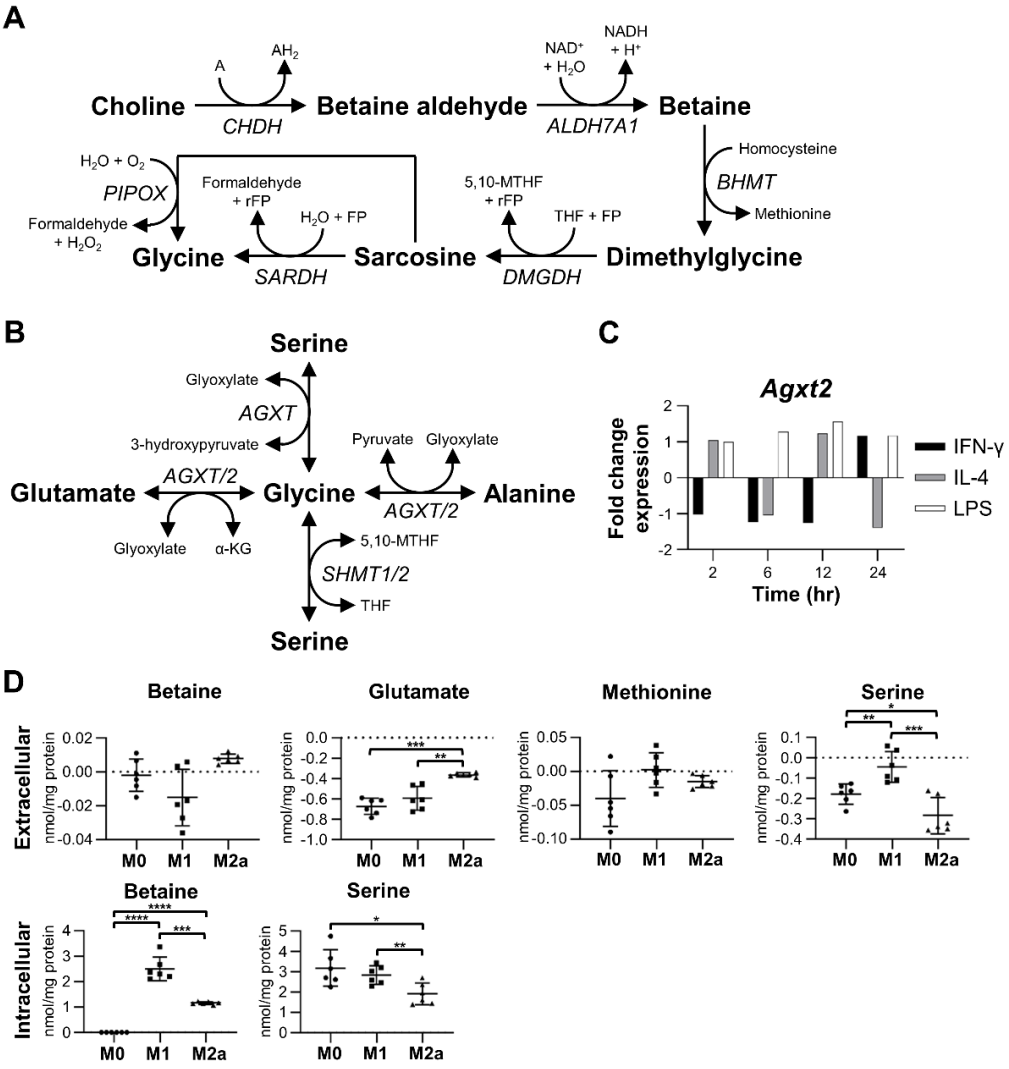

Figure S5. Generation of glycine from (A) choline or (B) glutamate, serine, and alanine. (C) Fold change expression of *Agxt2* in bone marrow-derived murine MΦs upon differential stimuli. Data has been derived from Zhang *et al.* to generate this plot [39]. (D) Quantitative levels of corresponding metabolites detected in intra- and extracellular MΦ metabolite extracts (mean ± SD). Statistical significance (*p*) was measured using two-tailed unpaired parametric t-tests with Welch's correction, whereby *, $p < 0.05$; **, $p < 0.01$; ***, $p < 0.001$; ****, $p < 0.0001$. Abbreviations denote: 5,10-MTHF, 5,10-methylenetetrahydrofolate; α-KG, α-ketoglutarate; A, acceptor; AH2, reduced acceptor; *ALDH7A1*, betaine aldehyde dehydrogenase; *AGXT*, alanine-glyoxylate aminotransferase; *BHMT*, betaine-homocysteine S-methyltransferase; *CHDH*, choline dehydrogenase; *DMGDH*, dimethylglycine dehydrogenase; FP, electron-transfer flavoprotein; IFN-γ, interferon-γ; IL-4, interleukin-4; LPS, lipopolysaccharide; NAD^+, nicotinamide adenine dinucleotide; NADH, reduced nicotinamide adenine dinucleotide; *PIPOX*, sarcosine oxidase; rFP, reduced electron-transfer flavoprotein; *SARDH*, sarcosine dehydrogenase; *SHMT*, serine hydroxymethyltransferase; THF, tetrahydrofolate.

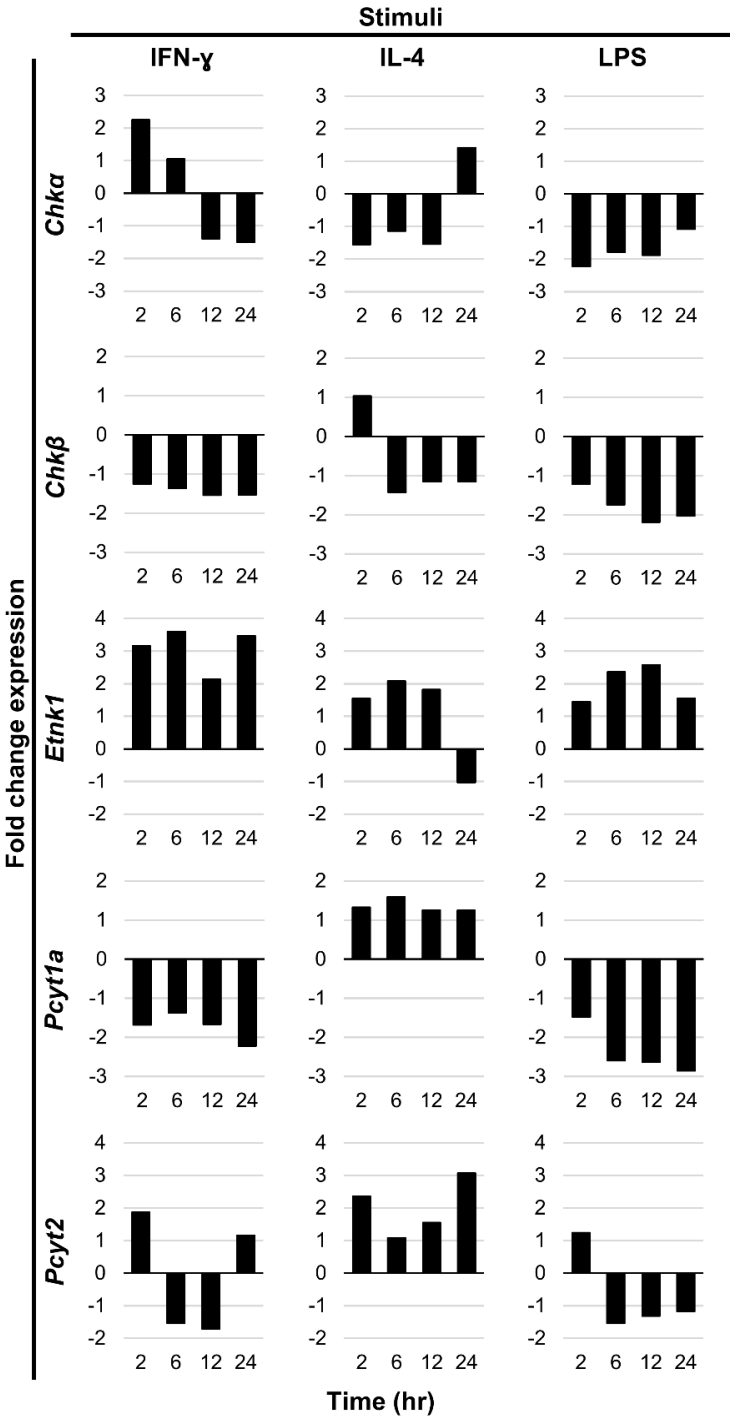

Figure S6. Fold change expression of *Chkα*, *Chkβ*, *Etnk1*, *Pcyt1a*, and *Pcyt2* in bone marrow-derived murine MΦs upon differential stimuli. Data has been derived from Zhang *et al.* to generate these plots [39]. Abbreviations denote: *Chkα*, choline kinase α; *Chkβ*, choline kinase β; *Etnk1*, ethanolamine kinase 1; IFN-γ, interferon-γ; IL-4, interleukin-4; LPS, lipopolysaccharide; *Pcyt1a*, phosphate cytidylyltransferase 1α; *Pcyt2*, phosphate cytidylyltransferase 2.

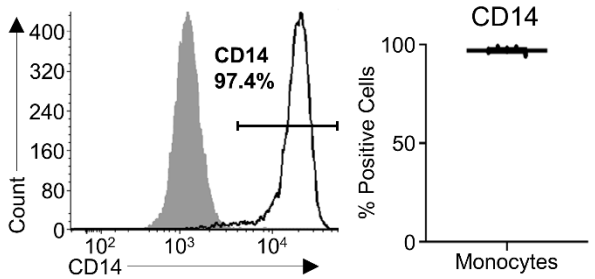

Figure S7. Purity of isolated monocytes. Representative histogram of purified $CD14^+$ monocytes (left) and pooled data from 5 independent experiments, mean ± SEM (right).

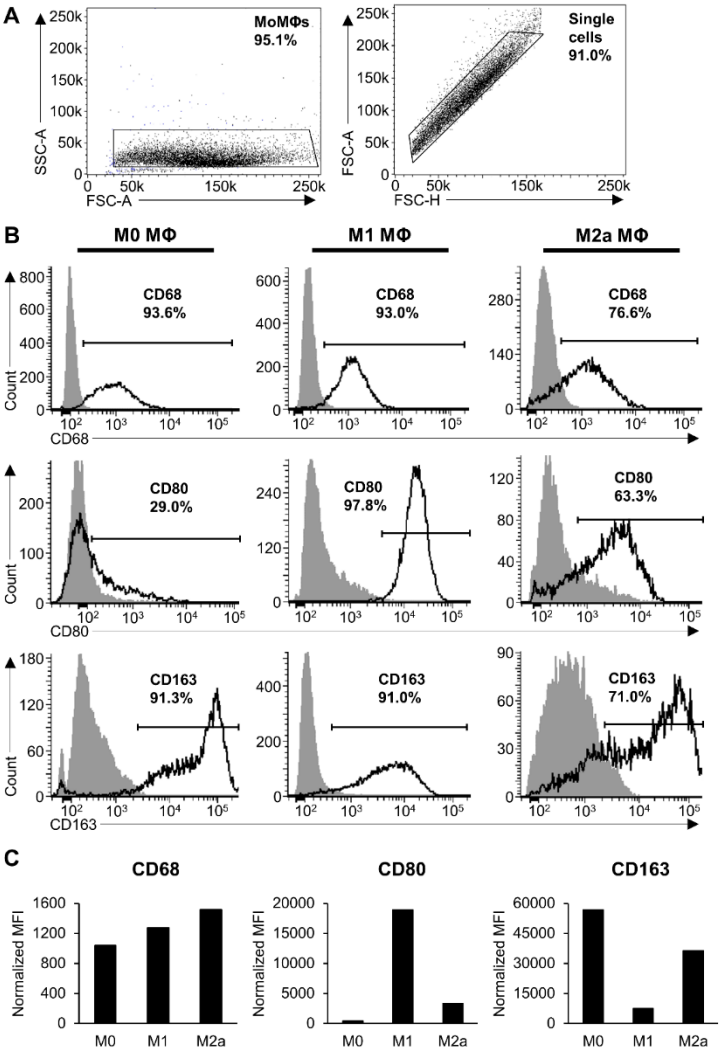

Figure S8. Phenotype of primary human monocyte-derived macrophages (MoMΦs). (A) Gating strategy for FACS analysis of MoMΦs; (B) Dot plots of CD68, CD80, and CD163 expression by M0, M1, and M2a MoMΦs; (C) Normalized mean fluorescence intensity (MFI) of CD68, CD80, and CD163 expression by M0, M1, and M2a MoMΦs.

Table S1. 1D ^{1}H NMR intra- and extracellular metabolite limit of detection (LOD) values.[1]

Extract	Metabolite	LOD (μM)
Intracellular	Arginine	3
	ATP	1
	Betaine	1
	Glucose-1-phosphate	1
	NAD^+	0.5
	Niacinamide	1
	Quinolinate	1
Extracellular	Fumarate	1

[1] LOD values were established by evaluation of signal to noise ratios in our experimental 1D ^{1}H NMR spectra, Chenomx NMR Suite software, and its accompanying Chenomx 600 MHz metabolite library. Abbreviations denote: ATP, adenosine triphosphate; NAD^+, nicotinamide adenine dinucleotide.

Table S2. Discriminatory metabolites in intracellular extracts associated with M1 vs. M2a MΦ activation.[1]

Metabolite	M1 vs. M2a MΦs	
	FC	*p*-value
Acetate	1.27	**
ADP	-1.36	***
AMP	-1.83	****
Aspartate	-1.32	**
ATP	9.14[2]	****
Betaine	2.16	***
Choline	1.91	****
Creatine	-1.46	*
Creatine phosphate	1.32	***
Fumarate	-1.86	****
Glucose	-1.47	*
Glutamate	-2.19	***
Glutamine	1.36	**
GSH	-1.34	**
GTP	-1.49	***
myo-Inositol	-4.57	****
NAD^+	-4.06	****
NADPH	-3.20	****
Niacinamide	5.19[2]	****
O-phosphocholine	-9.51	***
O-phosphoethanolamine	2.03	***
Proline	-1.39	*
Propionate	1.39	**
Quinolinate	25.90[2]	****
Serine	1.49	**
Succinate	1.48	*
Taurine	1.45	***
UMP	-1.61	****
Valine	1.18	*

[1] Metabolites were selected based upon fold change (FC) and statistical significance of intracellular metabolite concentrations between M1 and M2a MΦs; (nmol/mg protein; calculated from metabolite spectral fitting using the Chenomx NMR Suite software and the standard Chenomx 600 MHz metabolite library). Fold changes were calculated relative to M2a MΦs, whereby increases are shown as positive values and decreases are shown as negative values. Statistical significance (*p*) was measured using two-tailed unpaired parametric *t*-tests with Welch's correction, whereby *, $p < 0.05$; **, $p < 0.01$; ***, $p < 0.001$; ****, $p < 0.0001$. Abbreviations denote: ADP, adenosine diphosphate; AMP, adenosine monophosphate; ATP, adenosine triphosphate; GSH, reduced glutathione; GTP, guanosine triphosphate; NAD^+, nicotinamide adenine dinucleotide; NADPH, reduced nicotinamide adenine dinucleotide phosphate; UMP, uridine monophosphate. [2] Fold change (FC) was calculated using limit of detection (LOD) values (see Table S1) for MΦ activation state in which a given metabolite was not detected.

Table S3. Relative fold change expression of select genes in bone marrow-derived murine MΦs upon differential stimuli.[1]

Gene	Stimuli	Time (hr)			
		2	6	12	24
Agxt2	IFN-γ	-1.03	-1.24	-1.27	1.18
	IL-4	1.05	-1.05	1.23	-1.39
	LPS	1.01	1.28	1.56	1.17
Bdh1	IFN-γ	-1.37	-1.93	-1.47	-1.56
	IL-4	-1.01	-1.17	1.12	1.02
	LPS	1.06	1.03	-1.68	1.18
*Bdh1**	IFN-γ	1.47	1.21	1.25	1.27
	IL-4	1.08	-1.02	1.04	-1.08
	LPS	1.23	-1.07	-1.05	1.16
Chkα	IFN-γ	2.25	1.05	-1.39	-1.49
	IL-4	-1.55	-1.14	-1.54	1.42
	LPS	-2.22	-1.78	-1.88	-1.08
Chkβ	IFN-γ	-1.25	-1.37	-1.54	-1.54
	IL-4	1.04	-1.43	-1.15	-1.15
	LPS	-1.22	-1.74	-2.19	-2.03
Etnk1	IFN-γ	3.16	3.60	2.13	3.47
	IL-4	1.55	2.08	1.82	-1.03
	LPS	1.44	2.37	2.58	1.55
Gmppa	IFN-γ	1.12	-1.37	-1.20	1.01
	IL-4	1.30	-1.18	1.14	1.51
	LPS	1.19	-1.10	-1.57	1.12
Gmppb	IFN-γ	1.24	1.10	2.89	2.09
	IL-4	-1.48	-1.20	1.64	1.11
	LPS	1.55	1.31	2.32	2.44
Oxct1	IFN-γ	1.19	1.15	1.58	-1.44
	IL-4	1.08	1.86	2.17	2.03
	LPS	-1.29	-1.35	-1.41	-1.46
Oxct2	IFN-γ	1.27	1.55	1.18	1.24
	IL-4	1.26	1.44	1.25	-1.45
	LPS	1.05	1.13	1.06	1.10
Pcyt1a	IFN-γ	-1.68	-1.37	-1.66	-2.22
	IL-4	1.33	1.59	1.26	1.24
	LPS	-1.47	-2.59	-2.63	-2.85
Pcyt2	IFN-γ	1.87	-1.54	-1.71	1.15
	IL-4	2.36	1.08	1.55	3.07
	LPS	1.24	-1.54	-1.31	-1.17
Pmm1	IFN-γ	-1.12	-2.74	-3.45	-3.66
	IL-4	1.40	2.06	1.77	1.22
	LPS	1.11	-1.54	-3.83	-1.63
Pmm2	IFN-γ	2.71	1.63	1.27	2.41
	IL-4	1.90	2.29	1.76	2.20
	LPS	1.43	1.07	1.39	1.63

[1] Fold changes were calculated using supplementary microarray data for *Agxt2*, *Bdh1*, *Bdh1**, *Chkα*, *Chkβ*, *Etnk1*, *Gmppa*, *Gmppb*, *Oxct1*, *Oxct2*, *Pcyt1a*, *Pcyt2*, *Pmm1*, and *Pmm2* genes, with UNIQIDs of mMA035026, mMR028403, mMC011803, mMC011615, mMA034846, mMR029849, mMR028432, mMC009282, mMC013095, mMC019363, mMC002638, mMC007591, mMC004009, and mMA034923, respectively, relative to control MΦs (data derived from Zhang *et al.*) [39]. Increases are shown as positive values and decreases are shown as negative values. Abbreviations denote: *Agxt2*, alanine-glyoxylate aminotransferase 2; *Bdh1*, 3-hydroxybutyrate dehydrogenase 1; *Chkα*, choline kinase α; *Chkβ*, choline kinase β; *Etnk1*, ethanolamine kinase 1; *Gmppa*, GDP-mannose pyrophosphorylase A; *Gmppb*, GDP-mannose pyrophosphorylase B; IFN-γ, interferon-γ; IL-4, interleukin-4; LPS, lipopolysaccharide; *Ocxt1/2*, 3-oxoacid Co-A transferase 1/2; *Pcyt1a*, phosphate cytidylyltransferase 1α; *Pcyt2*, phosphate cytidylyltransferase 2; *Pmm1*, phosphomannomutase 1; *Pmm2*, phosphomannomutase 2.

Funding

This work was supported in part by the Montana Research Initiative Grant No. 51040-MUSRI2015-03, NIH Grant No. DK R01 DK1147-01A1 (A.L.F., W.J.K., B.E., B.T., V.C.), NIH Grant No. 1KO1GM103821-04 (M.C.B.A.), and funding from MSU's Vice President for Research and Economic Development's office (V.C.). Sage M. Schiller was supported by an INBRE undergraduate student research fellowship, provided by the National Institute of General Medical Sciences of the National Institutes of Health at MSI, under Award No. P20GM103474. Amanda L. Fuchs acknowledges support from the Kopriva graduate fellowship program of Montana State University's College of Letters and Sciences. The 1D ^{1}H NMR spectra included in this manuscript were recorded on a Bruker AVANCE III 600 MHz NMR spectrometer at MSU's NMR Center. Funding for the NMR instrument and corresponding upgrade was provided by the NIH SIG program (Grant No. 1S10RR13878 and 1S10RR026659). Support for MSU's NMR Center and new NMR spectrometer has been provided by the National Science Foundation (Grant No. NSF-MRI:DBI-1532078), the Murdock Charitable Trust Foundation (Grant No. 2015066:MNL), and MSU's Vice President for Research and Economic Development's office.

Acknowledgements

We thank Dr. Diane Bimczok and Mandi Roe for MACS training and guidance in primary human monocyte cell culture, and Larissa Jackiw, FACS/Flow Core Supervisor, for flow cytometry training and assistance.

Conflicts of Interest

The authors declare no conflict of interest. The funders had no role in study design, data collection and analysis, decision to publish, or preparation of the manuscript.

References

1. O'Neill, L.A.; Pearce, E.J. Immunometabolism governs dendritic cell and macrophage function. J. Exp. Med. 2016, 213, 15-23. doi: 10.1084/jem.20151570

2. Buck, M.D.; Sowell, R.T.; Kaech, S.M.; Pearce, E.L. Metabolic instruction of immunity. Cell 2017, 169, 570-586. doi: 10.1016/j.cell.2017.04.004

3. Nicholson, J.K.; Lindon, J.C. Systems biology: metabonomics. Nature 2008, 455, 1054-1056. doi: 10.1038/4551054a

4. Fiehn, O. Metabolomics—the link between genotypes and phenotypes. Plant Mol Biol. 2002, 48, 155-171. doi: 10.1007/978-94-010-0448-0_11

5. Tannahill, G.M.; Curtis, A.M.; Adamik, J.; Palsson-McDermott, E.M.; McGettrick, A.F.; Goel, G.; Frezza, C.; Bernard, N.J.; Kelly, B.; Foley, N.H.; et al. Succinate is an inflammatory signal that induces IL-1β through HIF-1α. Nature 2013, 496, 238-242. doi: 10.1038/nature11986

6. Lampropoulou, V.; Sergushichev, A.; Bambouskova, M.; Nair, S.; Vincent, E.E.; Loginicheva, E.; Cervantes-Barragan, L.; Ma, X.; Huang, S.C.; Griss, T.; et al. Itaconate links inhibition of succinate dehydrogenase with macrophage metabolic remodeling and regulation of inflammation. Cell Metab. 2016, 24, 158-166. doi: 10.1016/j.cmet.2016.06.004

7. Vats, D.; Mukundan, L.; Odegaard, J.I.; Zhang, L.; Smith, K.L.; Morel, C.R.; Wagner, R.A.; Greaves, D.R.; Murray, P.J.; Chawla, A. Oxidative metabolism and PGC-1β attenuate macrophage-mediated inflammation. Cell Metab. 2006, 4, 13-24. doi: 10.1016/j.cmet.2006.05.011

8. Galván-Peña, S.; O'Neill, L.A. Metabolic reprogramming in macrophage polarization. Front. Immunol. 2014, 5, 420. doi: 10.3389/fimmu.2014.00420

9. Jha, A.K.; Huang, S.C.; Sergushichev, A.; Lampropoulou, V.; Ivanova, Y.; Loginicheva, E.; Chmielewshi, K.; Stewart, K.M.; Ashall, J.; Everts, B.; et al. Network integration of parallel metabolic and transcriptional data reveals metabolic modules that regulate macrophage polarization. Immunity 2015, 42, 419-430. doi: 10.1016/j.immuni.2015.02.005

10. Murray, P.J.; Wynn, T.A. Protective and pathogenic functions of macrophage subsets. Nat. Rev. Immunol. 2011, 11, 723-737. doi: 10.1038/nri3073

11. Ginhoux, F.; Schultze, J.L.; Murray, P.J.; Ochando, J.; Biswas, S.K. New insights into the multidimensional concept of macrophage ontogeny, activation and function. Nat. Immunol. 2016, 17, 34-40. doi: 10.1038/ni.3324

12. Odegaard, J.I.; Ricardo-Gonzalez, R.R.; Goforth, M.H.; Morel, C.R.; Subramanian, V.; Mukundan, L.; Red Eagle, A.; Vats, D.; Brombacher, F.; Ferrante, A.W.; et al. Macrophage-specific PPARγ controls alternative activation and improves insulin resistance. Nature 2007, 447, 1116-1120. doi: 10.1038/nature05894

13. Woollard, K.J.; Geissmann, F. Monocytes in atherosclerosis: subsets and functions. Nat. Rev. Cardiol. 2010, 7, 77-86. doi: 10.1038/nrcardio.2009.228

14. Platt, A.M.; Bain, C.C.; Bordon, Y.; Sester, D.P.; Mowat, A.M. An independent subset of TLR expressing CCR2-dependent macrophages promotes colonic inflammation. J. Immunol. 2010, 184, 6843-6854. doi: 10.4049/jimmunol.0903987

15. Kamada, N.; Hisamatsu, T.; Okamoto, S.; Chinen, H.; Kobayashi, T.; Sato, T.; Sakuraba, A.; Kitazume, M.T.; Sugita, A.; Koganei, K.; et al. Unique CD14+ intestinal macrophages contribute to the pathogenesis of Crohn disease via IL-23/IFN-γ axis. J. Clin. Invest. 2008, 118, 2269-2280. doi: 10.1172/JCI34610

16. Kim, J.W.; Tchernyshyoc, I.; Semenza, G.L.; Dang, C.V. HIF-1-mediated expression of pyruvate dehydrogenase kinase: a metabolic switch required for cellular adaptation to hypoxia. Cell Metab. 2006, 3, 177-185. doi: 10.1016/j.cmet.2006.02.002

17. Diskin, C.; Pålsson-McDermott, E.M. Metabolic modulation in macrophage effector function. Front. Immunol. 2018, 9, 270. doi: 10.3389/fimmu.2018.00270

18. Pavlou, S.; Wang, L.; Xu, H.; Chen, M. Higher phagocytic activity of thioglycollate-elicited peritoneal macrophages is related to metabolic status of the cells. J. Inflamm. (Lond) 2017, 14, 4. doi: 10.1186/s12950-017-0151-x

19. Freemerman, A.J.; Johnson, A.R.; Sacks, G.N.; Milner, J.J.; Kirk, E.L.; Troester, M.A.; Macintyre, A.N.; Goraksha-Hicks, P.; Rathmell, J.C.; Makowski, L. Metabolic reprogramming of macrophages: glucose transporter 1 (GLUT1)-mediated glucose metabolism drives a proinflammatory phenotype. J. Biol. Chem. 2014, 289, 7884-7896. doi: 10.1074/jbc.M113.522037

20. Michl, J.; Ohlbaum, D.J.; Silverstein, S.C. 2-Deoxyglucose selectively inhibits Fc and complement receptor-mediated phagocytosis in mouse peritoneal macrophages II. Dissociation of the inhibitory effects of 2-deoxyglucose on phagocytosis and ATP generation. J. Exp. Med. 1976, 144, 1484-1493. doi: 10.1084/jem.144.6.1484

21. Rőszer, T. Understanding the mysterious M2 macrophage through activation markers and effector mechanisms. Mediators Inflamm. 2015, 2015, 816460. doi: 10.1155/2015/816460

22. Huang, S.C.; Everts, B.; Ivanova, Y.; O'Sullivan, D.; Nascimento, M.; Smith, A.M.; Beatty, W.; Love-Gregory, L.; Lam, W.Y.; O'Neill, C.M.; et al. Cell-intrinsic lysosomal lipolysis is essential for alternative activation of macrophages. Nat. Immunol. 2014, 15, 846-855. doi: 10.1038/ni.2956

23. Fang, F.C.; Nathan, C.F. Man is not a mouse: reply. J. Leukoc. Biol. 2007, 81, 580. doi: 10.1189/jlb.1206715

24. Thomas, A.C.; Mattila, J.T. "Of mice and men": arginine metabolism in macrophages. Front. Immunol. 2014, 5, 479. doi: 10.3389/fimmu.2014.00479

25. Martinez, F.O.; Helming, L.; Milde, R.; Varin, A.; Melgert, B.N.; Draijer, C.; Thomas, B.; Fabbri, M.; Crawshaw, A.; Ho, L.P.; et al. Genetic programs expressed in resting and IL-4 alternatively activated mouse and human macrophages: similarities and differences. Blood 2013, 121, e57-69. doi: 10.1182/blood-2012-06-436212

26. León, Z.; García-Cañaveras, J.C.; Donato, M.T.; Lahoz, A. Mammalian cell metabolomics: experimental design and sample preparation. Electrophoresis 2013, 34, 2762-2775. doi: 10.1002/elps.201200605

27. Wishart, D.S. Quantitative metabolomics using NMR. Trends Analyt. Chem. 2008, 27, 228-237. doi: 10.1016/j.trac.2007.12.001

28. Van den Bossche, J.; Baardman, J.; de Winther, M.P. Metabolic characterization of polarized M1 and M2 bone marrow-derived macrophages using real-time extracellular flux analysis. J. Vis. Exp. 2015, 105, e53424. doi: 10.3791/53424

29. Feng, J.; Li, L.; Ou, Z.; Li, Q.; Gong, B.; Zhao, Z.; Qi, W.; Zhou, T.; Zhong, J.; Cai, W.; et al. IL-25 stimulates M2 macrophage polarization and thereby promotes mitochondrial respiratory capacity and lipolysis in adipose tissues against obesity. Cell Mol. Immunol. 2018, 15, 493-505. doi: 10.1038/cmi.2016.71

30. Feingold, K.R.; Shigenaga, J.K.; Kazemi, M.R.; McDonald, C.M.; Patzek, S.M.; Cross, A.S.; Moser, A.; Grunfeld, C. Mechanisms of triglyceride accumulation in activated macrophages. J. Leukoc. Biol. 2012, 92, 829-839. doi: 10.1189/jlb.1111537

31. Longo, D.M.; Louie, B.; Wang, E.; Pos, Z.; Marincola, F.M.; Hawtin, R.E.; Cesano, A. Inter-donor variation in cell subset specific immune signaling responses in healthy individuals. Am. J. Clin. Exp. Immunol. 2012, 1, 1-11. PMCID: PMC3714187

32. Carpenter, D.J.; Granot, T.; Matsuoka, N.; Senda, T.; Kumar, B.V.; Thome, J.J.C.; Gordon, C.L.; Miron, M.; Weiner, J.; Connors, T.; et al. Human immunology studies using organ donors: impact of clinical variations on immune parameters in tissues and circulation. Am. J. Transplant. 2018, 18, 74-88. doi: 10.1111/ajt.14434

33. Tedesco, S.; De Majo, F.; Kim, J.; Trenti, A.; Trevisi, L.; Paolo Fadini, G.; Bolego, C.; Zandstra, P.W.; Cignarella, A.; Vitiello, L. Convenience versus biological significance: are PMA-differentiated THP-1 cells a reliable substitute for blood-derived macrophages when studying in vitro polarization? Front. Pharmacol. 2018, 9, 71. doi: 10.3389/fphar.2018.00071

34. Gibellini, F.; Smith, T.K. The Kennedy pathway--de novo synthesis of phosphatidylethanolamine and phosphatidylcholine. IUBMB Life 2010, 62, 414-428. doi: 10.1002/iub.337

35. Huang, S.C.; Smith, A.M.; Everts, B.; Colonna, M.; Pearce, E.L.; Schilling, J.D.; Pearce, E.J. Metabolic reprogramming mediated by the mTORC2-IRF4 signaling axis is essential for macrophage alternative activation. Immunity 2016, 45, 817-830. doi: 10.1016/j.immuni.2016.09.016

36. Tavakoli, S.; Short, J.D.; Downs, K.; Nguyen, H.N.; Lai, Y.; Zhang, W.; Jerabek, P.; Goins, B.; Sadeghi, M.M.; Asmis, R. Differential regulation of macrophage glucose metabolism by macrophage colony-stimulating factor and granulocyte-macrophage colony-stimulating factor: implications for ^{18}F FDG PET imaging of vessel wall inflammation. Radiology 2017, 283, 87-97. doi: 10.1148/radiol.2016160839

37. Rodríguez-Prados, J.C.; Través, P.G.; Cuenca, J.; Rico, D.; Aragonés, J.; Martín-Sanz, P.; Cascante, M.; Boscá, L. Substrate fate in activated macrophages: a comparison between innate, classic, and alternative activation. J. Immunol. 2010, 185, 605-614. doi: 10.4049/jimmunol.0901698

38. Sica, A.; Mantovani, A. Macrophage plasticity and polarization: In vivo veritas. J. Clin. Invest. 2012, 122, 787-795. doi: 10.1172/JCI59643

39. Zhang, S.; Kim, C.C.; Batra, S.; McKerrow, J.H.; Loke, P. Delineation of diverse macrophage activation programs in response to intracellular parasites and cytokines. PLoS Negl. Trop. Dis. 2010, 4, e648. doi: 10.1371/journal.pntd.0000648

40. Ryan, D.G.; O'Neill, L.A.J. Krebs cycle rewired for macrophage and dendritic cell effector functions. FEBS Lett. 2017, 591, 2992-3006. doi: 10.1002/1873-3468.12744

41. Meiser, J.; Krämer, L.; Sapcariu, S.C.; Battello, N.; Ghelfi, J.; D'Herouel, A.F.; Skupin, A.; Hiller, K. Pro-inflammatory macrophages sustain pyruvate oxidation

through pyruvate dehydrogenase for the synthesis of itaconate and to enable cytokine expression. J. Biol. Chem. 2016, 291, 3932-3946. doi: 10.1074/jbc.M115.676817

42. Liu, P.S.; Wang, H.; Li, X.; Chao, T.; Teav, T.; Christen, S.; Di Conza, G.; Cheng, W.C.; Chou, C.H.; Vavakova, M.; et al. α-ketoglutarate orchestrates macrophage activation through metabolic and epigenetic reprogramming. Nat. Immunol. 2017, 18, 985-994. doi: 10.1038/ni.3796

43. Vander Heiden, M.G.; Cantley, L.C.; Thompson, C.B. Understanding the Warburg effect: The metabolic requirements of cell proliferation. Science. 2009, 324, 1029-1033. doi: 10.1126/science.1160809

44. Warburg, O.; Wind, F.; Negelein, E. The metabolism of tumors in the body. J. Gen. Physiol. 1927, 8, 519-530. doi: 10.1085/jgp.8.6.519

45. Warburg, O. On the origin of cancer cells. Science. 1956, 123, 309-314. doi: 10.1126/science.123.3191.309

46. Cheng, T.; Sudderth, J.; Yang, C.; Mullen, A.R.; Jin, E.S.; Matés, J.M.; DeBerardinis, R.J. Pyruvate carboxylase is required for glutamine-in-dependent growth of tumor cells. Proc. Natl. Acad. Sci. USA. 2011, 108, 8674-8679. doi: 10.1073/pnas.1016627108

47. Nakaya, M.; Xiao, Y.; Zhou, X.; Chang, J.H.; Chang, M.; Cheng, X.; Blonska, M.; Lin, X.; Sun, S.C. Inflammatory T cell responses rely on amino acid transporter ASCT2 facilitation of glutamine uptake and mTORC1 kinase activation. Immunity. 2014, 40, 692-705. doi: 10.1016/j.immuni.2014.04.007

48. Mills, E.L.; Ryan, D.G.; Prag, H.A.; Dikovskaya, D.; Menon, D.; Zaslona, Z.; Jedrychowski, M.P.; Costa, A.S.H.; Higgins, M.; Hams, E.; et al. Itaconate is an anti-inflammatory metabolite that activates Nrf2 via alkylation of KEAP1. Nature 2018, 556, 113-117. doi: 10.1038/nature25986

49. Guzy, R.D.; Sharma, B.; Bell, E.; Chandel, N.S.; Schumacker, P.T. Loss of SdhB, but not SdhA, subunit of complex II triggers reactive oxygen species-dependent hypoxia-inducible factor activation and tumorigenesis. Mol. Cell Biol. 2008, 28, 718-731. doi: 10.1128/MCB.01338-07

50. Arts, R.J.; Novakovic, B.; Ter Horst, R.; Carvalho, A.; Bekkering, S.; Lachmandas, E.; Rodrigues, F.; Silvestre, R.; Cheng, S.C.; Wang, S.Y.; et al. Glutaminolysis and fumarate accumulation integrate immunometabolic and epigenetic programs in trained immunity. Cell Metab. 2016, 24, 807-819. doi:10.1016/j.cmet.2016.10.008

51. Quintin, J.; Saeed, S.; Martens, J.H.A.; Giamarellos-Bourboulis, E.J.; Ifrim, D.C.; Logie, C.; Jacobs, L.; Jansen, T.; Kullberg, B.J.; Wijmenga, C.; et al. Candida albicans infection affords protection against reinfection via functional reprogramming of monocytes. Cell Host Microbe. 2012, 12, 223-232, doi:10.1016/j.chom.2012.06.006

52. Saeed, S.; Quintin, J.; Kerstens, H.H.; Rao, N.A.; Aghajanirefah, A.; Matarese, F.; Cheng, S.C.; Ratter, J.; Berentsen, K.; van der Ent, M.A.; et al. Epigenetic programming of monocyte-to-macrophage differentiation and trained innate immunity. Science. 2014, 345, 1251086. doi:10.1126/science.1251086

53. Ghoreschi, K.; Brück, J.; Kellerer, C.; Deng, C.; Peng, H.; Rothfuss, O.; Hussain, R.Z.; Gocke, A.R.; Respa, A.; Glocova, I.; et al. Fumarates improve psoriasis and multiple sclerosis by inducing type II dendritic cells. J. Exp. Med. 2011, 208, 2291-2303. doi:10.1084/jem.20100977

54. Tan, H.; Wang, N.; Li, S.; Hong, M.; Wang, X.; Feng, Y. The reactive oxygen species in macrophage polarization: reflecting its dual role in progression and treatment of human diseases. Oxid. Med. Cell. Longev. 2016, 2016, 2795090. doi: 10.1155/2016/2795090

55. Piao, S.; Cha, Y.N.; Kim, C. Taurine chloramine protects RAW 264.7 macrophages against hydrogen peroxide-induced apoptosis by increasing antioxidants. J. Clin. Biochem. Nutr. 2011, 49, 50-56. doi: 10.3164/jcbn.10-120

56. Ray, P.D.; Huang, B.W.; Tsuji, Y. Reactive oxygen species (ROS) homeostasis and redox regulation in cellular signaling. Cell. Signal. 2012, 24, 981-990. doi: 10.1016/j.cellsig.2012.01.008

57. He, C.; Ryan, A.J.; Murthy, S.; Carter, A.B. Accelerated development of pulmonary fibrosis via Cu,Zn-superoxide dismutase-induced alternative activation of macrophages. J. Biol. Chem. 2013, 288, 20745-20757. doi: 10.1074/jbc.M112.410720

58. Marcinkiewicz, J.; Kontny, E. Taurine and inflammatory diseases. Amino Acids 2014, 46, 7-20. doi: 10.1007/s00726-012-1361-4

59. Snider, S.A.; Margison, K.D.; Ghorbani, P.; LeBlond, N.D.; O'Dwyer, C.; Nunes, J.R.C.; Nguyen, T.; Xu, H.; Bennett, S.A.L.; Fullerton, M.D. Choline transport links macrophage phospholipid metabolism and inflammation. J. Biol. Chem. 2018, 293, 11600-11611. doi: 10.1074/jbc.RA118.003180

60. Mehta, A.K.; Singh, B.P.; Arora, N.; Gaur, S.N. Choline attenuates inflammation and suppresses oxidative stress in patients with asthma. Immunobiology 2010, 215, 527-534. doi: 10.1016/j.imbio.2009.09.004

61. Richter, K.; Mathes, V.; Fronius, M.; Althaus, M.; Hecker, A.; Krasteva-Christ, G.; Padberg, W.; Hone, A.J.; McIntosh, J.M.; Zakrzewicz, A.; et al. Phosphocholine – an agonist of metabotropic but not of ionotropic functions of α9-containing nicotinic acetylcholine receptors. Sci. Rep. 2016, 6, 28660. doi: 10.1038/srep28660

62. Garcia, M.; Mamedova, L.K.; Barton, B.; Bradford, B.J. Choline regulates the function of bovine immune cells and alters the mRNA abundance of enzymes and receptors involved in its metabolism in vitro. Front. Immunol. 2018, 9, 2448. doi: 10.3389/fimmu.2018.02448

63. Gohil, V.M.; Zhu, L.; Baker, C.D.; Cracan, V.; Yaseen, A.; Jain, M.; Clish, C.B.; Brookes, P.S.; Bakovic, M.; Mootha, V.K. Meclizine inhibits mitochondrial respiration through direct targeting of cytosolic phosphoethanolamine metabolism. J. Biol. Chem. 2013, 288, 35387-35395. doi: 10.1074/jbc.M113.489237

64. Guillemin, G.J.; Smith, D.G.; Smythe, G.A.; Armati, P.J.; Brew, B.J. Expression of the kynurenine pathway enzymes in human microglia and macrophages. Adv. Exp. Med. Biol. 2003, 527, 105-112. doi: 10.1007/978-1-4615-0135-0_12

65. Sävman, K.; Heyes, M.P.; Svedin, P.; Karlsson, A. Microglia/macrophage-derived inflammatory mediators galectin-3 and quinolinic acid are elevated in cerebrospinal fluid from newborn infants after birth asphyxia. Transl. Stroke Res. 2013, 4, 228-235. doi: 10.1007/s12975-012-0216-3

66. Braidy, N.; Grant, R.; Adams, S.; Brew, B.J.; Guillemin, G.J. Mechanism for quinolinic acid cytotoxicity in human astrocytes and neurons. Neurotox. Res. 2009, 16, 77-86. doi: 10.1007/s12640-009-9051-z

67. Pláteník, J.; Stopka, P.; Vejrazka, M.; Stípek, S. Quinolinic acid-iron(II) complexes: slow autoxidation, but enhanced hydroxyl radical production in the Fenton reaction. Free Radic. Res. 2001, 34, 445-459. doi: 10.1080/10715760100300391

68. Minhas, P.S.; Liu, L.; Moon, P.K.; Joshi, A.U.; Dove, C.; Mhatre, S.; Contrepois, K.; Wang, Q.; Lee, B.A.; Coronado, M.; et al. Macrophage de novo NAD^+ synthesis specifies immune function in aging and inflammation. Nat. Immunol. 2019, 20, 50-63. doi: 10.1038/s41590-018-0255-3

69. García-Cañaveras, J.C.; López, S.; Castell, J.V.; Donato, M.T.; Lahoz, A. Extending metabolome coverage for untargeted metabolite profiling of adherent cultured hepatic cells. Anal. Bioanal. Chem. 2016, 408, 1217-1230. doi: 10.1007/s00216-015-9227-8

70. Ammons, M.C.; Tripet, B.P.; Carlson, R.P.; Kirker, K.R.; Gross, M.A.; Stanisich, J.J.; Copié, V. Quantitative NMR metabolite profiling of methicillin-resistant and methicillin-susceptible Staphylococcus aureus discriminates between biofilm and planktonic phenotypes. J. Proteome Res. 2014, 13, 2973-2985. doi: 10.1021/pr500120c

71. Fathi, F.; Brun, A.; Rott, K.H.; Falco Cobra, P.; Tonelli, M.; Eghbalnia, H.R.; Caviedes-Vidal, E.; Karasov, W.H.; Markley, J.L. NMR-based identification of metabolites in polar and non-polar extracts of avian liver. Metabolites 2017, 7, 61. doi: 10.3390/metabo7040061

72. Ramm Sander, P.; Peer, M.; Grandl, M.; Bogdahn, U.; Schmitz, G.; Robert Kalbitzer, H. NMR spectroscopy of macrophages loaded with native, oxidized or enzymatically degraded lipoproteins. PLoS One 2013, 8, e56360. doi: 10.1371/journal.pone.0056360

73. Weaver, A.J.; Peters, T.R.; Tripet, B.; Van Vuren, A.; Rakesh; Lee, R.E.; Copié, V.; Teintze, M. Exposure of methicillin-resistant Staphylococcus aureus to low levels of the antibacterial THAM-3ΦG generates a small colony drug-resistant phenotype. Sci. Rep. 2018, 8, 9850. doi: 10.1038/s41598-018-28283-3

74. Fuchs, A.L.; Weaver, A.J. Jr.; Tripet, B.P.; Ammons, M.C.B.; Teintze, M, Copié, V. Characterization of the antibacterial activity of Bald's eyesalve against drug resistant Staphylococcus aureus and Pseudomonas aeruginosa. PLoS One 2018, 13, e0208108. doi: 10.1371/journal.pone.0208108

75. Mercier, P.; Lewis, M.J.; Chang, D.; Baker, D.; Wishart, D.S. Towards automatic metabolomic profiling of high-resolution one-dimensional proton NMR spectra. J. Biomol. NMR 2011, 49, 307-323. doi: 10.1007/s10858-011-9480-x

76. Emwas, A.H.; Saccenti, E.; Gao, X.; McKay, R.T.; Dos Santos, V.A.P.M.; Roy, R.; Wishart, D.S. Recommended strategies for spectral processing and post-processing of 1D 1H-NMR data of biofluids with a particular focus on urine. Metabolomics 2018, 14, 31. doi: 10.1007/s11306-018-1321-4

77. Xia, J.; Wishart, D.S. Metabolomic data processing, analysis, and interpretation using MetaboAnalyst. Curr. Protoc. Bioinformatics 2011, 34, 14.10.1-14.10.48. doi: 10.1002/0471250953.bi1410s34

78. Araníbar, N.; Ott, K.H.; Roongta, V.; Mueller, L. Metabolomic analysis using optimized NMR and statistical methods. Anal. Biochem. 2006, 355, 62-70. doi: 10.1016/j.ab.2006.04.014

79. Weljie, A.M.; Newton, J.; Mercier, P.; Carlson, E.; Slupsky, C.M. Targeted profiling: quantitative analysis of 1H NMR metabolomics data. Anal. Chem. 2006, 78, 4430-4442. doi: 10.1021/ac060209g

80. Chong, J.; Soufan, O.; Li, C.; Caraus, I.; Li, S.; Bourgue, G.; Wishart, D.S.; Xia, J. MetaboAnalyst 4.0: towards more transparent and integrative metabolomics analysis. Nucleic Acids Res. 2018, 46, W486-W494. doi: 10.1093/nar/gky310

CHAPTER THREE

PSEUDOMONAS AERUGINOSA PLANKTONIC- AND BIOFILM-CONDITIONED MEDIA ELICIT DIVERGENT RESPONSES IN HUMAN MACROPHAGES

Contribution of Authors and Co-Authors

Manuscript in Chapter 3

Author: Amanda L. Fuchs

Contributions: Conceptualized the study, developed methodology, validated and visualized the data, conducted formal analysis and investigation, curated the data, wrote the original manuscript draft, reviewed and edited the manuscript, and supervised and administered the project.

Author: Sage M. Schiller

Contributions: Validated the data, conducted investigation, and reviewed and edited the manuscript.

Co-Author: Isaac R. Miller

Contributions: Validated the data, conducted formal analysis and investigation, curated the data, and reviewed and edited the manuscript.

Co-Author: Mary Cloud B. Ammons

Contributions: Conceptualized the study, developed methodology, provided resources, reviewed and edited the manuscript, supervised and administered the project, and acquired funding.

Co-Author: Brian Eilers

Contributions: Reviewed and edited the manuscript, and supervised the project.

Co-Author: Brian Tripet

Contributions: Developed methodology, reviewed and edited the manuscript, and supervised and administered the project.

Contribution of Authors and Co-Authors – Continued

Co-Author: Valérie Copié

Contributions: Conceptualized the study, provided software and resources, wrote the original manuscript draft, reviewed and edited the manuscript, supervised and administered the project, and acquired funding.

Manuscript Information Page

Amanda L. Fuchs, Sage M. Schiller, Isaac R. Miller, Mary Cloud B. Ammons, Brian Eilers, Brian Tripet, Valérie Copié

Journal Name: PLoS Pathogens

Status of Manuscript:
__x__ Prepared for submission to a peer-reviewed journal
_____ Officially submitted to a peer-reviewed journal
_____ Accepted by a peer-reviewed journal
_____ Published in a peer-reviewed journal

Publisher: PLoS

PSEUDOMONAS AERUGINOSA PLANKTONIC- AND BIOFILM-CONDITIONED MEDIA ELICIT DIVERGENT RESPONSES IN HUMAN MACROPHAGES

Amanda L. Fuchs[1*], Sage M. Schiller[1], Isaac R. Miller[1,#a], Mary Cloud B. Ammons[1,#b], Brian Eilers[1], Brian Tripet[1], Valérie Copié[1*]

[1]Department of Chemistry and Biochemistry, Montana State University, Bozeman, Montana, United States of America
[#a]Current Address: Department of Microbiology and Immunology, Montana State University, Bozeman, Montana, United States of America
[#b]Current Address: Boise Veterans Medical Center, Idaho Veterans Research and Education Foundation, Boise, Idaho, United States of America

[*] Corresponding authors
E-mail: vcopie@montana.edu (VC) and afuchs03143@gmail.com (ALF)

Abstract

Macrophages (MΦs) are innate immune cells that are nearly ubiquitous throughout human bodily tissues, where they orchestrate innate and adaptive immune responses to maintain cellular homeostasis. They have the capacity to display a spectrum of functional phenotypes due to the presence of different microenvironmental cues, particularly soluble bacterial secretory products. Recent evidence has emerged which demonstrates that metabolism supports MΦ function and plasticity, in addition to energy and biomolecular precursor production. In this study, 1D ^{1}H NMR-based metabolomics was used to determine the metabolic pathways that are modulated following primary human monocyte-derived MΦ exposure to *P. aeruginosa* planktonic- and biofilm-conditioned media (PCM and BCM). Metabolic profiling of PCM- and BCM-exposed MΦs indicated a significant depletion of intracellular glucose without equivalent

elevation of downstream glycolytic products, including pyruvate and lactic acid. These metabolic patterns also suggest that PCM- and BCM-exposed MΦs divert glycolytic intermediates towards inositol phosphate metabolism. Altogether, our study reveals novel findings concerning the metabolic modulation of human MΦs following exposure to secretory microbial products and contributes additional knowledge to the field of immunometabolism in MΦs.

Introduction

The host innate immune system provides the initial line of defense against invasive microbes and infection [1]. Macrophages (MΦs) are a type of phagocytic innate immune cell, which are crucial for host defense processes, including pathogen and infection clearance [2], and there is substantial evidence that MΦs are key regulators during wound healing [3,4]. Bacterial infection induces the migration and activation of immune cells, including neutrophils and monocytes, as a result of cytokine and chemokine secretion at the site of infection [5]. In acute wounds, MΦs phagocytose debris, bacteria, and apoptotic host cells from the wound bed during an inflammatory response before the subsequent proliferative phase and tissue regeneration can commence, which is marked by a phenotypic transition of MΦs from pro-inflammatory, M1 MΦs, to anti-inflammatory, M2 MΦs [6,7]. Progression from inflammation into the proliferative and remodeling phases of healing does not readily occur in chronic wounds; consequently, there is a prolonged presence of M1 MΦs in the chronic wound bed, which may contribute to delayed tissue regeneration [8,9]. Investigating the molecular events

and biological processes that support persistent inflammation in chronic wounds may provide insight for the development of more effective therapeutic treatments for chronic wounds.

Biofilms are structured communities of bacterial cells encased in a secreted extracellular polymeric matrix, which adhere to abiotic or biological surfaces [10,11]. Bacteria within biofilms have been demonstrated to be phenotypically distinct from planktonic, or free-living, bacteria; in addition, they are inherently more resistant to antibiotics and host defense mechanisms than planktonic microbes [12,13]. Chronic wounds are particularly susceptible to bacterial infection and subsequent biofilm colonization of the wound bed due to inadequate blood flow, hypoxia [14], delayed re-epithelialization [15], and impaired host defense mechanisms [16,17]. A previous study has demonstrated that bacteria present within chronic wounds are predominantly biofilm, whereas acute wounds exhibit minimal biofilm content [18]. Furthermore, it has been shown that partial thickness porcine model wounds inoculated with a wound isolate bacterial strain display biofilm structure formation within 48 hours [19]. Biofilm challenged diabetic murine punch biopsy wounds exhibit delayed healing, prolonged inflammation, and extensive tissue necrosis compared to control wounds [20], which suggests that biofilm formation within wounds contributes to deferred healing and wound chronicity. Although biofilm colonization within chronic wounds has been well established, their interactions with host innate immune cells, which may support pathogenesis, remain uncharacterized.

While chronic wound biofilms are known to maintain a diverse flora of microbes,

the most prevalent bacteria in diabetic foot, venous leg, and pressure ulcers include *Staphylococcus*, *Pseudomonas*, *Peptoniphilus*, *Enterobacter*, *Stenotrophomonas*, *Finegoldia*, and *Serratia* spp [21]. In addition, chronic wound microbiota varies markedly between different wound types and individuals, with most exhibiting colonization by multiple microbial species [21]. This complexity contributes to and often confounds the determination of a definitive host immune response. Consequently, in order to further understand and gain insight into the role of biofilms in pathogenesis, a single, opportunistic pathogen, *Pseudomonas aeruginosa*, was examined in our study. *P. aeruginosa* is a particularly virulent pathogen that is found predominantly in venous leg ulcers [21]. Moreover, chronic *P. aeruginosa* infection is correlated with increased morbidity, mortality, and worsened disease progression [22,23]. Previous studies have demonstrated that biofilm-conditioned media (BCM), containing soluble bacterial products, induces distinct morphological changes, diminished viability, apoptosis, and altered cytokine production in keratinocytes and fibroblasts, when compared to planktonic-conditioned media (PCM) [24,25].

Immunometabolism is a rapidly developing and expanding field at the forefront of immunology that studies the correlation between immune cell function and metabolism [26,27]. Metabolomics studies investigate the differential modulation of metabolic pathways in biological samples, such as cells, tissues, and biofluids, by identifying and quantitating perturbations in metabolite profiles [28,29]. Recent evidence has emerged indicating that metabolites, such as itaconate and succinate, can serve as signaling molecules, in addition to metabolic intermediates, that mediate the resultant functional

phenotype of MΦs [30,31]. Prior studies have shown that M1 and M2 MΦs demonstrate distinct metabolic patterns pertaining to central metabolism, including oxidative phosphorylation, fatty acid utilization, and glycolysis; therefore, immunometabolism is believed to be vital for competent functionality of immune cells [32-34]. However, further research is essential to better understand and elucidate the potential biochemical and functional differences concerning host MΦ responses to invasive pathogens, with specific emphasis placed upon discrepancies between planktonic versus biofilm challenge.

In the present study, we aimed to investigate the metabolic impact of *P. aeruginosa* planktonic- and biofilm-conditioned media exposure on primary human monocyte-derived resting (M0) MΦs, using $CD14^+$ magnetic-activated cell sorting (MACS) technology, *in vitro* MΦ differentiation and exposure schemes, 1D ^{1}H NMR metabolomics, metabolic profiling using Chenomx Suite software, and statistical analysis. M0 MΦs were differentiated from primary human monocytes using MΦ colony-stimulating factor (M-CSF) for 9 d before stimulation with PCM or BCM. Following exposure, both intra- and extracellular metabolites were extracted, 1D ^{1}H NMR data was acquired, and metabolite profiling of the extracts was conducted. Results from this study highlight metabolic pathways that are modulated in PCM- and BCM-exposed MΦs, relative to control MΦs, including glycolysis, lactic acid fermentation, and the tricarboxylic acid (TCA) cycle. The functional significance of the metabolic profiles found to be associated with PCM- and BCM-exposed MΦ phenotypes is also discussed.

Materials and Methods

Primary Human Monocyte Isolation

Heparinized whole blood was collected in accordance with proper guidelines, local Institutional Review Board (IRB) approval (ID# 00000799; Protocol #VC100118), and informed consent from healthy, adult donors in Bozeman, Montana, USA. A total of 5 donors, in the age range of 19 to 35 were included in this study, of whom 40% were female. Peripheral blood mononuclear cells (PBMCs) were isolated by centrifugation in lymphocyte separation media (Corning) at 800 x g for 25 min at room temperature. $CD14^+$ monocytes were isolated from PBMCs by MACS using CD14 human microbeads (Miltenyi Biotec), which resulted in an average purity of 97.1 ± 1.3% (Figure S2) when subjected to sorting on an LSR Fortessa cell analyzer (BD Biosciences).

In Vitro Differentiation of Primary Human Monocyte-Derived MΦs

To generate primary human monocyte-derived MΦs, $CD14^+$ monocytes were cultured in 25 cm2 tissue culture flasks (1×10^6 cells per mL; Falcon/Corning) in RPMI 1640 w/L-glutamine (Lonza) media, supplemented with 1 mM sodium pyruvate (Lonza), 1X MEM non-essential amino acids (NEAAs; Gibco), 10% (v/v) fetal bovine serum (FBS; ATCC), and 50 ng/mL recombinant human M-CSF (rHU-MCSF; PeproTech) for 9 d at 37 °C, 5% CO_2. Media and cytokines were replenished every 3 d. Following differentiation, phenotypic characterization of primary human monocyte-derived MΦs (MoMΦs) was conducted by flow cytometry (Figure S3).

Antibodies and Flow Cytometry

Primary human monocytes isolated using $CD14^+$ MACS technology were stained using anti-human antibodies directed against CD14 (BD Biosciences) and appropriate isotype controls. M0 MΦs were stained using anti-human antibodies directed against CD68, CD80, and CD163 (BD Biosciences) and appropriate isotype controls. Permeabilization of a cell subset was conducted using Cytofix/Cytoperm (BD Biosciences) for intracellular staining of CD68. Following staining, cells were resuspended in fluorescence-activated cell sorting (FACS) buffer for analysis on an LSR Fortessa Flow Cytometer (BD Biosciences). FACS data were analyzed using FCSalyzer software (version 0.9.14-alpha) with monocytes and MoMΦs gated based upon size and single cells. Since baseline fluorescence levels differed between fluorophores, mean fluorescence intensity (MFI) values were normalized by subtracting the appropriate isotype control MFI from the sample MFI (normalized MFI; Figure S3).

Biofilm-Conditioned Medium (BCM)

BCM was generated using methods similar to those described previously [24,25]. In brief, 6-well plate tissue culture inserts (0.4 µm; Falcon) were inoculated with five 10 µL droplets of overnight *P. aeruginosa* PAO1 culture grown in 10% BHI (Brain Heart Infusion, BD Bacto) at 37 °C and 220 rpm agitation. Following inoculation, tissue culture inserts were placed into a 6-well tissue culture plate, and 1.5 mL of 10% BHI was added to each well. The tissue culture plate was incubated at 37 °C, and media was refreshed every 24 hrs to maintain biofilm viability [35]. After 72 hrs of growth, biofilm-containing inserts were transferred to a new 6-well tissue culture plate, 1.5 mL of 1X phosphate

buffered saline (PBS) was added to each well, and biofilms were incubated at 37 °C for 30 min to remove excess growth media. These 72 hr mature biofilm-containing inserts were then transferred to a new 6-well tissue culture plate, 1.5 mL of MΦ culture medium, consisting of RPMI 1640 w/L-glutamine (Lonza) media, supplemented with 1 mM sodium pyruvate (Lonza), 1X MEM NEAAs, and 10% FBS, was added to each well, and biofilms were incubated at 37 °C. BCM was harvested after 24 hrs of conditioning, centrifuged at 5000 rpm for 10 min to remove cells, sterile-filtered (0.22 µm; Fisherbrand), and stored at -20 °C. Tissue culture wells were replenished with fresh cell culture media following BCM harvest. A total of five 24 hr BCM collections were pooled, pH-adjusted to 7.4 using sterile, concentrated HCl or NaOH, and stored at -20 °C until further use.

Colony-forming units (CFUs) for *P. aeruginosa* PAO1 biofilms were determined after initial maturation (72 hrs) using 10% BHI and following BCM generation using a serial dilution drop-plating method. In brief, biofilm colonies were removed from tissue culture inserts using 1X PBS, vortexed, agitated in a sonicator bath, serially diluted with PBS, plated on 100% tryptic soy agar (TSA) plates, and incubated at 37 °C. Bacterial colonies were then counted, and the number of CFUs per insert was calculated.

Planktonic-Conditioned Medium (PCM)

PCM was generated to yield a similar proportion of CFUs per unit of fluid volume to that of BCM, as previously described [24, 25]. In brief, an overnight culture of *P. aeruginosa* PAO1 was grown in 10% BHI at 37 °C with 220 rpm agitation. This overnight culture was then centrifuged at 5000 rpm for 5 min, and then the cells were

washed using 1X PBS to remove excess media. This cell suspension was centrifuged again at 5000 rpm for 5 min, and the cells were resuspended in MΦ culture medium, consisting of RPMI 1640 w/L-glutamine (Lonza) media, supplemented with 1 mM sodium pyruvate (Lonza), 1X MEM NEAAs, and 10% FBS, at a density equivalent to that of a mature PAO1 biofilm (6×10^9 CFUs/mL). This PAO1 suspension was cultured at 37 °C with 220 rpm agitation for 24 hrs. After the conditioning period, PCM was centrifuged at 5000 rpm for 10 min to remove cells, sterile-filtered (0.22 µm; Fisherbrand), pH-adjusted to 7.4 using sterile, concentrated HCl or NaOH, and stored at -20 °C until further use.

Exposure of Primary Human Monocyte-Derived MΦs to PCM and BCM

Before exposure experiments, equal volumes of PCM and BCM were mixed with equal volumes of MΦ culture medium, consisting of RPMI 1640 w/L-glutamine (Lonza) media, supplemented with 1 mM sodium pyruvate (Lonza), 1X MEM NEAAs, and 10% FBS, and pre-warmed to 37 °C.

Spent media was removed from 9 d *in vitro* M0 MΦ cultures and discarded. Adherent cells were then washed using 4 mL of pre-warmed (37 °C) Dulbecco's PBS (dPBS); this wash was then discarded. Pre-warmed PCM and/or BCM was transferred into 25 cm^2 tissue culture flasks containing M0 MΦs, and these flask were then placed at 37 °C, 5% CO_2 for 30 min or 1 hr before conducting metabolite extraction.

Intra- and Extracellular
Metabolite Extraction

Following exposure, spent cell culture medium was transferred into sterile 15 mL conical tubes and centrifuged at 2000 x g for 1 min at room temperature (RT) to pellet cellular debris. Two 1.5 mL aliquots of sham and spent cell culture medium were transferred to sterile 1.5 mL tubes and stored at -80 °C prior to extracellular metabolite extraction. Cell monolayers were washed with 1 mL of cold (4 °C) sterile 1X phosphate-buffered saline (PBS). Wash solutions were pipetted into a 15 mL conical tube, centrifuged at 2000 x g to pellet any remaining non-adherent cells, decanted, and then resuspended in 500 µL of -20 °C 50% aqueous methanol. 1.5 mL of -20 °C 50% aqueous methanol was added to 25 cm2 tissue culture flasks to simultaneously quench, extract, and detach cells from flask surface with the aid of a cell scraper. Cell suspensions were removed from 25 cm^2 tissue culture flasks, transferred to 15 mL conical tubes containing non-adherent cell suspensions, and thoroughly mixed.

Two aliquots of 1 mL cell suspensions were transferred into separate 2 mL lysis B matrix tubes (MP Biomedicals) and lysed using a FastPrep-24 5G homogenizer (MP Biomedicals) at a speed of 6.0 m/s for 2 cycles of 40 s each, with lysis tubes placed on ice between cycles. 50 µL of cell lysate was stored at -80 °C for protein determination, and then 500 µL of chloroform ($CHCl_3$) was added to each lysis tube. Tubes were vortexed for 3 cycles of 10 s each, and then placed at -20 °C for 20 min, prior to centrifugation at 10,000 x g for 10 min to separate aqueous and nonpolar phases [36]. The aqueous phase was transferred to a 1.5 mL tube, dried using a vacuum centrifuge (Speedvac) with no heat overnight, and stored at -80 °C until NMR metabolite sample

preparation.

Sham and spent cell culture medium aliquots were filtered through 3 kDa molecular weight cutoff (MWCO) centrifuge filters (Millipore Amicon), which had been prewashed extensively [35], prior to being dried using a vacuum centrifuge (Speedvac) with no heat overnight and stored at -80 °C until NMR sample preparation.

Protein Assay

Sample protein content was measured using a Pierce BCA Protein Assay Kit (ThermoFisher Scientific; Cat. No. 23225) for intra- and extracellular metabolite extract normalization.

NMR Sample Preparation

Intra- and extracellular metabolite extracts were resuspended in 600 µL of NMR buffer consisting of 25 mM NaH_2PO_4/Na_2HPO_4, 0.4 mM imidazole, 0.25 mM 4,4-dimethyl-4-silapentane-1-sulfonic acid (DSS) in 90% H_2O/10% D_2O at pH 7.0. Samples were centrifuged at 21000 rpm for 60 s to pellet insoluble material, and then transferred into 5 mm NMR tubes for metabolomics analysis.

NMR Data Acquisition and Preprocessing

NMR spectra were collected at 298 K (25 °C) using a Bruker 600 MHz (^{1}H Larmor frequency) AVANCE III solution NMR spectrometer, equipped with a SampleJet automatic sample loading system, a 5 mm triple resonance (^{1}H, ^{15}N, ^{13}C), liquid-helium-cooled TCI NMR cryoprobe, and Topspin software (Bruker version 3.6). 1D ^{1}H NMR spectra acquisition was performed using the Bruker-supplied ‘zgesgp’ pulse sequence

[37,38]; NMR spectra were recorded with 256 scans and a ^{1}H spectral window of 9615.38 Hz. Free induction decays (FIDs) were collected with 32K data points and a dwell time interval of 52 μsec, amounting to a data acquisition time of 1.7 s. Recovery delay (D1) times between acquisitions were set to 1 s, resulting in an overall 2.7 s relaxation recovery delay between scans [39,40]. Phase correction and DSS chemical shift referencing of 1D ^{1}H NMR spectra were performed using Topspin software (Bruker version 3.6).

NMR Data Analysis

Additional processing of 1D ^{1}H NMR spectra and metabolic profiling were performed using Chenomx NMR Suite software (version 8.1; Chenomx Inc., Edmonton, Alberta, Canada). Preprocessed '1r' NMR spectra files were imported into Chenomx and baseline correction was conducted using the automatic cubic spline function and manual breakpoint adjustment to procure a flat, well-defined baseline [41,42]. All ^{1}H chemical shifts were referenced to the DSS signal (0.0 ppm), and imidazole ^{1}H NMR signals were used to make adjustments arising from slight variations in sample pH. Identification and quantitation of metabolites was performed by manually peak-based fitting 1D ^{1}H spectral patterns, intensities, and chemical shifts with reference to small molecule spectral patterns present in the Chenomx database for 600 MHz (^{1}H Larmor frequency) magnetic field strength NMR; manual adjustments were performed to attain optimal spectral pattern fits based upon metabolite intensity and peak cluster location [43]. In addition to serving as a chemical shift reference, the internal DSS (0.25 mM) standard was also used for metabolite quantitation.

Statistical Analysis

Metabolite concentrations were normalized to protein content and NMR buffer volume before multivariate statistical analysis by MetaboAnalyst 4.0 [44,45]. After normalization, metabolite concentrations were log-transformed and auto-scaled, mean-centered and divided by SD, to yield a Gaussian data distribution prior to multivariate statistical analysis, which included 2D-PCA and HCA. A Euclidean distance measure and Ward clustering algorithm were used when performing HCA in MetaboAnalyst. GraphPad Prism program version 8.2.1 (GraphPad Software, La Jolla, CA) was used to determine statistical significance by unpaired parametric *t*-test with Welch's correction.

Results

PCM- and BCM-Exposed MΦs Exhibit Distinct Metabolic Profiles Compared to Control MΦs

To determine the metabolic patterns associated with PCM- and BCM-exposed MΦs, metabolite profiles of 30 min. and 1 hr. control, PCM-exposed, and BCM-exposed MΦs cultured *in vitro* were characterized using untargeted ^{1}H NMR metabolomics. 1D ^{1}H NMR spectra of intra- and extracellular metabolite extracts were recorded on a 600 MHz (^{1}H Larmor frequency) solution NMR spectrometer at MSU. This approach facilitated the identification and quantitation of 44 metabolites in these cell cultures.

2D principal component analysis (2D-PCA) of intracellular metabolite profiles (Figure 1A) demonstrated that 30 min. and 1 hr. PCM- and BCM-exposed MΦs are metabolically distinct from 30 min. and 1 hr. control MΦs. In addition, 30 min. PCM-

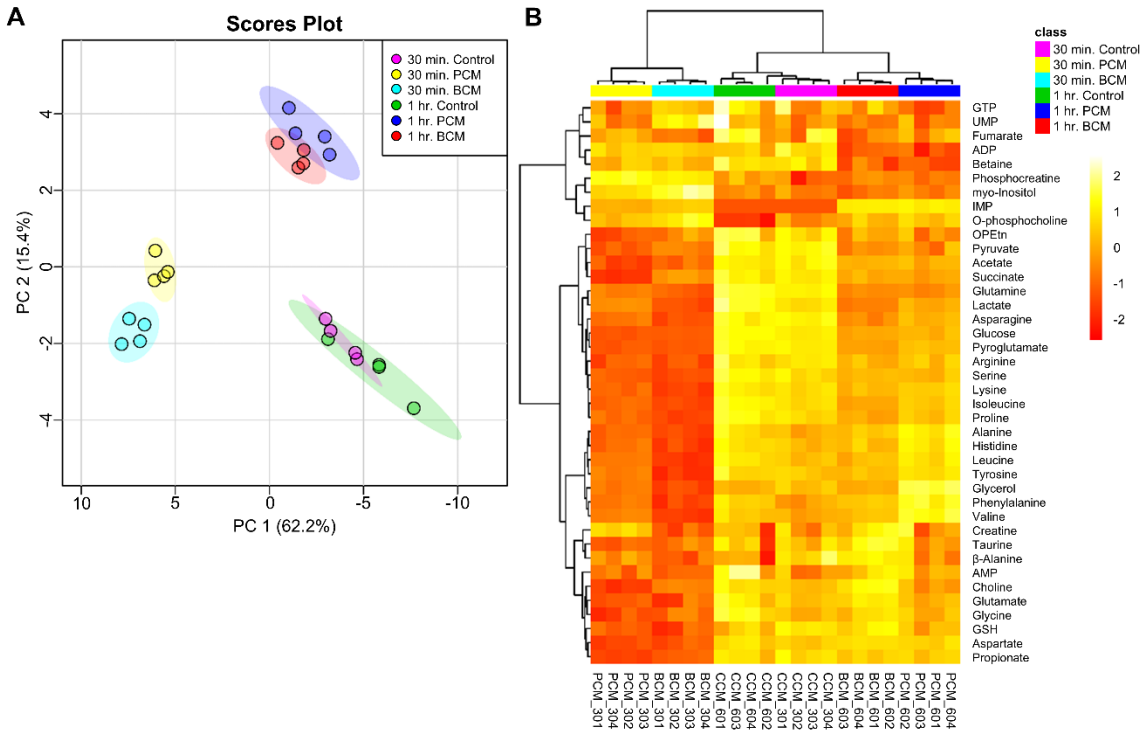

Figure 1. Multivariate statistical analysis reveals intracellular metabolic differences between 30 min. and 1 hr. control, PCM-exposed, and BCM-exposed MΦs. 2D principal component analysis (2D-PCA) scores plots generated by analysis of metabolic profiles from (A) intracellular MΦ metabolite extracts (30 min. control, pink; 30 min. PCM, yellow; 30 min. BCM, cyan; 1 hr. control, green; 1 hr. PCM, blue; 1 hr. BCM, red), with shaded regions illustrating respective 95% confidence intervals. Hierarchical clustering analysis (HCA) and heatmap visualization of metabolic profiles from (B) intracellular MΦ metabolite extracts was performed using a Euclidean distance calculated from metabolite abundance and a Ward clustering algorithm. The upmost column bar is colored according to MΦ group (30 min. control, pink; 30 min. PCM, yellow; 30 min. BCM, cyan; 1 hr. control, green; 1 hr. PCM, blue; 1 hr. BCM, red), and the color scale represents the scaled abundance of each metabolite, with yellow indicating high abundance and red indicating low abundance. Abbreviations denote: ADP, adenosine diphosphate; AMP, adenosine monophosphate; GSH, reduced glutathione; GTP, guanosine triphosphate; IMP, inosine monophosphate; OPEtn, o-phosphoethanolamine; UMP, uridine monophosphate.

and BCM- exposed MΦs displayed unique metabolic profiles from corresponding 1 hr. exposure samples. These intracellular metabolite profiles were also subjected to hierarchical clustering analysis (HCA) and heatmap generation to illustrate which

metabolites significantly contributed to group discrimination (Figure 1B). Some distinct patterns observed in the intracellular metabolite profiles of 30 min. PCM- and BCM-exposed MΦs included elevated concentrations of phosphocreatine, myo-inositol, inosine monophosphate (IMP), and phosphocholine, which were not observed in 30 min. control MΦs (Figure 1B). Although the intracellular metabolite profiles determined for 1 hr. PCM- and BCM-exposed MΦs were not as distinct from 1 hr. control MΦs as those observed for the 30 min. time point MΦ groups, one notable finding from our 1 hr. PCM- and BCM-exposed MΦs was an increased concentration of IMP relative to control MΦs (Figure 1B). Unfortunately, none of these MΦ groups (control, PCM-exposed, and BCM-exposed) were distinguishable based upon their extracellular metabolite profiles (Figure S1).

PCM- and BCM-Exposed MΦs Display Intriguing Glycolytic Trends

Metabolic profiling of intra- and extracellular 30 min. and 1 hr. control, PCM-exposed, and BCM-exposed MΦ metabolite extracts revealed that PCM- and BCM-exposed MΦs display similar metabolic changes with regard to glycolytic and lactic acid fermentation pathways (Figure 2A), when compared to control MΦs.

30 min. PCM- and BCM-exposed MΦs exhibited intracellular glucose levels that were -10.70 and -9.65-fold lower, respectively, intracellular pyruvate levels that were -3.05 and -2.30-fold lower, respectively, and intracellular lactate levels that were -1.83 and -2.94-fold lower, respectively, relative to those found in 30 min. control MΦs (Figure 2B and Table 1). However, 30 min. PCM- and BCM-exposed MΦs displayed no

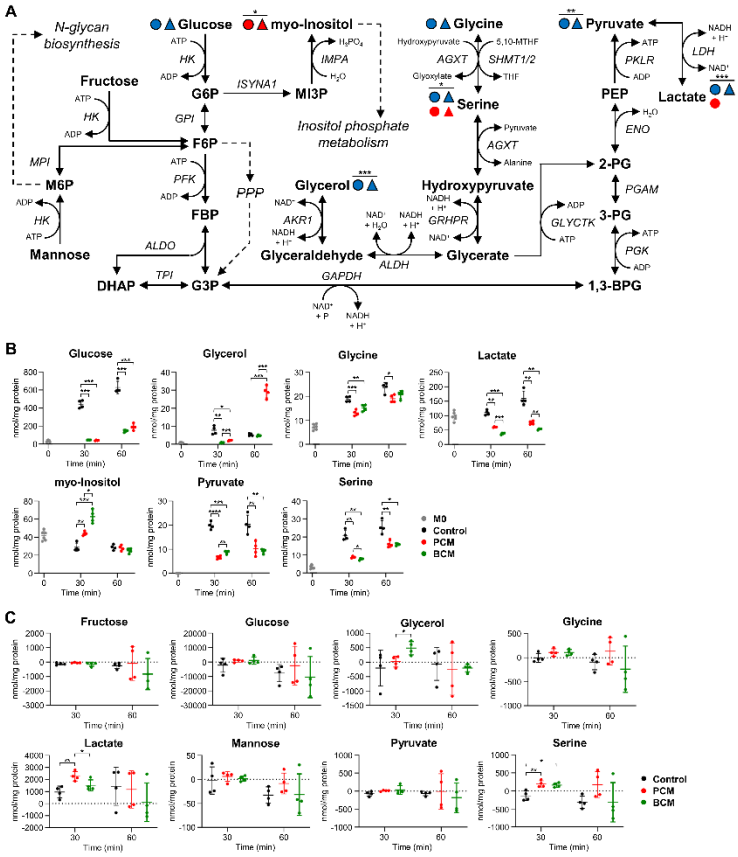

Figure 2. Depletion of intracellular glucose without equivalent generation of pyruvate or lactate in PCM- and BCM-exposed MΦs. Schematic diagram of glycolysis and lactic acid fermentation pathways (A), and quantitative levels of corresponding metabolites detected in (B) intra- and (C) extracellular metabolite extracts (mean ± SD). Unpaired parametric t-tests with Welch's correction (two-tailed; *$p < 0.05$; **$p < 0.01$; ***$p < 0.001$; ****$p < 0.0001$). Abbreviations denote: 2-PG, 2-phosphoglycerate; 3-PG, 3-phosphoglycerate; ADP, adenosine diphosphate; *AGXT*, serine—pyruvate aminotransferase; *AKR1*, aldo-keto reductase family 1; *ALDH*, aldehyde dehydrogenase; *ALDO*, aldolase; ATP, adenosine triphosphate; BPG, bisphosphoglycerate; DHAP, dihydroxyacetone phosphate; *ENO*, enolase; F6P, fructose 6-phosphate; FBP, fructose bisphosphate; G3P, glyceraldehyde 3-phosphate; G6P, glucose 6-phosphate; *GAPDH*, glyceraldehyde-3-phosphate dehydrogenase; *GLYCTK*, glycerate kinase; *GPI*, glucose-6-phosphate isomerase; *GRHPR*, glyoxylate and hydroxypyruvate reductase; *HK*, hexokinase; *IMPA*, inositol monophosphatase; *ISYNA1*, inositol-3-phosphate synthase 1; *LDH*, lactate dehydrogenase; M6P, mannose 6-phosphate; MI3P, myo-inositol-3-phosphate; *MPI*, mannose phosphate isomerase; MTHF, methylenetetrahydrofolate; NAD^+, nicotinamide adenine dinucleotide; NADH, reduced nicotinamide adenine dinucleotide; PEP, phosphoenolpyruvate; *PFK*, phosphofructokinase; *PGAM*, phosphoglycerate mutase; *PGK*, phosphoglycerate kinase; *PKLR*, pyruvate kinase L/R; PPP, pentose phosphate pathway; *SHMT1/2*, serine hydroxymethyltransferase 1/2; THF, tetrahydrofolate; *TPI*, triosephosphate isomerase.

Table 1. Discriminatory metabolites in intracellular extracts associated with 30 min. and 1 hr. PCM and BCM exposure.[1]

Metabolite	30 min.				1 hr.			
	PCM MΦs		BCM MΦs		PCM MΦs		BCM MΦs	
	FC	*p*-value	FC	*p*-value	FC	*p*-value	FC	*p*-value
Acetate	-1.50	**	-1.51	**	-1.50	**	-1.51	**
ADP	-1.19	NS	-1.21	NS	-2.04	**	-1.90	**
Alanine	-1.41	**	-1.67	**	1.08	NS	-1.15	NS
Arginine	-4.24	****	-4.96	****	-1.57	NS	-1.93	NS
Asparagine	-3.37	***	-4.73	***	-1.90	**	-2.79	**
Aspartate	-2.84	***	-2.47	***	-1.06	NS	1.02	NS
Betaine	-1.22	NS	-1.27	*	-2.27	**	-2.13	**
Choline	-2.58	***	-1.55	**	-1.62	*	1.16	NS
Creatine phosphate	3.18	***	2.66	**	-1.40	NS	-1.29	NS
Fumarate	-1.16	NS	-1.55	NS	-1.41	NS	-1.79	*
Glucose	-10.70	***	-9.65	***	-3.30	***	-4.30	***
Glutamate	-1.56	***	-1.54	**	-1.24	NS	-1.02	NS
Glutamine	-2.78	****	-3.72	****	-3.12	***	-3.23	***
Glutathione	-2.61	***	-2.89	****	-1.08	NS	1.29	NS
Glycerol	-3.57	*	-8.58	**	5.36	***	-1.12	NS
Glycine	-1.44	***	-1.24	**	-1.24	*	-1.14	NS
GTP	-1.19	NS	1.01	NS	-1.52	*	-1.20	NS
Histidine	-2.01	**	-3.10	**	1.09	NS	-1.40	*
IMP	1.63[2]	***	3.24[2]	***	8.70[2]	**	8.28[2]	***
Isoleucine	-2.65	***	-3.51	***	-1.52	**	-2.13	**
Lactate	-1.83	**	-2.94	***	-2.12	**	-3.01	**
Leucine	-1.61	**	-2.51	***	-1.04	NS	-1.38	*
Lysine	-2.91	***	-4.19	***	-1.33	NS	-1.66	*
Phosphocholine	1.19	*	1.45	**	1.81	***	1.69	***
Phosphoethanolamine	-1.60	***	-1.32	**	-1.40	*	-1.35	*
Phenylalanine	-1.29	*	-1.85	**	1.34	*	-1.11	NS
Proline	-2.11	***	-2.76	***	-1.45	**	-1.81	**
Propionate	-3.49	**	-2.74	**	-1.09	NS	-1.11	NS
Pyroglutamate	-6.20	***	-6.23	***	-2.18	**	-3.17	**
Pyruvate	-3.05	****	-2.30	***	-2.00	**	-2.24	**
Serine	-2.39	**	-2.72	**	-1.58	**	-1.60	*
Succinate	-4.88	***	-2.07	***	-2.01	*	-1.88	*
Taurine	-1.39	*	-1.29	*	-1.04	NS	1.24	NS
Tyrosine	-1.77	**	-3.29	***	-1.04	NS	-1.37	NS
UMP	-1.04	NS	1.45	**	-1.36	NS	-1.44	NS
Valine	-1.30	*	-2.16	**	1.47	**	-1.11	NS
myo-Inositol	1.54	**	2.19	***	-1.03	NS	-1.15	NS
β-alanine	-1.31	*	-1.54	**	1.06	NS	1.36	*

[1] Metabolites were selected based upon fold change (FC) of intracellular metabolite concentrations, and statistical significance, between exposure MΦ groups (PCM MΦs and BCM MΦs; nmol/mg protein; calculated from metabolite spectral fitting using the Chenomx NMR Suite software and the standard Chenomx 600 MHz metabolite library) relative to control MΦs. Fold changes were calculated relative to control MΦs, whereby increases are shown as positive values and decreases are shown as negative values. Statistical significance (*p*) was measured using two-tailed unpaired parametric t-tests with Welch's correction, whereby *, $p < 0.05$; **, $p < 0.01$; ***, $p < 0.001$; ****, $p < 0.0001$. Abbreviations denote: NS, not statistically significant; ADP, adenosine diphosphate; GTP, guanosine triphosphate; IMP, inosine monophosphate; UMP, uridine monophosphate. [2] Fold change (FC) was calculated using limit of detection (LOD) values (see Table S1) for MΦ group in which a given metabolite was not detected.

significant differences concerning extracellular fructose, glucose, mannose, or pyruvate consumption (Figure 2C). Extracellular lactate for the 30 min. PCM-exposed MΦs were significantly different from 30 min. control MΦs, where control and PCM-exposed MΦs displayed an average surplus of 952.61 and 2269.58 nmol lactate/mg protein, respectively (Figure 2C and Table 2), relative to sham extracellular metabolite extract controls. 1 hr. PCM- and BCM-exposed MΦs exhibited intracellular glucose levels that were -3.30 and -4.30-fold lower, respectively, intracellular pyruvate levels that were -2.00 and -2.24-fold lower, respectively, and intracellular lactate levels that were -2.12 and -3.01-fold lower, respectively, relative to those found in 1 hr. control MΦs (Figure 2B and Table 1). Similar to the 30 min. time point MΦ groups, 1 hr. PCM- and BCM-exposed MΦs displayed no significant differences concerning extracellular fructose, glucose, mannose, or pyruvate consumption (Figure 2C). In addition, extracellular lactate for the 1 hr. PCM- and BCM-exposed MΦs was also not significantly different from 1 hr. control MΦs (Figure 2C).

Since there appeared to be discrepancies regarding the depletion of intracellular glucose relative to the levels of intracellular pyruvate and lactate, other relevant intra- and extracellular metabolites that were detected in control, PCM-exposed, and BCM-exposed MΦs were examined, including glycerol, glycine, myo-inositol, and serine (Figure 2A). 30 min. PCM- and BCM-exposed MΦs exhibited intracellular glycerol levels that were -3.57 and -8.58-fold lower, respectively, intracellular glycine levels that were -1.44 and -1.24-fold lower, respectively, intracellular myo-inositol levels that were 1.54 and 2.19-fold higher, respectively, and intracellular serine levels that were -2.39 and -2.72-fold

Table 2. Discriminatory metabolites in extracellular extracts associated with 30 min. PCM and BCM exposure.[1]

Metabolite	Concentration (mean ± SD)			*p*-value		
	Control MΦs	PCM MΦs	BCM MΦs	PCM[2]	BCM[2]	PCM vs. BCM
3-hydroxybutyrate	-2.27 ± 4.45	-16.68 ± 4.87	-2.04 ± 21.42	**	NS	NS
Alanine	-13.26 ± 18.86	158.23 ± 63.84	127.83 ± 57.81	**	*	NS
Asparagine	91.23 ± 225.36	198.11 ± 69.82	80.02 ± 23.81	NS	NS	*
Aspartate	-209.86 ± 116.33	47.27 ± 46.36	119.78 ± 197.75	*	*	NS
Betaine	-2.42 ± 2.94	1.63 ± 1.21	-14.23 ± 2.65	NS	**	***
Choline	6.99 ± 4.92	-13.50 ± 3.39	0.13 ± 19.43	***	NS	NS
Glutamate	-128.12 ± 9.12	-113.96 ± 32.48	280.37 ± 244.28	NS	*	*
Glycerol	-204.47 ± 620.34	20.36 ± 186.36	489.34 ± 231.78	NS	NS	*
Lactate	952.61 ± 490.23	2269.58 ± 390.78	1516.06 ± 455.25	**	NS	*
Lysine	-53.70 ± 25.58	61.03 ± 18.71	5.92 ± 37.24	***	*	NS
Methionine	-30.81 ± 33.63	65.52 ± 30.04	64.82 ± 14.75	**	**	NS
Phosphocholine	-3.84 ± 10.98	-25.25 ± 4.40	-11.95 ± 31.81	*	NS	NS
Phenylalanine	-41.11 ± 43.58	59.64 ± 31.75	32.97 ± 16.83	*	*	NS
Serine	-132.54 ± 133.77	195.13 ± 88.48	161.81 ± 60.37	**	*	NS
Threonine	-51.72 ± 153.48	239.78 ± 107.86	134.26 ± 93.92	*	NS	NS
Tryptophan	-32.70 ± 12.44	10.95 ± 6.54	12.36 ± 3.91	**	**	NS
Tyrosine	-16.65 ± 46.03	68.98 ± 22.92	39.87 ± 35.98	*	NS	NS
myo-Inositol	-52.53 ± 102.00	25.75 ± 56.15	205.99 ± 130.96	NS	*	NS
trans-4-hydroxy-L-proline	-185.88 ± 82.02	87.15 ± 43.53	-26.79 ± 12.97	**	*	*

[1] Metabolites were selected based upon statistical significance of extracellular metabolite concentrations between exposure MΦ groups (PCM MΦs and BCM MΦs; nmol/mg protein; calculated from metabolite spectral fitting using the Chenomx NMR Suite software and the standard Chenomx 600 MHz metabolite library) relative to control MΦs. Metabolite concentrations were normalized to sham media controls, whereby increases are shown as positive values and decreases are shown as negative values. Statistical significance (p) was measured using two-tailed unpaired parametric t-tests with Welch's correction, whereby *, $p < 0.05$; **, $p < 0.01$; ***, $p < 0.001$; ****, $p < 0.0001$; NS, not statistically significant. [2] Relative to control MΦs.

lower, respectively, relative to those found in 30 min. control MΦs (Figure 2B and Table 1). 30 min. PCM- and BCM-exposed MΦs displayed no significant differences concerning extracellular glycerol or glycine consumption (Figure 2C), relative to control MΦs. Extracellular serine levels for 30 min. PCM- and BCM-exposed MΦs were significantly different from 30 min. control MΦs, where control, PCM-exposed, and BCM-exposed MΦs displayed an average concentration of -132.54, 195.13, and 161.81 nmol serine/mg protein, respectively (Figure 2C and Table 2), relative to sham extracellular metabolite extract controls. 1 hr. PCM-exposed MΦs exhibited intracellular glycerol levels that were 5.36-fold higher, intracellular glycine levels that were -1.24-fold lower, and intracellular serine levels that were -1.58-fold lower, relative to those found in 30 min. control MΦs (Figure 2B and Table 1). 1 hr. BCM-exposed MΦs exhibited

intracellular serine levels that were -1.60-fold lower, relative to those found in 30 min. control MΦs (Figure 2B and Table 1). 1 hr. PCM- and BCM-exposed MΦs displayed no significant differences concerning extracellular glycerol, glycine, or serine consumption (Figure 2C), relative to control MΦs.

Although the majority of these results concern the metabolic distinctions found between PCM- and BCM-exposed MΦs relative to control MΦs, there were several significant differences observed between PCM- and BCM-exposed MΦs. 30 min. BCM-exposed MΦs demonstrated intracellular glycerol levels that were -2.40-fold lower, intracellular lactate levels that were -1.61-fold lower, intracellular pyruvate levels that were 1.33-fold higher, intracellular serine levels that were -1.14-fold lower, and intracellular myo-inositol levels that were 1.42-fold higher, relative to those found in 30 min. PCM-exposed MΦs (Figure 2B and Table S2). In addition, 1 hr. BCM-exposed MΦs displayed intracellular glycerol levels that were -5.99-fold lower and intracellular lactate levels that were -1.42-fold lower, relative to those found in 30 min. PCM-exposed MΦs (Figure 2B and Table S2). Much of the extracellular data were similar for both PCM- and BCM-exposed MΦs; however, 30 min. BCM-exposed MΦs exhibited significantly increased levels of extracellular glycerol and significantly decreased levels of extracellular lactate, relative to those found for the 30 min. PCM-exposed MΦs (Figure 2C and Table 2).

Discussion

Increased glycolytic flux in the presence of oxygen (i.e. aerobic glycolysis) is

considered a universal metabolic characteristic of M1, or pro-inflammatory, MΦs. In fact, it has been shown to be critical for the regulation and support of M1 MΦ function, such as the generation of ROS, phagocytosis of pathogens and apoptotic cells, and the secretion of pro-inflammatory cytokines [46-48]. In this study, we determined that PCM- and BCM-exposed MΦs exhibit significant depletion of their intracellular glucose levels compared to control MΦs. Surprisingly, we did not observe a corresponding significant increase in either intracellular pyruvate or lactate in PCM- and BCM-exposed MΦs relative to control MΦs. An even greater puzzling result was that PCM- and BCM-exposed MΦs do not consume any extracellular carbohydrate sources, such as fructose, glucose, or mannose, to a larger extent than our control MΦs. If glycolysis was indeed upregulated, we would expect to see significant consumption of glucose from the extracellular environment similar to what we and others in the immunometabolism field have demonstrated for M1 MΦs. Although intracellular glucose depletion in PCM- and BCM-exposed MΦs does not correspondingly reflect in our observed intracellular pyruvate and lactate levels, we believe that some intracellular glucose is being used to generate ATP and pyruvate given that previous studies have found Warburg-like metabolic traits in inflammatory M1 MΦs [34,46,49].

Lipopolysaccharide (LPS)-stimulated, or M1, MΦs have been shown to increase fatty acid synthesis to support their pro-inflammatory effector functions, particularly phagocytic activity [30,34]. Monocytic differentiation to MΦs is associated with upregulation of fatty acid synthesis genes and a metabolic switch from cholesterol synthesis to phosphatidylcholine synthesis in MΦs [50]. Our metabolic findings in PCM-

and BCM-exposed MΦs revealed significant depression of intracellular glycerol levels at 30 min.; however, 1 hr. PCM-exposed MΦs exhibit significantly increased levels of intracellular glycerol. Although Figure 2A illustrates the anaplerotic regeneration of the glycolytic intermediate 2-phosphoglycerate (2-PG) from glycerol, glycerol can also be generated from the glycolytic intermediate glyceraldehyde 3-phosphate (G3P) and then utilized for fatty acid synthesis [51]. We believe that our metabolic data indicate that PCM-exposed MΦs may be accumulating intracellular glycerol at the 1 hr. time point in order to upregulate the synthesis of fatty acids, which are critical for the proper function of MΦ phagocytosis. In addition, additional metabolic data obtained in our study demonstrates consumption of extracellular choline and phosphocholine, which are essential metabolic precursors for phosphatidylcholine (PC) synthesis [50], uniquely in our PCM-exposed MΦs. Absence of glycerol accumulation and consumption of choline and phosphocholine in our BCM-exposed MΦs suggests that secretory bacterial biofilm products inhibit MΦ phagocytic activity. This result may be considered consistent with previous studies that have demonstrated attenuated MΦ effector function in the presence of *P. aeruginosa* biofilms [52].

Previous studies have suggested that myo-inositol is involved in the regulation of phagocytosis [53,54]. Chen *et al.* demonstrated that low and intermediate dose administration of exogenous myo-inositol induced significant depolarization of MΦ membrane potential *in vitro* [55]. However, this MΦ depolarization effect was lost when higher myo-inositol dosages, 80 mM, were used in *in vivo* murine models [55]. MΦs in mice pre-treated with exogenous myo-inositol exhibited greater membrane potential

depolarization, which led to significantly increased phagocytic capacity in MΦs exposed to antibiotic-susceptible and antibiotic-resistant *Escherichia coli* [55]. In the absence of exogenous myo-inositol pre-treatment, murine MΦs displayed reduced phagocytosis of antibiotic-resistant *E. coli* relative to antibiotic-susceptible *E. coli* and reduced membrane potential polarization [55]. Myo-inositol metabolism leads to the generation of two products, phosphatidylinositol-3,4,5-trisphosphate (PtdIns(3,4,5)P3) and inositol 1,3,4,5-tetrakisphosphate (Ins(1,3,4,5)P4). While the latter product, Ins(1,3,4,5)P4, suppresses PH domain-containing proteins, such as Akt1, the former product, PtdIns(3,4,5)P3, binds to PD domain-containing proteins and as a result initiates downstream cellular signaling pathways which include the modulation of membrane potential [53,54,56]. We hypothesize that elevation of intracellular myo-inositol in our PCM-exposed MΦs modulates the ratio of Ins(1,3,4,5)P4 and PtdIns(3,4,5)P3, which regulate Akt1 activity, therefore manipulating membrane potential depolarization.

Conclusions

In conclusion, our metabolite profiling data generated using *in vitro* primary human monocyte-derived MΦs exposed to *P. aeruginosa* PCM and BCM indicate that both PCM- and BCM-exposed MΦs utilize glycolysis without any apparent consumption of extracellular carbohydrate sources. Furthermore, at our 30 min. exposure time points it appears as through PCM- and BCM-exposed MΦs may be diverting a significant portion of early glycolytic intermediates towards inositol phosphate metabolism instead of pyruvate generation. Moreover, we found that although 30 min. PCM- and BCM-exposed

MΦs seem to use glycerol as a catabolic substrate, our 1 hr. PCM-exposed MΦs contain significantly increased levels of glycerol compared to both 1 hr. BCM-exposed and control MΦs. Results from this study highlight the importance of elucidating the differential metabolic modulation of physiologically relevant immune cell populations under disparate microbial growth mode stress. This work also emphasizes the application of NMR metabolomics to determine characteristic metabotypes associated with specific pathogen-derived stimuli. In addition, these methods can be used to further understand how metabolic adaptations in human MΦs correspond to functional dysregulation of MΦs in the presence of pathogenic biofilms and potentially yield targets or insight into the development of more efficacious chronic wound therapeutics.

Supporting Information

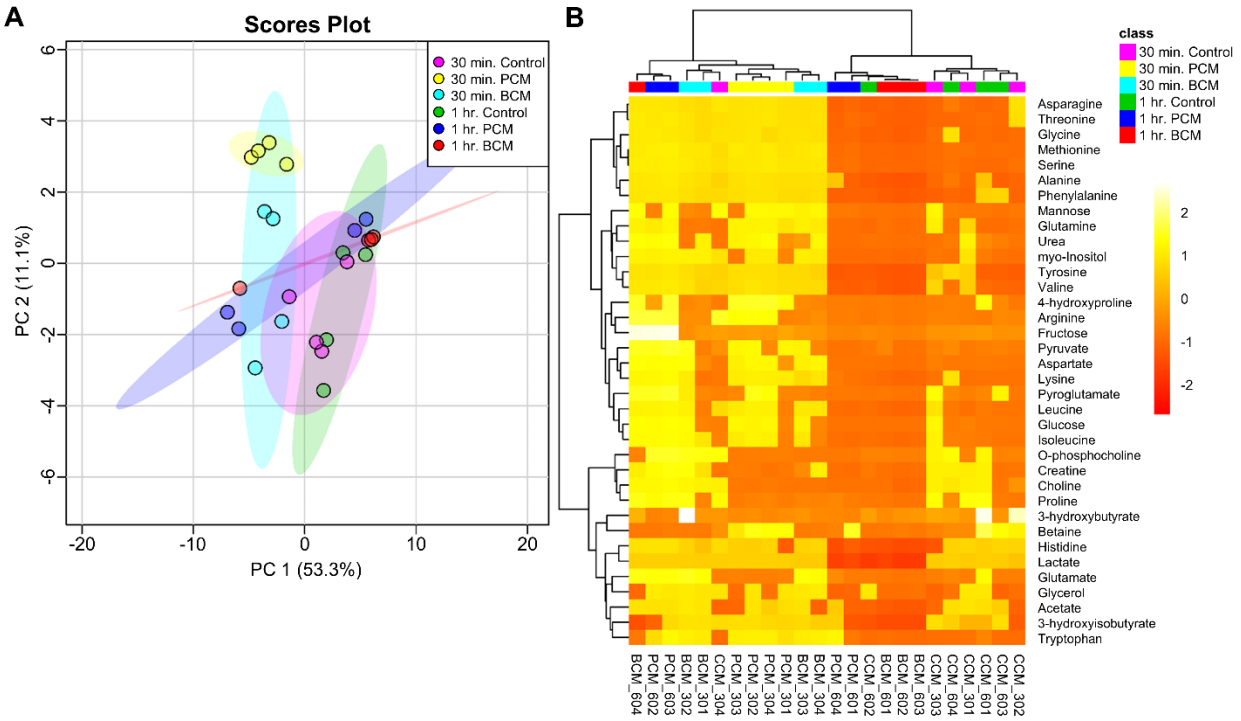

Figure S1. Multivariate statistical analysis reveals limited differences between extracellular metabolite profiles from 30 min. and 1 hr. control, PCM-exposed, and BCM-exposed MΦs. 2D principal component analysis (2D-PCA) scores plots generated by analysis of metabolic profiles from (A) extracellular MΦ metabolite extracts (30 min. control, pink; 30 min. PCM, yellow; 30 min. BCM, cyan; 1 hr. control, green; 1 hr. PCM, blue; 1 hr. BCM, red), with shaded regions illustrating respective 95% confidence intervals. Hierarchical clustering analysis (HCA) and heatmap visualization of metabolic profiles from (B) extracellular MΦ metabolite extracts was performed using a Euclidean distance calculated from metabolite abundance and a Ward clustering algorithm. The upmost column bar is colored according to MΦ group (30 min. control, pink; 30 min. PCM, yellow; 30 min. BCM, cyan; 1 hr. control, green; 1 hr. PCM, blue; 1 hr. BCM, red), and the color scale represents the scaled abundance of each metabolite, with yellow indicating high abundance and red indicating low abundance.

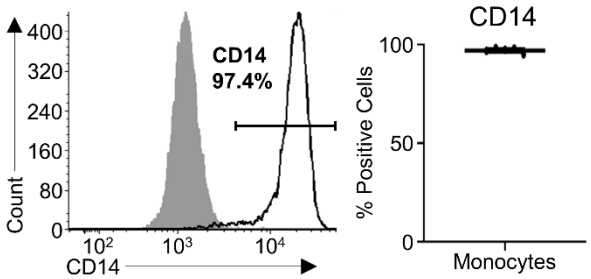

Figure S2. Purity of isolated monocytes. Representative histogram of purified $CD14^+$ monocytes (left) and pooled data from 5 independent experiments, mean ± SEM (right).

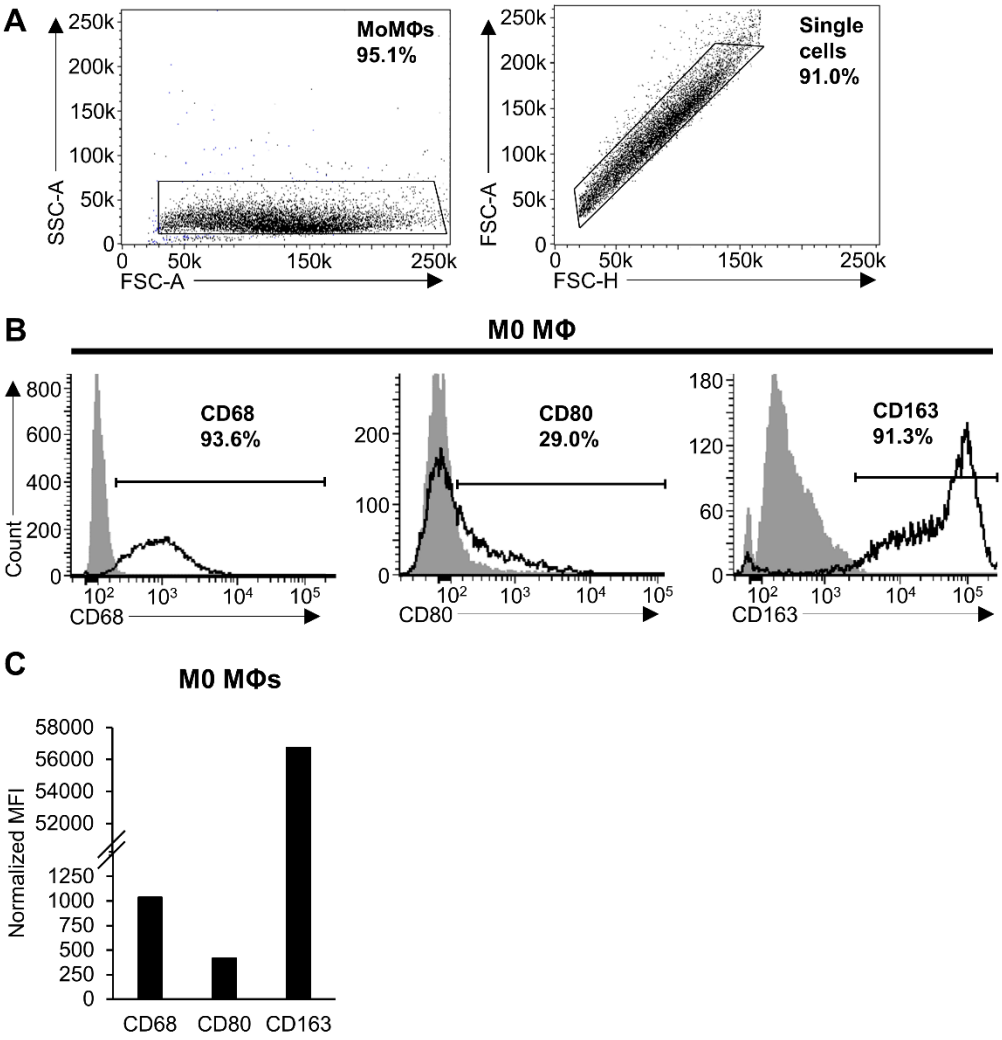

Figure S3. Phenotype of primary human monocyte-derived macrophages (MoMΦs). (A) Gating strategy for FACS analysis of MoMΦs; (B) Dot plots of CD68, CD80, and CD163 expression by M0 MoMΦs; (C) Normalized mean fluorescence intensity (MFI) of CD68, CD80, and CD163 expression by M0 MoMΦs.

Table S1. 1D ^{1}H NMR intra- and extracellular metabolite limit of detection (LOD) values.[1]		
Extract	Metabolite	LOD (μM)
Intracellular	IMP	0.5

[1] LOD values were established by evaluation of signal to noise ratios in our experimental 1D ^{1}H NMR spectra, Chenomx NMR Suite software, and its accompanying Chenomx 600 MHz metabolite library. Abbreviations denote: IMP, inosine monophosphate.

Table S2. Discriminatory metabolites in intracellular extracts associated with 30 min. and 1 hr. BCM vs. PCM exposure.[1]

Metabolite	30 min. BCM vs. PCM MΦs		1 hr. BCM vs. PCM MΦs	
	FC	*p*-value	FC	*p*-value
Alanine	-1.18	**	-1.24	*
Asparagine	-1.40	**	-1.47	**
Choline	1.66	****	1.88	**
Creatine	-1.20	***	1.09	NS
Creatine phosphate	-1.20	**	1.09	NS
Fumarate	-1.33	**	-1.27	NS
GTP	1.20	*	1.27	*
Glutamate	1.01	NS	1.21	**
Glutamine	-1.34	**	-1.03	NS
Glutathione	-1.11	NS	1.39	*
Glycerol	-2.40	***	-5.99	***
Histidine	-1.54	**	-1.53	*
IMP	1.99	**	-1.05	NS
Isoleucine	-1.32	**	-1.40	**
Lactate	-1.61	***	-1.42	**
Leucine	-1.57	****	-1.33	*
Lysine	-1.44	**	-1.25	*
Phosphocholine	1.22	*	-1.07	NS
Phosphoethanolamine	1.21	*	1.04	NS
Phenylalanine	-1.44	**	-1.48	**
Proline	-1.31	**	-1.24	*
Propionate	1.27	**	-1.02	NS
Pyroglutamate	-1.00	NS	-1.46	***
Pyruvate	1.33	**	-1.12	NS
Serine	-1.14	*	-1.01	NS
Succinate	2.35	**	1.07	NS
Taurine	1.08	NS	1.28	*
Tyrosine	-1.86	****	-1.32	**
UMP	1.51	**	-1.06	NS
Valine	-1.66	****	-1.64	**
myo-Inositol	1.42	*	-1.12	NS
β-alanine	-1.17	*	1.28	NS

[1] Metabolites were selected based upon fold change (FC) and statistical significance of intracellular metabolite concentrations between BCM- and PCM-exposed MΦs; (nmol/mg protein; calculated from metabolite spectral fitting using the Chenomx NMR Suite software and the standard Chenomx 600 MHz metabolite library). Fold changes were calculated relative to PCM-exposed MΦs, whereby increases are shown as positive values and decreases are shown as negative values. Statistical significance (*p*) was measured using two-tailed unpaired parametric t-tests with Welch's correction, whereby *, $p < 0.05$; **, $p < 0.01$; ***, $p < 0.001$; ****, $p < 0.0001$. Abbreviations denote: GTP, guanosine triphosphate; IMP, inosine monophosphate; UMP, uridine monophosphate.

Acknowledgements

We thank Dr. Michael Franklin at Montana State University for providing the bacterial strain *P. aeruginosa* PAO1.

References

1. Clarke TB. Microbial programming of systemic innate immunity and resistance to infection. PLoS Pathog. 2014; 10(12): e1004506.

2. Aderem A. Phagocytosis and the inflammatory response. J Infect Dis. 2003; 187(Suppl. 2): S340-5.

3. Mosser DM, Edwards JP. Exploring the full spectrum of macrophage activation. Nat Rev Immunol. 2008; 8(12): 958-69.

4. Ferrante CJ, Leibovich SJ. Regulation of macrophage polarization and wound healing. Adv Wound Care (New Rochelle). 2012; 1(1): 10-16.

5. Zhang L, Wang CC. Inflammatory response of macrophages in infection. Hepatobiliary Pancreat Dis Int. 2014; 13(2): 138-52.

6. Frykberg RG, Banks J. Challenges in the treatment of chronic wounds. Adv Wound Care (New Rochelle). 2015; 4(9): 560-582.

7. Baum CL, Arpey CJ. Normal cutaneous wound healing: clinical correlation with cellular and molecular events. Dermatol Surg. 2005; 31(6): 674-86, discussion 86.

8. Zhao R, Liang H, Clarke E, Jackson C, Xue M. Inflammation in chronic wounds. Int J Mol Sci. 2016; 17(12): E2085.

9. Hesketh M, Sahin KB, West ZE, Murray RZ. Macrophage phenotypes regulate scar formation and chronic wound healing. Int J Mol Sci. 2017; 18(7): E1545.

10. Costerton JW, Stewart PS, Greenberg EP. Bacterial biofilms: a common cause of persistent infections. Science. 1999; 284(5418): 1318-22.

11. Mann EE, Wozniak DJ. *Pseudomonas* biofilm matrix composition and niche biology. FEMS Microbiol Rev. 2012; 36(4): 893-916.

12. Lebeaux D, Ghigo JM, Beloin C. Biofilm-related infections: bridging the gap between clinical management and fundamental aspects of recalcitrance toward antibiotics. Microbiol Mol Biol Rev. 2014; 78(3): 510-43.

13. Lewis K. Multidrug tolerance of biofilms and persister cells. Curr Top Microbiol Immunol. 2008; 322: 107-31.

14. Sen CK. Wound healing essentials: let there be oxygen. Wound Repair Regen. 2009; 17(1): 1-18.

15. Goren I, Müller E, Schiefelbein D, Christen U, Pfeilschifter J, Mühl H, et al. Systemativ anti-TNFalpha treatment restores diabetes-impaired skin repair in ob/ob mice by inactivation of macrophages. J Invest Dermatol. 2007; 127(9): 2259-67.

16. Loots MA, Lamme EN, Zeegelaar J, Mekkes JR, Bos JD, Middelkoop E. Differences in cellular infiltrate and extracellular matrix of chronic diabetic and venous ulcers versus acute wounds. J Invest Dermatol. 1998; 111(5): 850-7.

17. Vannella KM, Wynn TA. Mechanisms of organ injury and repair by macrophages. Annu Rev Physiol. 2017; 79: 593-617.

18. James GA, Swogger E, Wolcott R, Pulcini Ed, Secor P, Sestrich J, et al. Biofilms in chronic wounds. Wound Repair Regen. 2008; 16(1): 37-44.

19. Davis SC, Ricotti C, Cazzaniga A, Welsh E, Eaglstein WH, Mertz PM. Microscopic and physiologic evidence for biofilm-associated wound colonization *in vivo*. Wound Repair Regen. 2008; 16(1): 23-9.

20. Zhao G, Hochwalt PC, Usui ML, Underwood RA, Singh PK, James GA, et al. Delayed wound healing in diabetic (db/db) mice with *Pseudomonas aeruginosa* biofilm challenge: a model for the study of chronic wounds. Wound Repair Regen. 2010; 18(5): 467-77.

21. Dowd SE, Sun Y, Secor PR, Rhoads DD, Wolcott BM, James GA, et al. Survey of bacterial diversity in chronic wounds using pyrosequencing, DGGE, and full ribosome shotgun sequencing. BMC Microbiol. 2008; 8: 43.

22. Maurice NM, Bedi B, Sadikot RT. *Pseudomonas aeruginosa* biofilms: host response and clinical implication in lung infections. Am J Respir Cell Mol Biol. 2018; 58(4): 428-439.

23. Nixon GM, Armstrong DS, Carzino R, Carlin JB, Olinsky A, Robertson CF, et al. Clinical outcome after early *Pseudomonas aeruginosa* infection in cystic fibrosis. J Pediatr. 2001; 138(5): 699-704.

24. Kirker KR, Secor PR, James GA, Fleckman P, Olerud JE, Stewart PS. Loss of viability and induction of apoptosis in human keratinocytes exposed to *Staphylococcus aureus* biofilms in vitro. Wound Repair Regen. 2009; 17(5): 690-699.

25. Kirker KR, James GA, Fleckman P, Olerud JE, Stewart PS. Differential effects of planktonic and biofilm MRSA on human fibroblasts. Wound Repair Regen. 2012; 20(2): 253-261.

26. O'Neill LA, Pearce EJ. Immunometabolism governs dendritic cell and macrophage function. J Exp Med. 2016; 213: 15-23.

27. Buck MD, Sowell RT, Kaech SM, Pearce EL. Metabolic instruction of immunity. Cell. 2017; 169: 570-586.

28. Nicholson JK, Lindon JC. Systems biology: metabonomics. Nature. 2008; 455: 1054-1056.

29. Fiehn O. Metabolomics—the link between genotypes and phenotypes. Plant Mol Biol. 2002; 48: 155-171.

30. Tannahill GM, Curtis AM, Adamik J, Palsson-McDermott EM, McGettrick AF, Goel G, et al. Succinate is an inflammatory signal that induces IL-1β through HIF-1α. Nature. 2013; 496: 238-242.

31. Lampropoulou V, Sergushichev A, Bambouskova M, Nair S, Vincent EE, Loginicheva E, et al. Itaconate links inhibition of succinate dehydrogenase with macrophage metabolic remodeling and regulation of inflammation. Cell Metab. 2016; 24: 158-166.

32. Vats D, Mukundan L, Odegaard JI, Zhang L, Smith KL, Morel CR, et al. Oxidative metabolism and PGC-1β attenuate macrophage-mediated inflammation. Cell Metab. 2006; 4: 13-24.

33. Galván-Peña S, O'Neill LA. Metabolic reprogramming in macrophage polarization. Front Immunol. 2014; 5: 420.

34. Jha AK, Huang SC, Sergushichev A, Lampropoulou V, Ivanova Y, Loginicheva E, et al. Network integration of parallel metabolic and transcriptional data reveals metabolic modules that regulate macrophage polarization. Immunity. 2015; 42: 419-430.

35. Ammons MCB, Tripet BP, Carlson RP, Kirker KR, Gross MA, Stanisich JJ, Copié V. Quantitative NMR metabolite profiling of methicillin-resistant and methicillin-susceptible *Staphylococcus aureus* discriminates between biofilm and planktonic phenotypes. J Proteome Res. 2014; 13(6): 2973-2985.

36. García-Cañaveras JC, López S, Castell JV, Donato MT, Lahoz A. Extending metabolome coverage for untargeted metabolite profiling of adherent cultured hepatic cells. Anal Bioanal Chem. 2016; 408: 1217-1230.

37. Fathi F, Brun A, Rott KH, Falco Cobra P, Tonelli M, Eghbalnia HR, et al. NMR-based identification of metabolites in polar and non-polar extracts of avian liver. Metabolites. 2017; 7:61.

38. Ramm Sander P, Peer M, Grandl M, Bogdahn U, Schmitz G, Robert Kalbitzer H. NMR spectroscopy of macrophages loaded with native, oxidized or enzymatically degraded lipoproteins. PLoS One. 2013; 8: e56360.

39. Weaver AJ, Peters TR, Tripet B, Van Vuren A, Rakesh, Lee RE, et al. Exposure of methicillin-resistant *Staphylococcus aureus* to low levels of the antibacterial THAM-3ΦG generates a small colony drug-resistant phenotype. Sci Rep. 2018; 8: 9850.

40. Fuchs AL, Weaver AJ Jr, Tripet BP, Ammons MCB, Teintze M, Copié V. Characterization of the antibacterial activity of Bald's eyesalve against drug resistant *Staphylococcus aureus* and *Pseudomonas aeruginosa*. PLoS One. 2018; 13: e0208108.

41. Mercier P, Lewis MJ, Chang D, Baker D, Wishart DS. Towards automatic metabolomic profiling of high-resolution one-dimensional proton NMR spectra. J Biomol NMR. 2011; 49: 307-323.

42. Emwas AH, Saccenti E, Gao X, McKay RT, Dos Santos VAPM, Roy R, et al. Recommended strategies for spectral processing and post-processing of 1D ^{1}H-NMR data of biofluids with a particular focus on urine. Metabolomics. 2018; 14: 31.

43. Xia J, Wishart DS. Metabolomic data processing, analysis, and interpretation using MetaboAnalyst. Curr Protoc Bioinformatics. 2011; 34: 14.10.1-14.10.48.

44. Weljie AM, Newton J, Mercier P, Carlson E, Slupsky CM. Targeted profiling: quantitative analysis of ^{1}H NMR metabolomics data. Anal Chem. 2006; 78: 4430-4442.

45. Chong J, Soufan O, Li C, Caraus I, Li S, Bourgue G, et al. MetaboAnalyst 4.0: towards more transparent and integrative metabolomics analysis. Nucleic Acids Res. 2018; 46: W486-W494.

46. Pavlou S, Wang L, Xu H, Chen M. Higher phagocytic activity of thioglycollate-elicited peritoneal macrophages is related to metabolic status of the cells. J Inflamm (Lond). 2017; 14:4.

47. Freemerman AJ, Johnson AR, Sacks GN, Milner JJ, Kirk EL, Troester MA, et al. Metabolic reprogramming of macrophages: glucose transporter 1 (GLUT1)-mediated glucose metabolism drives a proinflammatory phenotype. J Biol Chem. 2014; 289: 7884-7896.

48. Michl J, Ohlbaum DJ, Silverstein SC. 2-deoxyglucose selectively inhibits Fc and complement receptor-mediated phagocytosis in mouse peritoneal macrophages. II. Dissociation of the inhibitory effects of 2-deoxyglucose on phagocytosis and ATP generation. J Exp Med. 1976; 144: 1484-1493.

49. Van den Bossche J, Baardman J, de Winther MP. Metabolic characterization of polarized M1 and M2 bone marrow-derived macrophages using real-time extracellular flux analysis. J Vis Exp. 2015; 105: e53424.

50. Diskin C, Pålsson-McDermott EM. Metabolic modulation in macrophage effector function. Front Immunol. 2018; 9: 270.

51. Feingold KR, Shigenaga JK, Kazemi MR, McDonald CM, Patzek SM, Cross AS, et al. Mechanisms of triglyceride accumulation in activated macrophages. J Leukoc Biol. 2012; 92(4): 829-39.

52. Jensen ET, Kharazmi A, Lam K, Costerton JW, Høiby N. Human polymorphonuclear leukocyte response to *Pseudomonas aeruginosa* grown in biofilms. Infect Immun. 1990; 58(7): 2383-5.

53. Stephens L, Ellson C, Hawkins P. Roles of PI3Ks in leukocyte chemotaxis and phagocytosis. Curr Opin Cell Biol. 2002; 14: 203-213.

54. Jia Y, Schurmans S, Luo HR. Regulation of innate immunity by inositol 1,3,4,5-tetakisphosphate. Cell Cycle. 2008; 7: 2803-2808.

55. Chen X, Zhang B, Li H, Peng X. Myo-inositol improves the host's ability to eliminate balofloxacin-resistant *Escherichia coli*. Sci Rep. 2015; 5: 10720.

56. Xu J, et al. Divergent signals and cytoskeletal assemblies regulate self-organizing polarity in neutrophils. Cell. 2003; 114: 201-214.

CHAPTER FOUR

ONGOING WORK AND CONCLUDING REMARKS

Metabolic Analysis of M2b/c/d MΦ Activation States

Although preliminary NMR metabolomics analysis of the intracellular metabolome of primary human monocyte-derived M2b, M2c, and M2d MΦ activation states has suggested that these cellular phenotypes are metabolically distinct from one another, the extracellular metabolic analysis of these MΦ populations has yet to be examined. As indicated by our metabolomics data from M0, M1, and M2a MΦs using the same primary monocyte isolation and *in vitro* differentiation protocols, metabolite extraction, and NMR analysis methods, the extracellular small molecule environment of *in vitro* activated MΦ cultures yields important insights and validating data with respect to the metabolic findings resulting from the analysis of intracellular MΦ metabolite extracts. In order to conduct a more comprehensive metabolic characterization of M2b, M2c, and M2d MΦ activation states, aliquots of sham and spent media from the same cultures used in our preliminary intracellular analysis, and which have already been collected and are currently stored at -80 °C, will be filtered using pre-washed 3 kDa MWCO centrifugal filters and dried using a Speedvac vacuum centrifuge prior to 1D ^{1}H NMR data acquisition and metabolic profiling analysis using Chenomx NMR Suite software. Furthermore, it would be beneficial to conduct FACS analysis of our M2b, M2c, and M2d MΦ phenotypes in order to integrate our metabolomics data with other -omics and functional analyses reported in previous studies [1]. Additional examination of

these MΦ activation states may provide further insights into the metabolic signatures of these immune cell phenotypes. Furthermore, comparison of these metabolite profiles to those exhibited by M0, M1, and M2a MΦs, which have been experimentally characterized in greater detail [2-7], could lead to the development of targeted therapeutics to manipulate the functional phenotypes of distinct MΦ populations.

MΦ-Biofilm *In Vitro* Co-Culture Model

While temporal exposure of human MΦs to cell culture media that has been conditioned with *P. aeruginosa* planktonic or biofilm bacteria coupled with NMR metabolomics analysis provides valuable and relevant information regarding host-pathogen interactions, this model is rather simplistic since it does not use live pathogens during host cell exposure. In order to conduct a more comprehensive evaluation of the metabolic cross talk between primary human monocyte-derived M0 MΦs and *P. aeruginosa* biofilms, we have performed temporal MΦ-biofilm co-culture experiments ranging from 30 minutes to 8 hours using a non-contact *in vitro* co-culture model (Figure 1) similar to that utilized in previous studies [8,9]. Following MΦ-biofilm co-culturing, samples were harvested, intra- and extracellular metabolites were extracted, and 1D ^{1}H NMR data was acquired. Metabolomics profiling and statistical analysis for all co-culture intracellular MΦ extracts has been completed; however, metabolite analyses for the corresponding extracellular MΦ extracts have yet to be undertaken. Furthermore, since the extracellular compartment of our *in vitro* co-culture model contains both host- and pathogen-derived molecules, we have also undertaken the metabolic profiling on *P.*

aeruginosa biofilm samples that were collected in parallel with our co-cultured MΦs. The goal of these studies is to investigate potential pertubations in pathogen metabolism during co-culture with MΦs.

In addition to the NMR metabolomics approach used in this study, we have also harvested MΦ-biofilm co-culture samples for RNA isolation, cDNA generation, and subsequent real-time polymerase chain reaction (RT-PCR) transcriptomics profiling of co-cultured MΦs with the aim of integrating transcriptomics data with our metabolomics findings. Biological triplicate RT-PCR arrays were completed earlier this year; however, statistical analysis and integration of this data with their corresponding metabolite profiles has yet to be conducted. To investigate the resulting functional phenotype of human MΦs upon co-culture with *P. aeruginosa* biofilms, we started collecting samples and conducting intracellular FACS analysis regarding the cytokine production profiles of these host cells, specifically examining levels of tumor necrosis factor α (TNF-α), interleukin 6 (IL-6), and interleukin 10 (IL-10), which represent a panel of both pro- and anti-inflammatory cytokines [10]. Although preliminary data has indicated divergent trends concerning IL-6, we have not performed a sufficient number of intracellular MΦ FACS replicates to generate any firm conclusions thus far. Further analysis and biological interpretations of these complementary datasets are needed to gain a better understanding and to generate more detailed insights into the molecular mechanisms mediating host-pathogen interactions.

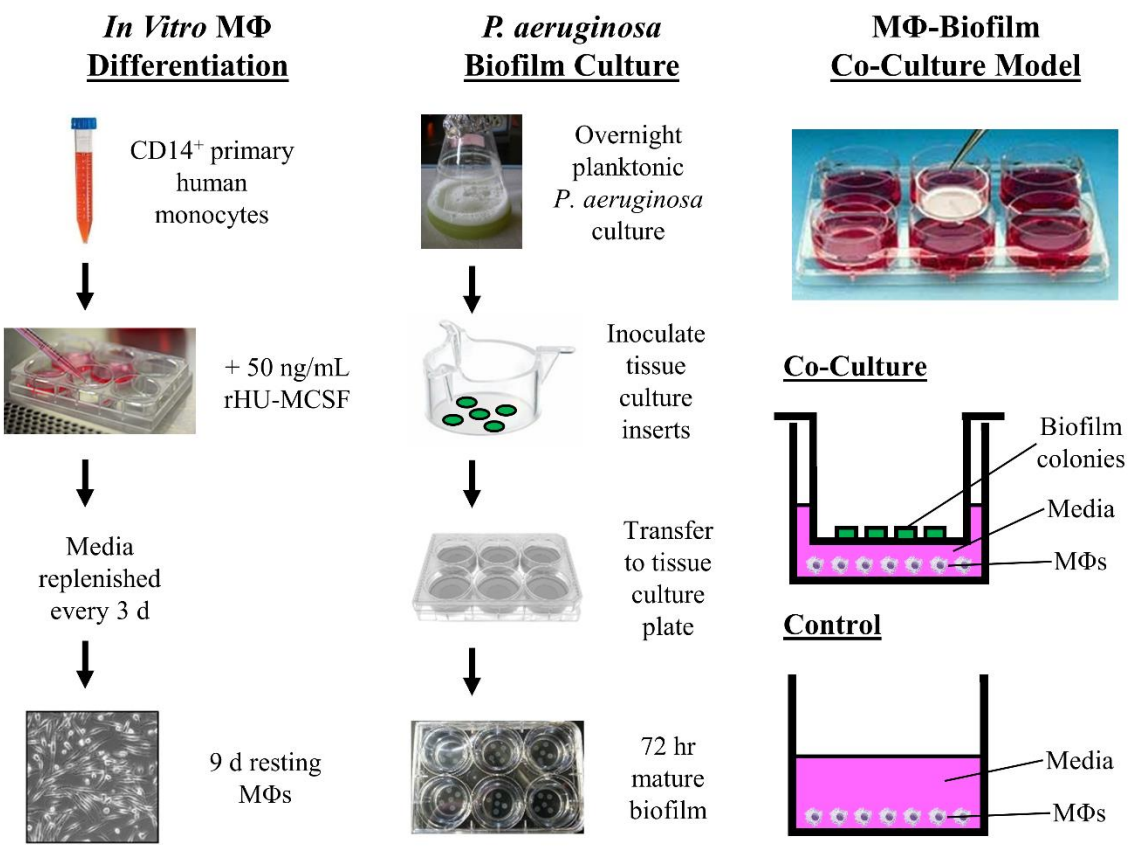

Figure 1. Depiction of our *in vitro* MΦ-biofilm co-culture model. This illustration highlights the preparation, *in vitro* differentiation/maturation, and co-culture model used for primary human monocyte-derived MΦs and *P. aeruginosa* biofilms. Abbreviations denote: MΦ, macrophage; rHU-MCSF, recombinant human macrophage colony stimulating factor.

Concluding Remarks

The dissertation research described herein focused on the metabolic characterization of distinct primary human monocyte-derived MΦ activation states and investigated the temporal metabolic modulation of resting, M0, MΦs during exposure to *P. aeruginosa* PCM or BCM. Metabolic profiling of human M0, M1, and M2a MΦs revealed how differential activation stimuli, pro- or anti-inflammatory, can induce markedly disparate adaptations in immune cell metabolism, including reprogramming of

glycolysis, the TCA cycle, *de novo* glycerophospholipid synthesis, and the promotion of oxidative stress, which track with MΦ biological functions and cellular phenotypes. Results from the metabolic analysis of human M2b, M2c, and M2d MΦs draw considerable attention to the need to better characterize and define MΦ phenotypes in a more comprehensive manner, rather than the traditional M1/M2 binary terminology used in the field of MΦ biology. Investigation into the metabolic perturbations of human MΦs upon exposure to *P. aeruginosa* PCM and BCM demonstrated that planktonic and biofilm bacteria elicit markedly different metabolic responses in MΦs, particularly at the 30 minute time point following PCM or BCM MΦ exposure. Moreover, the metabolic diversity of human MΦs, in response to cytokine or bacterial stimuli, highlighted using 1D ^{1}H NMR showcases the potential of NMR-based metabolomics for elucidating the metabolic networks underlying the dysregulation of innate immune cells, which have been implicated in several pathologies [11-14]. Taken together, the studies herein highlight the importance of distinguishing and interpreting immunometabolic differences between human MΦ activation states in the absence or presence of unique bacterial growth modes, whilst also demonstrating the particularly effective application of untargeted 1D ^{1}H NMR-based metabolomics for the characterization of intra- and extracellular metabolic networks utilized by primary human innate immune cells in response to varying environmental conditions.

References

1. Rőszer T. Understanding the mysterious M2 macrophage through activation markers and effector mechanisms. Mediators Inflamm. 2015; 2015: 816460.

2. O'Neill LA, Pearce EJ. Immunometabolism governs dendritic cell and macrophage function. J Exp Med. 2016; 213: 15-23.

3. Tannahill GM, Curtis AM, Adamik J, Palsson-McDermott EM, McGettrick AF, Goel G, et al. Succinate is an inflammatory signal that induces IL-1β through HIF-1α. Nature. 2013; 496: 238-242.

4. Lampropoulou V, Sergushichev A, Bambouskova M, Nair S, Vincent EE, Loginicheva E, et al. Itaconate links inhibition of succinate dehydrogenase with macrophage metabolic remodeling and regulation of inflammation. Cell Metab. 2016; 24: 158-166.

5. Vats D, Mukundan L, Odegaard JI, Zhang L, Smith KL, Morel CR, et al. Oxidative metabolism and PGC-1β attenuate macrophage-mediated inflammation. Cell Metab. 2006; 4: 13-24.

6. Kim JW, Tchernyshyoc I, Semenza GL, Dang CV. HIF-1-mediated expression of pyruvate dehydrogenase kinase: a metabolic switch required for cellular adaptation to hypoxia. Cell Metab. 2006; 3: 177-185.

7. Huang SC, Everts B, Ivanova Y, O'Sullivan D, Nascimento M, Smith AM, et al. Cell-intrinsic lysosomal lipolysis is essential for alternative activation of macrophages. Nat Immunol. 2014; 15: 846-855.

8. Kirker KR, Secor PR, James GA, Fleckman P, Olerud JE, Stewart PS. Loss of viability and induction of apoptosis in human keratinocytes exposed to *Staphylococcus aureus* biofilms in vitro. Wound Repair Regen. 2009; 17(5): 690-699.

9. Kirker KR, James GA, Fleckman P, Olerud JE, Stewart PS. Differential effects of planktonic and biofilm MRSA on human fibroblasts. Wound Repair Regen. 2012; 20(2): 253-261.

10. Wojdasiewicz P, Poniatowski LA, Szukiewicz D. The role of inflammatory and anti-inflammatory cytokines in pathogenesis of osteoarthritis. Mediators Inflamm. 2014; 2014: 561459.

11. Odegaard JI, Ricardo-Gonzalez RR, Goforth MH, Morel CR, Subramanian V, Mukundan L, et al. Macrophage-specific PPARγ controls alternative activation and improves insulin resistance. Nature. 2007; 447: 1116-1120.

12. Woollard KJ, Geissmann F. Monocytes in atherosclerosis: subsets and functions. Nat Rev Cardiol. 2010; 7: 77-86.

13. Platt AM, Bain CC, Bordon Y, Sester DP, Mowat AM. An independent subset of TLR expressing CCR2-dependent macrophages promotes colonic inflammation. J Immunol. 2010; 184: 6843-6854.

14. Kamada N, Hisamatsu T, Okamoto S, Chinen H, Kobayashi T, Sato T, et al. Unique $CD14^{+}$ intestinal macrophages contribute to the pathogenesis of Crohn disease via IL-23/IFN-γ axis. J Clin Invest. 2008; 118: 2269-2280.

APPENDICES

APPENDIX A

OPTIMIZATION OF METABOLITE EXTRACTION PROTOCOLS FOR THE IDENTIFICATION AND PROFILING OF SMALL MOLECULE METABOLITES FROM PLANKTONIC AND BIOFILM *PSEUDOMONAS AERUGINOSA* CULTURES

OPTIMIZATION OF METABOLITE EXTRACTION PROTOCOLS FOR THE IDENTIFICATION AND PROFILING OF SMALL MOLECULE METABOLITES FROM PLANKTONIC AND BIOFILM *PSEUDOMONAS AERUGINOSA* CULTURES

Contribution of Authors and Co-Authors

Manuscript in Appendix A

Author: Amanda Fuchs

Contributions: Conceptualized the study, curated the data, conducted formal analysis and investigation, developed methodology, administered the project, validated and visualized the data, wrote the original manuscript draft, and reviewed and edited the manuscript.

Author: Brian P. Tripet

Contributions: Conceptualized the study, developed methodology, administered the project, and reviewed and edited the manuscript.

Co-Author: Mary Cloud B. Ammons

Contributions: Conceptualized the study, acquired funding, provided resources, and reviewed and edited the manuscript.

Co-Author: Valérie Copié

Contributions: Acquired funding, administered the project, provided resources and software, supervised the project, and reviewed and edited the manuscript.

Manuscript Information Page

Amanda Fuchs, Brian P. Tripet, Mary Cloud B. Ammons, Valérie Copié

Journal Name: Current Metabolomics

Status of Manuscript:
_____ Prepared for submission to a peer-reviewed journal
_____ Officially submitted to a peer-reviewed journal
_____ Accepted by a peer-reviewed journal
__x__ Published in a peer-reviewed journal

Publisher: Bentham Science Publisher
Issue in which manuscript appears: Volume 4, Issue 2, 2016

OPTIMIZATION OF METABOLITE EXTRACTION PROTOCOLS FOR THE IDENTIFICATION AND PROFILING OF SMALL MOLECULE METABOLITES FROM PLANKTONIC AND BIOFILM *PSEUDOMONAS AERUGINOSA* CULTURES

Amanda Fuchs[a], Brian P. Tripet[a], Mary Cloud B. Ammons[a*], Valérie Copié[a*]

[a]Department of Chemistry and Biochemistry, Montana State University, Bozeman, 59717, Montana, USA

[*]Address correspondence to these authors at the Department of Chemistry and Biochemistry, Faculty of Montana State University, Bozeman, MT, USA; Tel: (406) 994-7244; Fax: (406) 994-4801; E-mails: vcopie@chemistry.montana.edu and mcammons@chemistry.montana.edu

Abstract

In order to rigorously assess metabolic differences between planktonic and biofilm *Pseudomonas aeruginosa* cultures, we found that a specific metabolite extraction method must be devised to be adequately suited for both phenotypes. Intracellular metabolite extraction efficiency was found to be dependent on the extraction method and varies between microbial growth modes. Three cell pellet wash solutions were compared for the potential to influence intracellular metabolite leakage of *P. aeruginosa*. Methods using the 60% methanol wash produced the greatest amount of cell leakage, which was also reflected in metabolite quantification. We also compared four different extraction methods using (i) methanol:chloroform (2:1); (ii) 50% methanol; (iii) 100% methanol; or (iv) 100% water to extract intracellular metabolites from *P. aeruginosa* planktonic and biofilm cultures. Quantification of intracellular metabolites via ^{1}H NMR showed that

extraction protocols using 100% water or 50% methanol achieved the greatest extraction efficiencies, while addition of sonication to facilitate cell lysis to the 50% methanol extraction method resulted in at least a two-fold increase in signal intensities for approximately half of the metabolites identified. Phosphate buffered saline (PBS) was determined to be the most appropriate wash solution, yielding little metabolite leakage from cells. We determined that washing in 1X PBS and extracting intracellular metabolites with 50% methanol is the most appropriate metabolite extraction protocol because (a) leakage is minimal; (b) a broad range of metabolites present at sufficiently high concentrations is detectable by NMR; and (c) this method proved suitable for metabolite extraction of both planktonic and biofilm *P. aeruginosa* cultures.

Introduction

As an analytical approach, metabolomics most directly characterizes the metabolic phenotype of a sample and reports on metabolic pathways utilized by a given microorganism when grown under certain conditions [1]. Most commonly used techniques for metabolite detection and identification include mass spectrometry (MS) and nuclear magnetic resonance (NMR). MS has the advantages of being more sensitive than NMR and can detect metabolites of wide ranging abundance [2]. However, mapping mass spectral features to specific metabolites and metabolite quantification by LC-MS is quite challenging. While NMR best detects more abundant metabolites (1 mM to 10 µM reliably) in a sample, identification of metabolites using spectral databases of small molecules such as those found in the Chenomx^{TM} compound libraries [3] is more

straightforward. In addition, the NMR approach is highly reproducible, non-destructive, and permits accurate quantification of metabolite concentrations in a given sample [2]. The Chenomx^{TM} software [3] uses a sophisticated linear analysis approach that allows the specific contribution of each metabolite to be assessed in an additive manner [4] until complete or nearly complete spectral intensity contribution, splitting patterns, and chemical shift matching have been realized.

A critical process in metabolomics research is the establishment of robust and reproducible methods for metabolite extraction. A key issue is how to handle and harvest cells prior to extracting intracellular metabolites. This step involves the separation of cells from growth medium via centrifugation followed by a series of washing procedures to separate and remove residual extracellular materials from pelleted cells. This wash step is particularly important for the biofilm phenotype due to the complex extracellular matrix that often contains extracellular DNA, proteins and, in the case of *P. aeruginosa*, alginate among other exopolysaccharides that serve as a protective barrier against harsh environmental conditions and as a structural scaffold [5]. A common approach used to wash cell pellets is 60% methanol, which also serves as a metabolic quenching step [6]. Chen *et al.* [7] observed a significant leakage of intracellular metabolites when *Lactobacillus bulgaricus* cells were quenched with both 60% and 80% methanol. It has also been demonstrated that low ionic strength solutions, such as deionized water, cause extensive metabolite leakage from Gram-negative bacterial cells [8]. As expected, such leakages result in a vast underestimation of intracellular metabolite levels present and skewed metabolite profiles. Significant intracellular ATP loss (>10%) also takes place

upon cell exposure to 60% methanol, which is particular striking because ATP, ADP, and AMP concentrations are often used to quantify the metabolic state of the cell via energy charge calculations [9].

Following cell culture harvesting and washing to remove residual extracellular materials, including extracellular small molecules, intracellular metabolites must be extracted efficiently. The ultimate goal of any extraction method is to extract all metabolites in a non-biased, reproducible, and consistent manner. However, most extraction methods used thus far are designed to target specific metabolite classes and often employ harsh conditions, such as high temperatures, that may lead to significant metabolite degradation [10].

The quintessential goal of an efficient extraction protocol is to be suitable for metabolomics studies of a variety of microbial cells; however, this is often not feasible due to different cellular characteristics that result in varying resistance to lysis across diverse microbial species. Therefore, metabolite extraction methodologies need to be optimized and evaluated for each species of interest. In the present study, several different cell wash solutions and metabolite extraction methods were tested and evaluated for their efficiency to most comprehensively profile the metabolome of *P. aeruginosa*, a Gram-negative bacterium that is of particular importance and concern in many areas of human health [11].

Materials and Methods

Bacterial Strain, Growth Conditions, and Sampling

This study utilized the well-characterized and genome sequenced PAO1 strain of *P. aeruginosa*. Growth media for both planktonic and biofilm cultures consisted of 10% BHI (Brain Heart Infusion, BD Bacto™). Inocula for both planktonic and biofilm growth conditions consisted of closed, batch cultures grown in 10% BHI at 37 °C shaking with 220 rpm to 20 hrs post inoculation (~2.2×10^9 CFUs/ml). Aliquots (10 µl) were collected for serial dilution, drop plating, and calculation of colony forming units (CFUs).

For planktonic studies, inoculum cultures were diluted 1:1000 in fresh 10% BHI and cultured at 37 °C in 250 ml flasks shaking at 220 rpm. Planktonic cultures were grown under aerobic conditions with flask-to-medium volume ratios of 5:1. Samples were harvested at 24 hrs post inoculation. Biofilm growth was cultured as previously described [12, 13]. In brief, tissue culture inserts (Millipore Millicell, 0.4 µm pore size) were inoculated with five 10 µl droplets of overnight inoculum culture (~10^9 CFUs/ml) and grown for 96 hrs at 37 °C. To maintain biofilm viability, the growth media was refreshed every 24 hrs. Biofilms were collected once they had reached 96 hrs post inoculation. Spent supernatant was collected from the plate wells and biofilm cells were harvested from the inserts by gently pipetting with 1 ml of sterile 1X PBS to dislodge the biofilms. Samples were immediately centrifuged at 5000 rpm for 10 min at 25 °C to pellet the cells. For both planktonic and biofilm growth conditions, samples were harvested in technical triplicates.

Extraction Procedures and
NMR Sample Preparation

NMR samples were prepared in triplicate for each metabolite extraction method. For ^{1}H NMR analysis, dried samples were resuspended in 700 µl of NMR buffer [25 mM NaH_2PO_4/Na_2HPO_4 containing 0.25 mM 4,4-dimethyl-4-silapentane-1-sulfonic acid (DSS) in 100% D_2O, pH 7] and transferred to 5 mm Wilmad NMR tubes.

Methanol/Chloroform Extraction. Cell pellets were resuspended twice in 600 µl of 60% ice-cold methanol and centrifuged at 5,000 rpm for 10 min. Each of the methanol washes were dried under vacuum (SpeedVac) and stored at -20 °C prior to analysis. Washed cell pellets were resuspended in 1 ml of ice-cold 2:1 methanol/chloroform and transferred to 8 ml glass tubes. Cells were lysed by sonication (BioLogics Inc. Model 3000 Ultrasonic Homogenizer; 30% of maximum instrument power, ~50 pulse); samples were pulsed 10 times for 3 cycles. 300 µl of each layer of a 1:1 aqueous chloroform solution was added to the samples and mixed by inversion, followed by centrifugation at 5,000 rpm for 10 min. The top aqueous phase of each sample was transferred to a clean microcentrifuge tube and dried under vacuum (SpeedVac) at room temperature overnight and then stored at -20 °C until further use.

50% Methanol Extraction. Cell pellets were resuspended and washed twice in 1 ml of 1X PBS and centrifuged at 5,000 rpm for 10 min. PBS washes were dried under vacuum (SpeedVac) and stored at -20 °C prior to analysis. Washed cell pellets were resuspended in 1.5 ml of 50% methanol and placed at -80 °C to freeze for a minimum of 2 hours. Cells were thawed in a circulating cold water bath and transferred to glass tubes.

Samples were then sonicated for 30 sec. (30% power, ~50 pulse). This freeze-thaw, sonication cycle was repeated 2 additional times. Cells were centrifuged at 14,000 x g for 5 min. at 4 °C, and the supernatants were transferred to separate microcentrifuge tubes. The cell debris was resuspended in 1 ml of deionized H_2O (diH_2O) and centrifuged at 14,000 x g for 5 min. at 4 °C, and the supernatants were pooled with the initial extract. Chloroform (1 ml) was added to the pooled supernatant and mixed by vortexing briefly. Phase separation was driven by centrifugation at 5,000 rpm for 5 min. The top aqueous phase of each sample was transferred to a new microcentrifuge tube, and dried under vacuum (SpeedVac) at room temperature overnight and then stored at -20 °C until further use.

100% Methanol Extraction. This method is similar to the 50% methanol extraction protocol; however, washed cell pellets were resuspended in 1.5 ml of 100% methanol instead of 50% methanol prior to beginning freeze-thaw, sonication cycles.

100% Water Extraction. This method is similar to the 50% methanol extraction protocol; however, washed cell pellets were resuspended in 1.5 ml of sterile diH_2O instead of 50% methanol prior to the start of the freeze-thaw, sonication cycles.

NMR Analysis

One dimensional ^{1}H NMR spectra were acquired as previously described [13]. Processing and analysis of spectra was performed using Chenomx^{TM} NMR software (version 8.0, Chenomx, CA). Each ^{1}H NMR spectrum was phased, baseline-corrected, and line-broadened (0.5 Hz) prior to metabolite quantification and identification. The

DSS internal standard was used to quantify identified metabolites. Compound identification was carried out by fitting NMR spectral patterns for each sample manually using the Chenomx^{TM} spectral database of small-molecules for 600 MHz (^{1}H Larmor frequency) magnetic field strength NMR spectrometers. From all the ^{1}H 1D NMR spectra acquired on biofilm and planktonic PAO1 cell extracts, an overall number of ~83 compounds were identified.

Results and Discussions

Cell Pellet Wash

In this optimization study of metabolite extraction in *P. aeruginosa*, three different wash solutions were evaluated for their impacts on intracellular metabolite leakage. The 60% methanol washes produced the greatest amount of leakage for nearly all of the metabolites identified whereas washes with PBS were determined to be optimal because no metabolites were found in the second wash conducted with PBS. Therefore, metabolites obtained from the first PBS wash were determined to be predominantly extracellular, and did not significantly result from leaked intracellular fractions. This finding is consistent with previous reports [8] in that the lower ionic strength of solutions such as 60% methanol and deionized water have a significant effect on intracellular metabolite leakage from cells. The ^{1}H NMR metabolite profile and corresponding spectral intensities resulting from the first PBS wash was used to normalize the NMR data obtained from other wash protocols in order to strictly identify those metabolites that may have been lost due to cellular leakage (Fig. 1). Metabolite concentrations

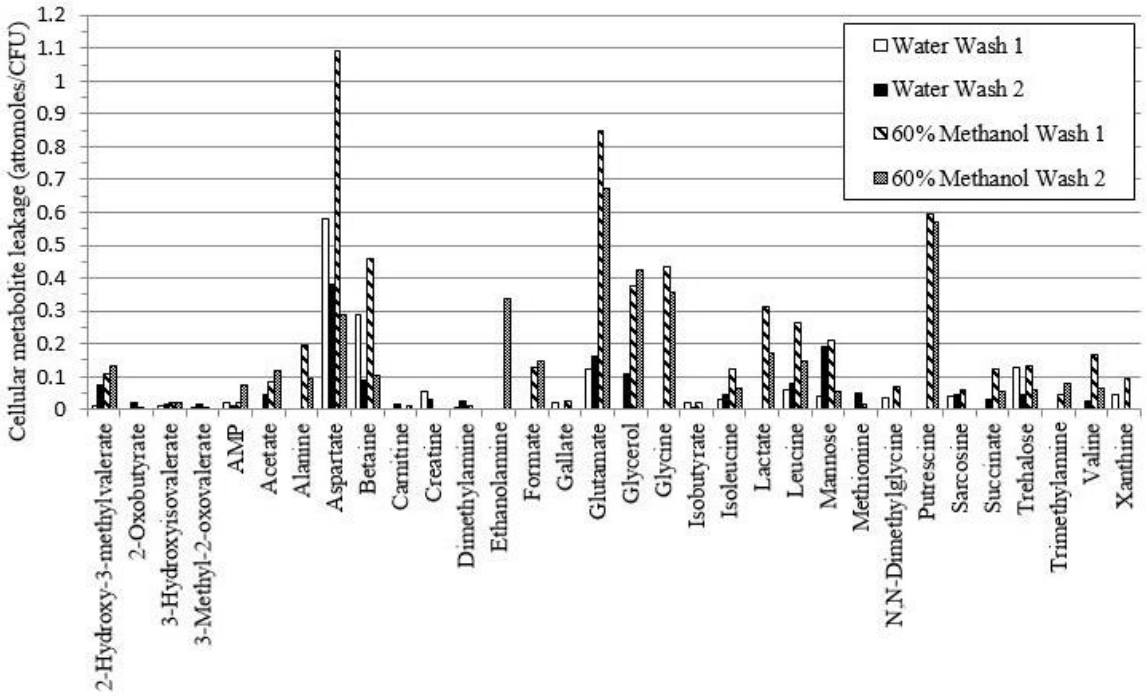

Fig. (1). Comparison of metabolite leakage caused by 60% methanol and water washes of *P. aeruginosa* cell pellets; cellular metabolite leakage is reported as metabolite abundance detected in addition to that observed in the first 1X PBS wash.

significantly impacted as a result of cell leakage from the 60% methanol washes included those from glutamate, betaine, and glycine. Loss of these intracellular metabolites may confound downstream characterization of different cellular phenotypes. This metabolite leakage is also reflected in the metabolite extraction efficiencies (attomoles/CFU) identified for the method using this wash solution – 2:1 methanol/chloroform – compared to other extraction methods (Table 1).

Metabolite Extraction

An optimal extraction method aims to recover as many intracellular metabolites as possible at adequate concentrations for quantification, accompanied by minimal degradation and cellular leakage. However, it has been previously demonstrated that an

Table 1. Sample metabolite sets (attomoles/CFU) extracted from *P. aeruginosa* cell pellets using different methods and detected by ^{1}H NMR. Metabolites were identified and quantified via Chenomx NMR Suite (v8.0); I (50% methanol); II (100% methanol); III (100% water); IV (2:1 methanol:chloroform); nd = not detected. All extraction methods were performed in triplicate. Amino acids are designated using their respective 3 letter abbreviations; GABA = 4-aminobutyrate; ADP = adenosine diphosphate; AMP = adenosine monophosphate; NAD^{+} = nicotinamide adenine dinucleotide; $NADP^{+}$ = nicotinamide adenine dinucleotide phosphate; UMP = uridine monophosphate.

	Planktonic				Biofilm			
Compound	IV	I	II	III	IV	I	II	III
GABA	nd	0.372±0.022	0.159±0.013	0.488±0.050	0.300±0.004	0.352±0.025	0.226±0.035	1.229±0.101
ADP	0.209±0.040	0.047±0.001	0.097±0.005	0.083±0.015	0.023±0.016	0.158±0.031	0.117±0.007	0.229±0.043
AMP	0.369±0.056	0.318±0.004	0.110±0.003	0.168±0.020	0.624±0.016	0.528±0.016	0.375±0.048	0.734±0.132
Acetate	0.016±0.003	0.591±0.002	0.195±0.034	1.12±0.09	0.085±0.012	5.532±0.090	6.409±2.072	31.16±0.05
Ala	0.601±0.030	1.54±0.36	0.484±0.083	3.42±0.92	0.204±0.016	2.423±0.313	0.307±0.007	3.716±0.632
Betaine	0.182±0.041	0.614±0.000	0.393±0.021	0.299±0.018	0.198±0.008	0.312±0.021	nd	nd
Choline	0.020±0.004	0.056±0.004	0.010±0.001	0.02±0.00	0.018±0.000	0.065±0.009	0.022±0.006	0.102±0.002
Formate	0.037±0.001	1.42±0.10	0.393±0.040	0.075±0.006	2.61±0.05	3.265±0.335	1.310±0.243	2.467±0.086
Glu	1.22±0.17	3.23±0.22	1.20±0.03	2.61±0.59	2.48±0.09	5.566±0.369	3.043±0.263	6.540±0.677
Gln	0.400±0.001	0.296±0.114	0.432±0.080	0.706±0.185	nd	nd	nd	nd
Gly	0.278±0.013	0.837±0.133	0.114±0.019	1.04±0.30	0.213±0.021	0.944±0.079	0.260±0.052	1.619±0.282
His	0.036±0.001	0.096±0.025	0.05±0.02	0.095±0.003	nd	0.142±0.040	nd	0.498±0.119
Ile	0.191±0.009	0.912±0.257	0.407±0.068	1.50±0.47	0.082±0.016	1.328±0.182	0.158±0.001	1.796±0.661
Leu	0.463±0.022	1.78±0.51	1.02±0.15	3.94±0.94	0.242±0.004	2.940±0.392	0.497±0.041	4.614±1.440
Mannose	0.131±0.032	0.400±0.000	0.183±0.011	0.077±0.012	0.178±0.062	0.107±0.021	nd	nd
Methanol	0.093±0.043	0.116±0.007	0.02±0.01	0.030±0.008	0.172±0.037	0.976±0.124	0.135±0.005	0.219±0.063
Met	0.065±0.009	0.309±0.082	0.189±0.030	0.808±0.206	0.108±0.004	0.529±0.074	0.085±0.009	0.842±0.184
NAD^{+}	0.117±0.001	0.167±0.059	0.173±0.004	nd	0.554±0.016	0.598±0.053	0.584±0.027	0.449±0.072
$NADP^{+}$	0.118±0.012	0.095±0.000	0.05±0.01	0.039±0.005	0.149±0.004	0.165±0.019	0.174±0.008	0.146±0.032
Trp	nd	0.133±0.036	nd	nd	nd	0.196±0.059	nd	0.425±0.202
Tyr	0.111±0.008	0.465±0.147	0.250±0.046	1.04±0.27	0.088±0.016	0.714±0.053	0.119±0.024	1.046±0.321
UMP	0.106±0.027	0.097±0.002	0.02±0.00	0.063±0.008	0.140±0.033	0.111±0.014	0.074±0.011	0.443±0.075
Val	0.304±0.024	1.49±0.44	0.704±0.137	3.00±0.78	0.073±0.020	1.978±0.258	0.217±0.003	2.607±0.897

extraction methodology optimized for a given microbe may not be suitable for the efficient extraction of metabolites originating from other microorganisms [8, 14]. Therefore, the development of an optimized extraction protocol for the microbial species

of interest is crucial for an appropriate examination of the intracellular metabolome. Initially, a 2:1 methanol/chloroform protocol previously adapted for the extraction of metabolites from *Staphylococcus aureus* [15] and effective for both planktonic and biofilm *S. aureus* [13] was used in this study. At the time, this method seemed appropriate for *P. aeruginosa* because it yielded a broad range of intracellular metabolites at sufficient concentrations for ^{1}H NMR quantification in the planktonic phenotype. Despite its efficacy with batch culture *P. aeruginosa*, the method produced inadequate and inconsistent results for the biofilm phenotype (Fig. 2, Table 1). As a result, three extraction methods adapted from the original protocol were assessed for their efficacy on planktonic and biofilm *P. aeruginosa* cultures.

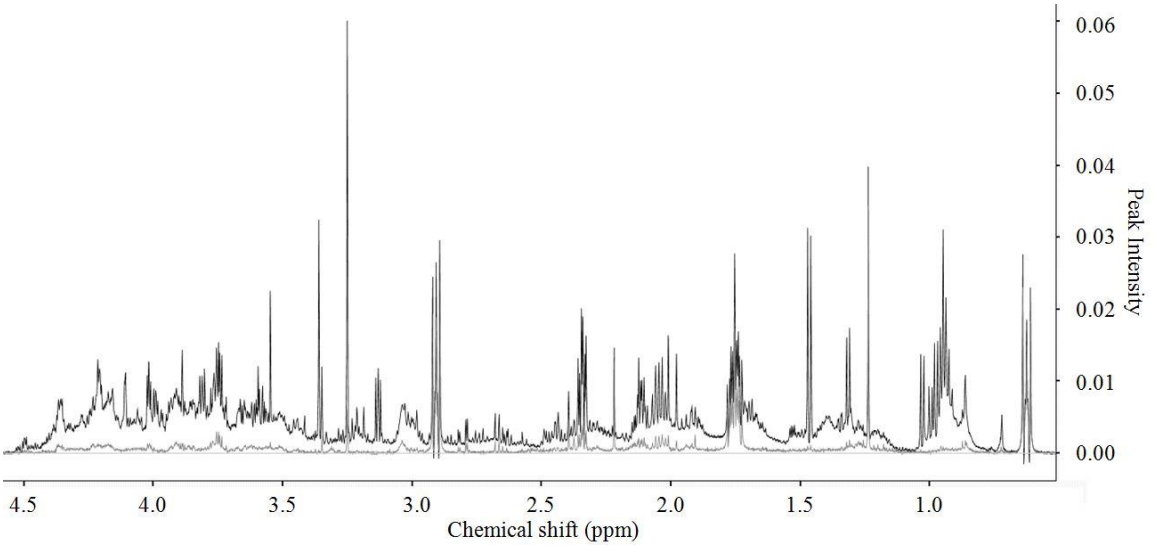

Fig. (2). Spectral overlay of intracellular metabolites extracted from planktonic (black) and biofilm *P. aeruginosa* (gray) using the 2:1 methanol:chloroform extraction method.

The extraction methods used here involved cell lysis with repeated freeze-thaw cycles in different solvents (100% methanol, 50% methanol, and 100% water) in combination with sonication. Efficiency of each extraction method was evaluated by

recording a series of 1D ^{1}H NMR spectra and determining the concentrations of intracellular metabolites obtained per viable bacterial cell count (CFU). Addition of a sonication step to the freeze-thaw extraction protocol did not yield any unique metabolites when compared to samples prepared without sonication; however, adding this mechanical cell disruption step to the extraction protocol resulted in a 2-fold increase in the concentrations of ~50% of the identified metabolites in the biofilm phenotype (Fig. 3). This finding is consistent with previous studies [16, 17] indicating that sonication can be used to enhance cell lysis for the recovery of intracellular molecules.

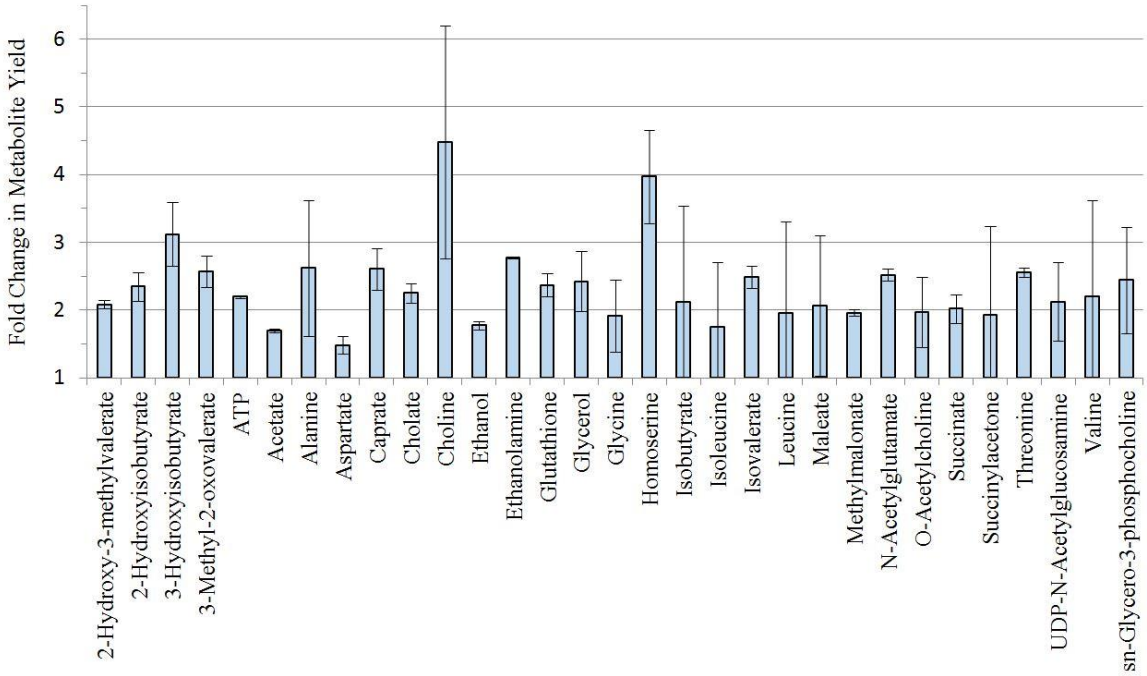

Fig. (3). Fold changes in metabolite yield of *P. aeruginosa* biofilm samples occurring when sonication is added to the 50% methanol freeze-thaw extraction method; data are reported as the mean of duplicate biological samples and standard deviation (SD) error bars.

However, sonication may lead to the degradation of some metabolites. We compared metabolite concentrations using 30 vs. 60 sonication pulses during

optimization of the 50% methanol extraction method. Increasing the number of sonication pulses showed a significant decrease in certain metabolite concentrations. Amino acids, such as isoleucine, leucine, methionine, tyrosine, and valine were reduced by at least 50%, and the amino acid tryptophan was not detectable by ^{1}H NMR following doubling of sonication pulses (data not shown). However, the concentrations of compounds such as ADP, acetate, choline, formate, methanol, and UMP were increased at least 25% upon additional sonication (data not shown). Although metabolite stability is an issue in extraction methods utilizing sonication, the most pressing issue is to be able to maximize metabolite extraction in a reproducible fashion (Table 1, Fig. S1).

We have also found metabolite stability to be dependent upon the extraction solvent used. ^{1}H NMR analysis of 7-day old metabolite samples revealed that biofilm metabolites extracted with methanol maintain their abundance levels better than those extracted with water. The concentrations of metabolites such as GABA, formate, and UMP were reduced by at least 10% in water-extracted samples; furthermore, NAD^{+} and $NADP^{+}$ were absent from these samples after 7 days of storage (data not shown). The only metabolites degraded by more than 10% in methanol-extracted biofilm samples were NAD^{+} and UMP (data not shown). One possible explanation for these results is that having methanol present during extraction may aid in the inactivation of degradative enzymes that could affect metabolite levels.

Metabolite extractions were performed in triplicate for each method and metabolite concentrations were determined and normalized to total viable cell counts (CFUs) (Table 1). The 100% water method yielded the highest concentrations for the

majority of the metabolites identified; the 50% methanol method yielded slightly lower metabolite concentrations, but permitted the identification of five and eight additional metabolites that were not observed in the 100% water extraction of the planktonic and biofilm samples, respectively (Fig. 4).

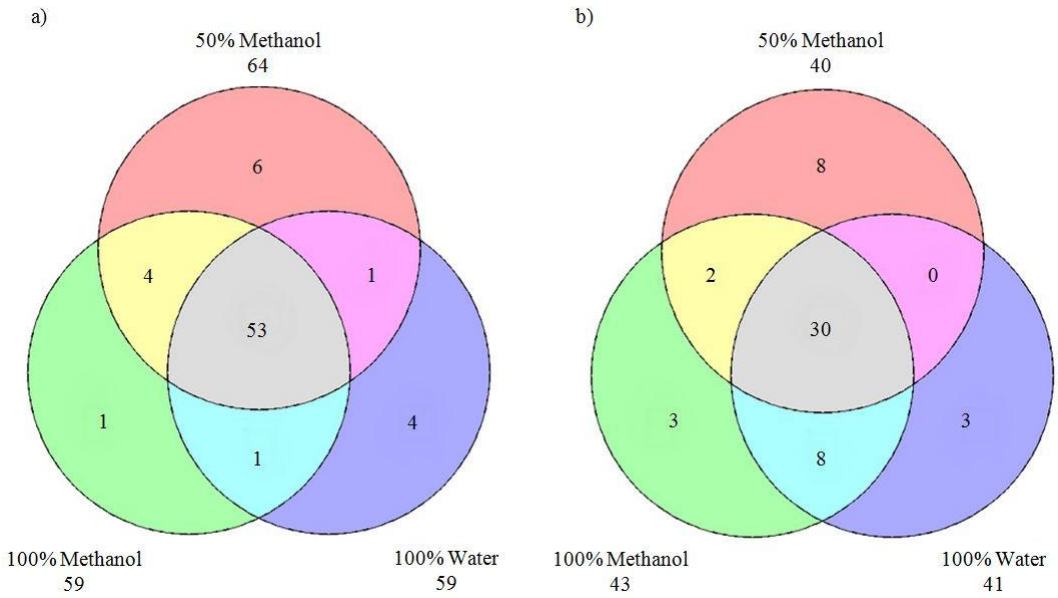

Fig. (4). Venn diagram of metabolites identified with each of the methods developed for a) planktonic and b) biofilm *P. aeruginosa* cell cultures.

The greater metabolite concentrations observed for the 100% water method could be due to the more ordered and compact ice crystal formation during freeze-thaw cycles. Integrity of the cellular membrane of another Gram-negative bacterium, *Escherichia coli*, has been shown to be compromised following freezing [18], and the majority of cells that experience intracellular ice formation at a rapid freezing rate, including *P. aeruginosa*, are damaged if not ruptured as a result of ice formation [19]. The method using 100% methanol yielded the lowest metabolite concentrations due, in all likelihood, to insufficient cell lysis as samples produced using the 100% methanol protocol did not

freeze during the -80 °C freeze-thaw cycles. The 50% methanol extraction was determined to be the optimal method for the profiling of the intracellular metabolome of *P. aeruginosa* as it yielded high metabolite recovery for both planktonic and biofilm phenotypes and proved to be very reproducible (Table 1, Fig. S1). Furthermore, the reduced polarity of methanol in comparison to water may enhance the solubility and subsequent extraction of marginally soluble metabolites; this may in part allow the 50% methanol method to yield a broader range of metabolites following extraction. In addition, methanol may aid in the release of metabolites from proteins present in their crude extracts.

Conclusion

In this study, an effective washing and metabolite extraction method was developed for metabolite profiling of *P. aeruginosa* grown both in planktonic and biofilm cultures. This optimized protocol includes washing with PBS to remove extracellular materials and extracellular small molecules while causing no detectable leakage of intracellular metabolites. In contrast to the 60% methanol procedure, the washing method developed here limits the loss of intracellular metabolites that are otherwise almost completely lost when using 60% methanol. For example, we observed loss of essential amino acids such as betaine, glycine, methionine, and tyrosine. In addition, this study demonstrated that the 50% methanol extraction method yields the largest number of metabolites, as well as several additional metabolites not seen with other protocols, at adequate concentrations for identification and quantification by 1D ^{1}H NMR. Inclusion of

sonication following each freeze-thaw cycle enhanced the metabolite extraction efficiency for nearly all metabolites of interest, including approximately half of those exhibiting at least a 2-fold concentration increase compared to metabolite profiles from samples prepared without a sonication step. The metabolite extraction method developed in this study has been optimized for planktonic and biofilm *P. aeruginosa* and demonstrates that it is crucial to develop and customize extraction methods for each microorganism and metabolic phenotype of interest, prior to undertaking extensive quantitative metabolite profiling studies.

Supplementary Materials

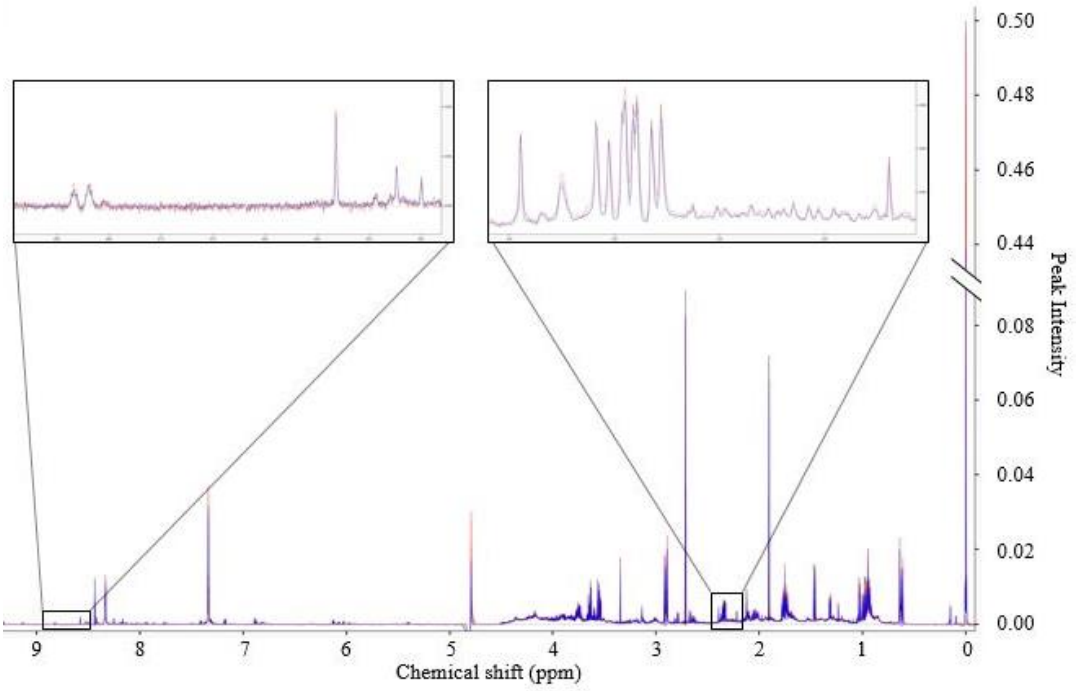

Fig. (S1). 1D ^{1}H NMR spectral overlays of technical metabolite samples extracted from *P. aeruginosa* biofilms using the 50% methanol method. ^{1}H spectral regions corresponding to aromatic and methylene protons have been expanded to demonstrate the excellent reproducibility of the data obtained as a result of this particular extraction method.

Conflict of Interest

The authors declare that they have no conflict of interest in the publication of these data.

Acknowledgements

This research was supported by NIH grant 1KO1GM103821-01 (to MCBA). The NMR metabolomics experiments were performed at MSU on a 600 MHz solution NMR spectrometer purchased in part, and recently upgraded to an AVANCE III console and TCI cryoprobe with, funds from NIH grants 1-S10RR13878-01 and S10RR026659-01A1. The content is solely the responsibility of the authors and does not necessarily represent the official views of the NIH.

References

1. Zhang, A.; Sun, H.; Xu, H.; Qiu, S.; Wang, X. Cell metabolomics. *OMICS*, **2013**, *17*(10), 495-501.

2. Zhang, B.; Powers, R. Analysis of bacterial biofilms using NMR-based metabolomics. *Future Med Chem*, **2012**, *4*(10), 1273-1306.

3. Weljie, A. M.; Newton, J.; Mercier, P.; Carlson, E.; Slupsky, C. M. Targeted profiling: quantitative analysis of ^{1}H NMR metabolomics data. *Anal Chem*, **2006**, *78*(13), 4430-4442.

4. Wishart, D. Applications of metabolomics in drug discovery and development. *Drugs R D*, **2008**, *9*(5), 307-322.

5. Wei, Q.; Ma, L. Z. Biofilm matrix and its regulation in *Pseudomonas aeruginosa*. *Int J Mol Sci*, **2013**, *14*, 20983-21005.

6. Spura, J.; Reimer, L. C.; Wieloch, P.; Schreiber, K.; Buchinger, S.; Schomburg, D. A method for enzyme quenching in microbial metabolome analysis successfully applied to gram-positive and gram-negative bacteria and yeast. *Anal Biochem*, **2009**, *394*, 192-201.

7. Chen, M.; Li, A.; Sun, M.; Feng, Z.; Meng, X.; Wang, Y. Optimization of the quenching method for metabolomics analysis of *Lactobacillus bulgaricus*. *J Zhejiang Univ Sci B*, **2014**, *15*(4), 333-342.

8. Bolten, C. J.; Kiefer, P.; Letisse, F.; Portais, J.; Wittmann, C. Sampling for metabolome analysis of microorganisms. *Anal Chem*, **2007**, *79*, 3843-3849.

9. Faijes, M.; Mars, A. E.; Smid, E. J. Comparison of quenching and extraction methodologies for metabolome analysis of *Lactobacillus plantarum*. *Microb Cell Fact*, **2007**, *6*, 27-34.

10. Gonzalez, B.; Francois, J.; Renaud, M. A rapid and reliable method for metabolite extraction in yeast using boiling buffered ethanol. *Yeast*, **1997**, *13*, 1347-1356.

11. Cigana, C.; Lore, N. I.; Bernardini, M. L.; Bragonzi, A. Dampening host sensing and avoiding recognition in *Pseudomonas aeruginosa* pneumonia. *J Biomed Biotechnol*, **2011**, *2011*, 852513.

12. Kirker, K. R.; Secor, P. R.; James, G. A.; Fleckman, P.; Olerud, J. E.; Stewart, P. S. Loss of viability and induction of apoptosis in human keratinocytes exposed to

Staphylococcus aureus biofilms in vitro. *Wound Repair and Regener*, **2009**, *17*(5), 690-699.

13. Ammons, M. C. B.; Tripet, B. P.; Carlson, R. P.; Kirker, K. R.; Gross, M. A.; Stanisich, J. J.; Copie, V. Quantitative NMR metabolite profiling of methicillin-resistant and methicillin-susceptible *Staphylococcus aureus* discriminates between biofilm and planktonic phenotypes. *J Proteome Res*, **2014**, *13*(6), 2973-2985.

14. Maharjan, R. P.; Ferenci, T. Global metabolite analysis: the influence of extraction methodology on metabolome profiles of *Escherichia coli*. *Anal Biochem*, **2003**, *313*, 145-154.

15. Wu, X.; Yu, H.; Ba, Z.; Chen, J.; Sun, H.; Han, B. Sampling methods for NMR-based metabolomics of *Staphylococcus aureus*. *Biotechnol J*, **2010**, *5*(1), 75-84.

16. Johnson, B. H.; Hecht, M. H. Recombinant proteins can be isolated from *E. coli* cells by repeated cycles of freezing and thawing. *Nat Biotechnol*, **1994**, *12*, 1357-1360.

17. Ho, C. W.; Chew, T. K.; Ling, T. C.; Kamaruddin, S.; Tan, W. S.; Tey, B. T. Efficient mechanical cell disruption of *Escherichia coli* by an ultrasonicator and recovery of intracellular hepatitis B core antigen. *Process Biochem*, **2006**, *41*, 1829-1834.

18. Kempler, G.; Ray, B. Nature of freezing damage on the lipopolysaccharide molecule of *Escherichia coli* B. *Cryobiology*, **1978**, *15*, 578-584.

19. Li, Y.; Wang, H.; Pan, T. Intracellular ice formation (IIF) during freeze-thaw repetitions. *Int J Heat and Mass Transfer*, **2013**, *64*, 436-443.

APPENDIX B

CHARACTERIZATION OF THE ANTIBACTERIAL ACTIVITY OF BALD'S EYESALVE AGAINST DRUG RESISTANT *STAPHYLOCOCCUS AUREUS* AND *PSEUDOMONAS AERUGINOSA*

CHARACTERIZATION OF THE ANTIBACTERIAL ACTIVITY OF BALD'S EYESALVE AGAINST DRUG RESISTANT *STAPHYLOCOCCUS AUREUS* AND *PSEUDOMONAS AERUGINOSA*

Contribution of Authors and Co-Authors

Manuscript in Appendix B

Author: Amanda L. Fuchs

Contributions: Conceptualized the study, curated the data, conducted formal analysis and investigation, developed methodology, administered the project, validated and visualized the data, wrote the original manuscript draft, and reviewed and edited the manuscript.

Author: Alan J. Weaver, Jr.

Contributions: Conceptualized the study, curated the data, conducted formal analysis and investigation, developed methodology, administered the project, validated and visualized the data, wrote the original manuscript draft, and reviewed and edited the manuscript.

Co-Author: Brian P. Tripet

Contributions: Conceptualized the study, developed methodology, administered the project, supervised the project, and reviewed and edited the manuscript.

Co-Author: Mary Cloud B. Ammons

Contributions: Conceptualized the study, acquired funding, provided resources, and reviewed and edited the manuscript.

Co-Author: Martin Teintze

Contributions: Acquired funding and reviewed and edited the manuscript.

Co-Author: Valérie Copié

Contributions: Acquired funding, administered the project, provided resources and software, supervised the project, and reviewed and edited the manuscript.

Manuscript Information Page

Amanda L. Fuchs*, Alan J. Weaver, Jr.*, Brian P. Tripet, Mary Cloud B. Ammons, Martin Teintze, Valérie Copié (*These authors contributed equally to this work.)

Journal Name: PLoS ONE

Status of Manuscript:
_____ Prepared for submission to a peer-reviewed journal
_____ Officially submitted to a peer-reviewed journal
_____ Accepted by a peer-reviewed journal
__x__ Published in a peer-reviewed journal

Publisher: PLoS
Issue in which manuscript appears: Volume 13, Issue 11, 2018

CHARACTERIZATION OF THE ANTIBACTERIAL ACTIVITY OF BALD'S EYESALVE AGAINST DRUG RESISTANT *STAPHYLOCOCCUS AUREUS* AND *PSEUDOMONAS AERUGINOSA*

Amanda L. Fuchs[1¶*], Alan J. Weaver, Jr.[1,#a¶], Brian P. Tripet[1], Mary Cloud B. Ammons[1,#b], Martin Teintze[1], Valérie Copié[1*]

[1]Department of Chemistry and Biochemistry, Montana State University, Bozeman, Montana, United States of America
[#a]Current Address: Dental and Craniofacial Trauma Research and Tissue Regeneration Directorate, U.S. Army Institute of Surgical Research, JBSA Fort Sam Houston, Texas, United States of America
[#b]Current Address: Boise Veterans Medical Center, Idaho Veterans Research and Education Foundation, Boise, Idaho, United States of America

[*] Corresponding authors
E-mail: vcopie@montana.edu (VC) and afuchs03143@gmail.com (ALF)

[¶]These authors contributed equally to this work.

Abstract

Bald's eyesalve is an Anglo-Saxon medicinal remedy that has been used through ancient times to treat eye sty infections and may represent a source of ancientbiotics. This study assessed the efficacy of Bald's eyesalve against several strains of *Staphylococcus aureus* and *Pseudomonas aeruginosa*, including a multi-drug resistant phenotype, and identified the principal compound conveying antibacterial activity. Bald's eyesalve formulations were produced by combining garlic, onion or leek, wine, bovine bile, and brass, with specific ingredient omissions in several formulations, followed by incubation at 4 °C for 9 days. Bald's eyesalve formulation ES-GBBr exhibited the greatest

antibacterial activity against *S.* aureus *and P. aeruginosa*. Fractionation of ES-GBBr using molecular size exclusion and organic solvent partitioning isolated its antibacterial activity to the small molecule nonpolar fraction, and 1D ^{1}H NMR revealed the identity of the antibacterial agent to be allicin. Depletion of allicin from this fraction by addition of exogenous cysteine established that all observable growth inhibition originated from allicin. Quantification of allicin demonstrated that its concentration was significantly greater in ES-GBBr compared to the ES-O formulation; however, this was not due to greater yield. The antibacterial activity of allicin against *S. aureus* was antagonized by other ingredients within Bald's eyesalve, whereas they were additive or synergistic against *P. aeruginosa*. These results suggest that neither leek nor onion is necessary for the antibacterial efficacy of Bald's eyesalve against *S. aureus* or *P. aeruginosa*, and while allicin was identified as the principal antibacterial agent present, its activity is influenced differentially in the presence of additional Bald's eyesalve ingredients when used against *S. aureus* compared to *P. aeruginosa*. Ancientbiotics may provide a source of promising antibacterials; however, identifying the source of activity and assessing distinct formulations for cooperative effects are essential to using ancient remedies, such as Bald's eyesalve, effectively against drug resistant pathogens.

Introduction

Ancient Anglo-Saxon medicinal remedies have been receiving renewed scrutiny concerning their potential as rich sources of antibacterial compounds that could help combat modern drug-resistant bacterial infections [1]. As the discovery and development

of novel antibiotics declines, the emergence of antibiotic resistant pathogens is an alarming threat to human health, with an estimated 700,000 deaths resulting from drug-resistant infections per year. Predictions indicate that such infections will cause 10 million deaths annually by the year 2050 if new antimicrobial compounds are not developed soon [2]. While ancient medical formulations, such as Bald's eyesalve, are being revisited for their antibacterial potency, little is known regarding the specific agents responsible for their efficacy, the cooperative effects within these complex mixtures, or whether such natural remedies could be utilized to effectively address the threat of modern antibiotic resistant microbes.

The development of bacterial resistance to modern antibiotics is startling and has thus prompted the investigation of ancient medieval remedies for promising antibiotic compounds. Bald's eyesalve originates from a 10th century English medicinal text, *Bald's Leechbook*, and has been used to treat bacterial infections of the eyelash follicle, commonly known as a sty. The formulation consists of wine, garlic, an additional *Allium* species, such as onion or leek, and bovine bile; these ingredients are combined within a brass or bronze vessel and left to incubate for 9 days prior to use [3]. Common pathogens found in modern bacterial eye infections include *Staphylococcus aureus* and *Pseudomonas aeruginosa*, including methicillin-resistant *S. aureus* (MRSA) and drug resistant *P. aeruginosa* strains. In addition, these pathogens are responsible for a wide variety of severe, chronic infections, including sepsis, pneumonia, and chronic wound infections [4, 5].

In a 2015 study, Bald's eyesalve was found to exhibit bactericidal activity against

MRSA biofilms in an *in vitro* synthetic wound model; however, its mechanism of action and the antimicrobial agent(s) responsible for its efficacy were never elucidated [6]. In the present study, we sought to identify the principal antibacterial compound within Bald's eyesalve using various formulations, a multi-step fractionation process, 1D ^{1}H NMR analysis, and minimum inhibitory concentration (MIC) assays. Furthermore, we aimed to establish the efficacy of Bald's eyesalve against both Gram-positive and Gram-negative bacteria, such as *S. aureus* and *P. aeruginosa*, including the MRSA strain LAC and clinical wound isolate *P. aeruginosa* PA215.

Materials and Methods

Bald's Eyesalve Materials

The garlic (*Allium sativum*), yellow onion (*Allium cepa* L.), and leek (*Allium ampeloprasum* L.) used in this study originated from Montana Stinking Rose Farm in Bozeman, Montana, Easterday Farms Produce Company in Pasco, Washington, and Associated Food Stores Inc. in Salt Lake City, Utah, respectively. Plant materials and white wine (2016 Pinot Grigio, La Fiera Veneto; UPC 0-89832-90007-8) were purchased from Town & Country Foods in Bozeman, Montana. Following purchase, produce and wine were stored at 4 °C prior to Bald's eyesalve preparation.

Bovine bile salts were purchased from Sigma Aldrich (product no. B3883; lot no. SLBH1798V), and 0.51-mm brass sheet (24 gauge; alloy 260) was purchased from Ace Hardware in Bozeman, Montana (product no. 5024864).

Preparation of Crude Bald's Eyesalve

Bald's eyesalve formulations (Table 1) were prepared as previously described [6] unless noted otherwise. In brief, garlic bulbs and yellow onion were peeled and coarsely chopped prior to being minced in a food processor (Mainstays Food Chopper, model no. FPMEMC3002). Leeks were chopped in half, and the leeks greens were coarsely chopped and the minced using a food processor as described above, while the white root end of the leek was discarded.

Table 1. Composition of Bald's eyesalve (ES) formulations.

	ES-O	ES-L	ES-GBBr	ES-GB	ES-GBr	ES-G
Garlic	+	+	+	+	+	+
Wine	+	+	+	+	+	+
Onion	+	-	-	-	-	-
Leek	-	+	-	-	-	-
Bovine bile[a]	+	+	+	+	-	-
Brass[b]	+	+	+	-	+	-

Bald's eyesalve was prepared by combining equal volumes (25 mL) of garlic, wine, onion or leek, and bovine bile followed by addition of brass prior to incubation at 4 °C for 9 days. + designates ingredients that were included, while - denotes those which were excluded.

[a]87 mg/mL dissolved in sterile water

[b]Nine 15-mm squares of 24 gauge (0.51-mm) brass sheet metal (alloy 260)

Immediately following plant material preparation, equivalent volumes (25 mL) of minced garlic bulb (~14.2 g), minced yellow onion (~22.2 g) or minced leek leaves (~8.8 g), white wine, and bovine bile salts (87 mg/mL dissolved in sterile water) were combined in sterile 250 mL glass bottles. Nine 15-mm squares of 0.51-mm brass sheet were added to each bottle prior to being wrapped in foil and placed at 4 °C for 9 days. One or more ingredients were omitted from several formulations as described in Table 1. After incubation, formulations were centrifuged at 5000 rpm for 10 min. Supernatants

were transferred to sterile 50 mL tubes and stored at 4 °C, while insoluble materials were discarded.

Bacterial Strains

Methicillin-susceptible *S. aureus* (MSSA) strain ATCC 6538 [7] was purchased commercially. Community-associated methicillin-resistant *S. aureus* (CA-MRSA) strain LAC, pulsed-field gel-electrophoresis type USA300 [8] was provided by Dr. Jovanka M. Voyich. *P. aeruginosa* wild-type strain PAO1 [9] and clinical wound isolate strain PA215 [10] were provided by Dr. Michael J. Franklin and Dr. Garth A. James, respectively.

Determination of Minimal Inhibitory Concentration

MIC values were determined for each of the bacterial strains using a microdilution method in 96-well microtiter plates with cation-adjusted Mueller-Hinton broth (MHB). Inoculum culture growth conditions consisted of batch cultures grown at 37 °C, 220 rpm agitation to an optical density reading at 600 nm of 0.45–0.5 for *S. aureus* (~ 2.5×10^8 colony-forming units per mL (CFU/mL)) and 0.48 for *P. aeruginosa* (~ 3×10^8 CFU/mL). Inoculum was diluted 1:200 (v/v) with 2X MHB and then 1:1 (v/v) into 96-well microtiter plates containing serial diluted eyesalve (40% to 0.3125% (v/v)) along with positive and negative control wells, containing no eyesalve with and without inoculum respectively, for a total of 200 μL per well. Microtiter plates were incubated at 37 °C for 20 hrs prior to evaluation for growth inhibition. This method was based upon recommendations from the Clinical and Laboratory Standards Institute [11]. An allicin standard (LKT Labs) was assayed using the same protocol, but

with *S. aureus* stain LAC and *P. aeruginosa* strain PA215 only.

Molecular Size Exclusion and
Solvent Partitioning Fractionation
of Bald's Eyesalve

The ES-GBBr formulation, consisting of garlic, wine, bovine bile, and brass, was centrifuged at 21000 x g for 10 min to remove any residual debris prior to fractionation. An aliquot of resultant supernatant was removed and stored at 4 °C as crude eyesalve, while the remaining supernatant was fractionated as described below.

Small molecule (SM) fraction was prepared by means of filtering 40 ml of the initially prepared crude eyesalve through a pre-washed Amicon Ultra-15 (cellulose) centrifugal filter unit with a 3 kDa molecular weight cut-off by centrifugation at 4000 x g, 4 °C for 60 min. The proteinaceous (PRT) fraction was prepared by restoring concentrate volume to 40 ml with sterile water. Both SM and PRT fractions were stored at 4 °C.

Small molecule, polar (SM-P) and nonpolar (SM-NP) fractions were prepared by combining 6 ml of SM fraction with 3.6 ml of chloroform. This mixture was vortexed for 1 min prior to phase separation by centrifugation at 5000 rpm for 10 min. The polar phase was removed and stored at 4 °C. The nonpolar phase was dried under a stream of N_2 gas and reconstituted in 6 ml of sterile water prior to being stored at 4 °C.

NMR Sample Preparation

Bald's eyesalve formulations/fractions prepared as described above were centrifuged at 21000 rpm for 10 min to remove insoluble debris. A 300 µL aliquot of resultant supernatant was added to 300 µL of 2X NMR stock buffer (50 mM

NaH_2PO_4/Na_2HPO_4, 0.8 mM imidazole as a pH indicator, and 0.5 mM 4,4-dimethyl-4-silapentane-1-sulfonic acid (DSS) in 20% D_2O, pH 7) and then transferred to a 5 mm Bruker NMR tube.

NMR Experiments

All NMR spectra were collected at 298 K (25 °C) on a Bruker 600 MHz (^{1}H Larmor frequency) AVANCE III solution NMR spectrometer, equipped with an automatic sample loading system (SampleJet), a 5 mm triple resonance (^{1}H, ^{15}N, ^{13}C) liquid-helium-cooled TCI NMR probe (Cryoprobe), and Topspin software (Bruker version 3.1).

1D ^{1}H NMR experiments were performed using the Bruker "zgesgp" pulse sequence and recorded with 256 scans and a ^{1}H spectral window of 9615.38 Hz. Free induction decays were collected with 32K data points and a dwell time interval of 52 μsec amounting to a data acquisition time of ~ 1.7 s, and a 1 s delay between acquisitions, which resulted in an overall ~ 2.7 sec relaxation recovery delay between scans. 1D ^{1}H NMR spectra were phase-corrected using Topspin software (Bruker version 3.1), and baseline correction was applied following import of the NMR spectra into the Chenomx NMR Suite program (version 8.0; Chenomx, Inc., Alberta, Canada). Subsequently, a recorded 1D ^{1}H NMR spectrum of an allicin standard was added to the Chenomx small-molecule library for 600 MHz (^{1}H Larmor frequency) magnetic field strength NMR using the 'Compound Builder' module of the Chenomx NMR Suite program (version 8.0) and was used as a reference spectrum for this compound. Allicin and ethanol were identified and quantified using the 'Profiler' module of Chenomx for each Bald's eyesalve

formulation and/or fraction. The internal DSS (0.25 mM) standard was used for quantification of metabolite concentrations.

Depletion of Allicin

An aliquot of the SM-NP fraction of the ES-GBBr formulation was titrated with L-cysteine to a final concentration of 15 mM and incubated at 4 °C for 1 hr. Allicin standard (0.5 mM), diluted from stock using sterile water, was also incubated in the presence of 15 mM L-cysteine under the same conditions, and resultant samples were analyzed by 1D ^{1}H NMR.

Statistical Analysis

Data analysis was performed on 4 independent replicates of each Bald's eyesalve formulation. Statistical significance was assessed by one-way analysis of variance (ANOVA), followed by Tukey's multiple comparisons post-test using GraphPad Prism program version 7.1 (GraphPad Software, La Jolla, CA).

Results

Antibacterial Efficacy of Bald's Eyesalve Formulations Against *S. aureus* and *P. aeruginosa*

The antibacterial activity of four different Bald's eyesalve formulations, prepared as described in Table 1, was assessed against two strains of *S. aureus* and *P. aeruginosa*, including LAC and PA215. This initial formulation selection included those denoted as ES-O, ES-L, ES-GBBr, and ES-GB (Table 1). All crude Bald's eyesalve formulations

predominantly demonstrated strong growth inhibition for *S. aureus* strains ATCC 6538 and LAC with MIC values ranging from 0.625 to 2.5% (v/v) (Table 2). ES-O, ES-L, and ES-GB largely exhibited weak activity towards *P. aeruginosa* strains PAO1 and PA215 with MIC values ranging from 2.5 to 10% (v/v); however, the ES-GBBr formulation displayed moderate growth suppression for both *P. aeruginosa* strains with an MIC value of 2.5% (v/v) (Table 2).

Table 2. Susceptibility of bacterial strains to crude Bald's eyesalve formulations.

Bacterial strains	MIC[a]			
	ES-O	ES-L	ES-GBBr	ES-GB
S. aureus				
ATCC 6538	0.625	0.625	0.625	0.625
LAC	2.5	1.25	1.25	1.25
P. aeruginosa				
PAO1	5	5	2.5	2.5
PA215	10	5	2.5	5

MIC was determined using a broth microdilution method as described by the Clinical and Laboratory Standards Institute. Reported values represent the median of at least 3 biological replicates.

[a]MIC values indicated the concentrations of Bald's eyesalve formulation in % (v/v)

Isolation of Antibacterial Activity Present in ES-GBBr Formulation by Fractionation

The ES-GBBr formulation was fractionated using molecular size exclusion into a proteinaceous (PRT) and small molecule (SM) fraction, and the antibacterial activity of these fractions was evaluated against the aforementioned bacterial strains. The PRT fraction showed notably weak activity against all strains with MIC values ranging from 10 to greater than 40% (v/v); furthermore, this reflected an MIC increase of 16-fold for *S. aureus* strain ATCC 6538, greater than 16-fold for *S. aureus* strain LAC, and greater than 32-fold for *P. aeruginosa* strains PAO1 and PA215 when compared to crude ES-GBBr

(Table 3). The SM fraction demonstrated strong growth inhibition activity for *S. aureus* strains ATCC 6538 and LAC with MIC values ranging from 0.625 to 1.25% (v/v), and moderate to weak activity towards *P. aeruginosa* strains PAO1 and PA215 with MIC values ranging from 2.5 to 5% (v/v) (Table 3). These results indicated that the SM fraction sustained full antibacterial activity relative to crude ES-GBBr against all strains, except for *P. aeruginosa* strain PA215 which exhibited a 2-fold MIC increase (Table 3).

Table 3. Susceptibility of bacterial strains to ES-GBBr formulation fractions.

Bacterial strains	MIC[a] (FC[b])			
	PRT	SM	SM-P	SM-NP
S. aureus				
ATCC 6538	10 (16)	0.625 (1)	10 (16)	1.25 (2)
LAC	>40 (>32)	1.25 (1)	20 (16)	2.5 (2)
P. aeruginosa				
PAO1	>40 (>16)	2.5 (1)	40 (16)	5 (2)
PA215	>40 (>16)	5 (2)	>40 (>16)	10 (4)

MIC was determined using a broth microdilution method as described by the Clinical and Laboratory Standards Institute. Reported values represent the median of at least 3 biological replicates.
[a]MIC values indicate the concentration of ES-GBBr formulation fraction in % (v/v)
[b]FC values indicate the fold change in the MIC relative to that of crude ES-GBBr

Organic solvent partitioning was used to further fractionate the SM fraction of the ES-GBBr formulation into a small molecule polar and small molecule nonpolar fraction, and the antibacterial activity of these fractions was evaluated against all bacterial strains. The SM-P fraction showed weak activity against all strains with MIC values ranging from 10 to greater than 40% (v/v); correspondingly, this reflected an MIC increase of 16-fold for *S. aureus* strains ATCC 6538 and LAC, 16-fold for *P. aeruginosa* strain PAO1, and greater than 8-fold for *P. aeruginosa* strain PA215 when compared to the SM fraction (Table 3). The SM-NP fraction demonstrated strong to moderate growth

inhibition activity for *S. aureus* strains ATCC 6538 and LAC with MIC values ranging from 1.25 to 2.5% (v/v), and weak activity towards *P. aeruginosa* strains PAO1 and PA215 with MIC values ranging from 5 to 10% (v/v) (Table 3). These results indicated that the SM-NP fraction sustained partial antibacterial activity, relative to the SM fraction, demonstrating a 2-fold MIC increase against all bacterial strains (Table 3).

Identification and Validation of the Principal Agent in Bald's Eyesalve

To identify the principal antibacterial agent in Bald's eyesalve, 1D ^{1}H NMR spectra of the SM, SM-P, and SM-NP fractions of the ES-GBBr formulation were recorded (S1 Fig). These 1D ^{1}H NMR spectra revealed notable NMR signals within the 5.1 to 6.1 ppm chemical shift range that were present in the SM and SM-NP fractions while absent in the SM-P fraction (Fig 1). A 1D ^{1}H NMR spectrum of an allicin standard was recorded, and this spectrum correlated with the NMR signals observed within the 5.1 to 6.1 ppm chemical shift range in the 1D ^{1}H NMR spectra of the SM and SM-NP fractions (Fig 2, S3 Fig).

To demonstrate that the antibacterial activity observed in the SM-NP fraction of the ES-GBBr formulation originated from allicin, depletion experiments were conducted by addition of exogenous free cysteine to the SM-NP fraction. Allicin depletion within this fraction and an allicin standard was confirmed using 1D ^{1}H NMR spectroscopy (S2 Fig) prior to evaluation of antibacterial activity against *S. aureus* stain LAC and *P. aeruginosa* strain PA215. The allicin-depleted SM-NP fraction demonstrated no observable antibacterial activity against the aforementioned bacterial strains with an MIC

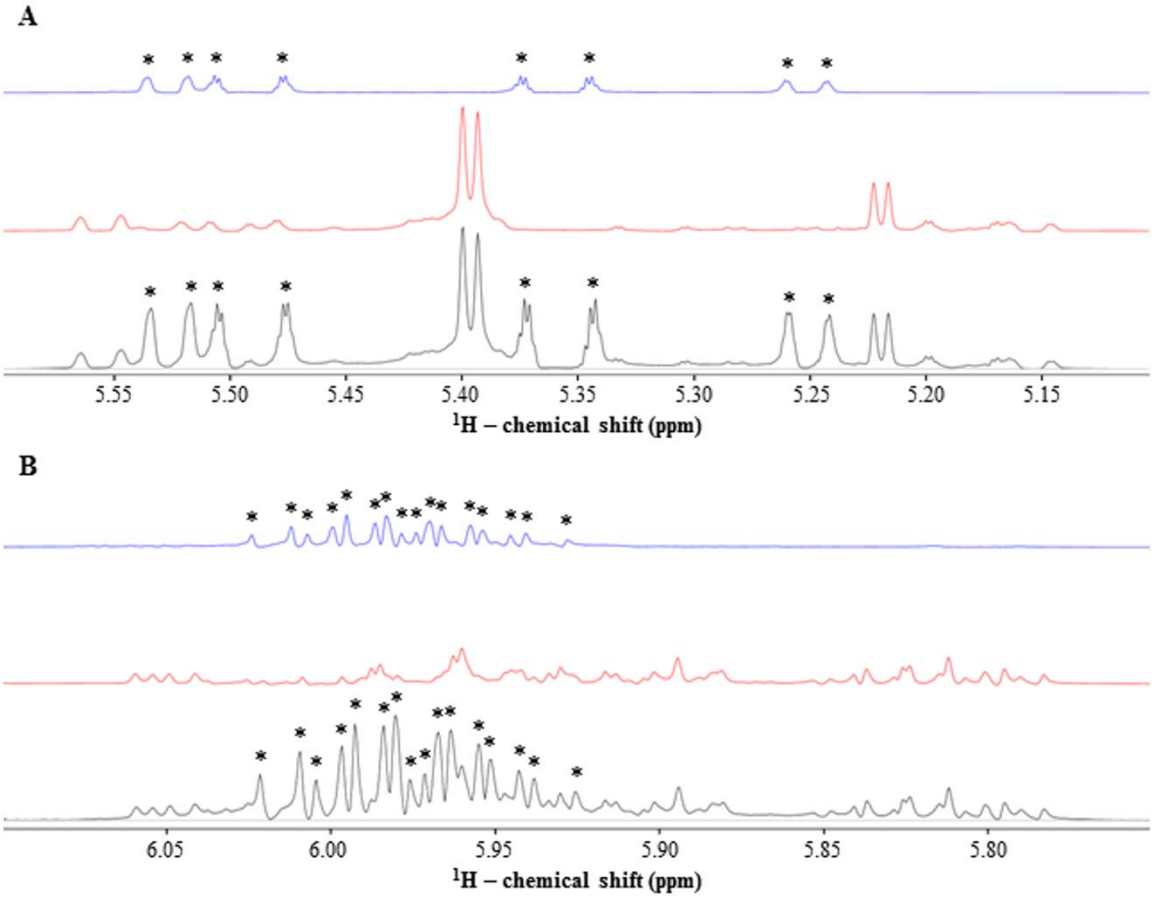

Fig 1. ^{1}H NMR analysis of ES-GBBr formulation fractions establishes presence of unknown compound(s). Stacked 1D ^{1}H NMR spectra (600 MHz, 10% D_2O) in chemical shift regions (A) 5.1-5.6 ppm and (B) 5.75-6.1 ppm for ES-GBBr SM (black), SM-P (red), and SM-NP (blue) fractions. Asterisks indicate NMR signals from molecule(s) of interest.

value greater than 40% (v/v); furthermore, this reflected an MIC increase greater than 16-fold for *S. aureus* strain LAC and greater than 4-fold for *P. aeruginosa* strain PA215 relative to control SM-NP fraction (Table 4).

Allicin Concentration and Production Within Distinct Bald's Eyesalve Formulations

To assess whether the enhanced antibacterial activity of the ES-GBBr formulation

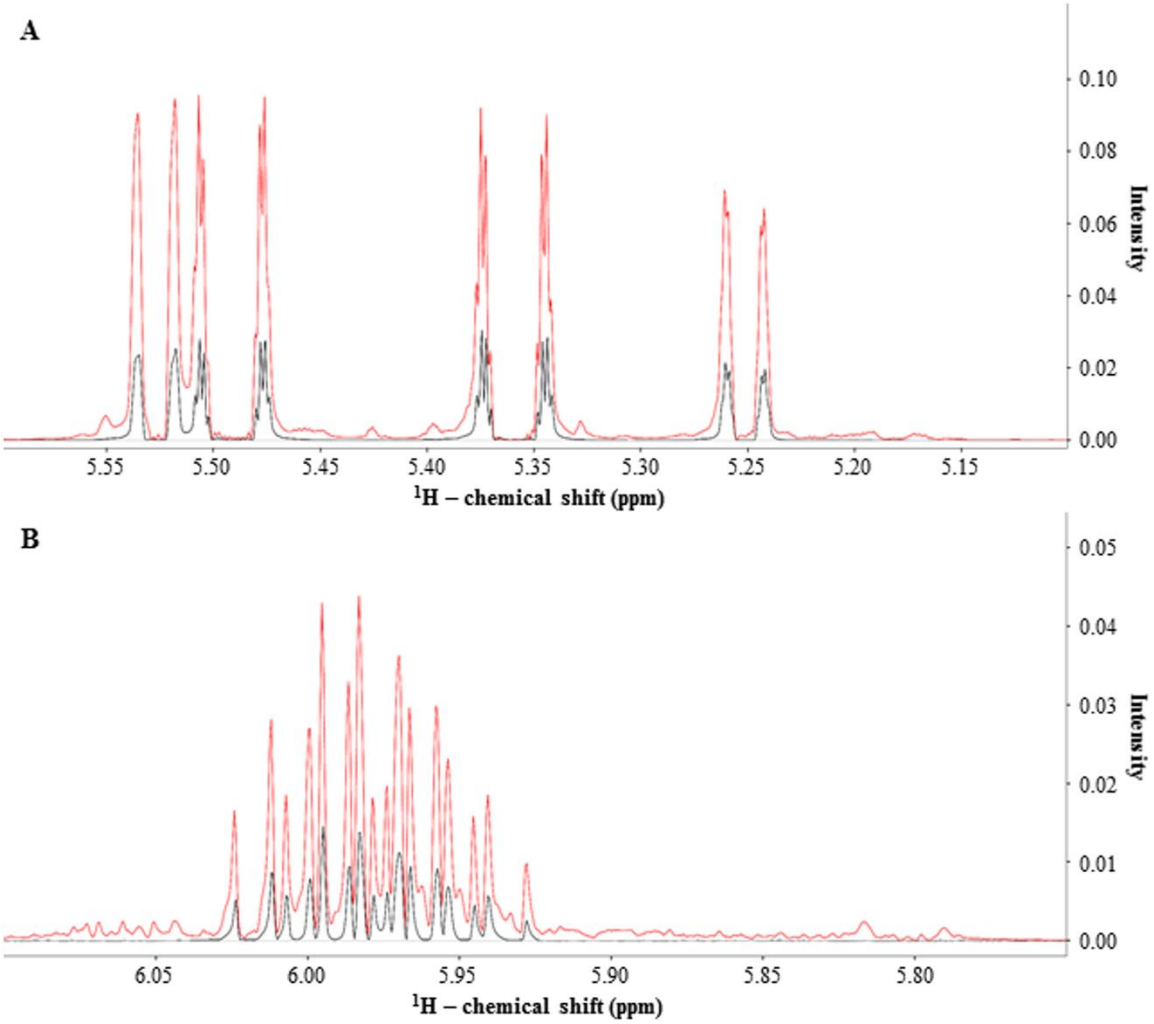

Fig 2. Identity of unknown determined to be an organosulfur compound originating from garlic known as allicin. An overlay of 1D ^{1}H NMR spectra (600 MHz, 10% D_2O) in chemical shift regions (A) 5.1-5.6 ppm and (B) 5.75-6.1 ppm for an allicin standard (black) and ES-GBBr formulation SM-NP fraction (red).

was due to a greater concentration of allicin, 1D ^{1}H NMR and Chenomx NMR Suite software was used to quantify the concentration of allicin in all Bald's eyesalve formulations described in Table 1. The ES-GBBr formulation exhibited a significantly greater concentration of allicin than the ES-O formulation, with mean values of 1476.6 and 836.2 µg/mL, respectively (Fig 3A). Although not significantly distinct from the ES-GBBr formulation, the average allicin concentration in the ES-L, ES-GB, ES-GBr, and

Table 4. Effect of allicin depletion on susceptibility of multi-drug resistant bacterial strains to ES-GBBr formulation SM-NP fraction.

Bacterial strains	MIC[a] (FC[b])	
	Control	Allicin-Depleted
S. aureus		
LAC	2.5 (1)	>40 (>16)
P. aeruginosa		
PA215	10 (1)	>40 (>4)

MIC was determined using a broth microdilution method as described by the Clinical and Laboratory Standards Institute. Allicin depletion was conducted by addition of free cysteine and incubation for 1 hr at 4 °C prior to MIC evaluation. Control was not subjected to allicin depletion. Reported values represent the median of at least 3 biological replicates.
[a]MIC values indicate the concentration of ES-GBBr SM-NP fraction in % (v/v)
[b]FC values indicate the fold change in the MIC relative to that of ES-GBBr SM-NP fraction

ES-G formulations were 977.3, 1127.3, 1170.4, and 1050.6 µg/mL respectively (Fig 3A).

Due to variations in final volume resulting from ingredient omission(s), allicin yield (mg) was also calculated for each formulation. The average amount of allicin produced in the ES-O, ES-L, ES-GBBr, ES-GB, ES-GBr, and ES-G formulations was 56.2, 64.2, 74.4, 50.0, 62.5, and 50.4 mg respectively; however, there was no significant difference in the amount of allicin present between any of these formulations (Fig 3B).

Cumulative Effects Regarding the Antibacterial Activity of Allicin Within Bald's Eyesalve Against *S. aureus* and *P. aeruginosa*

To evaluate whether interactions between ingredients within the Bald's eyesalve ES-GBBr formulation impact the efficacy of allicin against drug resistant phenotypes, the MIC values of an allicin standard and allicin within crude ES-GBBr were determined against *S. aureus* strain LAC and *P. aeruginosa* strain PA215. The allicin standard

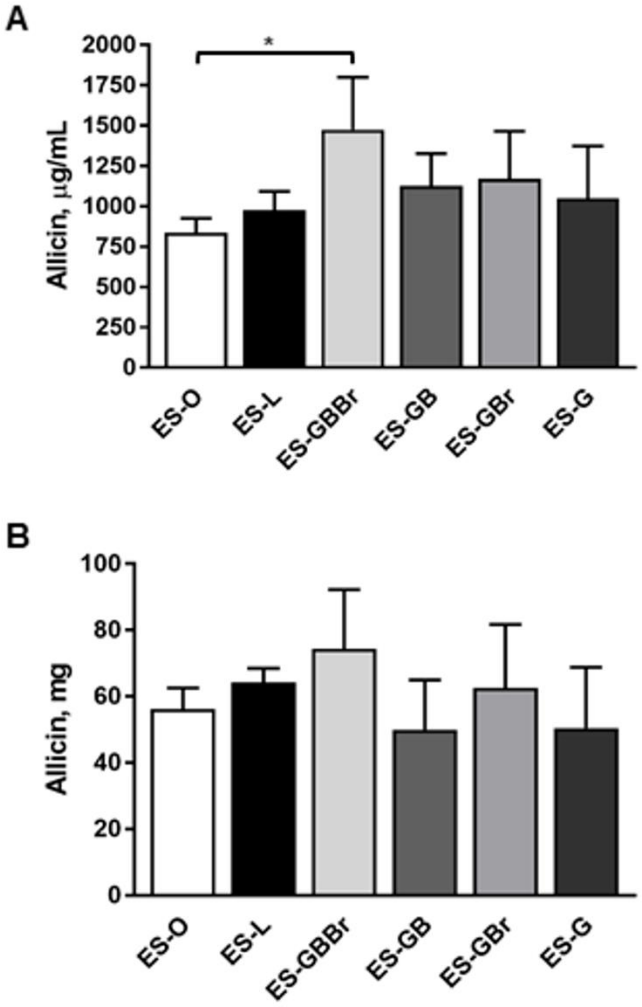

Fig 3. Quantitation of allicin in eyesalve formulations reveals significant differences in concentration but not overall yield. (A) Allicin concentration (µg/mL) was determined using Chenomx small-molecule library for 600 MHz (^{1}H Larmor frequency) magnetic field strength NMR. (B) Allicin production (mg) was calculated by accounting for volume differences between formulations. Data are presented as mean ± SD (n = 4). Significant differences ($p < 0.05$, one-way ANOVA, Tukey's multiple comparisons post-test) between formulations are indicated with asterisks.

exhibited an MIC value of 12.2 µg/ml against *S. aureus* strain LAC and 97.4 µg/ml against *P. aeruginosa* strain PA215, while allicin within crude ES-GBBr displayed an MIC value of 24.3 µg/ml against *S. aureus* strain LAC and 48.7 µg/ml against *P. aeruginosa* strain PA215 (Table 5). These results suggested that additional components

within the Bald's eyesalve ES-GBBr formulation act in an antagonistic manner with the antibacterial activity of allicin against *S. aureus* strain LAC, but additively or synergistically against *P. aeruginosa* strain PA215 (Table 5).

Table 5. Evaluation of conjugative effects within crude ES-GBBr formulation against multi-drug resistant bacterial strains.

Bacterial strains	MIC[a] (FC[b])		Interaction
	Control	ES-GBBr	ES-GBBr
S. aureus			
LAC	12.2 (1)	24.3 (2)	Antagonistic
P. aeruginosa			
PA215	97.4 (1)	48.7 (-2)	Additive or Synergistic

MIC was determined using a broth microdilution as described by the Clinical and Laboratory Standards Institute. Control MIC values were determined using an allicin standard. Reported values represent the median of at least 3 biological replicates.
[a]MIC values indicate the concentration of allicin in µg/mL
[b]FC values indicate the fold change in the MIC relative to control

Discussion

In this study, we have shown that Bald's eyesalve, an Anglo-Saxon remedy for eye sty infections, displays growth inhibitory activity against *S. aureus* and *P. aeruginosa*, including a multi-drug resistant strain. This activity was more pronounced against *S. aureus* than *P. aeruginosa*, which is consistent with the fact that Gram-negative bacteria, particularly *Pseudomonads*, are notably more resistant to antibacterial agents than Gram-positive bacteria, including *Staphylococcus sp.* [12]. Our data indicate that the specific formulation composition had little impact on the inhibition of *S. aureus*. This is inconsistent with a previous report where the presence of an additional *Allium* species, onion or leek, was found to significantly contribute to the antibacterial activity of Bald's eyesalve [6]; however, this previous study evaluated the antibacterial activity using a

synthetic wound model in which *S. aureus* inoculum was grown as a biofilm for 24 hr prior to treatment and based upon colony-forming units [6]. Our conflicting results may be due to our assessment of the antibacterial activity of Bald's eyesalve exclusively against planktonic *S. aureus* rather than *S. aureus* biofilms, and we did not investigate whether onion or leek are necessary for specific efficacy against bacterial biofilms. Previous studies have shown that quercetin, an antibacterial flavonoid found in onion [13], and its derivatives demonstrate anti-biofilm and anti-quorum sensing activity against *S. aureus* and *P. aeruginosa* [14, 15]. Although plant extracts have been shown to display growth inhibitory activity against *P. aeruginosa* [16, 17], to our knowledge our study represents the first report of the antibacterial efficacy of Bald's eyesalve against *P. aeruginosa*.

Although all known *Allium* species contain organosulfur compounds, the chemical composition and resultant antibacterial activity of their extracts greatly varies [18]. Prior investigations have determined the main constituents of garlic essential oil to be diallyl disulfide (DADS), diallyl trisulfide (DATS), allyl methyl trisulfide, diallyl sulfide (DAS), and diallyl tetrasulfide (DATTS), while the main constituents of onion and leek essential oils were found to be dipropyl disulfide, dipropyl trisulfide, methyl propyl disulfide, methyl propyl trisulfide, and 1-propenyl propyl disulfide [18, 19]. Tsao *et al*. previously demonstrated that DAS, DADS, DATS, and DATTS exhibit MICs of 20, 4, 2, and 0.5 µg/ml against *S. aureus*, respectively, and 80, 64, 32, and 12 µg/ml against *P. aeruginosa*, respectively [20, 21]. Little is known regarding the antibacterial activity of dipropyl disulfide and dipropyl trisulfide against *P. aeruginosa*; however, Kim *et al.*

established the MICs of dipropyl disulfide and dipropyl trisulfide against *S. aureus* to be >500 µg/ml and 50 µg/ml, respectively [22]. These findings suggest that the antibacterial activity of the *Allium* species used in our study would be in the following order: garlic > onion > leek. However, our data indicate that addition of leek to Bald's eyesalve results in greater antibacterial activity, in particular against clinical isolate strains, relative to the addition of onion (Table 2). Additional studies are necessary to elucidate the activity of organosulfur compounds derived from onion and leek, especially dipropyl disulfide and dipropyl trisulfide with regard to clinical isolates.

Crude botanical extracts that display antibacterial activity are often subjected to repetitive cycles of fractionation until relatively pure biologically active compounds are identified [23]. Many fractionation scheme variations have been utilized for the isolation of natural compounds, with each offering its own specific advantages [24, 25]. Sub-fractions generated are often less complex than the crude parent extract, thus simplifying the process of identifying the active component(s) [26]. We fractionated Bald's eyesalve formulation ES-GBBr using a combination of molecular size exclusion and organic solvent partitioning methods to isolate and identify its principal antibacterial agent. A review of the literature suggests that our study is the first to characterize the activity of Bald's eyesalve using fractionation in conjunction with growth inhibitory assays; however, there are several limitations to bioassay-guided fractionation. These include an inherent bias towards the most dominant bioactive compounds in the extract or fraction, which can lead to a disregard of low abundant, yet biologically active, components [27]. In addition, activity may be lost during fractionation, particularly if the bioactive agent is

temperature-sensitive or binds to the chromatographic resins employed [28, 29]. Due to the instability of allicin at room temperature and in organic solvents [30, 31], a significant amount of allicin may have been lost from our ES-GBBr formulation SM-NP fraction as suggested by the NMR spectral features shown in Fig. 1. In an attempt to reduce activity loss, we stored our ES-GBBr formulation SM-NP fraction in water. This could explain the 2-fold MIC increase observed for all bacterial strains upon exposure to the SM-NP fraction relative to the SM fraction of our ES-GBBr formulation (Table 3); furthermore, these observations reinforce our findings that allicin is the dominant antibacterial agent in Bald's eyesalve.

This study identified allicin as the principal antibacterial compound present in Bald's eyesalve. Allicin (3-[(prop-2-ene-1-sulfinyl)sulfanyl]prop-1-ene) is a reactive sulfur species that is used as a defense mechanism in garlic following tissue damage [32] and is known to be the most significant bioactive component within fresh garlic extract; furthermore, allicin has been shown to exhibit antibacterial activity against a diverse range of both Gram-positive and Gram-negative bacteria, including *Streptococcus* spp., methicillin-sensitive and methicillin-resistant *S. aureus*, *Salmonella typhimurium*, *Escherichia coli*, and *Vibrio cholerae* [33-36]. Previous studies have demonstrated that the mechanism of action of allicin is highly dependent upon the capacity of its thiosulfinate group to alter the intracellular glutathione pool and inhibit metabolic and oxidative stress enzymes by oxidation of thiols within cells [34, 37]. Unlike most modern clinical antibiotics, allicin has an inherent advantage in that it does not target any specific cellular component; therefore, the development of resistance by targeted mutation is

improbable, making allicin particularly suitable for application against drug resistant bacteria [34]. We exploited the thiol-reactive nature of allicin to facilitate its depletion from the ES-GBBr formulation SM-NP fraction by addition of exogenous free cysteine and found that there was no observable antibacterial activity against either *S. aureus* or *P. aeruginosa* following depletion of allicin. These results identify allicin as the primary antibacterial compound present in Bald's eyesalve.

Considering that the primary targets of allicin are intracellular thiols, such as those found in reduced glutathione, we evaluated the concentration and yield of allicin between several Bald's eyesalve formulations. Our results indicated that there was a significant difference in the concentration of allicin present in the ES-GBBr formulation when compared to the ES-O formulation (Fig 3A); therefore, the enhanced antibacterial activity demonstrated by our ES-GBBr formulation can be attributed to a greater concentration of allicin. Consequently, we assessed total mg of allicin in all of our Bald's eyesalve formulations to determine whether distinct ingredient combinations were more favorable for allicin production. Based upon previous studies demonstrating aqueous ethanol to be a superior extraction solvent for allicin [30, 38], we conclude that allicin is extracted from minced garlic in our Bald's eyesalve formulations and stabilized by the presence of ethanol from the addition of wine, which was determined to be 3-4% v/v (S1 Table). Although there was no statistically significant difference in the yield of allicin among our formulations (Fig 3B), the formulations containing brass (ES-O, ES-L, ES-GBBr, and ES-GBr) amassed on average more allicin than those that omitted this ingredient (ES-GB and ES-G). In particular, the ES-GBBr formulation accrued the most

allicin at 74.4 mg. These results suggest that the combination of brass and bovine bile in Bald's eyesalve may be favorable for extraction of allicin from minced garlic. A previous study demonstrated that alliinase, the enzyme responsible for the conversion of alliin to allicin, displays increased activity in the presence of metal ions, most notably Fe^{2+}, Mn^{2+}, and Zn^{2+} [39]. We hypothesize that dezincification [40, 41] of the brass 260 alloy included in several of our formulations takes place due to the mildly acidic pH of Bald's eyesalve (S1 Table) which may cause corrosion. In addition, we suspect that bile salts act as a metal ion buffer in Bald's eyesalve, increasing dezincification and solubility of Zn^{2+} by the formation of micellar complexes [42]. Future work is needed to identify the chemical processes by which brass and bile interact to alter allicin production in Bald's eyesalve.

While ethanol is a well-known and widely used disinfectant, its growth inhibitory activity due to the addition of wine in Bald's eyesalve can be considered minimal. Prior studies have established the MIC and minimum bactericidal concentration (MBC) for ethanol against *S. aureus* to be 6.25% and 25% (v/v), respectively, and against *P. aeruginosa* to be 1.56% and >12.5% (v/v), respectively [43, 44]. Given the concentration of ethanol in our Bald's eyesalve formulations (S1 Table) and their corresponding MIC values (Table 2), we determined that ethanol varied from 0.02 to 0.40% (v/v) at growth inhibitory concentrations of Bald's eyesalve. At bactericidal concentrations, ethanol can perturb the structure, function, pH gradient (ΔpH), membrane potential ($\Delta\Psi$), and composition of cellular membranes [45, 46], inhibit cell division and nutrient transport [45, 47], and reduce intracellular pH [47, 48]. Since ethanol is present in such low

concentrations within our Bald's eyesalve formulations, we conclude that any contribution ethanol could make to the overall antibacterial activity, aside from promoting the extraction and stabilization of allicin, is negligible.

In an attempt to mitigate the increasing prevalence of drug resistant bacterial infections, treatment regimens including multiple antibiotics are widely utilized. Antibiotic combinations can generate additive or synergistic effects that enhance antibacterial activity and/or reduce the dosage required to eradicate infection [49, 50]; in addition, using multiple antibiotics with distinct mechanisms of action reduces the risk of progressive resistance development following treatment [51]. A recent study suggested that the antibacterial efficacy of Bald's eyesalve may be due to the combined activity of compounds arising from several ingredients in the formulation, since it was determined that garlic, wine, and an additional *Allium* species were essential to obtain full activity [6]. Our study revealed that the principal antibacterial agent within Bald's eyesalve is allicin derived from garlic; however, our MIC data also indicate that the allicin present in this medieval remedy exhibits antagonistic antibacterial activity with other compounds present in the formulation when used against *S. aureus*, whereas it displays additive or synergistic activity against *P. aeruginosa*. Our data thus support the notion that the combinatorial formulation of Bald's eyesalve is not a more effective means of treatment than allicin alone against *S. aureus*, whereas it is more effective against *P. aeruginosa*. Previous studies have shown that combining allicin with additional antifungal and antibacterial agents, such as amphotericin B and silver nanoparticles, results in synergistic activity [52, 53]; however, we have yet to identify the accessory agent(s)

present in Bald's eyesalve that results in additional activity with allicin when used against *P. aeruginosa*. This study highlights the importance of evaluating cumulative effects of antibiotics within complex mixtures and multi-drug treatment regimens, particularly when the target bacteria responsible for the infection have been identified [54, 55].

Conclusions

Results from this study demonstrated that Bald's eyesalve possesses antibacterial activity against both Gram-positive and Gram-negative bacteria including phylogenetically distinct strains of *S. aureus* and *P. aeruginosa* that exhibit variable degrees of antibiotic resistance and virulence. In addition, our study identified allicin as the principal antibacterial agent present in Bald's eyesalve and determined that its activity among additional formulation components is antagonistic against *S. aureus*, whereas it acts in an additive or synergistic fashion with other Bald's eyesalve ingredients when used against *P. aeruginosa*. These results emphasize the value of establishing the source of antibacterial activity present in plant-derived natural products for therapeutic use, including how to use complex natural mixtures to treat drug resistant bacterial infections. Furthermore, our findings underline the importance of assessing the additive, synergistic, and/or antagonistic effects of combining different ingredients within these ancient formulae as these have significant consequences with regards to the antibacterial efficacy of these natural remedies.

Supporting Information

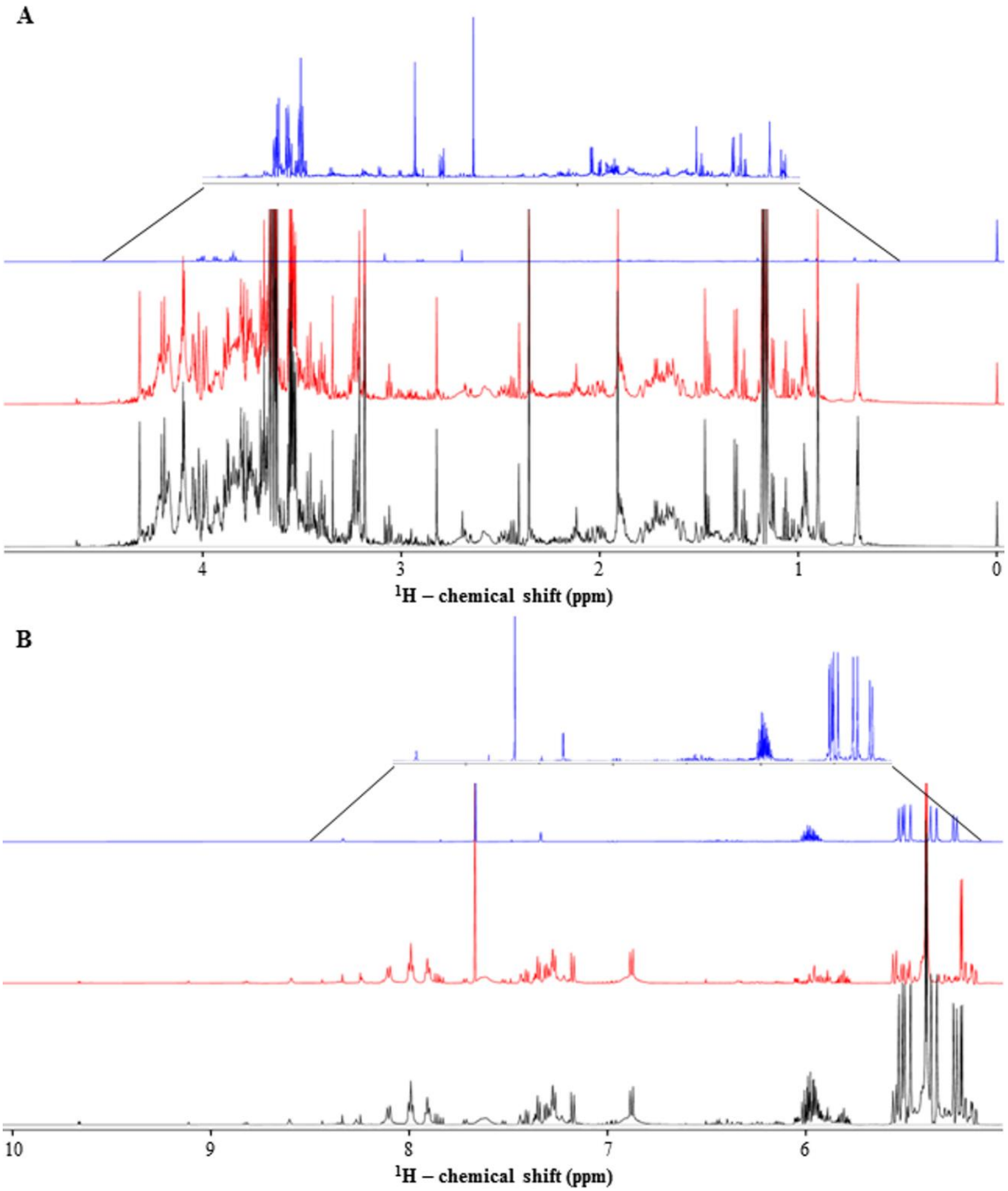

Figure S1. ^{1}H NMR analysis of ES-GBBr formulation fractions. Stacked 1D ^{1}H NMR spectra (600 MHz, 10% D_2O) in chemical shift regions (A) 0-5 ppm and (B) 5-10 ppm for ES-GBBr SM (black), SM-P (red), and SM-NP (blue) fractions. Insets display the expanded 1D ^{1}H NMR spectrum in chemical shift regions (A) 0.5-4.5 ppm and (B) 5.1-8.5 ppm for the ES-GBBr SM-NP (blue) fraction.

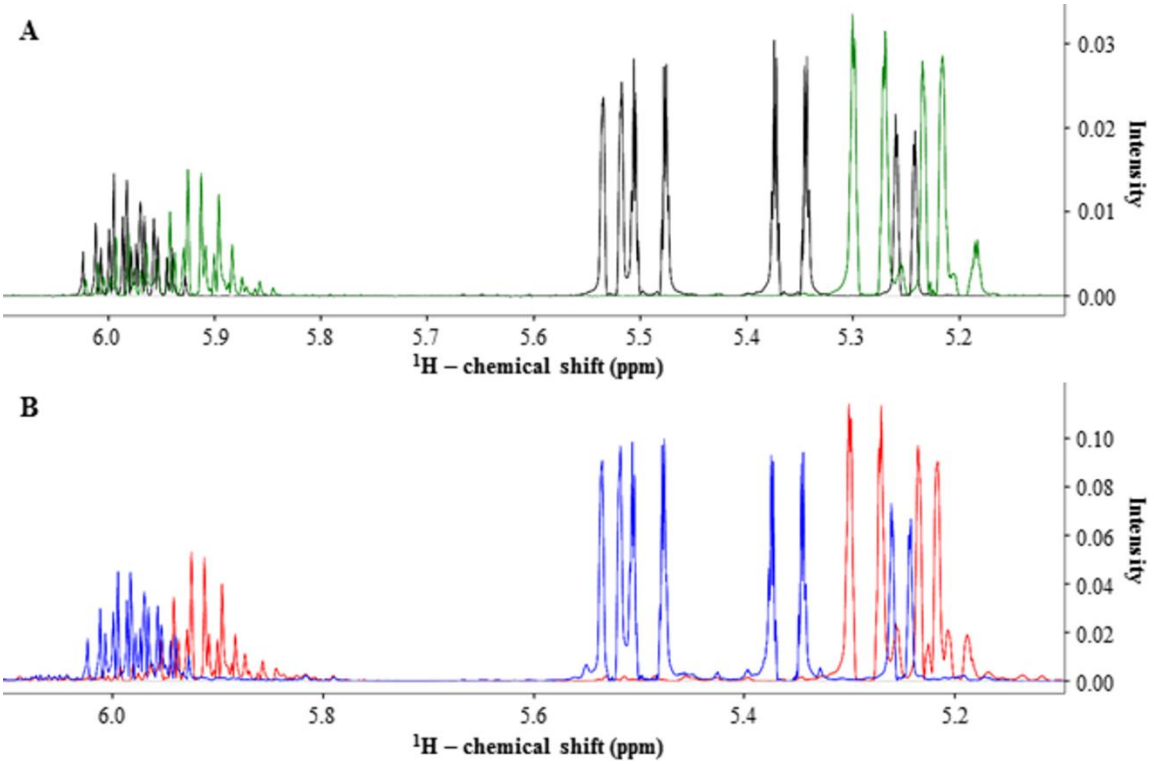

Figure S2. Thiol-reactive nature of allicin is exploited to facilitate depletion from ES-GBBr formulation SM-NP fraction. An overlay of 1D ^{1}H NMR spectra (600 MHz, 10% D_2O) in chemical shift region 5.1-6.1 ppm for (A) an allicin standard and (B) ES-GBBr formulation SM-NP fraction with (green/red) and without (black/blue) addition of exogenous free cysteine, respectively, followed by 4 °C incubation for 1 hr.

A

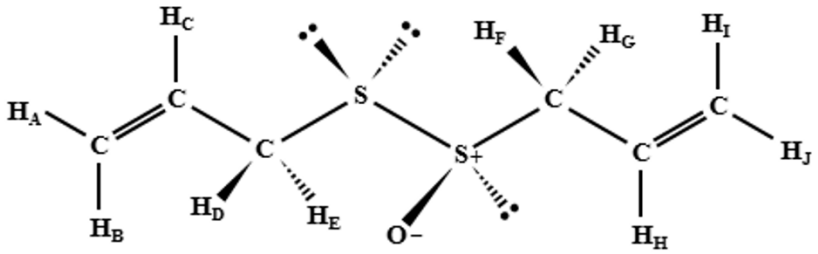

B

Allicin Standard				
^{1}H Assignment	Chemical shift (δ, ppm)	Relative Integrated Intensities	Multiplicity	Coupling (J, Hz)
A	5.25	1.00	dd	10.19, 0.99
B	5.36	1.45	dd	17.16, 1.35
C	5.99	0.61	m	17.27, 10.07, 7.37, 7.44
D	3.83	0.89	dd	14.37, 7.33
E	3.87	0.88	dd	14.25, 7.17
F	3.93	1.05	dd	12.89, 7.96
G	4.01	1.24	dd	13.21, 7.28
H	5.96	0.57	m	17.47, 9.91, 7.83, 7.62
I	5.49	1.39	dd	17.01, 1.16
J	5.53	1.28	dd	10.45, 1.01

C

Allicin in ES-GBBr Formulation SM-NP Fraction				
^{1}H Assignment	Chemical shift (δ, ppm)	Relative Integrated Intensities	Multiplicity	Coupling (J, Hz)
A	5.25	1.00	dd	10.18, 0.93
B	5.36	1.45	dd	17.02, 1.18
C	5.99	0.67	m	16.71, 9.69, 6.59, 7.20
D	3.83	0.90	dd	14.25, 7.50
E	3.87	0.90	dd	14.25, 7.16
F	3.93	1.15	dd	13.06, 8.06
G	4.01	1.20	dd	13.06, 7.54
H	5.96	0.58	m	17.60, 9.92, 7.64, 7.71
I	5.49	1.49	dd	17.02, 1.18
J	5.53	1.35	dd	10.32, 1.08

Figure S3. Allicin structure and ^{1}H NMR spectral data. The molecular structure of allicin in shown in (A). Assignments, chemical shifts (δ, ppm), relative integrated intensities, multiplicities, and coupling constants (J, Hz) from ^{1}H NMR spectra are displayed for (B) an allicin standard and (C) allicin in ES-GBBr formulation SM-NP fraction.

Table S1. pH and ethanol % v/v of Bald's eyesalve formulations.

Formulation	Replicate No.	pH	Ethanol % v/v	Average	
				pH	Ethanol % v/v
ES-O	1	5.41	2.86	5.37	2.70
	2	5.39	2.39		
	3	5.34	2.92		
	4	5.35	2.61		
ES-L	1	5.53	2.93	5.43	2.76
	2	5.38	2.51		
	3	5.37	2.80		
	4	5.45	2.78		
ES-GB	1	5.46	3.76	5.45	3.73
	2	5.47	3.49		
	3	5.43	3.91		
	4	5.44	3.74		
ES-GBBr	1	5.29	4.11	5.42	3.79
	2	5.46	3.77		
	3	5.45	3.74		
	4	5.48	3.53		
ES-GBr	1	5.09	3.63	5.01	3.83
	2	5.00	3.81		
	3	5.00	3.69		
	4	4.96	4.20		
ES-G	1	5.12	3.54	5.08	3.67
	2	5.09	3.87		
	3	5.10	3.61		
	4	5.02	3.66		

Acknowledgements

We thank Dr. Michael Franklin, Dr. Jovanka Voyich, and Dr. Garth James at Montana State University for providing the bacterial strains *P. aeruginosa* PAO1, *S. aureus* LAC, and *P. aeruginosa* PA215, respectively.

References

1. Watkins F, Pendry B, Corcoran O, Sanchez-Medina A. Anglo-Saxon pharmacopoeia revisited: a potential treasure in drug discovery. Drug Discov Today. 2011; doi:10.1016/j.drudis.2011.07.002.

2. The Review on Antimicrobial Resistance, chaired by Jim O'Neill. Tackling drug-resistant infections globally: final report and recommendations. 2016.

3. Cockayne TO. Leechdoms, wortcunning, and starcraft of early England. Being a collection of documents, for the most part never before printed, illustrating the history of science in this country before the Norman conquest. Rolls series 35th, 3 Vols. London: Longman, Green, Longman, Roberts, and Green. 1864-1866.

4. O'Callaghan RJ. The pathogenesis of *Staphylococcus aureus* eye infections. Pathogens. 2018; doi:10.3390/pathogens7010009.

5. Abidi SH, Sherwani SK, Siddiqui TR, Bashir A, Kazmi SU. Drug resistance profile and biofilm forming potential of *Pseudomonas aeruginosa* isolated from contact lenses in Karachi-Pakistan. BMC Ophthalmology. 2013; doi:10.1186/1471-2415-13-57.

6. Harrison F, Roberts AEL, Gabrilska R, Rumbaugh KP, Lee C, Diggle SP. A 1,000-year-old antimicrobial remedy with antistaphylococcal activity. mBio. 2015; doi:10.1128/mBio.01129-15.

7. Ammons MCB, Tripet BP, Carlson RP, Kirker KR, Gross MA, Stanisich JJ, Copié V. Quantitative NMR metabolite profiling of methicillin-resistant and methicillin-susceptible *Staphylococcus aureus* discriminates between biofilm and planktonic phenotypes. J Proteome Res. 2014; doi:10.1021/pr500120c.

8. Diep BA, Gill SR, Chang RF, Phan TH, Chen JH, Davidson MG, Lin F, Lin J, Carleton HA, Mongodin EF, Sensabaugh GF, Perdreau-Remington F. Complete genome sequence of USA300, an epidemic clone of community-acquired meticillin-resistant *Staphylococcus aureus*. Lancet. 2006; doi:10.1016/S0140-6736(06)68231-7.

9. Stewart PS, Franklin MJ, Williamson KS, Folsom JP, Boegli L, James GA. Contribution of stress responses to antibiotic tolerance in *Pseudomonas aeruginosa* biofilms. Antimicrob Agents Chemother. 2015; doi:10.1128/AAC.00433-15.

10. James GA, Swogger E, Wolcott R, Pulcini Ed, Secor P, Sestrich J, Costerton JW, Stewart PS. Biofilms in chronic wounds. Wound Repair Regen. 2008; doi:10.1111/j.1524-475X.2007.00321.x.

11. CLSI. Methods for dilution antimicrobial susceptibility tests for bacteria that grow aerobically; approved standard – tenth edition. CLSI document M07-A10. Wayne, PA: Clinical and Laboratory Standards Institute; 2015.

12. Silhavy TJ, Kahne D, Walker S. The bacterial cell envelope. Cold Spring Harb Perspect Biol. 2010; doi:10.1101/cshperspect.a000414.

13. Santas J, Almajano MP, Carbó R. Antimicrobial and antioxidant activity of crude onion (*Allium cepa*, L.) extracts. Int J Food Sci Technol. 2010; doi:10.1111/j.1365-2621.2009.02169.x.

14. Lee JH, Park JH, Cho HS, Joo SW, Cho MH, Lee J. Anti-biofilm activities of quercetin and tannic acid against *Staphylococcus aureus*. Biofouling. 2013; doi10.1080/08927014.2013.788692.

15. Vasavi HS, Arun AB, Rekha PD. Anti-quorum sensing activity of flavonoid-rich fraction from *Centella asiatica* L. against *Pseudomonas aeruginosa* PAO1. J Microb Immunol Infect. 2016; doi:10.1016/j.jmii.2014.03.012.

16. Musthafa KS, Ravi AV, Annapoorani A, Sybiya Vasantha Packiavathy IA, Pandian SK. Evaluation of anti-quorum-sensing activity of edible plants and fruits through inhibition of the N-acyl-homoserine lactone system in *Chromobacterium violaceum* and *Pseudomonas aeruginosa*. Chemotherapy. 2010; doi:10.1159/000320185.

17. Vandeputte OM, Kiendrebeogo M, Rasamiravaka T, Stévigny C, Duez P, Rajaonson S, Diallo B, Mol A, Baucher M, El JM. The flavanone naringenin reduces the production of quorum sensing-controlled virulence factors in *Pseudomonas aeruginosa* PAO1. Microbiology. 2011; doi:10.1099/mic.0.049338-0.

18. Lanzotti V, Bonanomi G, Scala F. What makes *Allium* species effective against pathogenic microbes? Phytochem Rev. 2013; doi:10.1007/s11101-013-9295-3.

19. Mnayer D, Fabiano-Tixier A, Petitcolas E, Hamieh T, Nehme N, Ferrant C, Fernandez X, Chemat F. Chemical composition, antibacterial and antioxidant activities of six essential oils from the *Alliaceae* family. Molecules. 2014; doi:10.3390/molecules191220034.

20. Tsao S, Yin M. In-vitro antimicrobial activity of four diallyl disulphides occurring naturally in garlic and Chinese leek oil. J Med Microbiol. 2001; doi:10.1099/0022-1317-50-7-646.

21. Tsao S, Yin M. *In vitro* activity of garlic oil and four diallyl sulphides against antibiotic-resistant *Psuedomonas aeruginosa* and *Klebsiella pneumoniae*. J Antimicrob Chemother. 2001; 47(5):665-670.

22. Kim JW, Huh JE, Kyung SH, Kyung KH. Antimicrobial activity of alk(en)yl sulfides found in essential oils of garlic and onion. Food Sci Biotechnol. 2004; 13(2):235-239.

23. Atanasov AG, Waltenberger B, Pferschy-Wenzig E, Linder T, Wawrosch C, Uhrin P, Temml V, Wang L, Schwaiger S, Heiss EH, Rollinger JM, Schuster D, Breuss JM, Bochkov V, Mihovilovic MD, Kopp B, Bauer R, Dirsch VM, Stuppner H. Discovery and resupply of pharmacologically active plant-derived natural products: a review. Biotechnol Adv. 2015; doi:10.1016/j.biotechadv.2015.08.001.

24. Eldridge GR, Vervoort HC, Lee CM, Cremin PA, Williams CT, Hart SM, Goering MG, O'Neill-Johnso M, Zeng L. High-throughput method for the production and analysis of large natural products libraries for drug discovery. Anal Chem. 2002; doi:10.1021/ac025534s.

25. Abel U, Koch C, Speitling M, Hansske FG. Modern methods to produce natural-product libraries. Curr Opin Chem Biol. 2002; doi:10.1016/S1367-5931(02)00338-1.

26. Koehn FE, Carter GT. The evolving role of natural products in drug discovery. Nat Rev Drug Discov. 2005; doi:10.1038/nrd1657.

27. Inui T, Wang Y, Pro SM, Franzblau SG, Pauli GF. Unbiased evaluation of bioactive secondary metabolites in complex matrices. Fitoterapia. 2012; doi:10.1016/j.fitote.2012.06.012.

28. Qiu F, Cai G, Jaki BU, Lankin DC, Franzblau SG, Pauli GF. Quantitative purity-activity relationships of natural products: the case of anti-tuberculosis active triterpenes from *Oplopanax horridus*. J Nat Prod. 2013; doi:10.1021/np3007809.

29. Liu Z. Preparation of botanical samples for biomedical research. Endocr Metab Immune Disord Drug Targets. 2008; doi:10.2174/187153008784534358.

30. Ilić D, Nikolić V, Stanković M, Nikolić L, Stanojević L, Mladenović-Ranisavljević I, Šmelcerović A. Transformation of synthetic allicin: the influence of ultrasound, microwaves, different solvents and temperatures, and the products isolation. ScientificWorldJournal. 2012; doi:10.1100/2012/561823.

31. Freeman F, Kodera Y. Garlic chemistry: stability of S-(2-propenyl)-2-propene-1-sulfinothioate (allicin) in blood, solvents, and simulated physiological fluids. J Agric Food Chem. 1995; doi:10.1021/jf00057a004.

32. Gruhlke MC, Nicco C, Batteux F, Slusarenko AJ. The effects of allicin, a reactive sulfur species from garlic, on a selection of mammalian cell lines. Antioxidants. 2016; doi:10.3390/antiox6010001.

33. Wu X, Santos RR, Fink-Gremmels J. Analyzing the antibacterial effects of food ingredients: model experiments with allicin and garlic extracts on biofilm formation and viability of *Staphylococcus epidermidis*. Food Sci Nutr. 2015; doi:10.1002/fsn3.199.

34. Müller A, Eller J, Albrecht F, Prochnow P, Kuhlmann K, Bandow JE, Slusarenko AJ, Leichert LI. Allicin induces thiol stress in bacteria through S-allylmercapto modification of protein cysteines. J Biol Chem. 2016; doi:10.1074/jbc.M115.702308.

35. Cavallito CJ, Bailey JH. Allicin, the antibacterial principle of *Allium sativum*. I. Isolation, physical properties and antibacterial action. J Am Chem Soc. 1944; doi:10.1021/ja01239a048.

36. Cutler RR, Wilson P. Antibacterial activity of a new, stable, aqueous extract of allicin against methicillin-resistant *Staphylococcus aureus*. Br J Biomed Sci. 2004; doi:10.1080/09674845.2004.11732646.

37. Borlinghaus J, Albrecht F, Gruhlke MCH, Nwachukwu ID, Slusarenko AJ. Allicin: chemistry and biological properties. Molecules. 2014; doi:10.3390/molecules190812591.

38. Fujisawa H, Suma K, Origuchi K, Kumagai H, Seki T, Ariga T. Biological and chemical stability of garlic-derived allicin. J Agric Food Chem. 2008; doi:10.1021/jf8000907.

39. Chhabria S, Desai K. Purification and characterization of alliinase produced by *Cupriavidus necator* and its application for generation of cytotoxic agent: allicin. Saudi J Biol Sci. 2016; doi:10.1016/j.sjbs.2016.01.003.

40. Marshakov IK. Corrosion resistance and dezincing of brasses. Prot Met. 2005; doi:10.1007/s11124-005-0031-2.

41. Natesan M, Selvaraj S, Manickam T, Venkatachari G. Corrosion behavior of metals and alloys in marine-industrial environment. Sci Technol Adv Mater. 2008; doi:10.1088/1468-6996/9/4/045002.

42. Feroci G, Fini A, Fazio G, Zuman P. Interaction between dihydroxyl bile salts and divalent heavy metal ions studied by polarography. Anal Chem. 1995; doi:10.1021/ac00118a008.

43. Man A, Gâz AS, Mare AD, Berţa L. Effects of low-molecular weight alcohols on bacterial viability. Rev Romana Med Lab. 2017; doi:10.1515/rrlm-2017-0028.

44. Mazzola PG, Jozala AF, Novaes LCL, Moriel P, Penna TCV. Minimal inhibitory concentration (MIC) determination of disinfectant and/or sterilizing agents. Braz J Pharm Sci. 2009; doi:10.1590/S1984-82502009000200008.

45. Fried VA, Novick A. Organic solvents as probes for the structure and function of the bacterial membrane: effects of ethanol on the wild type and an ethanol-resistant mutant of *Escherichia coli* K-12. J Bacteriol. 1973; 114(1):239-248.

46. Silveira, MG, Baumgärtner M, Rombouts FM, Abee T. Effect of adaptation to ethanol on cytoplasmic and membrane protein profiles of *Oenococcus oeni*. Appl Environ Microbiol. 2004; doi:10.1128/AEM.70.5.2748-2755.2004.

47. Bowles LK, Ellefson WL. Effects of butanol on *Clostridium acetobutylicum*. Appl Environ Microbiol. 1985; 50(5):1165-1170.

48. Huang L, Forsberg CW, Gibbins LN. Influence of external pH and fermentation products on *Clostridium acetobutylicum* intracellular pH and cellular distribution of fermentation products. Appl Environ Microbiol. 1986; 51(6):1230-1234.

49. Barrera NP, Morales B, Torres S, Villalón M. Principles: mechanisms and modeling of synergism in cellular responses. Trends Pharmacol Sci. 2005; doi:10.1016/j.tips.2005.08.003.

50. Wagner H, Ulrich-Merzenich G. Synergy research: approaching a new generation of phytopharmaceuticals. Phytomedicine. 2009; doi:10.1016/j.phymed.2008.12.018.

51. Rahal JJ. Novel antibiotic combinations against infections with almost completely resistant *Pseudomonas aeruginosa* and *Acinetobacter* species. Clin Infect Dis. 2006; doi:10.1086/504486.

52. Corral MJ, González-Sánchez E, Cuquerella M, Alunda JM. In vitro synergistic effect of amphotericin B and allicin on *Leishmania donovani* and *L. infantum*. Antimicrob Agents Chemother. 2014; doi:10.1128/AAC.00710-13.

53. Sharifi-Rad J, Hoseini Alfatemi SM, Sharifi Rad M, Iriti M. Antimicrobial synergic effect of allicin and silver nanoparticles on skin infection caused by methicillin-resistant *Staphylococcus aureus* spp. Ann Med Health Sci Res. 2014; doi:10.4103/2141-9248.144883.

54. Torella JP, Chait R, Kishony R. Optimal drug synergy in antimicrobial treatments. PLoS Comput Biol. 2010; doi:10.1371/journal.pcbi.1000796.

55. Li X, Plésiat P, Nikaido H. The challenge of efflux-mediated antibiotic resistance in Gram-negative bacteria. Clin Microbiol Rev. 2015; doi:10.1128/CMR.00117-14.

APPENDIX C

THE CLPCP COMPLEX MODULATES RESPIRATORY METABOLISM IN *STAPHYLOCOCCUS AUREUS* AND IS REGULATED IN A SRRAB-DEPENDENT MANNER

THE CLPCP COMPLEX MODULATES RESPIRATORY METABOLISM IN *STAPHYLOCOCCUS AUREUS* AND IS REGULATED IN A SRRAB-DEPENDENT MANNER

Contribution of Authors and Co-Authors

Manuscript in Appendix C

Author: Ameya A. Mashruwala

Contributions: Conceptualized the study, curated the data, conducted formal analysis and investigation, developed methodology, administered the project, validated and visualized the data, wrote the original manuscript draft, and reviewed and edited the manuscript.

Author: Brian J. Eilers

Contributions: Curated the data, conducted formal analysis and investigation, developed methodology, administered the project, validated and visualized the data, and reviewed and edited the manuscript.

Co-Author: Amanda L. Fuchs

Contributions: Conducted formal analysis and investigation, developed methodology, administered the project, and reviewed and edited the manuscript.

Co-Author: Javiera Norambuena

Contributions: Conducted formal analysis and investigation and reviewed and edited the manuscript.

Co-Author: Carly A. Earle

Contributions: Conducted formal analysis and investigation and reviewed and edited the manuscript.

Co-Author: Adriana van de Guchte

Contributions: Conducted formal analysis and investigation and reviewed and edited the manuscript.

Contribution of Authors and Co-Authors – Continued

Co-Author: Brian P. Tripet

Contributions: Conducted formal analysis and investigation, developed methodology, administered the project, and reviewed and edited the manuscript.

Co-Author: Valérie Copié

Contributions: Acquired funding, administered the project, provided resources and software, supervised the project, and reviewed and edited the manuscript.

Co-Author: Jeffrey M. Boyd

Contributions: Acquired funding, administered the project, provided resources and software, supervised the project, and reviewed and edited the manuscript.

Manuscript Information Page

Ameya A. Mashruwala, Brian J. Eilers, Amanda L. Fuchs, Javiera Norambuena, Carly A. Earle, Adriana van de Guchte, Brian P. Tripet, Valérie Copié, Jeffrey M. Boyd

Journal Name: Journal of Bacteriology

Status of Manuscript:
_____ Prepared for submission to a peer-reviewed journal
_____ Officially submitted to a peer-reviewed journal
_____ Accepted by a peer-reviewed journal
__x__ Published in a peer-reviewed journal

Publisher: American Society for Microbiology
Issue in which manuscript appears: Volume 201, Issue 15, 2019

THE CLPCP COMPLEX MODULATES RESPIRATORY METABOLISM IN *STAPHYLOCOCCUS AUREUS* AND IS REGULATED IN A SRRAB-DEPENDENT MANNER

Ameya A. Mashruwala[a*], Brian J. Eilers[b], Amanda L. Fuchs[b], Javiera Norambuena[a], Carly A. Earle[a], Adriana van de Guchte[a], Brian P. Tripet[b], Valérie Copié[b], Jeffrey M. Boyd[a]

[a]Department of Biochemistry and Microbiology, Rutgers, The State University of New Jersey, New Brunswick, New Jersey, USA
[b]Department of Chemistry and Biochemistry, Montana State University, Bozeman, Montana, USA
[*]Present address: Department of Molecular Biology, Princeton University, Princeton, New Jersey, USA

Address correspondence to Jeffrey M. Boyd, jeffboyd@SEBS.Rutgers.edu

Abstract

The staphylococcal respiratory regulator (SrrAB) modulates energy metabolism in *Staphylococcus aureus*. Studies have suggested that regulated protein catabolism facilitates energy homeostasis. Regulated proteolysis in *S. aureus* is achieved through protein complexes composed of a peptidase (ClpQ or ClpP) in association with an AAA family ATPase (typically, ClpC or ClpX). In the present report, we tested the hypothesis that SrrAB regulates a Clp complex to facilitate energy homeostasis in *S. aureus*. Strains deficient in one or more Clp complexes were attenuated for growth in the presence of puromycin, which causes enrichment of misfolded proteins. A Δ*srrAB* strain had increased sensitivity to puromycin. Epistasis experiments suggested that the puromycin

sensitivity phenotype of the Δ*srrAB* strain was a result of decreased ClpC activity. Consistent with this, transcriptional activity of *clpC* was decreased in the Δ*srrAB* mutant, and overexpression of *clpC* suppressed the puromycin sensitivity of the Δ*srrAB* strain. We also found that ClpC positively influenced respiration and that it did so upon association with ClpP. In contrast, ClpC limited fermentative growth, while ClpP was required for optimal fermentative growth. Metabolomics studies demonstrated that intracellular metabolic profiles of the Δ*clpC* and Δ*srrAB* mutants were distinct from those of the wild-type strain, supporting the notion that both ClpC and SrrAB affect central metabolism. We propose a model wherein SrrAB regulates energy homeostasis, in part, via modulation of regulated proteolysis.

Importance

Oxygen is used as a substrate to derive energy by the bacterial pathogen *Staphylococcus aureus* during infection; however, *S. aureus* can also grow fermentatively in the absence of oxygen. To successfully cause infection, *S. aureus* must tailor its metabolism to take advantage of respiratory activity. Different proteins are required for growth in the presence or absence of oxygen; therefore, when cells transition between these conditions, several proteins would be expected to become unnecessary. In this report, we show that regulated proteolysis is used to modulate energy metabolism in *S. aureus*. We report that the ClpCP protein complex is involved in specifically modulating aerobic respiratory growth but is dispensable for fermentative growth.

Introduction

Staphylococcus aureus is a commensal bacterium that colonizes between 20% and 50% of the healthy human population (1–4). Typically, *S. aureus* does not cause the human carrier harm; however, it is capable of causing both invasive and noninvasive infections (5–7). Historically, *S. aureus* infections were acquired within a hospital environment (8), but the onset or occurrence of *S. aureus* infections is increasing in community settings (5, 9).

S. aureus is a facultative anaerobe. It can derive energy for growth using either fermentative or respiratory pathways (10). Oxygen concentrations vary within healthy human tissues (between 1.5% and 19.7%), and in infected tissues, they are estimated to be less than 1% (11–13). In the context of *S. aureus* infections, the concentration of oxygen at the site of infection progressively decreases as an infection proceeds (14). Consequently, the ability of *S. aureus* to fine-tune respiratory or fermentative metabolism with respect to the oxygen concentration is likely to be crucial for achieving optimum energy production and utilization. Consistent with this idea, the pathogenesis of strains with an impaired ability to respire or ferment is attenuated (15–17).

Bacteria use a variety of regulatory mechanisms to facilitate adaptation toward changes in their environments. Regulation by means of proteolysis is a strategy adopted in processes as diverse as stress response to cell division (18, 19). It has been argued that regulated proteolysis allows cells to efficiently remove proteins that have been rendered superfluous to cellular needs (20). Two rather distinct sets of proteins are required to facilitate fermentative and respiratory growth; therefore, when cells transition between

either of the conditions, a number of proteins will be rendered unnecessary. The concentration and availability of a terminal electron acceptor (TEA) constitute one factor that could necessitate reliance of cells upon regulated proteolysis to facilitate energetic homeostasis. Regulated proteolysis is employed to modulate respiratory metabolism in yeast (21, 22). It is unclear whether regulated proteolysis and respiratory/fermentative metabolism are linked in *S. aureus*.

Proteolysis of *S. aureus* cytoplasmic proteins is achieved by chaperone-protease complexes (Clp complexes) (19). The complexes are two-component proteases consisting of peptidase and ATPase subunits (19). *S. aureus* harbors two peptidase subunits: ClpP and ClpQ (19, 23, 24). ClpP is the dominant peptidase under standard laboratory growth conditions (23, 24). *S. aureus* harbors multiple ATPase subunits that each carry a domain typical of the AAA protein superfamily (19). Only a subset of ATPases contain the ClpP recognition tripeptide and can interact with ClpP (25, 26). In *S. aureus*, ClpC and ClpX are capable of interacting with ClpP, while ClpL and ClpB are thought to not interact with ClpP (19). Apart from interacting with ClpP, the ATPases also interact with a second class of proteins termed cofactor or adaptor proteins. The adaptor proteins facilitate the recognition and targeting of proteins for degradation. Three adaptor proteins have been identified in *S. aureus*: YjbH (27), TrfA (28), and McsB (29). TrfA, a homolog of MecA in *Bacillus subtilis*, has been suggested to function as an adaptor for ClpC (30). ClpP-dependent complexes are integral for numerous cellular processes, thereby establishing regulated proteolysis as a global modulator of cellular physiology.

Bacteria utilize two-component regulatory systems (TCRS) to adapt to their

surroundings. TCRS allow bacteria to integrate several stimuli into signaling circuits, allowing for a tailored response toward their environment (reviewed in reference 31). Classical TCRS consist of two proteins: a histidine kinase (HK) and a response regulator (RR). The HK is capable of interacting with intracellular and/or extracellular stimuli. The RR is typically cytosolic and may also be a transcription factor with one or more of the following functionalities: it can undergo autophosphorylation, transfer phosphoryl groups to the RR, or remove phosphoryl groups from the RR. Interaction with a signal molecule alters the functionality of the HK, thereby affecting the levels of the phosphoryl group on the RR. In most cases but not all, the levels of phosphoryl groups on the RR at any given point determine whether system output is increased or decreased.

The staphylococcal respiratory regulator (SrrAB) TCRS was identified as a system that modulates the expression of staphylococcal virulence factors when oxygen tension is decreased (32–34). SrrA is a DNA binding RR (33, 35). SrrB is the HK and is membrane spanning (33). Proteomic and microarray studies have established SrrAB as a pleiotropic regulator of energy metabolism (14, 36, 37), and SrrAB positively influences aerobic respiration (14, 35, 36). In the absence of oxygen or upon its limitation, SrrAB positively influences fermentative growth (37). Biofilms are crucial in staphylococcal pathogenesis (6, 38, 39), and SrrAB positively influences the formation of biofilms in low-oxygen environments (36, 40). *S. aureus* strains lacking SrrAB also display attenuated survival in models of infection (17, 41).

Results

A *SrrAB* Strain has Increased Sensitivity to Puromycin

We reasoned that if SrrAB regulates a factor involved in protein turnover, then a Δ*srrAB* strain would display altered growth under conditions that cause protein misfolding. Puromycin is a tRNA analog that causes premature termination of protein translation; therefore, puromycin imposes a high demand for the proteolytic machinery (24). The USA300_LAC Δ*srrAB* mutant strain displayed a pronounced growth defect in solid and liquid aerobic media supplemented with puromycin but not in its absence (Fig. 1; see also Fig. S1 in the supplemental material). Growth on both solid and liquid media was examined, since regulatory networks in *S. aureus* can be altered between these two growth environments (42). Serial dilutions of the USA300_LAC (WT) and Δ*srrAB* strains were placed upon solid tryptic soy broth (TSB) medium in the presence or absence of puromycin and growth was analyzed. In the presence of puromycin, the Δ*srrAB* strain formed colonies that were smaller in size and the number of colonies formed was decreased by 10- to 100-fold (Fig. 1), while in the absence of puromycin, the Δ*srrAB* strain formed colonies of the same size and frequency as the WT strain. Likewise, in liquid medium, the *ΔsrrAB* strain displayed an increased generation time, and its growth was inhibited at lower concentrations of puromycin than for the WT (Fig. S1B and C). The return of *srrAB* genes to the chromosome of the *ΔsrrAB* strain, in a nonendogenous location, restored puromycin sensitivity to WT levels (Fig. 1 and S1). Puromycin resistance was mildly, but consistently, enhanced in a WT strain carrying *srrAB* in a

multicopy plasmid (Fig. S1D).

Regulatory networks can differ between isolates of *S. aureus* (43, 44). The influence of SrrAB on puromycin resistance was examined in alternate isolates of *S. aureus* (Newman, MW2, and N315) that differ in their physiologies and in their expression of virulence factors. In the Newman strain, the global virulence regulator SaeS contains a point mutation (SaeS P18) that imparts constitutive kinase activity (45). The growth of strains lacking SrrAB was attenuated on solid medium containing puromycin for each isolate examined (Fig. 1). The data in Fig. 1 and S1 suggested that SrrAB positively influences puromycin resistance in *S. aureus*.

Genetic Evidence Suggests that Decreased Expression of *ClpC* in the *SrrAB* Strain Results in Sensitivity to Puromycin

We tested the hypothesis that SrrAB controls the activity of a factor that facilitates protein turnover. Strains deficient in the activity of Clp proteolytic complexes have deficient growth in the presence of puromycin (24). Proteomic analyses by Throup et al. identified a putative ATPase, with homology to the *Lactococcus lactis* protein CAA44207, which had altered abundance in an *S. aureus* strain lacking SrrAB (37). Basic Local Alignment Search Tool (BLAST) analyses found that ClpL (SAUSA300_2486) and ClpC (SAUSA300_0510) had the highest similarity to CAA44207. We found that a *ΔclpC* strain had deficient growth on solid medium containing puromycin, whereas a *clpL*::Tn strain did not (Fig. 2A).

Epistasis experiments were used to examine potential interactions between *srrAB* and *clpC*. The puromycin sensitivities of the Δ*srrAB*, Δ*clpC*, and Δ*srrAB* Δ*clpC* strains

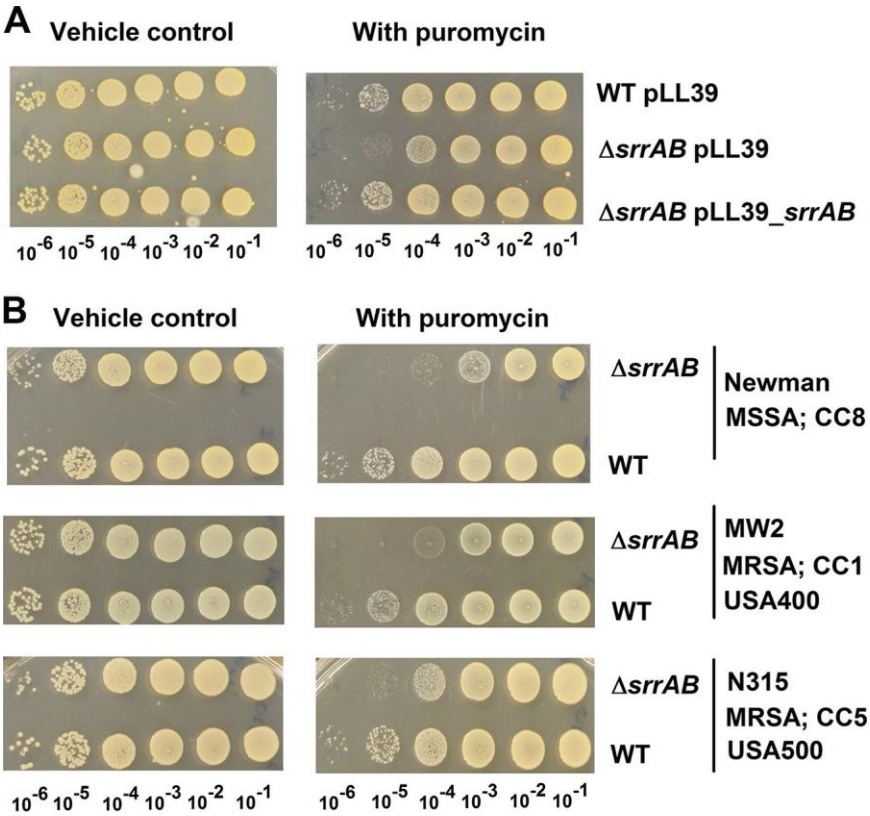

Figure 1. SrrAB is involved in puromycin resistance in diverse isolates of *S. aureus*. (A) A Δ*srrAB* strain is deficient in growth upon solid TSB medium containing puromycin. Growth for the WT with pLL39 or the Δ*srrAB* strain with pLL39 or pLL39_*srrAB* is displayed on solid TSB medium with or without puromycin. (B) Growth for the Newman (JMB 1422), Newman Δ*srrAB* (JMB 4751), MW2 (JMB 1324), MW2 Δ*srrAB* (JMB 7573), N315 (JMB 7570), and N315 Δ*srrAB* (JMB 7574) strains is displayed on solid TSB medium with or without puromycin. MRSA, methicillin-resistant *S. aureus*; MSSA, methicillin-sensitive *S. aureus*; CC, clonal-complex type, USA number, the pulsed-field gel electrophoresis type. Photographs are representative of at least three independent experiments. The numbers beneath each photograph denote the serial dilution that cells were removed from before plating.

were analyzed in liquid medium and on solid medium. The puromycin sensitivity phenotypes associated with the Δ*srrAB* and Δ*clpC* mutations were nonadditive. The size and frequency of colonies formed by the Δ*srrAB* Δ*clpC* double mutant were similar to those observed for the Δ*clpC* strain (Fig. 2B). We found that the presence of puromycin increased the lag times necessary to initiate outgrowth (see Fig. S2A). The puromycin

dependent growth inhibition levels associated with the Δ*srrAB* and Δ*clpC* mutations were not additive in liquid medium (Fig. S2B). These data suggest that SrrAB may affect puromycin resistance via ClpC.

We introduced *clpC*, under the transcriptional control of a xylose-inducible promoter (pEPSA5_*clpC*), into the WT and Δ*srrAB* strains and assessed puromycin sensitivities. In the presence of puromycin, the Δ*srrAB* strain carrying empty vector formed 10-fold fewer colonies than the WT strain carrying an empty vector (Fig. 2C). However, the Δ*srrAB* strain carrying pEPSA5_*clpC* formed a similar number of colonies as the WT carrying an empty vector. The presence of pEPSA5_*clpC* had no noticeable effect on the WT at the puromycin concentration utilized.

The influence of SrrAB on *clpC* transcription was examined. A transcriptional reporter was constructed wherein the gene encoding green fluorescent protein (GFP) was placed under the transcriptional control of the *clpC* promoter. SrrA is a transcriptional repressor of the gene encoding protein A (Spa) (33), and a *spa* transcriptional reporter was included as a positive control. The transcriptional activities of *clpC* and *spa* were decreased and increased, respectively, in the Δ*srrAB* strain (Fig. 2D). The transcriptional activities of both genes were restored to near WT levels by the reintroduction of *srrAB* to the Δ*srrAB* strain.

Metabolomics Analyses Demonstrate the Influence of SrrAB and ClpC on Metabolism

We tested the hypothesis that SrrAB affects energy homeostasis via ClpC. To this

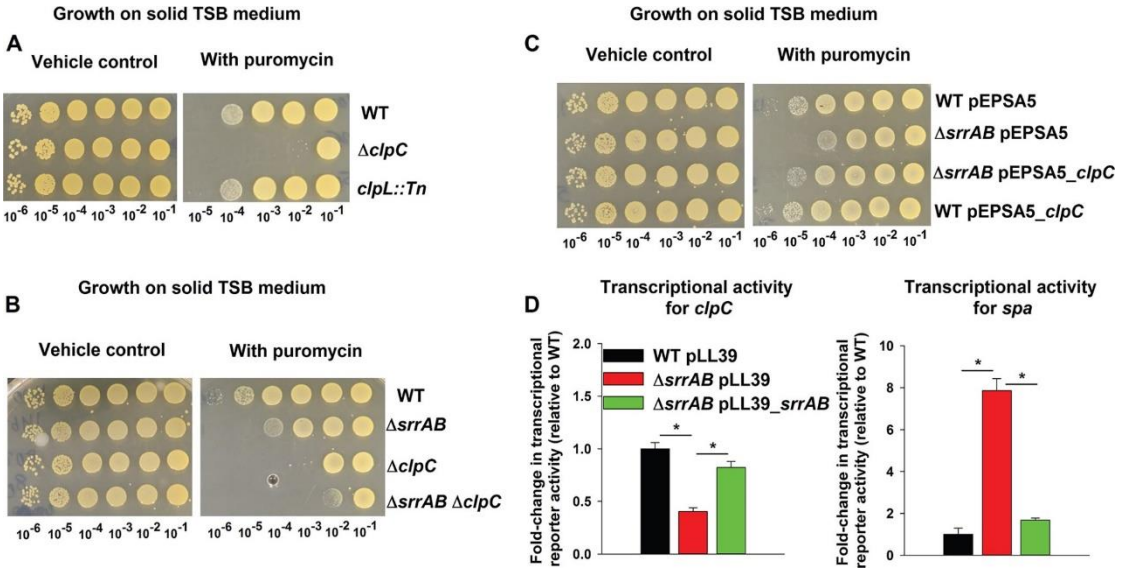

Figure 2. Genetic evidence suggests that decreased expression of ClpC in a *ΔsrrAB* strain results in sensitivity to puromycin. (A) ClpC is required for puromycin resistance, while ClpL is dispensable. Growth for the WT (JMB 1100), *ΔclpC* (JMB 8025), and *clpL*::Tn (JMB 4850) strains is displayed on solid TSB medium with or without puromycin. (B) The puromycin sensitivity phenotypes of the *ΔsrrAB* and *ΔclpC* mutations are not additive. Growth for the WT, *ΔsrrAB* (JMB 1467), *ΔclpC*, and *ΔsrrAB ΔclpC* (JMB 8027) strains is displayed on solid TSB medium with or without puromycin. (C) Overexpression of *clpC* suppresses the puromycin sensitivity phenotype of the *ΔsrrAB* strain. The growth profiles of WT and *ΔsrrAB* strains with either pEPSA5 (empty vector) or pEPSA5 *clpC* are displayed on solid TSB medium with or without puromycin. (D) Transcriptional activity of *clpC* is decreased, while that for *spa* is increased, in a strain lacking SrrAB. Transcriptional activities are displayed for the WT with pLL39 and the *ΔsrrAB* strain with pLL39 or pLL39 *srrAB* and simultaneously carrying a multicopy plasmid containing *gfp* under the transcriptional control of either the *clpC* or *spa* promoter. Data in panel D represent the averages from triplicate cultures and error bars represent standard deviations. Photographs shown in panels A, B, and C are representative of at least three independent experiments, and the numbers beneath each photograph denote the derail dilution that cells were removed from before plating. Where indicated, Student t-tests (two tailed) were performed. *, *P* 0.05.

end, we examined the effect of SrrAB and ClpC upon cellular energetics using one-dimensional (1D) ^{1}H nuclear magnetic resonance (NMR) for the global profiling of cellular metabolites following aerobic growth, as previously described (46). Intracellular metabolite levels were quantified in the WT, Δ*srrAB*, Δ*clpC*, and Δ*srrAB* Δ*clpC* strains.

A previous study found that a strain lacking ClpC, cultured to stationary phase, had altered transcript levels for genes encoding components of the electron transfer chain and oxidative phosphorylation (46). To allow comparisons with previous studies, our analyses were also conducted in stationary phase, following 48 h of growth. Two dimensional principal-component analysis (2D-PCA) and two-dimensional partial least squares discriminant (2D PLS-DA) multivariate statistical analyses demonstrated that the WT, Δ*srrAB,* Δ*clpC*, and Δ*srrAB* Δ*clpC* strains exhibit distinct metabolic profiles (Fig. 3A) (relative metabolite concentrations are listed in Table S1). Associated variable importance in projection (VIP) scores resulting from the 2D PLS-DA analysis highlighted the metabolites whose concentration changes contributed the most to the separation (VIP score 1.0) of the metabolic profiles of the four strains (Fig. 3B). Most notably, the mutant strains displayed higher levels of NAD than the WT (with NAD concentrations in the following order: Δ*clpC* Δ*srrAB* Δ*clpC* Δ*srrAB* WT). Other interesting metabolite pattern changes included higher levels of formate, niacinamide (Δ*clpC* Δ*srrAB* Δ*clpC* Δ*srrAB* WT), and ADP (Δ*clpC* Δ*srrAB* Δ*srrAB* Δ*clpC* WT) in the mutant strains than in the WT. In addition, GTP levels were lower in the Δ*clpC* and Δ*srrAB* Δ*clpC* mutants than in the WT.

We compared the metabolite profile of each strain to that of the WT. The 2D-PCA plot and heat map representation of metabolites whose levels were significantly altered between Δ*clpC* and WT are shown in Fig. 4. The 2D-PCA plot separates Δ*clpC* and WT primarily in the principal component 1 (PC1) dimension, where PC1 accounts for 60% of the variance and PC2 accounts for 22% of the variance (Fig. 4A). We found

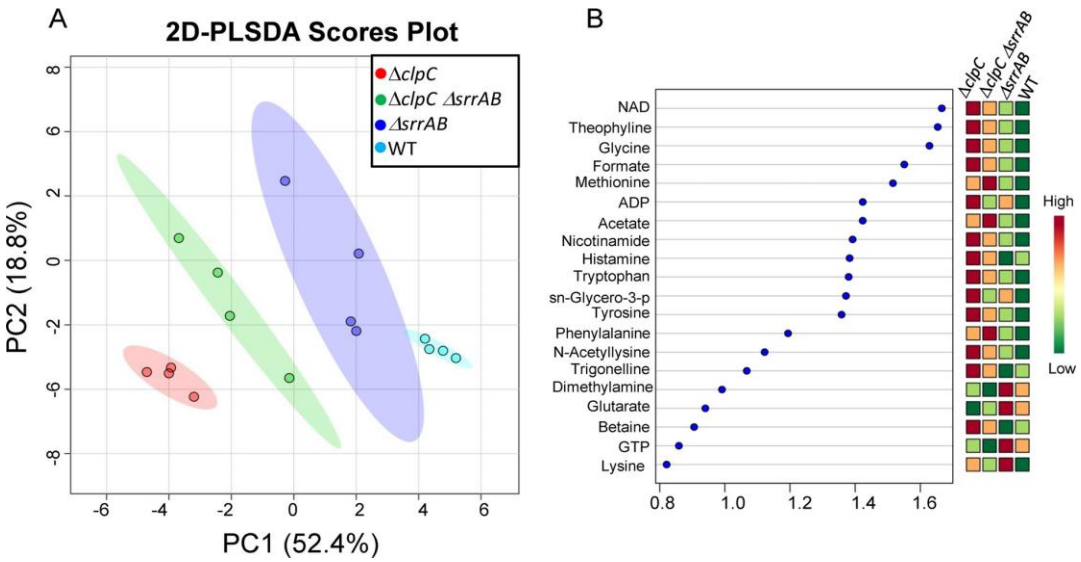

Figure 3. 2D partial least-square discriminant analysis (2D PLS-DA) score plot and associated VIP scores following aerobic growth for 48 h. (A) 2D PLS-DA score plot separating the WT (JMB 1100), Δ*srrAB* (JMB 1467), Δ*clpC* (JMB 8025), and Δ*srrAB* Δ*clpC* (JMB 8027) *S. aureus* strains according to their distinct metabolic profiles, with principal component 1 (PC1) and PC2 accounting for ~52% and ~19% of the variance, respectively. (B) Variable importance in projection (VIP) scores ranking the most important metabolites that contributed to the separation of the different strains in the 2D PLS-DA score plot. Metabolites with associated VIP scores of 1.0 were considered to be significant contributors to the separation between the metabolic profiles of the different strains. sn-Glycero-3-p, *sn*-glycero-3-phosphocholine.

that ADP, NAD, lactate, acetate, and formate levels were higher in the Δ*clpC* sample group (Fig. 4B), supporting the notion that the energy status of the Δ*clpC* strain is decreased. Levels of GTP and 2-oxo-glutarate were also lower in the Δ*clpC* strain. Taken together, these data suggest that the Δ*clpC* strain is, in all likelihood, exhibiting reduced oxidative phosphorylation and tricarboxylic acid (TCA) cycle activity.

Similarly, the metabolic profile of the Δ*srrAB* strain separates from that of WT in the 2D-PCA score plot, primarily in the PC1 dimension, with PC1 and PC2 accounting for 59% and 22%, respectively, of the variance (Fig. 5A). Similarly to the Δ*clpC* strain, the ADP, NAD, acetate, formate, and lactate levels were higher in the Δ*srrAB* strain (Fig.

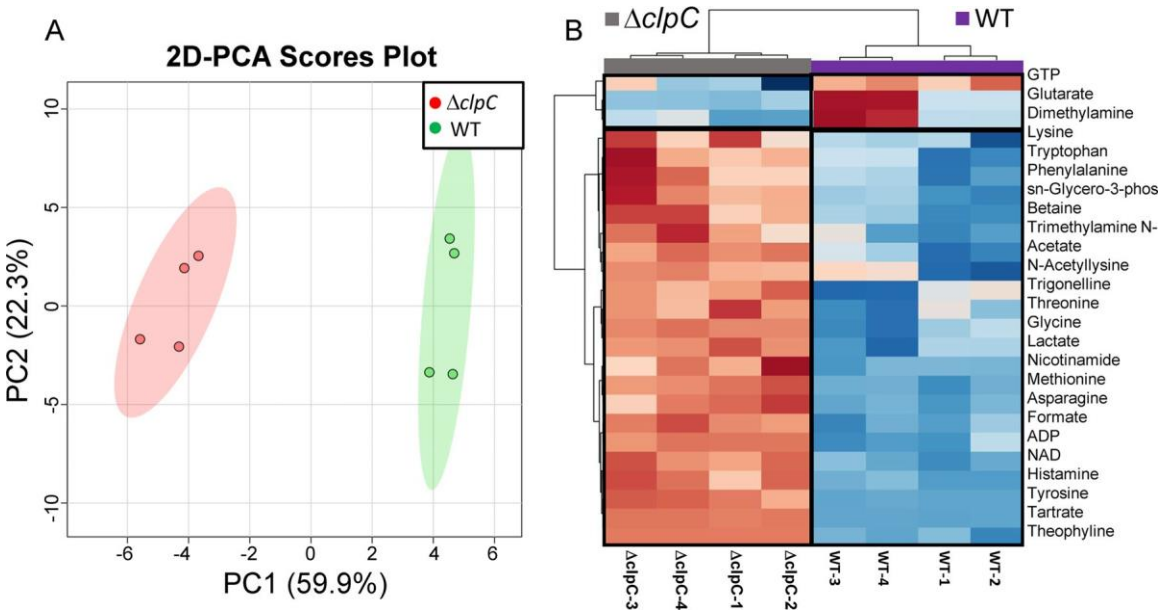

Figure 4. 2D-PCA score plot and corresponding hierarchical clustering analysis (HCA) of the metabolite profiles of Δ*clpC* and WT strains following aerobic growth for 48 h. (A) 2D-PCA score plot separating the Δ*clpC* (JMB 8025) and WT (JMB 1100) cell cultures and revealing that the two strains exhibit distinct metabolic profiles, with PC1 and PC2 accounting for 60% and 22% of the variance, respectively. (B) Heat map visualization of the top 25 metabolites that contributed most significantly to the metabolic profile separation of the Δ*clpC* mutant from the WT strain, based on Euclidean distance calculated from metabolite abundance and a Ward clustering algorithm. Boxed regions highlight metabolites whose levels were higher (red) or lower (blue) in the Δ*clpC* than in the WT groups, using a relative metabolite abundance scale of 2 (red) to 2 (blue). The HCA analysis indicates that, within these top 25 metabolites whose levels were significantly altered, a greater proportion of metabolites are found in higher levels in the Δ*clpC* mutant than in the WT. sn-Glycero-3-phos, *sn*-glycero-3-phosphocholine; Trimethylamine N-, trimethylamine *N*-oxide.

5B). Levels of AMP, UMP, succinate, and citrulline were also increased in the Δ*srrAB* strain. Importantly, metabolite abundance in the Δ*srrAB* Δ*clpC* strain was nonadditive with respect to the metabolite levels quantified for the individual Δ*srrAB* and Δ*clpC* mutations for 65% of the metabolites examined (25/39) (Table 1; see also Fig. S3). Notably, a number of the metabolites that displayed nonadditivity are crucial in the maintenance of cellular redox and energy homeostasis (for example, NAD, NADP, GTP,

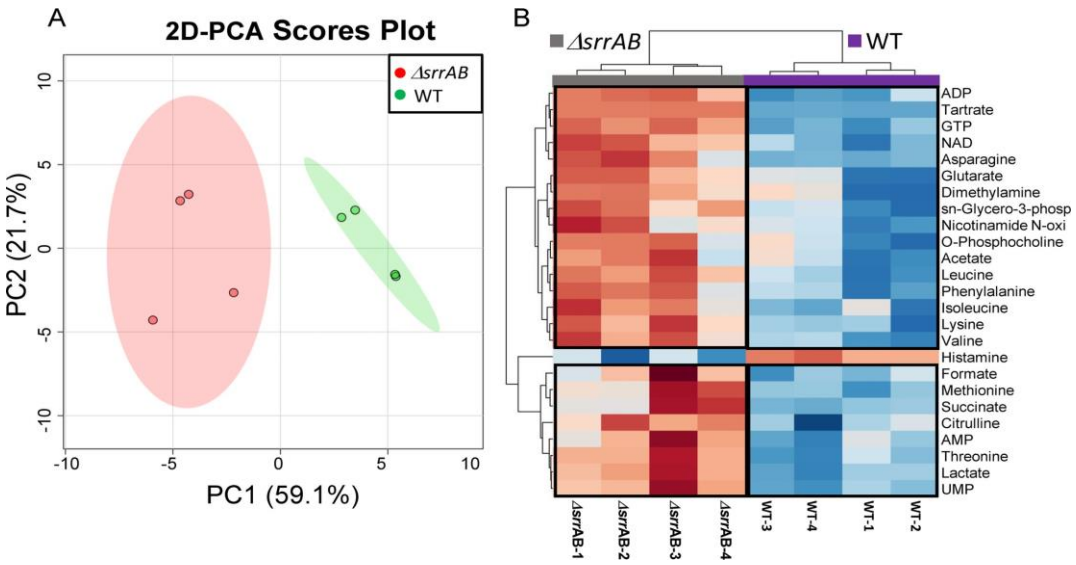

Figure 5. 2D-PCA score plot and hierarchical clustering analysis (HCA) of the metabolite profiles of the Δ*srrAB* and WT strains following aerobic growth for 48 h. (A) The 2D-PCA score plot separates the metabolic profile of Δ*srrAB* (JMB 1467) from that of WT (JMB 1100), with PC1 and PC2 accounting for 59% and 22% of the variance, respectively. (B) Heat map visualization of the top 25 metabolites whose level changes contributed the separation between the Δ*srrAB* and WT groups. Boxed regions indicate metabolites whose levels were higher (red) or lower (blue) when comparing the Δ*srrAB* and WT groups, using a relative metabolite abundance scale of 2 (red) to 2 (blue). Most of the metabolites contributing to the separation between the two groups were in higher relative abundance in the Δ*srrAB* strain than in the WT strain. sn-Glycero-3-phosp, *sn*-glycero-3-phosphocholine; Nicotinamide N-oxi, nicotinamide *N*-oxide.

and ADP). Consistent with the NMR analyses, the NAD/NADH ratios were significantly altered in strains lacking SrrAB or ClpC compared to that in the WT upon reexamination using a biochemical assay (Table 2). Moreover, the magnitude of change observed in the Δ*srrAB* Δ*clpC* double mutant strain was statistically indistinguishable from those in the single Δ*srrAB* strains. We do note that the metabolite level patterns were different between the Δ*srrAB*, Δ*clpC*, and the Δ*srrAB* Δ*clpC* strain mutants for 30% of the metabolites examined (Table S1). We conclude that while the Δ*clpC* and Δ*srrAB* mutations do not influence central metabolism in exactly the same way, it is likely that a

Table 1. Relative abundances of select metabolite levels for which the Δ*srrAB* and Δ*clpC* mutations are nonadditive.[a]

	clpC			*srrAB*			*srrAB clpC*		
Metabolite	FC		*P* value	FC		*P* value	FC		*P* value
Acetate	1.6	0.3	1.7E03	1.4	0.3	3.4E02	1.7	0.4	1.3E03
ADP	1.9	0.2	8.7E05	1.8	0.3	4.8E04	1.6	0.4	2.1E03
Asparagine	1.2	0.1	2.1E04	1.5	0.3	2.5E03	1.3	0.2	1.0E02
Citrulline	1.3	0.3	1.4E01	1.4	0.3	1.4E02	0.7	0.1	3.0E03
Formate	1.4	0.1	4.6E05	1.2	0.2	3.5E02	1.2	0.1	4.4E03
Glutarate	0.5	0.3	4.8E02	2.4	2.0	1.5E02	0.9	0.6	7.4E01
GTP	0.8	0.1	3.1E02	1.4	0.1	2.8E05	0.5	0.0	3.6E06
Lactate	1.3	0.1	7.3E04	1.5	0.3	1.6E03	1.2	0.3	2.0E01
Lysine	1.2	0.1	1.5E02	1.3	0.1	3.9E03	1.2	0.1	5.3E03
Methionine	1.9	0.2	6.5E06	1.4	0.2	1.1E02	2.0	0.4	2.7E03
NAD	1.9	0.2	2.1E05	1.3	0.2	1.4E03	1.9	0.2	4.2E04
NADP	1.2	0.3	3.4E01	1.1	0.3	4.9E01	1.0	0.2	8.5E01
N-Alpha-acetyllysine	1.7	0.6	3.6E02	1.2	1.0	5.8E01	1.4	1.1	1.9E01
Niacinamide	1.7	0.3	1.5E03	1.2	0.3	1.2E01	1.6	0.5	2.0E02
Nicotinamide *N*-oxide	1.2	0.1	1.7E01	1.6	0.7	2.9E02	1.2	0.3	2.0E01
O-Phosphocholine	1.2	0.3	1.7E01	1.5	0.5	3.0E02	1.6	0.5	1.1E02
Phenylalanine	1.3	0.1	6.4E03	1.3	0.2	6.3E03	1.3	0.2	5.2E03
sn-Glycero-3-phosphocholine	1.6	0.1	1.1E03	1.3	0.2	7.2E03	1.1	0.2	9.3E02
Succinate	0.9	0.0	2.6E01	2.1	0.9	1.7E02	1.2	0.5	3.3E01
Theophylline	7.5	0.7	2.5E06	1.4	0.6	3.5E01	7.0	1.9	3.2E06
Threonine	1.3	0.1	3.9E03	1.5	0.3	2.7E03	1.2	0.3	1.7E01
Trigonelline	1.9	0.7	1.5E02	1.1	1.3	8.9E01	1.5	1.1	1.1E01
Tryptophan	1.3	0.1	9.1E03	1.2	0.2	4.5E02	1.3	0.2	2.3E03
Tyrosine	1.4	0.1	5.9E06	1.2	0.2	3.6E02	1.3	0.2	2.3E02
UMP	1.1	0.1	1.1E01	1.5	0.3	2.7E03	0.9	0.2	1.5E01

[a]Data presented as fold changes (FC) and significance (*P* values) relative to the WT.

portion of the effect of SrrAB on metabolism is controlled via alterations in ClpC activity.

Table 2. NAD/NADH ratio after 48 h of growth.

Strain or genotype	NAD		NADH		NAD/NADH ratio[a]	
WT	17.02	1.75	0.23	0.12	99.0	15.3
Δ*clpC*	20.78	0.98	0.18	0.09	144.5	19.4[b]
Δ*srrAB*	20.86	1.13	0.34	0.02	61.0	3.5[b]
Δ*srrAB clpC*	22.06	1.35	0.46	0.20	56.2	6.0[b]

[a]Metabolite concentrations standardized to pmol per 10^8 bacteria before determining the ratios. [b]P 0.05 versus WT by Students *t* tests.

ClpCP is Required for Optimal Growth in a Medium that Only Supports Respiratory Growth

SrrAB regulates aerobic respiration, and the data presented suggested that a Δ*clpC* strain may be deficient in oxidative phosphorylation and tricarboxylic acid (TCA) cycle activity (35, 36). This prompted us to test the hypothesis that ClpC positively influences respiratory growth. We examined the growth profiles of strains in a medium that supports only respiratory growth. *S. aureus* is capable of utilizing glucose as well as glutamate as a source of carbon (47, 48). Glutamate feeds directly into the TCA cycle at the -ketoglutarate entry point, and we reasoned that glutamate would support respiratory growth almost exclusively. Defined medium containing glutamate as a carbon source (DFM-glutamate) did not support fermentative (anaerobic) growth but did support respiratory (aerobic) growth (Fig. 6A). Defined medium with glucose as a carbon source (DFM-glucose) supported both respiratory and fermentative growth (Fig. 6A). Heme is necessary for the function of *S. aureus* terminal oxidases, and consequently, a heme auxotroph is incapable of respiring. A *hemB*::Tn strain was capable of aerobic growth in DFM-glucose but not DFM-glutamate medium (Fig. 6B), leading to the conclusion that

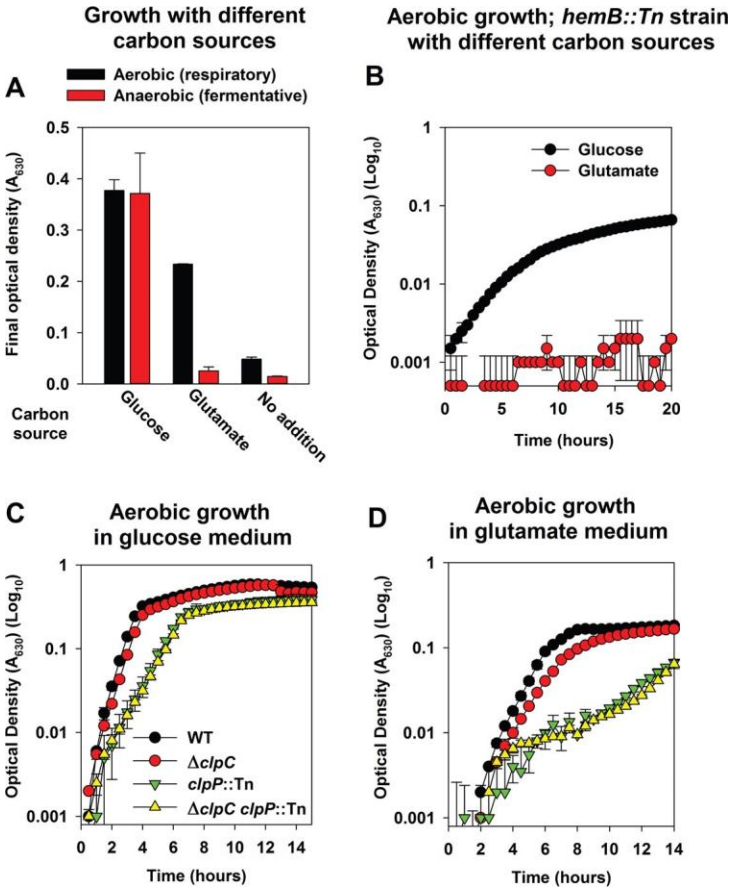

Figure 6. The ClpCP complex is required for optimal growth in a medium that only supports respiratory growth. (A) *S. aureus* can utilize glutamate as a source of carbon aerobically but not fermentatively. Final growth yields are displayed for the WT (JMB 1100) cultured in the presence or absence of oxygen (fermentative growth) and in defined minimal medium containing the canonical 20 amino acids and glucose (DFM-glucose) or glutamate (DFM-glutamate) as a carbon source or in the absence of a carbon source. (B) A heme auxotroph is unable to utilize glutamate as a carbon source during aerobic growth. Growth profiles are displayed for a *hemB*::Tn (JMB 6037) strain cultured aerobically in either DFM-glucose or DFM-glutamate. (C and D) A strain lacking ClpC or ClpCP is substantially attenuated for aerobic growth upon DFM-glutamate. Growth profiles are displayed for the WT, Δ*clpC* (JMB 8025), *clpP*::Tn (JMB 4898), and Δ*clpC clpP*::Tn (JMB 8029) strains cultured aerobically in either DFM-glucose (C) or DFM-glutamate (D). Data in all panels represent the averages from duplicate cultures and error bars represent standard deviations. Error bars are displayed for all points but may be too small to see on occasion.

DFM-glutamate supports only respiratory growth. The Δ*clpC* strain had a modest, but repeatable, growth defect in DFM-glutamate but not DFM-glucose medium (Fig. 6C and

D; black versus red circles).

ClpC can associate with a peptidase that forms a proteolytic complex. *S. aureus* harbors the ClpP and ClpQ peptidases. To understand which peptidase ClpC associates with to influence respiratory growth, the puromycin sensitivities of strains lacking ClpC, ClpP, or ClpQ were assessed. Concentrations of puromycin that attenuated growth of a Δ*clpC* strain also attenuated growth of a *clpP*::Tn strain, while the growth of a *clpQ*::Tn strain was unaffected (data not shown). This suggested that ClpC associates with ClpP; therefore, we conducted epistasis experiments to further understand the role of ClpP.

The growth of a Δ*clpC clpP*::Tn strain was examined relative to that of its parental strains in different media. The phenotypic effects of the Δ*clpC* and *clpP*::Tn mutations were nonadditive, and the Δ*clpC clpP*::Tn strain phenocopied the *clpP*::Tn strain in both DFM-glucose and DFM-glutamate media (Fig. 6C and D). The growth of the *clpP*::Tn strain was attenuated to a greater degree than for the Δ*clpC* strain in both media (Fig. 6C and D).

ClpP is Required for Optimal Fermentative Growth While ClpC is Dispensable

SrrAB positively influences fermentative growth (37). A previous study found that the transcription of *clpP* but not *clpC* is increased upon a shift to fermentative growth (49). In conjunction with the metabolomics data presented, we reasoned that ClpC was not required for fermentative growth and that SrrAB would not modulate *clpC* transcription during fermentative growth.

The transcript levels for *clpC* were examined in the WT and Δ*srrAB* strains

following fermentative growth. Transcript levels for *spa* and *cydB*, which are negatively and positively modulated by SrrAB, were assessed as controls (33, 35). Transcript levels were examined instead of transcriptional activity using the reporter constructs, since the folding of GFP is impaired in the absence of oxygen (50). Transcript levels for *spa* and *cydB* were increased and decreased, respectively, in the Δ*srrAB* strain (Fig. 7A). However, transcription of *clpC* was unaltered (Fig. 7A).

We examined whether ClpC, ClpP, or the ClpCP complex had a role during fermentative growth. Relative to that of the WT, the growth of the *clpP*::Tn strain was severely attenuated during fermentative culture (Fig. 7B). The Δ*clpC* strain was more proficient in fermentative growth than the WT and consistently formed bigger colonies (65% larger; relative sizes presented in Fig. S4, and representative image presented in Fig. 7B), suggesting ClpC limits fermentative growth. The phenotypic effects of the Δ*clpC* and *clpP*::Tn mutations were nonadditive (Fig. 7B).

The glycine at position 672 of ClpC is required for the interaction between ClpC and ClpP (51). The introduction of pEPSA5_*clpC* but not pEPSA5_*clpC*$_{G672R}$ inhibited fermentative growth of the WT strain (Fig. 7C). The WT strain carrying pEPSA5_*clpC* formed 100-fold fewer colonies that the WT carrying empty vector (Fig. 7C). The WT strain carrying pESPSA5_*clpC*$_{G672R}$ behaved similarly to the WT strain carrying empty vector (Fig. 7C). From Fig. 7, we concluded that ClpC is dispensable for fermentative growth, while ClpP is required. Further, dysregulation of ClpC levels during fermentative growth inhibits growth, which is likely due its interference with ClpP function(s).

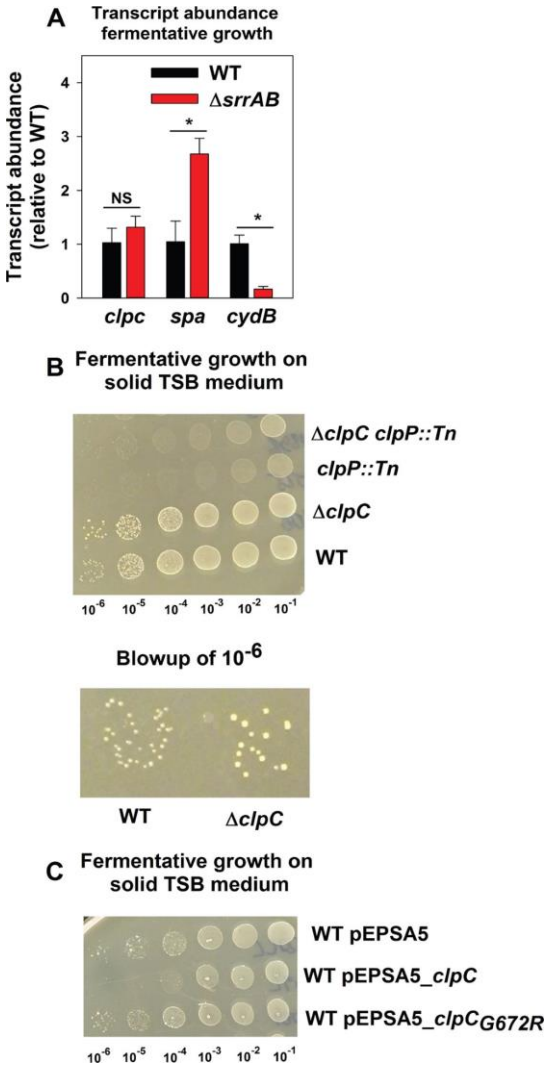

Figure 7. ClpP is required for optimal fermentative growth, while ClpC is dispensable. (A) SrrAB influences transcript levels for *spa* and *cydB* but not *clpC* during fermentative growth. The WT (JMB 1100) and Δ*srrAB* (JMB 1467) strains were cultured fermentatively, mRNA was extracted, and the abundances of the *clpC*, *spa*, and *cydB* transcripts were quantified. The data were normalized to 16S rRNA levels and thereafter to levels observed in the WT. (B) ClpP is required for optimal fermentative growth, while ClpC is dispensable. Fermentative growth is displayed for the WT, Δ*clpC* (JMB 8025), *clpP*::Tn (JMB 4898), and Δ*clpC clpP*::Tn (JMB 8029) strains on solid TSB medium. (C) Increased expression of *clpC* inhibits growth of fermenting *S. aureus*. Fermentative growth is displayed for the WT strain with pEPSA5 (empty vector), pEPSA5_*clpC*, or pEPSA5_$clpC_{G672R}$ on solid TSB medium. Data in panel A represent the averages from triplicate cultures and error bars represent standard deviations. Photographs in panels B and C are representative of at least three independent experiments, and the numbers beneath each photograph denote the serial dilution that cells were removed from before plating. Where indicated, Student *t* tests (two tailed) were performed on the data. *, *P* 0.05.

Discussion

Energy homeostasis is crucial for cellular physiology. SrrAB modulates aerobic respiration as well as fermentation in *S. aureus* (36, 37). Regulated proteolysis is involved in modulating respiratory metabolism in alternate organisms (18, 21); however, it is unclear whether a similar mechanism exists in *S. aureus*. We tested the hypothesis that the SrrAB TCRS links energy homeostasis and regulates proteolysis by modulating the levels of a factor involved in protein turnover. Our analyses using a combination of genetics and metabolomics lead us to propose a model wherein SrrAB affects puromycin resistance and energy homeostasis, at least in part, by modulating ClpC levels, which functions in protein turnover (Fig. 8). Consistent with our model, the growth of a Δ*srrAB* strain was deficient on media that impose a high demand for the cellular proteolytic machinery. Moreover, the transcriptional activity for *clpC* was decreased in a strain lacking SrrAB during respiratory growth, and overexpression of *clpC* suppressed the puromycin sensitivity phenotype of the *srrAB* mutant. We also note that early studies by Throup et al. (37) suggest that ClpC levels were altered in a *srrAB* mutant. One interpretation of this is that SrrAB regulates particular oxidative phosphorylation factors in a posttranslational manner. This idea would be consistent with our findings presented herein.

To understand whether SrrAB modulation of ClpC affects energy homeostasis, we conducted NMR-based metabolomics analyses. Our studies revealed that the Δ*srrAB* and Δ*clpC* mutations both result in altered concentrations of metabolites involved in balancing cellular redox and energy or of amino acids that serve as precursors for the

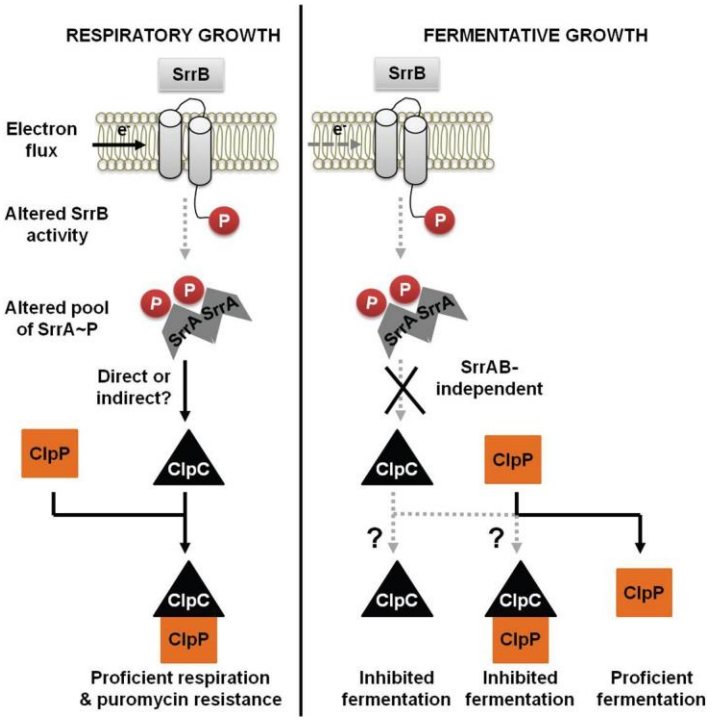

Figure 8. A working model for the influence of respiration upon SrrAB-dependent regulation of ClpC in *S. aureus*. Respiratory growth results in increased expression of *clpC* in an SrrAB-dependent manner. The increased ClpC leads to increased activity of the ClpCP proteolytic machinery and thereby facilitates proficient respiration and resistance toward protein misfolding stress. In contrast, during fermentative growth, SrrAB does not alter *clpC* expression and ClpP is necessary for proficient growth, while ClpC limits growth. Further experimentation is required to understand whether ClpC limits growth fermentatively solely upon association with ClpP or if it functions via an alternate mechanism.

TCA cycle. Importantly metabolite analyses in a Δ*srrAB* Δ*clpC* double mutant strain found that the effects of the Δ*clpC* and Δ*srrAB* mutations are not additive for 65% of the metabolites examined (25/39). A number of these metabolites serve as reporters of cellular energy status such as (ADP and NAD) and respiratory growth (acetate, formate, and lactate). Moreover, the growth of the Δ*clpC* strain was deficient on a medium that supported only respiratory growth. Taken together, these data are highly suggestive of a role for ClpC in directing energy metabolism. However, we do note that the Δ*srrAB*

Δ*clpC* double mutant strain did not completely phenocopy the Δ*clpC* and Δ*srrAB* single mutants. Thus, while our data are supportive of our hypothesis that SrrAB affects energy homeostasis via ClpC, we do not rule out the possibility that mutations in either gene could have direct or indirect (or both) effects on metabolism. Alternatively, the results could arise as an indirect consequence of altering regulated proteolysis, which subsequently results in global changes in the cell.

The growth conditions of our NMR-based metabolomics experiments were selected to allow comparisons with previous studies conducted on ClpC function using transcriptomics and proteomics. Chatterjee et al. found that a strain lacking ClpC had decreased transcript levels for genes encoding NADH dehydrogenases and 2-oxoglutarate ferredoxin oxidoreductase (46). They also found that the protein levels for the ATP synthase subunits were decreased in abundance in a *clpC* mutant (46). These data align well with our results indicating that a Δ*clpC* strain alters the NAD/ NADH ratio in the cell. A separate study found that a number of proteins that are involved in the synthesis of cofactors, which are essential for respiration, are substrates for ClpC (52). Prominent among these were SufCD, which are required to synthesize iron-sulfur (Fe-S) cofactors (52). *S. aureus* strains unable to properly process Fe-S proteins into their mature forms display global shifts in carbon flux and metabolic defects (47, 51, 53–55). Consistent with these studies, we found that a *clpC* mutant had deficient respiratory growth. ClpC acts either independently as a molecular chaperone or in conjunction with the ClpP peptidase. A *clpP*::Tn strain had attenuated growth on media supporting only respiratory growth, and the phenotypic effects of the Δ*clpC* and *clpP*::Tn mutations were not

additive. Thus, we concluded that the ClpCP proteolytic complex functions in directing respiratory metabolism. These findings are consistent with previous observations that several proteins involved in energy metabolism may be direct substrates of the ClpCP system (56).

We also examined the roles of ClpC, ClpP, and ClpCP during fermentative growth. ClpP was required for optimal growth during fermentative culture. Interestingly, the Δ*clpC* strain consistently formed bigger colonies than the WT strain when growing fermentatively but not aerobically. This suggested that the presence of ClpC limits fermentative growth. SrrAB did not affect *clpC* transcript levels during fermentative growth. Our metabolic profile analyses support this observation, as elevated levels of fermentative products/metabolites were measured in the Δ*clpC* mutant compared to that in the WT. These data are also consistent with previous findings that the transcription of *clpP* but not *clpC* is increased upon transition to fermentative growth (49).

Overexpression of *clpC* but not $clpC_{G627R}$ inhibited fermentative growth of the WT strain. Therefore, we propose that dysregulated levels of ClpC interfere with ClpP function and thereby limit fermentative growth. However, future experiments are necessary to uncover the precise mechanism by which overexpression of *clpC* decreases fermentative growth.

In summary, this study demonstrates that both SrrAB and ClpC affect energy metabolism. The data presented suggest that SrrAB influences energy metabolism, in part, by modulating ClpCP-directed regulated proteolysis. Metabolomics and physiological analyses establish that ClpCP is involved in altering aerobic respiratory

metabolism but is dispensable for fermentative growth.

Materials and Methods

Materials

Restriction enzymes, deoxynucleoside triphosphates, quick DNA ligase kit, and Phusion DNA polymerase were purchased from New England BioLabs. The plasmid miniprep kit, RNAprotect, and the gel extraction kit were purchased from Qiagen. Lysostaphin was purchased from Ambi Products. DNase I was purchased from Ambion. High-Capacity cDNA reverse transcription kits and TRIzol were purchased from Life Technologies. Oligonucleotides were purchased from Integrated DNA Technologies, and sequences are listed in Table S2 in the supplemental material. Tryptic soy broth (TSB) was purchased from MP Biomedicals. Unless specified, all chemicals were purchased from Sigma-Aldrich and were of the highest purity available.

Bacterial Growth Conditions

Unless specifically stated otherwise, the *S. aureus* strains used in this study (Table 3) were constructed in the community-associated USA300 strain LAC that was cured of the native plasmid pUSA03, which confers erythromycin resistance (57). *S. aureus* strains were cultured at 37°C. For aerobic growth in liquid, cultures were grown with shaking at 200 rpm at a flask/tube headspace-to-culture medium volume ratio of 10 (with the exception of analyses conducted in 96-well microtiter plates). Anaerobic growth was achieved by either incubation with a flask/tube headspace-to-culture medium volume ratio of 0, as described earlier (47, 53), or by incubation in a Coy anaerobic chamber

Table 3. Strains and plasmids used in this study.

Strain or plasmid	Genotype or description	Genetic background	Source and/or reference
Strains			
S. aureus			
JMB 1100	USA300_LAC (Erm sensitive), MRSA, USA300, CC8	LAC	57
JMB 1467	Δ*srrAB* (SAUSA300_1441-42)	LAC	62
JMB 2047	Δ*srrAB*::*tet*	LAC	35
JMB 1103	Restriction minus, MSSA, CC8	RN4220	63
JMB 1422	Parent, MSSA, CC8	Newman	64
JMB 4751	Δ*srrAB*::*tet*	Newman	This work
JMB 1324	Parent, MRSA, USA400, CC1	MW2	65
JMB 7573	Δ*srrAB*::*tet*	MW2	This work
JMB 7570	Parent, MRSA, USA100, CC5	N315	66
JMB 7574	Δ*srrAB*::*tet*	N315	This work
JMB 4898	*clpP*::Tn(*erm*)	LAC	BEI Resources, 67
JMB 8025	Δ*clpC*::*tet*	LAC	51
JMB 8027	Δ*srrAB* Δ*clpC*::*tet*	LAC	This work
JMB 8029	Δ*clpC*::*tet clpP*::Tn(*erm*)	LAC	This work
JMB 7714	*clpQ*::Tn(*erm*)	LAC	BEI Resources, 67
JMB 4850	*clpL*::Tn(*erm*)	LAC	BEI Resources, 67
JMB 6037	*hemB*::Tn(*erm*)	LAC	BEI Resources, 67
Escherichia coli PX5			Protein Express
Saccharomyces cerevisiae FY2			W. Belden
Plasmids			
pCM28	Insertless cloning vector, genetic complementation, multicopy		62
pCM11	Parent vector for construction of transcriptional reporter, multicopy		68
pCM11_P*clpC*	*clpC* transcriptional reporter		This work
pCM11_P*spa*	*spa* transcriptional reporter		This work
pCM28_*srrAB*	*srrAB* complementation, multicopy		35
pLL39	Insertless cloning vector, genetic complementation, episome		69
pLL39_*srrAB*	*srrAB* complementation, episome		40
pEPSA5	Cloning vector, genetic complementation, xylose-inducible promoter, multicopy		70
pEPSA5_*clpC*	*clpC* complementation, multicopy		51
pEPSA5_$clpC_{G672R}$	*clpC* complementation, multicopy		51

equipped with an oxygen-scavenging catalyst to maintain oxygen levels lower than 1

ppm. For culture in 96-well microtiter plates, each well contained 200 l total volume (detailed procedure below). Difco BioTek agar was added (15 g liter^{-1}) for solid medium. The staphylococcal defined medium recipe was as described previously and contained 10 mg ml^{-1} $(NH_4)_2SO_4$, 45 mg ml^{-1} KH_2PO_4, 105 mg ml^{-1} K_2HPO_4, 6.42 mg ml^{-1} NaCl, 2.23 mg ml^{-1} KCl, 0.5 g ml^{-1} nicotinic acid, 0.5 g ml^{-1} thiamine, 0.5 g ml^{-1} pantothenic acid, 3 ng ml^{-1} biotin, and 0.25 ng ml^{-1} of each individual amino acid (47, 53). All components were prepared using distilled and deionized water, but the water added to the medium was only deionized. Glutamate and glucose were added as carbon sources at 44 mM and 22 mM, respectively. When selecting for plasmids or episome insertions, antibiotics were added at the final following concentrations: 150 g ml^{-1} ampicillin, 30 g ml^{-1} chloramphenicol (Cm), 10 g ml^{-1} erythromycin (Erm), and 3 g ml^{-1} tetracycline (Tet). For routine plasmid maintenance, media were supplemented with 10 g ml^{-1} or 3.3 g ml^{-1} of chloramphenicol or erythromycin, respectively.

Liquid Growth Analysis. Strains were cultured overnight in TSB (18 h of growth) and subsequently inoculated in minimal medium to a final optical density (OD) of 0.02 (A_{600}) unit. For assessing nutritional requirements in chemically defined medium, the cell pellet was washed twice with phosphate-buffered saline (PBS) prior to inoculation to prevent carryover of rich medium components.

Puromycin sensitivities were examined in TSB medium, and the media were amended with antibiotic at the point of inoculation. The puromycin concentrations ranged between 0.5 and 10 g ml^{-1}. Aerobic growth was monitored using a BioTek 808E visible absorption spectrophotometer equipped with an incubator and set at medium shake speed.

For anaerobic growth, the microtiter plate was incubated in an air incubator inside a Coy anaerobic chamber. Where final optical densities are presented, growth was assessed after overnight growth (18 h).

Solid Growth Analyses. Strains were cultured overnight in TSB (18 h of growth). The strains were serial diluted using 1X PBS, and 5-l aliquots of the dilutions were spot plated on solid medium. Where mentioned, the TSB solid medium was amended with between 4.5 and 7 g ml^{-1} of puromycin. Plates were subsequently incubated at 37°C overnight before photographs were taken. Where mentioned, anaerobic growth was achieved by incubation in an air incubator inside a Coy anaerobic chamber.

Colony Size Analysis. Relative colony sizes were determined using the particle size tool in the ImageJ software. Sizes for at least ten colonies for each strain were determined.

Recombinant DNA and Genetic Techniques

Plasmids were passaged through RN4220 and subsequently transduced into the appropriate strains using bacteriophage 80 (58). Mutant strains and plasmids were verified using PCR or by sequencing PCR products or plasmids. DNA sequencing was performed at Genewiz (South Plainfield, NJ).

Creation of Plasmids and Mutant Strains

pCM11_*clpC* was created using the *clpC* hindIII and *clpC* kpnI primer pair. pCM11_*spa* was made using the *spa* Pro for HindIII and *spa* Pro Rev KpnI primer pair.

Digested PCR products were ligated into similar digested vectors.

Transcriptional Reporter Fusion Assay

Strains cultured overnight in liquid TSB-Erm medium were diluted in fresh liquid TSB-Erm medium to a final OD of 0.1 (A_{600}) and cultured with shaking. At periodic intervals, culture density and fluorescence were assessed as described previously (47, 53). Fluorescence data were normalized with respect to a strain not carrying a GFP-based transcriptional reporter to normalize for background fluorescence values. The resulting data were normalized to the culture OD. Finally, the data were normalized relative to the wild-type (WT) strain, or as specified in the figure legend.

RNA Extractions and
Real-Time Quantitative PCR

The abundances of RNAs were determined using a previously described cDNA library (35, 53). Briefly, cells were cultured in capped microcentrifuge tubes at a headspace-to-volume (H/V) ratio of 0. Anaerobic conditions were verified by the addition of resazurin to control tubes. Cultures were grown for 4.5 h. Thereafter, cells were treated with RNAprotect reagent, mRNA was obtained, cDNA libraries were constructed, and real-time quantitative PCR (RT-qPCR) was performed as described earlier (35, 53).

NMR Metabolomics

Bacterial Strains and Growth Conditions. Aerobic growth for all strains was assessed on four biological replicates for each cell group. Overnight cultures diluted 1:1,000 were used to inoculate 25 ml of fresh TSB in a 250-ml flask with 220-rpm

agitation at 37 °C. Aliquots of 10 ml were collected at 48 h, centrifuged at 5,000 rpm for 5 min, rinsed once with 1 ml of 1X PBS, and centrifuged at 5,000 rpm for 5 min. The supernatant was discarded, and cell pellets were frozen at -80 °C until further use. An additional 10 µl of the culture was utilized to determine the CFU, and 5 ml was utilized for NAD/NADH assays.

Polar Metabolite Extraction. Frozen cell pellets were resuspended in 1 ml of a 2:1 methanol:chloroform mixture and transferred to FastPrep lysis B matrix tubes (MP Biomedicals). Cells were lysed using the FastPrep-24 5^{G} instrument and designated *S. aureus* settings (2 cycles at a speed of 6.0 m/s for 40 s); 300 l of each layer of a 1:1 aqueous chloroform solution was added to each cell lysate. The tubes were vortexed, placed at 20°C for 20 min, and centrifuged at 14,000 *g* for 10 min. 800 l of the aqueous phase was transferred to microcentrifuge tubes and placed in a SpeedVac (no heat, manual run, volatile solvent) to dry overnight. Samples were resuspended in 600 l of NMR buffer (0.25 mM 4,4-dimethyl-4-silapentane-1-sulfonic acid [DSS], 0.4 mM imidazole, 25 mM phosphate buffer, 90% H_2O– 10% D_2O) and transferred to 5-mm Bruker NMR tubes.

NMR Experiments. 1D ^{1}H NMR spectra for each sample were obtained at 298 K on a Bruker 600-MHz (^{1}H Larmor frequency) AVANCE III solution NMR spectrometer, equipped with an automatic SampleJet sample loading system as well as a 5-mm triple resonance (^{1}H, ^{15}N, and ^{13}C) liquid helium cooled TCI probe (cryoprobe) and Topspin software (Bruker version 3.2). 1D ^{1}H experiments were performed using the “zgesgp”

Bruker pulse sequence with 256 scans, ^{1}H spectral window of 9,615.38 Hz. Free induction decays (FIDs) were collected in 32K data points, with a dwell time interval of 52 s amounting to an acquisition time of 1.7 s, and using an additional 1-s relaxation recovery delay between spectrum acquisitions. For each sample, the Topspin software (Bruker version 3.2) was used for phasing, baseline correction, and suppression of the water NMR signal using the baseline correction module "qfil" with a filter width (BCFW) of 0.2 ppm. Spectral analysis and metabolite identification and quantitation were performed using Chenomx software (version 8.0) (Chenomx Inc., Edmonton, AB, Canada) (59). For each NMR spectrum, the baseline was further corrected prior to metabolite identification and quantitation using the Chenomx small-molecule spectral database for 600-MHz (^{1}H Larmor frequency) magnetic field strength NMR spectrometers. NMR spectral patterns were fitted for each sample independently, and an internal DSS (0.25 mM) standard was used for metabolite quantitation. Metabolite concentrations were further normalized to viable cell counts (i.e., CFU). Metabolite identification (ID), when ambiguous due to partial ^{1}H NMR signal overlap, was further confirmed by recording 2D ^{1}H-^{1}H total correlation spectroscopy (TOCSY) NMR spectra or by spiking, when available, pure metabolite standards into samples. A total of 42 compounds were identified upon analysis of the 1D ^{1}H NMR spectra, and concentrations reported in millimolar were exported to Excel spreadsheets for further analysis using the MetaboAnalyst software (60).

Multivariate Data Analysis. Metabolite concentrations (in mM) for all four biological replicates obtained from the Chenomx software data analysis were normalized

to the total number of viable cells as determined by CFU, converted to attomoles/CFU, and saved as a CSV file. These data sets were analyzed, and metabolic profile trends between different sample groups were assessed using multivariate statistical analysis methods, including unsupervised 2D principal-component analysis (2D-PCA) and supervised 2D partial least-squares discriminant (2D PLS-DA) analyses using the multivariate statistical analysis modules of MetaboAnalyst (60). All metabolite concentration data sets were imported into MetaboAnalyst using log transformation and autoscaling settings. Log transformation was used to ensure Gaussian distribution of the data, and autoscaling was used for data scaling. This approach ensures that the variance from the more abundant metabolites does not dominate the variance covariance matrix of the multivariate statistical analysis and ensures that all changes from metabolites whose concentrations span several orders of magnitude contribute to the analysis, as described in reference 61.

Metabolic Pathway Analysis/VIP Scores. The most important metabolites contributing to the variance were ranked by 2D PLS-DA VIP (variable importance in projection) scores. Metabolites with VIP scores of 1.0 were considered the most significant contributors to the separation of the metabolic profiles of the different *S. aureus* sample groups, as shown in the 2D PLS-DA score plots. VIP scores resulting from the MetaboAnalyst data analysis are shown in Fig. 4B.

Data Interpretation and Analyses. Heat maps were generated using the Cluster Analysis module in MetaboAnalyst. Except for displaying the top 25 metabolites using

the *t* test/analysis of variance (ANOVA) setting, default settings were used (Euclidian distance measure and Ward clustering algorithm). During analyses, data were curated using the interquartile range (IQR) rule. The lower and upper outlier bounds were determined by 1.5 IQR subtraction from the first quartile and 1.5 IQR addition to the third quartile, respectively. Data values falling outside these bounds were omitted as outliers.

NAD/NADH Analysis

Total NAD and NADH concentrations were determined using 5-ml aliquots of cell culture and standard NAD/NADH enzymatic quantitation kits (BioVision, K337-100) according to the manufacturer's protocol and by normalizing resultant data to viable cell counts (i.e., CFU). After 48 h of culture, cells were washed with 1 PBS and lysed via 2 cycles of freeze/thaw in NADH/NAD extraction buffer. The resulting supernatant was split into two reactions for each sample, and one was used to measure the concentration of NADH present and the other to measure total NAD (NADt) corresponding to [NADH] [NAD]. NADH samples were heated to 60°C for 30 min to remove any NAD present. NADH and NADt samples were then loaded into 96-well plates, and NAD cycling enzyme mix was added. The reactions were allowed to incubate at room temperature for 5 min prior to the addition of developer mix, and the reactions were allowed to sit for 1 h prior to the measurement of optical density at 450 nm. Standard curves were generated using standards of 10 pmol/l NADH and NAD provided by the manufacturer. NAD/NADH concentration measurements were conducted on four biological replicates for each sample group.

Data Availability

We have deposited all the NMR metabolomics data and associated data processing files into the Metabolomics Workbench database under data accession number ST001174.

Supplemental Material

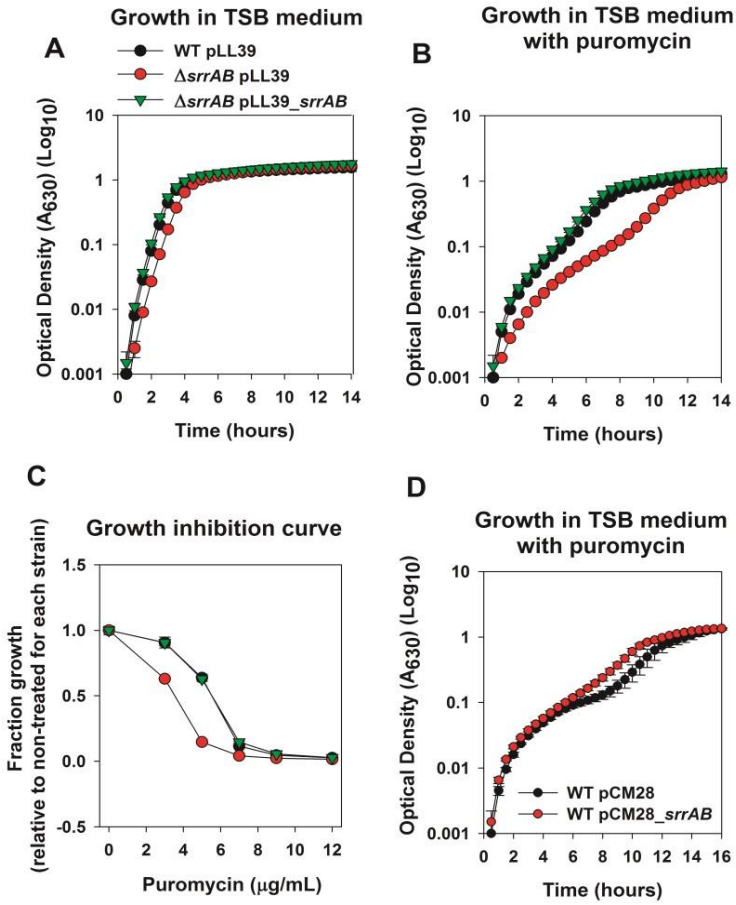

Figure S1. A Δ*srrAB* strain has increased sensitivity to puromycin. Panel A and B; A Δ*srrAB* strain is deficient in growth upon co-culture with puromycin. Growth profiles are presented for the WT (JMB1100) with the pLL39 episome (empty vector) and the Δ*srrAB* strain (JMB1467) with pLL39 or pLL39_*srrAB* in tryptic soy broth (TSB) medium in the absence (Panel A) or presence (Panel B) of puromycin. Panel C; The growth of a Δ*srrAB* strain is inhibited at lower concentrations of puromycin than the WT. The WT with pLL39 or the Δ*srrAB* strain with pLL39 or pLL39_*srrAB* was diluted into TSB containing varying amounts of puromycin. The strains were cultured for 5 hours and optical densities were recorded. Data are presented as fraction growth achieved relative to the non-treated control for each strain. Panel D; Increased dosage of *srrAB* improves the puromycin resistance of the WT strain. Growth profiles are presented for the WT carrying the multicopy vector pCM28 or pCM28_*srrAB* and diluted into TSB in the presence of puromycin. Data in Panels A-D represent the average of duplicate cultures and error bars represent standard deviations. Error bars are shown in all figures but may not be visible where error is low. Data in panel E are representative of at least three independent experiments.

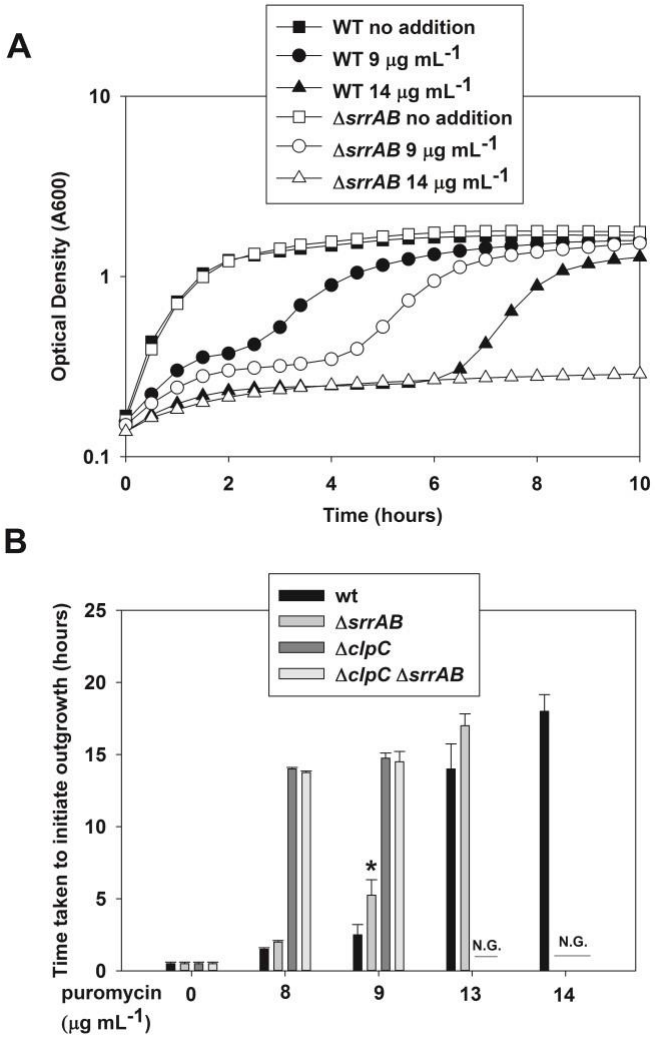

Figure S2. The puromycin sensitivity phenotypes associated with the Δ*srrAB* and Δ*clpC* mutation are not additive. Panel A; Representative growth profiles are displayed for the WT (JMB 1100) and Δ*srrAB* (JMB 1467) strains in TSB medium in the presence or absence of various concentrations of puromycin. Panel B; The time taken for strains to initiate outgrowth is plotted vs. the concentration of puromycin present in the TSB medium. The data in Panel B represents the average of triplicate cultures and error bars represent standard deviations. Students t-tests were conducted against the WT and * represents $p < 0.05$.

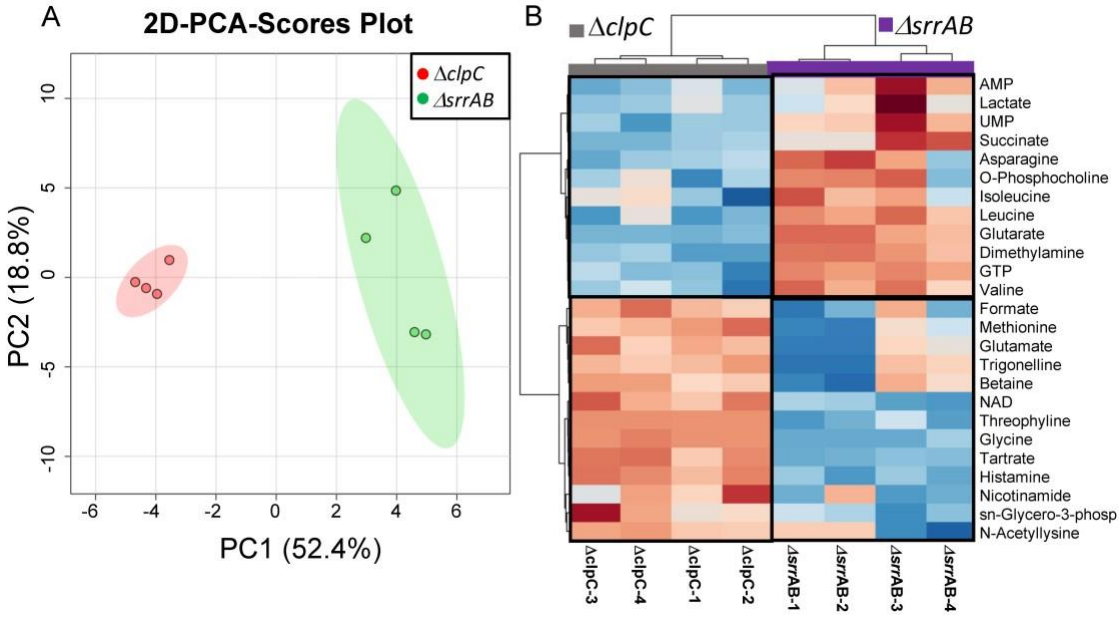

Figure S3. 2D PCA scores plot and corresponding hierarchical clustering analysis (HCA) of the metabolic profiles of Δ*clpC* and Δ*srrAB*, following aerobic growth for 48 hours. Panel A: 2D-PCA scores plot separating the metabolic profiles of Δ*clpC* (JMB 8025) and Δ*srrAB* (JMB 1467), with PC1 and PC 2 accounting for 52.4% and 18.8% of the variance, respectively. Panel B: Heatmap visualization of the top 25 metabolites contributing the most to the separation of the Δ*clpC* and Δ*srrAB* strains based of their distinct metabolite profiles, and indicating elevated levels of GTP, AMP, and lactate in Δ*srrAB* compared to Δ*clpC*. Levels of AMP, UMP, succinate, and citrulline are also increased in the Δ*srrAB* strain, indicating that the Δ*clpC* and Δ*srrAB* mutations are not affecting central metabolism in exactly the same way. Boxed regions indicate regions of higher (red) or lower (blue) metabolite levels between groups, with relative scale ranging from +2 (red) to -2 (blue); The heatmap also reveals that, within these top 25 metabolites whose levels are significantly altered between the two strains, a comparable distribution of increased or decreased metabolite levels is observed between Δ*clpC* and Δ*srrAB*.

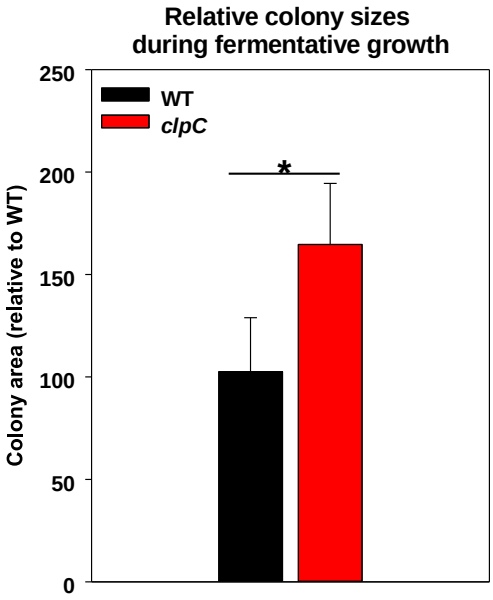

Figure S4. Quantification of colony size of the WT and Δ*clpC* strains after fermentative growth. Relative colony sizes of the WT (JMB1100) and Δ*clpC* (JMB 8025) strains were determined using the particle size tool in the ImageJ software. Sizes for at least ten colonies for each strain were determined.

Supplemental Table 1. Metabolite levels for the WT, Δ*srrAB*, Δ*clpC*, and Δ*srrAB* Δ*clpC* strains*

	WT	Δ*clpC*		Δ*srrAB*		Δ*srrAB* Δ*clpC*	
Metabolite	fc	fc	p.value	fc	p.value	fc	p.value
Acetate	1	1.6 ± 0.29	1.7E-03	1.4 ± 0.30	3.4E-02	1.7 ± 0.40	1.33E-03
ADP	1	1.9 ± 0.22	8.7E-05	1.8 ± 0.26	4.8E-04	1.6 ± 0.38	2.09E-03
AMP	1	1.0 ± 0.05	4.6E-01	1.2 ± 0.18	1.7E-02	0.8 ± 0.20	6.16E-02
Asparagine	1	1.2 ± 0.05	2.1E-04	1.5 ± 0.25	2.5E-03	1.3 ± 0.21	9.96E-03
Aspartate	1	0.9 ± 0.12	6.0E-01	1.1 ± 0.65	5.6E-01	1.3 ± 0.76	2.66E-01
Betaine	1	1.4 ± 0.04	1.4E-03	1.0 ± 0.30	7.8E-01	1.1 ± 0.14	5.57E-01
Citrulline	1	1.3 ± 0.33	1.4E-01	1.4 ± 0.30	1.4E-02	0.7 ± 0.14	3.00E-03
Dimethylamine	1	0.7 ± 0.14	8.9E-02	1.6 ± 0.81	3.4E-02	0.6 ± 0.40	8.57E-02
Formate	1	1.4 ± 0.10	4.6E-05	1.2 ± 0.19	3.5E-02	1.2 ± 0.09	4.44E-03
Glutamate	1	1.1 ± 0.13	2.2E-01	0.7 ± 0.23	6.2E-02	0.5 ± 0.05	9.55E-06
Glutarate	1	0.5 ± 0.25	4.8E-02	2.4 ± 1.99	1.5E-02	0.9 ± 0.59	7.39E-01
Glycine	1	2.5 ± 0.58	4.9E-04	1.0 ± 0.40	9.9E-01	2.0 ± 0.85	3.98E-03
GTP	1	0.8 ± 0.14	3.1E-02	1.4 ± 0.12	2.8E-05	0.5 ± 0.03	3.62E-06
Histamine	1	1.8 ± 0.17	1.0E-04	0.8 ± 0.10	5.6E-03	1.6 ± 0.23	2.03E-03
Histidine	1	1.0 ± 0.25	9.6E-01	1.2 ± 0.07	1.3E-01	1.4 ± 0.14	3.53E-03
Isoleucine	1	1.1 ± 0.14	2.9E-01	1.3 ± 0.10	8.8E-03	1.1 ± 0.12	6.39E-01
Lactate	1	1.3 ± 0.06	7.3E-04	1.5 ± 0.27	1.6E-03	1.2 ± 0.29	2.05E-01
Leucine	1	1.0 ± 0.14	7.3E-01	1.4 ± 0.18	2.1E-03	1.1 ± 0.25	5.20E-01
Lysine	1	1.2 ± 0.08	1.5E-02	1.3 ± 0.12	3.9E-03	1.2 ± 0.14	5.25E-03
Methionine	1	1.9 ± 0.18	6.5E-06	1.4 ± 0.21	1.1E-02	2.0 ± 0.43	2.69E-03
NAD	1	1.9 ± 0.07	2.1E-05	1.3 ± 0.17	1.4E-03	1.9 ± 0.20	4.22E-04
NADP	1	1.2 ± 0.26	3.4E-01	1.1 ± 0.27	4.9E-01	1.0 ± 0.22	8.50E-01
N-alpha-Acetyllysine	1	1.7 ± 0.62	3.6E-02	1.2 ± 1.04	5.8E-01	1.4 ± 1.11	1.91E-01
Niacinamide	1	1.7 ± 0.30	1.5E-03	1.2 ± 0.28	1.2E-01	1.6 ± 0.47	2.00E-02
Nicotinamide N-oxide	1	1.2 ± 0.09	1.7E-01	1.6 ± 0.7	2.9E-02	1.2 ± 0.33	1.96E-01
O-Phosphocholine	1	1.2 ± 0.28	1.7E-01	1.5 ± 0.49	3.0E-02	1.6 ± 0.49	1.11E-02
Phenylalanine	1	1.3 ± 0.06	6.4E-03	1.3 ± 0.19	6.3E-03	1.3 ± 0.23	5.21E-03
sn-Glycero-3-phosphocholine	1	1.6 ± 0.13	1.1E-03	1.3 ± 0.19	7.2E-03	1.1 ± 0.17	9.34E-02
Succinate	1	0.9 ± 0.03	2.6E-01	2.1 ± 0.95	1.7E-02	1.2 ± 0.45	3.32E-01
Tartrate	1	1.1 ± 0.01	4.8E-11	1.1 ± 0.01	6.8E-13	1.0 ± 0.01	7.74E-08
Theophylline	1	7.5 ± 0.72	2.5E-06	1.4 ± 0.62	3.5E-01	7.0 ± 1.85	3.16E-06
Threonine	1	1.3 ± 0.07	3.9E-03	1.5 ± 0.29	2.7E-03	1.2 ± 0.29	1.74E-01
Trigonelline	1	1.9 ± 0.69	1.5E-02	1.1 ± 1.26	8.9E-01	1.5 ± 1.07	1.09E-01
Trimethylamine N-oxide	1	1.2 ± 0.08	5.6E-03	0.9 ± 0.43	4.6E-01	0.9 ± 0.19	3.24E-01
Tryptophan	1	1.3 ± 0.11	9.1E-03	1.2 ± 0.15	4.5E-02	1.3 ± 0.16	2.32E-03
Tyrosine	1	1.4 ± 0.06	5.9E-06	1.2 ± 0.18	3.6E-02	1.3 ± 0.19	2.27E-02
UMP	1	1.1 ± 0.05	1.1E-01	1.5 ± 0.29	2.7E-03	0.9 ± 0.22	1.54E-01
Valine	1	0.9 ± 0.05	2.0E-01	1.2 ± 0.12	4.3E-03	1.0 ± 0.16	5.02E-01

Supplementary Table 2: Oligonucleotides used in this study.

RT- PCR primers

clpC For	CGTCGTTTCCAACCTGTACAAG
*clpC*Rev	TGGTGTGCTTCGTAACGATCTC
*spa*For	GATGGTAACGGAGTACATGTCGTT
spa Rev	GTGCCGTTTGCTTTTGCAAT
cydB For	GCCTTGGATTGTTCGTGGTT
*cydB*Rev	CCGCCTGCTTGTGTTGCT

Cloning primers

pCM28_IsceI_yeast For	AAAAACCTACAGAAGCTTGCATGCCTGCAAGTTACGCTAGGGATAACAGGGTAATATAG
srrB_pCM28 reverse	TGATTACGAATTCATGATCGAATGCTAGCGGATCTTTTATTCTGGTTTTGGTAGTTTA
spa (0113) Pro For HindIII	CCCAAGCTTTGTAGAATTCACAATTCTAGCTATTATCACTTCTCAAAAT
spa(0113) Pro Rev Kpn1	CCCGGTACCAATAAATGTTTT TCT TTT TCA AAT TAA TACCCCCTGTATG
clpC hindIII	CCCAAGCTTATTATATTATTGATGGGCTTTTAGATAAAATG
clpC kpnI	CCCGGTACCGTGGTGTCTTTCCAACGTGCTC

Acknowledgements

The Boyd lab is supported by the Charles and Johanna Busch foundation, USDA MRF project NE-1028, and grant 1R01AI139100-01 from the NIAID. A.A.M. was supported by the Douglas Eveleigh fellowship from the Microbial Biology Graduate Program and an Excellence Fellowship from Rutgers University. C.A.E. was supported by a Rutgers Aresty undergraduate research fellowship. The research in the Copié lab was supported by a grant from the Montana University System Research Initiative (51040-MUSRI2015-03). The NMR metabolomics studies were conducted on Montana State University s (MSU's) 600-MHz Bruker AVANCE III solution NMR spectrometer. Support for the NMR instruments, console upgrades, and MSU's NMR Center has been provided by the NIH Shared Instrumentation Grant (SIG) program (grant numbers 1S10RR13878 and 1S10RR026659), the NSF MRI program (NSF grant number DBI-

1532078), the Murdock Charitable Trust, and MSU's Vice President for Research Economic Development's office.

We thank William Belden for use of his real-time thermocycler.

References

1. Enright MC, Robinson DA, Randle G, Feil EJ, Grundmann H, Spratt BG.2002. The evolutionary history of methicillin-resistant *Staphylococcus aureus* (MRSA). Proc Natl Acad Sci U S A 99:7687–7692. https://doi.org/ 10.1073/pnas.122108599.

2. Graham PL, III, Lin SX, Larson EL. 2006. A U.S. population-based survey of *Staphylococcus aureus* colonization. Ann Intern Med 144:318–325. https://doi.org/10.7326/0003-4819-144-5-200603070-00006.

3. Ohara-Nemoto Y, Haraga H, Kimura S, Nemoto TK. 2008. Occurrence of staphylococci in the oral cavities of healthy adults and nasal oral trafficking of the bacteria. J Med Microbiol 57:95–99. https://doi.org/10 .1099/jmm.0.47561-0.

4. Zafar U, Johnson LB, Hanna M, Riederer K, Sharma M, Fakih MG, Thirumoorthi MC, Farjo R, Khatib R. 2007. Prevalence of nasal colonization among patients with community-associated methicillin-resistant *Staphylococcus aureus* infection and their household contacts. Infect Control Hosp Epidemiol 28:966–969. https://doi.org/10.1086/518965.

5. Klevens RM, Morrison MA, Nadle J, Petit S, Gershman K, Ray S, Harrison LH, Lynfield R, Dumyati G, Townes JM, Craig AS, Zell ER, Fosheim GE, McDougal LK, Carey RB, Fridkin SK. 2007. Invasive methicillin-resistant *Staphylococcus aureus* infections in the United States. JAMA 298: 1763–1771. https://doi.org/10.1001/jama.298.15.1763.

6. Tong SY, Davis JS, Eichenberger E, Holland TL, Fowler VG, Jr. 2015. *Staphylococcus aureus* infections: epidemiology, pathophysiology, clinical manifestations, and management. Clin Microbiol Rev 28:603–661. https://doi.org/10.1128/CMR.00134-14.

7. Williamson DA, Lim A, Thomas MG, Baker MG, Roberts SA, Fraser JD, Ritchie SR. 2013. Incidence, trends and demographics of *Staphylococcus aureus* infections in Auckland, New Zealand, 2001-2011. BMC Infect Dis 13:569. https://doi.org/10.1186/1471-2334-13-569.

8. Said-Salim B, Mathema B, Kreiswirth BN. 2003. Community-acquiredmethicillin-resistant *Staphylococcus aureus*: an emerging pathogen. Infect Control Hosp Epidemiol 24:451–455. https://doi.org/10.1086/ 502231.

9. Tenover FC, McDougal LK, Goering RV, Killgore G, Projan SJ, Patel JB, Dunman PM. 2006. Characterization of a strain of community-associated methicillin-resistant

Staphylococcus aureus widely disseminated in the United States. J Clin Microbiol 44:108–118. https://doi.org/10.1128/JCM .44.1.108-118.2006.

10. Mashruwala AA, Gries CM, Scherr TD, Kielian T, Boyd JM. 2017. SaeRS is responsive to cellular respiratory status and regulates fermentative biofilm formation in *Staphylococcus aureus*. Infect Immun 85:e00157-17. https://doi.org/10.1128/IAI.00157-17.

11. Arnold F, West D, Kumar S. 1987. Wound healing: the effect of macrophage and tumour derived angiogenesis factors on skin graft vascularization. Br J Exp Pathol 68:569–574.

12. Carreau A, El Hafny-Rahbi B, Matejuk A, Grillon C, Kieda C. 2011. Why isthe partial oxygen pressure of human tissues a crucial parameter? Small molecules and hypoxia. J Cell Mol Med 15:1239–1253. https://doi.org/ 10.1111/j.1582-4934.2011.01258.x.

13. Vogelberg KH, Konig M. 1993. Hypoxia of diabetic feet with abnormal arterial blood flow. Clin Investig 71:466–470.

14. Wilde AD, Snyder DJ, Putnam NE, Valentino MD, Hammer ND, Lonergan ZR, Hinger SA, Aysanoa EE, Blanchard C, Dunman PM, Wasserman GA, Chen J, Shopsin B, Gilmore MS, Skaar EP, Cassat JE. 2015. Bacterial hypoxic responses revealed as critical determinants of the host-pathogen outcome by TnSeq analysis of *Staphylococcus aureus* invasive infection. PLoS Pathog 11:e1005341. https://doi.org/ 10.1371/journal.ppat.1005341.

15. Hammer ND, Reniere ML, Cassat JE, Zhang Y, Hirsch AO, Indriati Hood M, Skaar EP. 2013. Two heme-dependent terminal oxidases power *Staphylococcus aureu*s organ-specific colonization of the vertebrate host. mBio 4:e00241-13. https://doi.org/10.1128/mBio.00241-13.

16. Vitko NP, Grosser MR, Khatri D, Lance TR, Richardson AR. 2016. Expanded glucose import capability affords *Staphylococcus aureus* optimized glycolytic flux during infection. mBio 7:e00296-16. https://doi.org/10.1128/ mBio.00296-16.

17. Richardson AR, Libby SJ, Fang FC. 2008. A nitric oxide-inducible lactate dehydrogenase enables *Staphylococcus aureus* to resist innate immunity. Science 319:1672–1676. https://doi.org/10.1126/science.1155207.

18. Gottesman S. 1999. Regulation by proteolysis: developmental switches. Curr Opin Microbiol 2:142–147. https://doi.org/10.1016/ S1369-5274(99)80025-3.

19. Frees D, Savijoki K, Varmanen P, Ingmer H. 2007. Clp ATPases and ClpP proteolytic complexes regulate vital biological processes in low GC, Gram-positive bacteria. Mol Microbiol 63:1285–1295. https://doi.org/10 .1111/j.1365-2958.2007.05598.x.

20. Michalik S, Liebeke M, Zuhlke D, Lalk M, Bernhardt J, Gerth U, HeckerM. 2009. Proteolysis during long-term glucose starvation in *Staphylococcus aureus* COL. Proteomics 9:4468–4477. https://doi.org/10 .1002/pmic.200900168.

21. van Dijl JM, Kutejova E, Suda K, Perecko D, Schatz G, Suzuki CK. 1998. The ATPase and protease domains of yeast mitochondrial Lon: roles in proteolysis and respiration-dependent growth. Proc Natl Acad Sci U S A 95:10584–10589. https://doi.org/10.1073/pnas.95.18.10584.

22. Suzuki CK, Suda K, Wang N, Schatz G. 1994. Requirement for the yeast gene LON in intramitochondrial proteolysis and maintenance of respiration. Science 264:891. https://doi.org/10.1126/science.8178144.

23. Frees D, Thomsen LE, Ingmer H. 2005. *Staphylococcus aureus* ClpYQ plays a minor role in stress survival. Arch Microbiol 183:286–291. https://doi .org/10.1007/s00203-005-0773-x.

24. Frees D, Qazi SN, Hill PJ, Ingmer H. 2003. Alternative roles of ClpX and ClpP in *Staphylococcus aureus* stress tolerance and virulence. Mol Microbiol 48:1565–1578. https://doi.org/10.1046/j.1365-2958.2003.03524.x.

25. Kim YI, Levchenko I, Fraczkowska K, Woodruff RV, Sauer RT, Baker TA. 2001. Molecular determinants of complex formation between Clp/ Hsp100 ATPases and the ClpP peptidase. Nat Struct Biol 8:230–233. https://doi.org/10.1038/84967.

26. Singh SK, Rozycki J, Ortega J, Ishikawa T, Lo J, Steven AC, Maurizi MR. 2001. Functional domains of the ClpA and ClpX molecular chaperones identified by limited proteolysis and deletion analysis. J Biol Chem 276:29420–29429. https://doi.org/10.1074/jbc.M103489200.

27. Gohring N, Fedtke I, Xia G, Jorge AM, Pinho MG, Bertsche U, Peschel A. 2011. New role of the disulfide stress effector YjbH in beta-lactam susceptibility of *Staphylococcus aureus*. Antimicrob Agents Chemother 55:5452–5458. https://doi.org/10.1128/AAC.00286-11.

28. Jousselin A, Kelley WL, Barras C, Lew DP, Renzoni A. 2013. The *Staphylococcus aureus* thiol/oxidative stress global regulator Spx controls *trfA*, a gene implicated in cell wall antibiotic resistance. Antimicrob Agents Chemother 57:3283–3292. https://doi.org/10.1128/AAC.00220-13.

29. Elsholz AK, Hempel K, Michalik S, Gronau K, Becher D, Hecker M, Gerth U. 2011. Activity control of the ClpC adaptor McsB in *Bacillus subtilis*. J Bacteriol 193:3887–3893. https://doi.org/10.1128/JB.00079-11.

30. Donegan NP, Marvin JS, Cheung AL. 2014. Role of adaptor TrfA and ClpPC in controlling levels of SsrA-tagged proteins and antitoxins in *Staphylococcus aureus*. J Bacteriol 196:4140–4151. https://doi.org/10 .1128/JB.02222-14.

31. Stock AM, Robinson VL, Goudreau PN. 2000. Two-component signal transduction. Annu Rev Biochem 69:183–215. https://doi.org/10.1146/ annurev.biochem.69.1.183.

32. Pragman AA, Ji Y, Schlievert PM. 2007. Repression of *Staphylococcus aureus* SrrAB using inducible antisense *srrA* alters growth and virulence factor transcript levels. Biochemistry 46:314–321. https://doi .org/10.1021/bi0603266.

33. Pragman AA, Yarwood JM, Tripp TJ, Schlievert PM. 2004. Characterization of virulence factor regulation by SrrAB, a two-component system in *Staphylococcus aureus*. J Bacteriol 186:2430–2438. https://doi.org/10 .1128/jb.186.8.2430-2438.2004.

34. Yarwood JM, McCormick JK, Schlievert PM. 2001. Identification of a novel two-component regulatory system that acts in global regulation of virulence factors of *Staphylococcus aureus*. J Bacteriol 183:1113–1123. https://doi.org/10.1128/JB.183.4.1113-1123.2001.

35. Mashruwala AA, Boyd JM. 2017. The *Staphylococcus aureus* SrrAB regulatory system modulates hydrogen peroxide resistance factors, which imparts protection to aconitase during aerobic growth. PLoS One 12: e0170283. https://doi.org/10.1371/journal.pone.0170283.

36. Kinkel TL, Roux CM, Dunman PM, Fang FC. 2013. The *Staphylococcus aureus* SrrAB two-component system promotes resistance to nitrosative stress and hypoxia. mBio 4:e00696-13. https://doi.org/10.1128/ mBio.00696-13.

37. Throup JP, Zappacosta F, Lunsford RD, Annan RS, Carr SA, Lonsdale JT, Bryant AP, McDevitt D, Rosenberg M, Burnham MK. 2001. The srhSR gene pair from *Staphylococcus aureus*: genomic and proteomic approaches to the identification and characterization of gene function. Biochemistry 40:10392–10401. https://doi.org/10.1021/bi0102959.

38. Joo HS, Otto M. 2012. Molecular basis of *in vivo* biofilm formation by bacterial pathogens. Chem Biol 19:1503–1513. https://doi.org/10.1016/j .chembiol.2012.10.022.

39. Otto M. 2008. Staphylococcal biofilms. Curr Top Microbiol Immunol 322:207–228.

40. Mashruwala AA, Van De Guchte A, Boyd JM. 2017. Impaired respiration elicits SrrAB-dependent programmed cell lysis and biofilm formation in *Staphylococcus aureus*. Elife 6:e23845. https://doi.org/10 .7554/eLife.23845.

41. Richardson AR, Dunman PM, Fang FC. 2006. The nitrosative stressresponse of *Staphylococcus aureus* is required for resistance to innate immunity. Mol Microbiol 61:927–939. https://doi.org/10.1111/j.1365 -2958.2006.05290.x.

42. Bose JL, Daly SM, Hall PR, Bayles KW. 2014. Identification of the *Staphylococcus aureus vfrAB* operon, a novel virulence factor regulatory locus. Infect Immun 82:1813–1822. https://doi.org/10.1128/IAI.01655-13.

43. Herbert S, Ziebandt AK, Ohlsen K, Schafer T, Hecker M, Albrecht D, Novick R, Gotz F. 2010. Repair of global regulators in *Staphylococcus aureus* 8325 and comparative analysis with other clinical isolates. Infect Immun 78:2877–2889. https://doi.org/10.1128/IAI.00088-10.

44. Memmi G, Nair DR, Cheung A. 2012. Role of ArlRS in autolysis in methicillin-sensitive and methicillin-resistant *Staphylococcus aureus* strains. J Bacteriol 194:759–767. https://doi.org/10.1128/JB.06261-11.

45. Mainiero M, Goerke C, Geiger T, Gonser C, Herbert S, Wolz C. 2010. Differential target gene activation by the *Staphylococcus aureus* twocomponent system SaeRS. J Bacteriol 192:613–623. https://doi.org/10 .1128/JB.01242-09.

46. Chatterjee I, Schmitt S, Batzilla CF, Engelmann S, Keller A, Ring MW, Kautenburger R, Ziebuhr W, Hecker M, Preissner KT, Bischoff M, Proctor RA, Beck HP, Lenhof HP, Somerville GA, Herrmann M. 2009. *Staphylococcus aureus* ClpC ATPase is a late growth phase effector of metabolism and persistence. Proteomics 9:1152–1176. https://doi.org/10.1002/pmic .200800586.

47. Mashruwala AA, Bhatt S, Poudel S, Boyd ES, Boyd JM. 2016. The DUF59 containing protein SufT is involved in the maturation of iron-sulfur (FeS) proteins during conditions of high FeS cofactor demand in *Staphylococcus aureus*. PLoS Genet 12:e1006233. https://doi.org/10.1371/journal .pgen.1006233.

48. Miller RD, Fung DY. 1973. Amino acid requirements for the production of enterotoxin B by *Staphylococcus aureus* S-6 in a chemically defined medium. Appl Microbiol 25:800–806.

49. Fuchs S, Pane-Farre J, Kohler C, Hecker M, Engelmann S. 2007. Anaerobicgene expression in *Staphylococcus aureus*. J Bacteriol 189:4275–4289. https://doi.org/10.1128/JB.00081-07.

50. Cubitt AB, Heim R, Adams SR, Boyd AE, Gross LA, Tsien RY. 1995. Understanding, improving and using green fluorescent proteins. Trends Biochem Sci 20:448–455. https://doi.org/10.1016/S0968-0004(00)89099-4.

51. Mashruwala AA, Roberts CA, Bhatt S, May KL, Carroll RK, Shaw LN, Boyd JM. 2016. *Staphylococcus aureus* SufT: an essential iron-sulphur cluster assembly factor in cells experiencing a high-demand for lipoic acid. Mol Microbiol 102:1099–1119. https://doi.org/10.1111/mmi.13539.

52. Graham JW, Lei MG, Lee CY. 2013. Trapping and identification of cellular substrates of the *Staphylococcus aureus* ClpC chaperone. J Bacteriol 195:4506–4516. https://doi.org/10.1128/JB.00758-13.

53. Mashruwala AA, Pang YY, Rosario-Cruz Z, Chahal HK, Benson MA, Mike LA, Skaar EP, Torres VJ, Nauseef WM, Boyd JM. 2015. Nfu facilitates the maturation of iron-sulfur proteins and participates in virulence in *Staphylococcus aureus*. Mol Microbiol 95:383–409. https://doi.org/10.1111/ mmi.12860.

54. Roberts CA, Al-Tameemi HM, Mashruwala AA, Rosario-Cruz Z, Chauhan U, Sause WE, Torres VJ, Belden WJ, Boyd JM. 2017. The Suf iron-sulfur cluster biosynthetic system is essential in *Staphylococcus aureus*, and decreased Suf function results in global metabolic defects and reduced survival in human neutrophils. Infect Immun 85:e00100-17. https://doi .org/10.1128/IAI.00100-17.

55. Rosario-Cruz Z, Boyd JM. 2016. Physiological roles of bacillithiol in intracellular metal processing. Curr Genet 62:59–65. https://doi.org/10 .1007/s00294-015-0511-0.

56. Feng J, Michalik S, Varming AN, Andersen JH, Albrecht D, Jelsbak L, Krieger S, Ohlsen K, Hecker M, Gerth U, Ingmer H, Frees D. 2013. Trapping and proteomic identification of cellular substrates of the ClpP protease in *Staphylococcus aureus*. J Proteome Res 12:547–558. https:// doi.org/10.1021/pr300394r.

57. Boles BR, Thoendel M, Roth AJ, Horswill AR. 2010. Identification ofgenes involved in polysaccharide-independent *Staphylococcus aureus* biofilm formation. PLoS One 5:e10146. https://doi.org/10.1371/ journal.pone.0010146.

58. Novick RP. 1991. Genetic systems in staphylococci. Methods Enzymol 204:587–636. https://doi.org/10.1016/0076-6879(91)04029-N.

59. Mercier P, Lewis MJ, Chang D, Baker D, Wishart DS. 2011. Towards automatic metabolomic profiling of high-resolution one-dimensional proton NMR spectra. J Biomol NMR 49:307–323. https://doi.org/10.1007/ s10858-011-9480-x.

60. Xia J, Wishart DS. 2011. Web-based inference of biological patterns, functions and pathways from metabolomic data using MetaboAnalyst. Nat Protoc 6:743–760. https://doi.org/10.1038/nprot.2011.319.

61. Xia J, Wishart DS. 2016. Using MetaboAnalyst 3.0 for comprehensive metabolomics data analysis. Curr Protoc Bioinformatics 55: 14.10.1–14.10.91. https://doi.org/10.1002/cpbi.11.

62. Pang YY, Schwartz J, Bloomberg S, Boyd JM, Horswill AR, Nauseef WM. 2014. Methionine sulfoxide reductases protect against oxidative stress in *Staphylococcus aureus* encountering exogenous oxidants and human neutrophils. J Innate Immun 6:353–364. https://doi.org/10.1159/000355915.

63. Kreiswirth BN, Lofdahl S, Betley MJ, O'Reilly M, Schlievert PM, Bergdoll MS, Novick RP. 1983. The toxic shock syndrome exotoxin structural gene is not detectably transmitted by a prophage. Nature 305:709–712. https://doi.org/10.1038/305709a0.

64. Duthie ES, Lorenz LL. 1952. Staphylococcal coagulase; mode of action and antigenicity. J Gen Microbiol 6:95–107. https://doi.org/10.1099/ 00221287-6-1-2-95.

65. Anonymous. 1999. From the Centers for Disease Control and Prevention. Four pediatric deaths from community-acquired methicillin-resistant *Staphylococcus aureus*—Minnesota and North Dakota, 1997-1999. JAMA 282:1123–1125.

66. Kuroda M, Ohta T, Uchiyama I, Baba T, Yuzawa H, Kobayashi I, Cui L,Oguchi A, Aoki K, Nagai Y, Lian J, Ito T, Kanamori M, Matsumaru H, Maruyama A, Murakami H, Hosoyama A, Mizutani-Ui Y, Takahashi NK, Sawano T, Inoue R, Kaito C, Sekimizu K, Hirakawa H, Kuhara S, Goto S, Yabuzaki J, Kanehisa M, Yamashita A, Oshima K, Furuya K, Yoshino C, Shiba T, Hattori M, Ogasawara N, Hayashi H, Hiramatsu K. 2001. Whole genome sequencing of methicillin-resistant *Staphylococcus aureus*. Lancet 357:1225–1240. https://doi.org/10.1016/S0140-6736(00)04403-2.

67. Fey PD, Endres JL, Yajjala VK, Widhelm TJ, Boissy RJ, Bose JL, Bayles KW. 2013. A genetic resource for rapid and comprehensive phenotype screening of nonessential *Staphylococcus aureus* genes. mBio 4:e00537. https://doi.org/10.1128/mBio.00537-12.

68. Malone CL, Boles BR, Lauderdale KJ, Thoendel M, Kavanaugh JS, HorswillAR. 2009. Fluorescent reporters for *Staphylococcus aureus*. J Microbiol Methods 77:251–260. https://doi.org/10.1016/j.mimet.2009.02.011.

69. Luong TT, Lee CY. 2007. Improved single-copy integration vectors for *Staphylococcus aureus*. J Microbiol Methods 70:186–190. https://doi.org/10.1016/j.mimet.2007.04.007.

70. Forsyth RA, Haselbeck RJ, Ohlsen KL, Yamamoto RT, Xu H, Trawick JD, WallD, Wang LS, Brown-Driver V, Froelich JM, Kedar GC, King P, McCarthy M, Malone C, Misiner B, Robbins D, Tan ZH, Zhu ZY, Carr G, Mosca DA, Zamudio C, Foulkes JG, Zyskind JW. 2002. A genome-wide strategy for the identification of essential genes in *Staphylococcus aureus*. Mol Microbiol 43: 1387–1400. https://doi.org/10.1046/j.1365-2958.2002.02832.x.

REFERENCES CITED

Abel U, Koch C, Speitling M, Hansske FG. Modern methods to produce natural-product libraries. Curr Opin Chem Biol. 2002; 6(4): 453-458.

Abidi SH, Sherwani SK, Siddiqui TR, Bashir A, Kazmi SU. Drug resistance profile and biofilm forming potential of *Pseudomonas aeruginosa* isolated from contact lenses in Karachi-Pakistan. BMC Ophthalmology. 2013; 13: 57.

Aderem A. Phagocytosis and the inflammatory response. J Infect Dis. 2003; 187(Suppl. 2): S340-5.

Alhede M, Bjarnsholt T, Givskov M, Alhede M. *Pseudomonas aeruginosa* biofilms: mechanisms of immune evasion. Adv Appl Microbiol. 2014; 86: 1-40.

Alhede M, Bjarnsholt T, Jensen PØ, Phipps RK, Moser C, Christophersen L, et al. *Pseudomonas aeruginosa* recognizes and responds aggressively to the presence of polymorphonuclear leukocytes. Microbiology. 2009; 155(Pt 11): 3500-8.

Ammons MCB, Tripet BP, Carlson RP, Kirker KR, Gross MA, Stanisich JJ, et al. Quantitative NMR metabolite profiling of methicillin-resistant and methicillin-susceptible *Staphylococcus aureus* discriminates between biofilm and planktonic phenotypes. J Proteome Res. 2014; 13(6): 2973-2985.

Anonymous. From the Centers for Disease Control and Prevention. Four pediatric deaths from community-acquired methicillin-resistant *Staphylococcus aureus*— Minnesota and North Dakota, 1997-1999. JAMA. 1999; 282: 1123-1125.

Araníbar N, Ott KH, Roongta V, Mueller L. Metabolomic analysis using optimized NMR and statistical methods. Anal Biochem. 2006; 355: 62-70.

Arnold F, West D, Kumar S. Wound healing: the effect of macrophage and tumour derived angiogenesis factors on skin graft vascularization. Br J Exp Pathol. 1987; 68: 569-574.

Arts RJ, Novakovic B, Ter Horst R, Carvalho A, Bekkering S, Lachmandas E, et al. Glutaminolysis and fumarate accumulation integrate immunometabolic and epigenetic programs in trained immunity. Cell Metab. 2016; 24(6): 807-819.

Atanasov AG, Waltenberger B, Pferschy-Wenzig E, Linder T, Wawrosch C, Uhrin P, et al. Discovery and resupply of pharmacologically active plant-derived natural products: a review. Biotechnol Adv. 2015; 33(8): 1582-1614.

Barrera NP, Morales B, Torres S, Villalón M. Principles: mechanisms and modeling of synergism in cellular responses. Trends Pharmacol Sci. 2005; 26(10): 526-532.

Baum CL, Arpey CJ. Normal cutaneous would healing: clinical correction with cellular and molecular events. Dermatol Surg. 2005; 31(6): 674-86; discussion 686.

Bax A. Multidimensional nuclear magnetic resonance methods for protein studies. Curr Opin Struct Biol. 1994; 4(5): 738-744.

Beckonert O, Keun HC, Ebbels TM, Bundy J, Holmes E, Lindon JC, et al. Metabolic profiling, metabolomic and metabonomic procedures for NMR spectroscopy of urine, plasma, serum and tissue extracts. Nat Protoc. 2007; 2(11): 2692-703.

Bingol K, Brüschweiler R. Multidimensional approaches to NMR-based metabolomics. Anal Chem. 2014; 86(1): 47-57.

Birungi G, Chen SM, Loy BP, Ng ML, Li SF. Metabolomics approach for investigation of effects of dengue virus infection using the EA.hy926 cell line. J Proteome Res. 2010; 9(12): 6523-34.

Biswas SK, Chittezhath M, Shalova IN, Lim JY. Macrophage polarization and plasticity in health and disease. Immunol Res. 2012; 53(1-3): 11-24.

Biswas SK, Mantovani A. Macrophage plasticity and interaction with lymphocyte subsets: cancer as a paradigm. Nat Immunol. 2010; 11(10): 889-96.

Bjarnsholt T, Jensen PØ, Fiandaca MJ, Pedersen J, Hansen CR, Andersen CB, et al. *Pseudomonas aeruginosa* biofilms in the respiratory tract of cystic fibrosis patients. Pediatr Pulmonol. 2009; 44(6): 547-58.

Blakytny R, Jude E. The molecular biology of chronic wounds and delayed healing in diabetes. Diabet Med. 2006; 23(6): 594-608.

Boles BR, Thoendel M, Roth AJ, Horswill AR. Identification ofgenes involved in polysaccharide-independent *Staphylococcus aureus* biofilm formation. PLoS One. 2010; 5: e10146.

Bolten CJ, Kiefer P, Letisse F, Portais J, Wittmann C. Sampling for metabolome analysis of microorganisms. Anal Chem. 2007; 79: 3843-3849.

Borlinghaus J, Albrecht F, Gruhlke MCH, Nwachukwu ID, Slusarenko AJ. Allicin: chemistry and biological properties. Molecules. 2014; 19(8): 12591-12618.

Bose JL, Daly SM, Hall PR, Bayles KW. Identification of the *Staphylococcus aureus vfrAB* operon, a novel virulence factor regulatory locus. Infect Immun. 2014; 82: 1813-1822.

Bowles LK, Ellefson WL. Effects of butanol on *Clostridium acetobutylicum*. Appl Environ Microbiol. 1985; 50(5): v1165-1170.

Braidy N, Grant R, Adams S, Brew BJ, Guillemin GJ. Mechanism for quinolinic acid cytotoxicity in human astrocytes and neurons. Neurotox Res. 2009; 16: 77-86.

Brindle JT, Nicholson JK, Schofield PM, Grainger DJ, Holmes E. Application of chemometrics to ^{1}H NMR spectroscopic data to investigate a relationship between human serum metabolic profiles and hypertension. Analyst. 2003; 128(1): 32-6.

Buck MD, Sowell RT, Kaech SM, Pearce EL. Metabolic instruction of immunity. Cell. 2017; 169: 570-586.

Buescher JM, Antoniewicz MR, Boros LG, Burgess SC, Brunengraber H, Clish CB, et al. A roadmap for interpreting ^{13}C metabolite labeling patterns from cells. Curr Opin Biotechnol. 2015; 34: 189-201.

Cairo G, Recalcati S, Mantovani A, Locati M. Iron trafficking and metabolism in macrophages: contribution to the polarized phenotype. Trends Immunol. 2011; 32(6): 241-7.

Canton J, Neculai D, Grinstein S. Scavenger receptors in homeostasis and immunity. Nat Rev Immunol. 2013; 13(9): 621-34.

Carls GS, Gibson TB, Driver VR, Wrobel JS, Garoufalis MG, Defrancis RR, et al. The economic value of specialized lower-extremity medical care by podiatric physicians in the treatment of diabetic foot ulcers. J Am Podiatr Med Assoc. 2011; 101(2): 93-115.

Carpenter DJ, Granot T, Matsuoka N, Senda T, Kumar BV, Thome JJC, et al. Human immunology studies using organ donors: impact of clinical variations on immune parameters in tissues and circulation. Am J Transplant. 2018; 18: 74-88.

Carreau A, El Hafny-Rahbi B, Matejuk A, Grillon C, Kieda C. Why is the partial oxygen pressure of human tissues a crucial parameter? Small molecules and hypoxia. J Cell Mol Med. 2011; 15: 1239-1253.

Cavallito CJ, Bailey JH. Allicin, the antibacterial principle of *Allium sativum*. I. Isolation, physical properties and antibacterial action. J Am Chem Soc. 1944; 66(11): 1950-1951.

Chastre J, Fagon JY. Ventilator-associated pneumonia. Am J Respir Crit Care Med. 2002; 165(7): 867-903.

Chatterjee I, Schmitt S, Batzilla CF, Engelmann S, Keller A, Ring MW, et al. *Staphylococcus aureus* ClpC ATPase is a late growth phase effector of metabolism and persistence. Proteomics. 2009; 9: 1152-1176.

Chen M, Li A, Sun M, Feng Z, Meng X, Wang Y. Optimization of the quenching method for metabolomics analysis of *Lactobacillus bulgaricus*. J Zhejiang Univ Sci B. 2014; 15(4): 333-342.

Chen X, Zhang B, Li H, Peng X. Myo-inositol improves the host's ability to eliminate balofloxacin-resistant *Escherichia coli*. Sci Rep. 2015; 5: 10720.

Cheng T, Sudderth J, Yang C, Mullen AR, Jin ES, Matés JM, et al. Pyruvate carboxylase is required for glutamine-in-dependent growth of tumor cells. Proc Natl Acad Sci USA. 2011; 108: 8674-8679.

Chhabria S, Desai K. Purification and characterization of alliinase produced by *Cupriavidus necator* and its application for generation of cytotoxic agent: allicin. Saudi J Biol Sci. 2018; 25(7): 1429-1438.

Chong J, Soufan O, Li C, Caraus I, Li S, Bourgue G, et al. MetaboAnalyst 4.0: towards more transparent and integrative metabolomics analysis. Nucleic Acids Res. 2018; 46: W486-W494.

Cigana C, Lore NI, Bernardini ML, Bragonzi A. Dampening host sensing and avoiding recognition in *Pseudomonas aeruginosa* pneumonia. J Biomed Biotechnol. 2011; 2011: 852513.

Clarke TB. Microbial programming of systemic innate immunity and resistance to infection. PLoS Pathog. 2014; 10(12): e1004506.

Clore M, Potts J. Recent developments in biomolecular NMR. RSC Publishing. 2012.

CLSI. Methods for dilution antimicrobial susceptibility tests for bacteria that grow aerobically; approved standard – tenth edition. CLSI document M07-A10. Wayne, PA: Clinical and Laboratory Standards Institute; 2015.

Cockayne TO. Leechdoms, wortcunning, and starcraft of early England. Being a collection of documents, for the most part never before printed, illustrating the history of science in this country before the Norman conquest. Rolls series 35th, 3 Vols. London: Longman, Green, Longman, Roberts, and Green. 1864-1866.

Corral MJ, González-Sánchez E, Cuquerella M, Alunda JM. *In vitro* synergistic effect of amphotericin B and allicin on *Leishmania donovani* and *L. infantum*. Antimicrob Agents Chemother. 2014; 58(3): 1596-1602.

Costerton JW, Stewart PS, Greenberg EP. Bacterial biofilms: a common cause of persistent infections. Science. 1999; 284(5418): 1318-22.

Cubitt AB, Heim R, Adams SR, Boyd AE, Gross LA, Tsien RY. Understanding, improving and using green fluorescent proteins. Trends Biochem Sci. 1995; 20: 448-455.

Currie GA, Gyure L, Cifuentes L. Microenvironmental arginine depletion by macrophages in vivo. Br J Cancer. 1979; 39(6): 613-20.

Cutler RR, Wilson P. Antibacterial activity of a new, stable, aqueous extract of allicin against methicillin-resistant *Staphylococcus aureus*. Br J Biomed Sci. 2004; 61(2): 71-74.

Davis SC, Ricotti C, Cazzaniga A, Welsh E, Eaglstein WH, Mertz PM. Microscopic and physiologic evidence for biofilm-associated wound colonization *in vivo*. Wound Repair Regen. 2008; 16(1): 23-9.

Dettmer K, Aronov PA, Hammock BD. Mass spectrometry-based metabolomics. Mass Spectrom Rev. 2007; 26(1): 51-78.

Diep BA, Gill SR, Chang RF, Phan TH, Chen JH, Davidson MG, et al. Complete genome sequence of USA300, an epidemic clone of community-acquired meticillin-resistant *Staphylococcus aureus*. Lancet. 2006; 367(9512): P731-739.

Diskin C, Pålsson-McDermott EM. Metabolic modulation in macrophage effector function. Front Immunol. 2018; 9: 270.

Donegan NP, Marvin JS, Cheung AL. Role of adaptor TrfA and ClpPC in controlling levels of SsrA-tagged proteins and antitoxins in *Staphylococcus aureus*. J Bacteriol. 2014; 196: 4140-4151.

Dowd SE, Sun Y, Secor PR, Rhoads DD, Wolcott BM, James GA, et al. Survey of bacterial diversity in chronic wounds using pyrosequencing, DGGE, and full ribosome shotgun sequencing. BMC Microbiol. 2008; 8: 43.

Dumas ME, Canlet C, André F, Vercauteren J, Paris A. Metabonomic assessment of physiological disruptions using ^{1}H-^{13}C HMBC-NMR spectroscopy combined with pattern recognition procedures performed on filtered variables. Anal Chem. 2002; 74(10): 2261-73.

Duthie ES, Lorenz LL. Staphylococcal coagulase; mode of action and antigenicity. J Gen Microbiol. 1952; 6: 95-107.

Eldridge GR, Vervoort HC, Lee CM, Cremin PA, Williams CT, Hart SM, et al. High-throughput method for the production and analysis of large natural products libraries for drug discovery. Anal Chem. 2002; 74(16): 3963-3971.

Ellis JK, Athersuch TJ, Cavill R, Radford R, Slattery C, Jennings P, et al. Metabolic response to low-level toxicant exposure in novel renal tubule epithelial cell system. Mol Biosyst. 2011; 7(1): 247-57.

Ellis JK, Athersuch TJ, Thomas LD, Teichert F, Pérez-Trujillo M, Svendsen C, et al. Metabolic profiling detects early effects of environmental and lifestyle exposure to cadmium in a human population. BMC Med. 2012; 10: 61.

Elsholz AK, Hempel K, Michalik S, Gronau K, Becher D, Hecker M, Gerth U. Activity control of the ClpC adaptor McsB in *Bacillus subtilis*. 2011; J Bacteriol. 193: 3887-3893.

Emwas AH, Saccenti E, Gao X, McKay RT, Dos Santos, VAPM, Roy R, et al. Recommended strategies for spectral processing and post-processing of 1D ^{1}H-NMR data of biofluids with a particular focus on urine. Metabolomics. 2018; 14: 31.

Emwas AHM, Salek RM, Griffin JL, Merzaban J. NMR-based metabolomics in human disease diagnosis: applications, limitations, and recommendations. Metabolomics. 2013; 9(5): 1048-1072.

Enright MC, Robinson DA, Randle G, Feil EJ, Grundmann H, Spratt BG. The evolutionary history of methicillin-resistant *Staphylococcus aureus* (MRSA). Proc Natl Acad Sci U S A. 2002; 99: 7687-7692.

Faijes M, Mars AE, Smid EJ. Comparison of quenching and extraction methodologies for metabolome analysis of *Lactobacillus plantarum*. Microb Cell Fact. 2007; 6: 27-34.

Falanga V. Wound healing and its impairment in the diabetic foot. Lancet. 2005; 366(9498): 1736-43.

Fan TW, Lane AN. Applications of NMR spectroscopy to systems biochemistry. Prog Nucl Magn Reson Spectrosc. 2016; 92-93: 18-53.

Fan TW, Lane AN, Higashi RM, Farag MA, Gao H, Bousamra M, et al. Altered regulation of metabolic pathways in human lung cancer discerned by (13)C stable isotope-resolved metabolomics (SIRM). Mol Cancer. 2009; 8: 41.

Fan TW, Lorkiewicz PK, Sellers K, Moseley HN, Higashi RM, Lane AN. Stable isotope-resolved metabolomics and applications for drug development. Pharmacol Ther. 2012; 133(3): 366-91.

Fan TW, Yuan P, Lane AN, Higashi RM, Wang Y, Hamidi AB, et al. Stable isotope-resolved metabolomic analysis of lithium effects on glial-neuronal metabolism and interactions. Metabolomics. 2010; 6(2): 165-179.

Fan X, Bai J, Shen P. Diagnosis of breast cancer using HPLC metabonomics fingerprints coupled with computational methods. Conf Proc IEEE Eng Med Biol Soc. 2005; 6: 6081-4.

Fang FC, Nathan CF. Man is not a mouse: reply. J Leukoc Biol. 2007; 81: 580.

Fantin A, Vieira JM, Gestri G, Denti L, Schwarz Q, Prykhozhij S, et al. Tissue macrophages act as cellular chaperones for vascular anastomosis downstream of VEGF-mediated endothelial tip cell induction. Blood. 2010; 116(5): 829-40.

Fathi F, Brun A, Rott KH, Falco Cobra P, Tonelli M, Eghbalnia HR, et al. NMR-based identification of metabolites in polar and non-polar extracts of avian liver. Metabolites. 2017; 7: 61.

Feingold KR, Shigenaga JK, Kazemi MR, McDonald CM, Patzek SM, Cross AS, et al. Mechanisms of triglyceride accumulation in activated macrophages. J Leukoc Biol. 2012; 92: 829-839.

Feng J, Li L, Ou Z, Li Q, Gong B, Zhao Z, et al. IL-25 stimulates M2 macrophage polarization and thereby promotes mitochondrial respiratory capacity and lipolysis in adipose tissues against obesity. Cell Mol Immunol. 2018; 15: 493-505.

Feng J, Michalik S, Varming AN, Andersen JH, Albrecht D, Jelsbak L, et al. Trapping and proteomic identification of cellular substrates of the ClpP protease in *Staphylococcus aureus*. J Proteome Res. 2013; 12: 547-558.

Feroci G, Fini A, Fazio G, Zuman P. Interaction between dihydroxyl bile salts and divalent heavy metal ions studied by polarography. Anal Chem. 1995; 67(22): 4077-4085.

Ferrante CJ, Leibovich SJ. Regulation of macrophage polarization and wound healing. Adv Wound Care (New Rochelle). 2012; 1(1): 10-16.

Fesik SW, Zuiderweg ER. Heteronuclear three-dimensional NMR spectroscopy of isotopically labelled biological macromolecules. Q Rev Biophys. 1990; 23(2): 97-131.

Fey PD, Endres JL, Yajjala VK, Widhelm TJ, Boissy RJ, Bose JL, et al. A genetic resource for rapid and comprehensive phenotype screening of nonessential *Staphylococcus aureus* genes. mBio. 2013; 4: e00537.

Fiehn O. Metabolomics—the link between genotypes and phenotypes. Plant Mol Biol. 2002; 48: 155-171.

Fonville JM, Maher AD, Coen M, Holmes E, Lindon JC, Nicholson JK. Evaluation of full-resolution J-resolved ^{1}H NMR projections of biofluids for metabonomics information retrieval and biomarker identification. Anal Chem. 2010; 82(5): 1811-21.

Forsyth RA, Haselbeck RJ, Ohlsen KL, Yamamoto RT, Xu H, Trawick JD, et al. A genome-wide strategy for the identification of essential genes in *Staphylococcus aureus*. Mol Microbiol. 2002; 43: 1387-1400.

Freeman F, Kodera Y. Garlic chemistry: stability of S-(2-propenyl)-2-propene-1-sulfinothioate (allicin) in blood, solvents, and simulated physiological fluids. J Agric Food Chem. 1995; 43(9): 2332-2338.

Freemerman AJ, Johnson AR, Sacks GN, Milner JJ, Kirk EL, Troester MA, et al. Metabolic reprogramming of macrophages: glucose transporter 1 (GLUT1)-mediated glucose metabolism drives a proinflammatory phenotype. J Biol Chem. 2014; 289: 7884-7896.

Frees D, Qazi SN, Hill PJ, Ingmer H. Alternative roles of ClpX and ClpP in *Staphylococcus aureus* stress tolerance and virulence. Mol Microbiol. 2003; 48: 1565-1578.

Frees D, Savijoki K, Varmanen P, Ingmer H. Clp ATPases and ClpP proteolytic complexes regulate vital biological processes in low GC, Gram-positive bacteria. Mol Microbiol. 2007; 63: 1285-1295.

Frees D, Thomsen LE, Ingmer H. *Staphylococcus aureus* ClpYQ plays a minor role in stress survival. Arch Microbiol. 2005; 183: 286-291.

Fried VA, Novick A. Organic solvents as probes for the structure and function of the bacterial membrane: effects of ethanol on the wild type and an ethanol-resistant mutant of *Escherichia coli* K-12. J Bacteriol. 1973; 114(1): 239-248.

Frykberg RG, Banks J. Challenges in the treatment of chronic wounds. Adv Wound Care (New Rochelle). 2015; 4(9): 560-582.

Fuchs AL, Weaver AJ Jr, Tripet BP, Ammons MCB, Teintze M, Copié V. Characterization of the antibacterial activity of Bald's eyesalve against drug resistant *Staphylococcus aureus* and *Pseudomonas aeruginosa*. PLoS One. 2018; 13: e0208108.

Fuchs S, Pane-Farre J, Kohler C, Hecker M, Engelmann S. Anaerobicgene expression in *Staphylococcus aureus*. J Bacteriol. 2007; 189: 4275-4289.

Fujisawa H, Suma K, Origuchi K, Kumagai H, Seki T, Ariga T. Biological and chemical stability of garlic-derived allicin. J Agric Food Chem. 2008; 56(11): 4229-4235.

Fukuzumi M, Shinomiya H, Shimizu Y, Ohishi K, Utsumi S. Endotoxin-induced enhancement of glucose influx into murine peritoneal macrophages via GLUT1. Infect Immun. 1996; 64(1): 108-12.

Funk JL, Feingold KR, Moser AH, Grunfeld C. Lipopolysaccharide stimulation of RAW 264.7 macrophages induces lipid accumulation and foam cell formation. Atherosclerosis. 1993; 98(1): 67-82.

Galván-Peña S, O'Neill LA. Metabolic reprogramming in macrophage polarization. Front Immunol. 2014; 5: 420.

Garcia M, Mamedova LK, Barton B, Bradford BJ. Choline regulates the function of bovine immune cells and alters the mRNA abundance of enzymes and receptors involved in its metabolism *in vitro*. Front Immunol. 2018; 9: 2448.

García-Cañaveras JC, López S, Castell JV, Donato MT, Lahoz A. Extending metabolome coverage for untargeted metabolite profiling of adherent cultured hepatic cells. Anal Bioanal Chem. 2016; 408: 1217-1230.

Gebregiworgis T, Powers R. Application of NMR metabolomics to search for human disease biomarkers. Comb Chem High Throughput Screen. 2012; 15(8): 595-610.

Ghoreschi K, Brück J, Kellerer C, Deng C, Peng H, Rothfuss O, et al. Fumarates improve psoriasis and multiple sclerosis by inducing type II dendritic cells. J Exp Med. 2011; 208: 2291-2303.

Gibellini F, Smith TK. The Kennedy pathway--*de novo* synthesis of phosphatidylethanolamine and phosphatidylcholine. IUBMB Life. 2010; 62: 414-428.

Gika HG, Theodoridis GA, Plumb RS, Wilson ID. Current practice of liquid chromatography-mass spectrometry in metabolomics and metabonomics. J Pharm Biomed Anal. 2014; 87: 12-25.

Ginhoux F, Jung S. Monocytes and macrophages: developmental pathways and tissue homeostasis. Nat Rev Immunol. 2014; 14(6): 392-404.

Ginhoux F, Schultze JL, Murray PJ, Ochando J, Biswas SK. New insights into the multidimensional concept of macrophage ontogeny, activation and function. Nat Immunol. 2016; 17: 34-40.

Gohil VM, Zhu L, Baker CD, Cracan V, Yaseen A, Jain M, et al. Meclizine inhibits mitochondrial respiration through direct targeting of cytosolic phosphoethanolamine metabolism. J Biol Chem. 2013; 288: 35387-35395.

Gohring N, Fedtke I, Xia G, Jorge AM, Pinho MG, Bertsche U, et al. New role of the disulfide stress effector YjbH in beta-lactam susceptibility of *Staphylococcus aureus*. Antimicrob Agents Chemother. 2011; 55: 5452-5458.

Gonzalez B, Francois J, Renaud M. A rapid and reliable method for metabolite extraction in yeast using boiled buffered ethanol. Yeast. 1997; 13: 1347-1356.

Gordois A, Scuffham P, Shearer A, Oglesby A, Tobian JA. The health care costs of diabetic peripheral neuropathy in the US. Diabetes Care. 2003; 26(6): 1790-5.

Gordon S, Taylor PR. Monocyte and macrophage heterogeneity. Nat Rev Immunol. 2005; 5(12): 259-70.

Goren I, Müller E, Schiefelbein D, Christen U, Pfeilschifter J, Mühl H, et al. Systematic anti-TNFalpha treatment restores diabetes-impaired skin repair in ob/ob mice by inactivation of macrophages. J Invest Dermatol. 2007; 127(9): 2259-67.

Gottesman S. Regulation by proteolysis: developmental switches. Curr Opin Microbiol. 1999; 2: 142-147.

Graham JW, Lei MG, Lee CY. Trapping and identification of cellular substrates of the *Staphylococcus aureus* ClpC chaperone. J Bacteriol. 2013; 195: 4506-4516.

Graham PL, III, Lin SX, Larson EL. A U.S. population-based survey of *Staphylococcus aureus* colonization. Ann Intern Med. 2006; 144: 318-325.

Gruhlke MC, Nicco C, Batteux F, Slusarenko AJ. The effects of allicin, a reactive sulfur species from garlic, on a selection of mammalian cell lines. Antioxidants. 2016; 6(1): 1.

Guillemin GJ, Smith DG, Smythe GA, Armati PJ, Brew BJ. Expression of the kynurenine pathway enzymes in human microglia and macrophages. Adv Exp Med Biol. 2003; 527: 105-112.

Guzy RD, Sharma B, Bell E, Chandel NS, Schumacker PT. Loss of SdhB, but not SdhA, subunit of complex II triggers reactive oxygen species-dependent hypoxia-inducible factor activation and tumorigenesis. Mol Cell Biol. 2008; 28: 718-731.

Han X, Holtzman DM, McKeel DW Jr, Kelley J, Morris JC. Substantial sulfatide deficiency and ceramide elevation in very early Alzheimer's disease: potential role in disease pathogenesis. J Neurochem. 2002; 82(4): 809-18.

Hammer ND, Reniere ML, Cassat JE, Zhang Y, Hirsch AO, Indriati Hood M, et al. Two heme-dependent terminal oxidases power *Staphylococcus aureu*s organ-specific colonization of the vertebrate host. mBio. 2013; 4: e00241-13.

Harrison F, Roberts AEL, Gabrilska R, Rumbaugh KP, Lee C, Diggle SP. A 1,000-year-old antimicrobial remedy with antistaphylococcal activity. mBio. 2015; 6(4): e01129-15.

Haschemi A, Kosma P, Gille L, Evans CR, Burant CF, Starkl P, et al. The sedoheptulose kinase CARKL directs macrophage polarization through control of glucose metabolism. Cell Metab. 2012; 15(6): 813-26.

He C, Ryan AJ, Murthy S, Carter AB. Accelerated development of pulmonary fibrosis via Cu,Zn-superoxide dismutase-induced alternative activation of macrophages. J Biol Chem. 2013; 288: 20745-20757.

Herbert S, Ziebandt AK, Ohlsen K, Schafer T, Hecker M, Albrecht D, et al. Repair of global regulators in *Staphylococcus aureus* 8325 and comparative analysis with other clinical isolates. Infect Immun. 2010; 78: 2877-2889.

Hesketh M, Sahin KB, West ZE, Murray RZ. Macrophage phenotypes regulate scar formation and chronic wound healing. Int J Mol Sci. 2017; 18(7): E1545.

Ho CW, Chew TK, Ling TC, Kamaruddin S, Tan WS, Tey BT. Efficient mechanical cell disruption of *Escherichia coli* by an ultrasonicator and recovery of intracellular hepatitis B core antigen. Process Biochem. 2006; 41: 1829-1834.

Holmes E, Tsang TM, Huang JT, Leweke FM, Koethe D, Gerth CW, et al. Metabolic profiling of CSF: evidence that early intervention may impact on disease progression and outcome in schizophrenia. PLoS Med. 2006; 3(8): e327.

Hotamisligil GS. Inflammation and metabolic disorders. Nature. 2006; 444(7121): 860-7.

Huang L, Forsberg CW, Gibbins LN. Influence of external pH and fermentation products on *Clostridium acetobutylicum* intracellular pH and cellular distribution of fermentation products. Appl Environ Microbiol. 1986; 51(6): 1230-1234.

Huang SC, Everts B, Ivanova Y, O'Sullivan D, Nascimento M, Smith AM, et al. Cell-intrinsic lysosomal lipolysis is essential for alternative activation of macrophages. Nat Immunol. 2014; 15: 846-855.

Huang SC, Smith AM, Everts B, Colonna M, Pearce EL, Schilling JD, et al. Metabolic reprogramming mediated by the mTORC2-IRF4 signaling axis is essential for macrophage alternative activation. Immunity. 2016; 45: 817-830.

Huang Z, Chen Y, Hang W, Gao Y, Lin L, Li DY, et al. Holistic metabonomic profiling of urine affords potential early diagnosis for bladder and kidney cancers. Metabolomics. 2013; 9(1): 119-129.

Hussell T, Bell TJ. Alveolar macrophages: plasticity in a tissue-specific context. Nat Rev Immunol. 2014; 14(2): 81-93.

Hyberts SG, Heffron GJ, Tarragona NG, Solanky K, Edmonds KA, Luithardt H, et al. Ultrahigh-resolution ^{1}H-^{13}C HSQC spectra of metabolite mixtures using nonlinear sampling and forward maximum entropy reconstruction. J Am Chem Soc. 2007; 129(16): 5108-16.

Ilić D, Nikolić V, Stanković M, Nikolić L, Stanojević L, Mladenović-Ranisavljević I, et al. Transformation of synthetic allicin: the influence of ultrasound, microwaves, different solvents and temperatures, and the products isolation. ScientificWorldJournal. 2012; 2012: 561823.

Inui T, Wang Y, Pro SM, Franzblau SG, Pauli GF. Unbiased evaluation of bioactive secondary metabolites in complex matrices. Fitoterapia. 2012; 83(7): 1218-25.

Iwańska A, Nowak J, Skorupa W, Augustynowicz-Kopeć E. Analysis of the frequency of isolation and drug resistance of microorganisms isolated from the airways of adult CF patients treated in the Institute of Tuberculosis and Lung Disease during 2008-2011. Pneumonol Alergol Pol. 2013; 81(2): 105-13.

James GA, Swogger E, Wolcott R, Pulcini Ed, Secor P, Sestrich J, et al. Biofilms in chronic wounds. Wound Repair Regen. 2008; 16: 37-44.

Jensen ET, Kharazmi A, Lam K, Costerton JW, Høiby N. Human polymorphonuclear leukocyte response to *Pseudomonas aeruginosa* grown in biofilms. Infect Immun. 1990; 58(7): 2383-5.

Jensen PØ, Bjarnsholt T, Phipps R, Rasmussen TB, Calum H, Christoffersen L, et al. Rapid necrotic killing of polymorphonuclear leukocytes is caused by quorum-sensing-controlled production of rhamnolipid by *Pseudomonas aeruginosa*. Microbiology. 2007; 153(Pt 5): 1329-38.

Jensen PØ, Moser C, Kobayashi O, Hougen HP, Kharazmi A, Høiby N. Faster activation of polymorphonuclear neutrophils in resistant mice during early innate response to *Pseudomonas aeruginosa* lung infection. Clin Exp Immunol. 2004; 137(3): 478-85.

Jesaitis AJ, Franklin MJ, Berglund D, Sasaki M, Lord CI, Bleazard JB, et al. Compromised host defense on *Pseudomonas aeruginosa* biofilms: characterization of neutrophil and biofilm interactions. J Immunol. 2003; 171(8): 4329-39.

Jha AK, Huang SC, Sergushichev A, Lampropoulou V, Ivanova Y, Loginicheva E, et al. Network integration of parallel metabolic and transcriptional data reveals metabolic modules that regulate macrophage polarization. Immunity. 2015; 42: 419-430.

Jia Y, Schurmans S, Luo HR. Regulation of innate immunity by inositol 1,3,4,5-tetakisphosphate. Cell Cycle. 2008; 7: 2803-2808.

Johnson BH, Hecht MH. Recombinant proteins can be isolated from *E. coli* cells by repeated cycles of freezing and thawing. Nat Biotechnol. 1994; 12: 1357-1360.

Johnson CH, Gonzalez FJ. Challenges and opportunities of metabolomics. J Cell Physiol. 2012; 227(8): 2975-81.

Johnson CH, Ivanisevic J, Siuzdak G. Metabolomics: beyond biomarkers and towards mechanisms. Nat Rev Mol Cell Biol. 2016; 17(7): 451-9.

Joo HS, Otto M. Molecular basis of *in vivo* biofilm formation by bacterial pathogens. Chem Biol. 2012; 19: 1503-1513.

Jousselin A, Kelley WL, Barras C, Lew DP, Renzoni A. The *Staphylococcus aureus* thiol/oxidative stress global regulator Spx controls *trfA*, a gene implicated in cell wall antibiotic resistance. Antimicrob Agents Chemother. 2013; 57: 3283-3292.

Kaddurah-Daouk R. Metabolic profiling of patients with schizophrenia. PLoS Med. 2006; 3(8): e363.

Kaddurah-Daouk R, Kristal BS, Weinshilboum RM. Metabolomics: a global biochemical approach to drug response and disease. Annu Rev Pharmacol Toxicol. 2008; 48: 653-83.

Kaddurah-Daouk R, McEvoy J, Baillie RA, Lee D, Yao JK, Doraiswamy PM, et al. Metabolomic mapping of atypical antipsychotic effects in schizophrenia. Mol Psychiatry. 2007; 12(10): 934-45.

Kamada N, Hisamatsu T, Okamoto S, Chinen H, Kobayashi T, Sato T, et al. Unique $CD14^+$ intestinal macrophages contribute to the pathogenesis of Crohn disease via IL-23/IFN-γ axis. J Clin Invest. 2008; 118: 2269-2280.

Kaplan O, van Zijl PC, Cohen JS. Information from combined ^{1}H and ^{31}P NMR studies of cell extracts: differences in metabolism between drug-sensitive and drug-resistant MCF-7 human breast cancer cells. Biochem Biophys Res Commun. 1990; 169(2): 383-90.

Kawai T, Akira S. The role of pattern-recognition receptors in innate immunity: update on Toll-like receptors. Nat Immunol. 2010; 11(5): 373-84.

Keller R, Geiges M, Keist R. L-arginine-dependent reactive nitrogen intermediates as mediators of tumor cell killing by activated macrophages. Cancer Res. 1990; 50(5): 1421-5.

Kempler G, Ray B, Nature of freezing damage on the lipopolysaccharide molecule of *Escherichia coli* B. Cryobiology. 1978; 15: 578-584.

Kenny LC, Dunn WB, Ellis DI, Myers J, Baker PN, Consortium GOPEC, et al. Novel biomarkers for pre-eclampsia detected using metabolomics and machine learning. Metabolomics. 2005; 1: 227-34.

Kim IY, Suh SH, Lee IK, Wolfe RR. Applications of stable, nonradioactive isotope tracers in *in vivo* human metabolic research. Exp Mol Med. 2016; 48(1): e203.

Kim JW, Huh JE, Kyung SH, Kyung KH. Antimicrobial activity of alk(en)yl sulfides found in essential oils of garlic and onion. Food Sci Biotechnol. 2004; 13(2): 235-239.

Kim JW, Tchernyshyoc I, Semenza GL, Dang CV. HIF-1-mediated expression of pyruvate dehydrogenase kinase: a metabolic switch required for cellular adaptation to hypoxia. Cell Metab. 2006; 3: 177-185.

Kim YI, Levchenko I, Fraczkowska K, Woodruff RV, Sauer RT, Baker TA. Molecular determinants of complex formation between Clp/ Hsp100 ATPases and the ClpP peptidase. Nat Struct Biol. 2001; 8: 230-233.

Kinkel TL, Roux CM, Dunman PM, Fang FC. The *Staphylococcus aureus* SrrAB two-component system promotes resistance to nitrosative stress and hypoxia. mBio. 2013; 4: e00696-13.

Kirker KR, James GA, Fleckman P, Olerud JE, Stewart PS. Differential effects of planktonic and biofilm MRSA on human fibroblasts. Wound Repair Regen. 2012; 20(2): 253-261.

Kirker KR, Secor PR, James GA, Fleckman P, Olerud JE, Stewart PS. Loss of viability and induction of apoptosis in human keratinocytes exposed to *Staphylococcus aureus* biofilms *in vitro*. Wound Repair and Regener. 2009; 17(5): 690-699.

Klevens RM, Morrison MA, Nadle J, Petit S, Gershman K, Ray S, et al. Invasive methicillin-resistant *Staphylococcus aureus* infections in the United States. JAMA. 2007; 298: 1763-1771.

Koehn FE, Carter GT. The evolving role of natural products in drug discovery. Nat Rev Drug Discov. 2005; 4(3): 206-220.

Kohyama M, Ise W, Edelson BT, Wilker PR, Hildner K, Mejia C, et al. Nature. 2009; 457(7227): 318-21.

Kosteli A, Sugaru E, Haemmerle G, Martin JF, Lei J, Zechner R, et al. Weight loss and lipolysis promote a dynamic immune response in murine adipose tissue. J Clin Invest. 2010; 120(10): 3466-79.

Kreiswirth BN, Lofdahl S, Betley MJ, O'Reilly M, Schlievert PM, Bergdoll MS, et al. The toxic shock syndrome exotoxin structural gene is not detectably transmitted by a prophage. Nature. 1983; 305: 709-712.

Krzyszczyk P, Schloss R, Palmer A, Berthiaume F. The role of macrophages in acute and chronic wound healing and interventions to promote pro-wound healing phenotypes. Front Physiol. 2018; 9: 419.

Kuroda M, Ohta T, Uchiyama I, Baba T, Yuzawa H, Kobayashi I, et al. Whole genome sequencing of methicillin-resistant *Staphylococcus aureus*. Lancet. 2001; 357: 1225-1240.

Lampropoulou V, Sergushichev A, Bambouskova M, Nair S, Vincent EE, Loginicheva E, et al. Itaconate links inhibition of succinate dehydrogenase with macrophage metabolic remodeling and regulation of inflammation. Cell Metab. 2016; 24: 158-166.

Lane AN, Fan TW. Regulation of mammalian nucleotide metabolism and biosynthesis. Nucleic Acids Res. 2015; 43(4): 2466-85.

Lanzotti V, Bonanomi G, Scala F. What makes *Allium* species effective against pathogenic microbes? Phytochem Rev. 2013; 12(4): 751-772.

Lavin Y, Mortha A, Rahman A, Merad M. Regulation of macrophage development and function in peripheral tissues. Nat Rev Immunol. 2015; 15(12): 731-44.

Lebeaux D, Ghigo JM, Beloin C. Biofilm-related infections: bridging the gap between clinical management and fundamental aspects of recalcitrance toward antibiotics. Microbiol Mol Biol Rev. 2014; 78(3): 510-43.

Lee JH, Park JH, Cho HS, Joo SW, Cho MH, Lee J. Anti-biofilm activities of quercetin and tannic acid against *Staphylococcus aureus*. Biofouling. 2013; 29(5): 491-9.

Leid JG, Willson CJ, Shirtliff ME, Hassett DJ, Parsek MR, Jeffers AK. The exopolysaccharide alginate protects *Pseudomonas aeruginosa* biofilm bacteria from IFN-γ-mediated macrophage killing. J Immunol. 2005; 175(11): 7512-8.

León Z, García-Cañaveras JC, Donato MT, Lahoz A. Mammalian cell metabolomics: experimental design and sample preparation. Electrophoresis. 2013; 34: 2762-2775.

Lewis IA, Schommer SC, Hodis B, Robb KA, Tonelli M, Westler WM, et al. Method for determining molar concentrations of metabolites in complex solutions from two-dimensional ^{1}H-^{13}C NMR spectra. Anal Chem. 2007; 79(24): 9385-90.

Lewis K. Multidrug tolerance of biofilms and persister cells. Curr Top Microbiol Immunol. 2008; 322: 107-31.

Li XZ, Plésiat P, Nikaido H. The challenge of efflux-mediated antibiotic resistance in Gram-negative bacteria. Clin Microbiol Rev. 2015; 28(2): 337-418.

Li Y, Wang H, Pan T. Intracellular ice formation (IIF) during freeze-thaw repetitions. Int J Heat and Mass Transfer. 2013; 64: 436-443.

Lindon JC, Holmes E, Bollard ME, Stanley EG, Nicholson JK. Metabonomics technologies and their applications in physiological monitoring, drug safety assessment and disease diagnosis. Biomarkers. 2004; 9(1): 1-31.

Liu PS, Wang H, Li X, Chao T, Teav T, Christen S, et al. α-ketoglutarate orchestrates macrophage activation through metabolic and epigenetic reprogramming. Nat Immunol. 2017; 18: 985-994.

Liu Z. Preparation of botanical samples for biomedical research. Endocr Metab Immune Disord Drug Targets. 2008; 8(2): 112-121.

Liu ZJ, Velazquez OC. Hyperoxia, endothelial progenitor cell mobilization, and diabetic wound healing. Antioxid Redox Signal. 2008; 10(11): 1869-82.

Longo DM, Louie B, Wang E, Pos Z, Marincola FM, Hawtin RE, et al. Inter-donor variation in cell subset specific immune signaling responses in healthy individuals. Am J Clin Exp Immunol. 2012; 1: 1-11.

Loots MA, Lamme EN, Zeegelaar J, Mekkes JR, Bos JD, Middelkoop E. Differences in cellular infiltrate and extracellular matrix of chronic diabetic and venous ulcers versus acute wounds. J Invest Dermatol. 1998; 111(5): 850-7.

Lumeng CN, Bodzin JL, Saltiel AR. Obesity induces a phenotypic switch in adipose tissue macrophage polarization. J Clin Invest. 2007; 117(1): 175-84.

Luong TT, Lee CY. Improved single-copy integration vectors for *Staphylococcus aureus*. J Microbiol Methods. 2007; 70: 186-190.

Maharjan RP, Ferenci T. Global metabolite analysis: the influence of extraction methodology on metabolome profiles of *Escherichia coli*. Anal Biochem. 2003; 313: 145-154.

Mainiero M, Goerke C, Geiger T, Gonser C, Herbert S, Wolz C. Differential target gene activation by the *Staphylococcus aureus* twocomponent system SaeRS. J Bacteriol. 2010; 192: 613-623.

Malone CL, Boles BR, Lauderdale KJ, Thoendel M, Kavanaugh JS, Horswill AR. Fluorescent reporters for *Staphylococcus aureus*. J Microbiol Methods. 2009; 77: 251-260.

Man A, Gâz AS, Mare AD, Berţa L. Effects of low-molecular weight alcohols on bacterial viability. Rev Romana Med Lab. 2017; 25(4): 335-343.

Mann EE, Wozniak DJ. *Pseudomonas* biofilm matrix composition and niche biology. FEMS Microbiol Rev. 2012; 36(4): 893-916.

Mannina L, Sobolev AP, Capitani D, Iaffaldano N, Rosato MP, Ragni P, et al. NMR metabolic profiling of organic and aqueous sea bass extracts: implications in the discrimination of wild and cultured sea bass. Talanta. 2008; 77(1): 433-44.

Marchesi JR, Holmes E, Khan F, Kochhar S, Scanlan P, Shanahan F, et al. Rapid and noninvasive metabonomic characterization of inflammatory bowel disease. J Proteome Res. 2007; 6(2): 546-51.

Marcinkiewicz J, Kontny E. Taurine and inflammatory diseases. Amino Acids. 2014; 46: 7-20.

Markley JL, Brüschweiler R, Edison AS, Eghbalnia HR, Powers R, Raftery D, et al. The future of NMR-based metabolomics. Curr Opin Biotechnol. 2017; 43: 34-40.

Marshakov IK. Corrosion resistance and dezincing of brasses. Prot Met. 2005; 41(3): 205-210.

Martinez FO, Gordon S. The M1 and M2 paradigm of macrophage activation: time for reassessment. F1000Prime Rep. 2014; 6:13.

Martinez FO, Helming L, Milde R, Varin A, Melgert BN, Draijer C, et al. Genetic programs expressed in resting and IL-4 alternatively activated mouse and human macrophages: similarities and differences. Blood. 2013; 121: e57-69.

Mashruwala AA, Bhatt S, Poudel S, Boyd ES, Boyd JM. The DUF59 containing protein SufT is involved in the maturation of iron-sulfur (FeS) proteins during conditions of high FeS cofactor demand in *Staphylococcus aureus*. PLoS Genet. 2016; 12: e1006233.

Mashruwala AA, Boyd JM. The *Staphylococcus aureus* SrrAB regulatory system modulates hydrogen peroxide resistance factors, which imparts protection to aconitase during aerobic growth. PLoS One. 2017; 12: e0170283.

Mashruwala AA, Gries CM, Scherr TD, Kielian T, Boyd JM. SaeRS is responsive to cellular respiratory status and regulates fermentative biofilm formation in *Staphylococcus aureus*. Infect Immun. 2017; 85: e00157-17.

Mashruwala AA, Pang YY, Rosario-Cruz Z, Chahal HK, Benson MA, Mike LA, et al. Nfu facilitates the maturation of iron-sulfur proteins and participates in virulence in *Staphylococcus aureus*. Mol Microbiol. 2015; 95: 383-409.

Mashruwala AA, Roberts CA, Bhatt S, May KL, Carroll RK, Shaw LN, et al. *Staphylococcus aureus* SufT: an essential iron-sulphur cluster assembly factor in cells experiencing a high-demand for lipoic acid. Mol Microbiol. 2016; 102: 1099-1119.

Mashruwala AA, Van De Guchte A, Boyd JM. Impaired respiration elicits SrrAB-dependent programmed cell lysis and biofilm formation in *Staphylococcus aureus*. Elife. 2017; 6: e23845.

Mathé EA, Patterson AD, Haznadar M, Manna SK, Krausz KW, Bowman ED, et al. Noninvasive urinary metabolomic profiling identifies diagnostic and prognostic markers in lung cancer. Cancer Res. 2014; 74(12): 3259-70.

Maurice NM, Bedi B, Sadikot RT. *Pseudomonas aeruginosa* biofilms: host response and clinical implication in lung infections. Am J Respir Cell Mol Biol. 2018; 58(4): 428-439.

Mazzola PG, Jozala AF, Novaes LCL, Moriel P, Penna TCV. Minimal inhibitory concentration (MIC) determination of disinfectant and/or sterilizing agents. Braz J Pharm Sci. 2009; 45(2): 241-248.

Mehta AK, Singh BP, Arora N, Gaur SN. Choline attenuates inflammation and suppresses oxidative stress in patients with asthma. Immunobiology. 2010; 215: 527-534.

Meiser J, Krämer L, Sapcariu SC, Battello N, Ghelfi J, D'Herouel AF, et al. Pro-inflammatory macrophages sustain pyruvate oxidation through pyruvate dehydrogenase for the synthesis of itaconate and to enable cytokine expression. J Biol Chem. 2016; 291: 3932-3946.

Memmi G, Nair DR, Cheung A. Role of ArlRS in autolysis in methicillin-sensitive and methicillin-resistant *Staphylococcus aureus* strains. J Bacteriol. 2012; 194: 759-767.

Mercier P, Lewis MJ, Chang D, Baker D, Wishart DS. Towards automatic metabolomic profiling of high-resolution one-dimensional proton NMR spectra. J Biomol NMR. 2011; 49: 307-323.

Michalik S, Liebeke M, Zuhlke D, Lalk M, Bernhardt J, Gerth U, et al. Proteolysis during long-term glucose starvation in *Staphylococcus aureus* COL. Proteomics. 2009; 9: 4468-4477.

Michl J, Ohlbaum DJ, Silverstein SC. 2-Deoxyglucose selectively inhibits Fc and complement receptor-mediated phagocytosis in mouse peritoneal macrophages II. Dissociation of the inhibitory effects of 2-deoxyglucose on phagocytosis and ATP generation. J Exp Med. 1976; 144: 1484-1493.

Miller RD, Fung DY. Amino acid requirements for the production of enterotoxin B by *Staphylococcus aureus* S-6 in a chemically defined medium. Appl Microbiol. 1973; 25: 800-806.

Mills EL, Ryan DG, Prag HA, Dikovskaya D, Menon D, Zaslona Z, et al. Itaconate is an anti-inflammatory metabolite that activates Nrf2 via alkylation of KEAP1. Nature. 2018; 556: 113-117.

Minhas PS, Liu L, Moon PK, Joshi AU, Dove C, Mhatre S, et al. Macrophage *de novo* NAD^+ synthesis specifies immune function in aging and inflammation. Nat Immunol. 2019; 20: 50-63.

Mirza R, Koh TJ. Dysregulation of monocyte/macrophage phenotype in wounds of diabetic mice. Cytokine. 2011; 56(2): 256-64.

Mittal R, Sharma S, Chhibber S, Harjai K. Effect of macrophage secretory products on elaboration of virulence factors by planktonic and biofilm cells of *Pseudomonas aeruginosa*. Comp Immunol Microbiol Infect Dis. 2006; 29(1): 12-26.

Mnayer D, Fabiano-Tixier A, Petitcolas E, Hamieh T, Nehme N, Ferrant C, et al. Chemical composition, antibacterial and antioxidant activities of six essential oils from the *Alliaceae* family. Molecules. 2014; 19(12): 20034-20053.

Moore K, Ruge F, Harding KG. T lymphocytes and the lack of activated macrophages in wound margin biopsies from chronic leg ulcers. Br J Dermatol. 1997; 137(2): 188-94.

Moore KJ, Tabas I. Macrophages in the pathogenesis of atherosclerosis. Cell. 2011; 145(3): 341-55.

Moser C, Pedersen HT, Lerche CJ, Kolpen M, Line L, Thomsen K, et al. Biofilms and host response – helpful or harmful. APMIS. 2017; 125(4): 320-338.

Mosser DM, Edwards JP. Exploring the full spectrum of macrophage activation. Nat Rev Immunol. 2008; 8(12): 958-69.

Müller A, Eller J, Albrecht F, Prochnow P, Kuhlmann K, Bandow JE, et al. Allicin induces thiol stress in bacteria through S-allylmercapto modification of protein cysteines. J Biol Chem. 2016; 291(22): 11477-90.

Murray PJ, Wynn TA. Protective and pathogenic functions of macrophage subsets. Nat Rev Immunol. 2011; 11: 723-737.

Musthafa KS, Ravi AV, Annapoorani A, Sybiya Vasantha Packiavathy IA, Pandian SK. Evaluation of anti-quorum-sensing activity of edible plants and fruits through inhibition of the N-acyl-homoserine lactone system in *Chromobacterium violaceum* and *Pseudomonas aeruginosa*. Chemotherapy. 2010; 56(4): 333-9.

Nagy C, Haschemi A. Time and demand are two critical dimensions of immunometabolism: the process of macrophage activation and the pentose phosphate pathway. Front Immunol. 2015; 6: 164.

Nakaya M, Xiao Y, Zhou X, Chang JH, Chang M, Cheng X, et al. Inflammatory T cell responses rely on amino acid transporter ASCT2 facilitation of glutamine uptake and mTORC1 kinase activation. Immunity. 2014; 40: 692-705.

Natesan M, Selvaraj S, Manickam T, Venkatachari G. Corrosion behavior of metals and alloys in marine-industrial environment. Sci Technol Adv Mater. 2008; 9(4): 045002.

Newby AC. Metalloproteinase expression in monocytes and macrophages and its relationship to atherosclerotic plaque instability. Arterioscler Thromb Vasc Biol. 2008; 28(12): 2108-14.

Nguyen MT, Favelyukis S, Nguyen AK, Reichart D, Scott PA, Jenn A, et al. A subpopulation of macrophages infiltrates hypertrophic adipose tissue and is activated by free fatty acids via Toll-like receptors 2 and 4 and JNK-dependent pathways. J Biol Chem. 2007; 282(48): 35279-92.

Nicholson JK, Lindon JC. Systems biology: metabonomics. Nature. 2008; 455: 1054-1056.

Nixon GM, Armstrong DS, Carzino R, Carlin JB, Olinsky A, Robertson CF, et al. Clinical outcome after early *Pseudomonas aeruginosa* infection in cystic fibrosis. J Pediatr. 2001; 138(5): 699-704.

Novick RP. Genetic systems in staphylococci. Methods Enzymol. 1991; 204: 587-636.

Nunan R, Harding KG, Martin P. Clinical challenges of chronic wounds: searching for an optimal animal model to recapitulate their complexity. Dis Model Mech. 2014; 7(11): 1205-13.

Nussbaum SR, Carter MJ, Fife CE, DaVanzo J, Haught R, Nusgart M, et al. An economic evaluation of the impact, cost, and medicare policy implications of chronic nonhealing wounds. Value Health. 2018; 21(1): 27-32.

O'Callaghan RJ. The pathogenesis of *Staphylococcus aureus* eye infections. Pathogens. 2018; 7(1): 9.

Odegaard JI, Chawla A. Alternative macrophage activation and metabolism. Annu Rev Pathol. 2011; 6: 275-97.

Odegaard JI, Ricardo-Gonzalez RR, Goforth MH, Morel CR, Subramanian V, Mukundan L, et al. Macrophage-specific PPARγ controls alternative activation and improves insulin resistance. Nature. 2007; 447: 1116-1120.

Ogle ME, Segar CE, Sridhar S, Botchwey EA. Monocytes and macrophages in tissue repair: implications for immunoregenerative biomaterial design. Exp Biol Med (Maywood). 2016; 241(10): 1084-97.

Ohara-Nemoto Y, Haraga H, Kimura S, Nemoto TK. Occurrence of staphylococci in the oral cavities of healthy adults and nasal oral trafficking of the bacteria. J Med Microbiol. 2008; 57: 95-99.

Oiknine J, Aviram M. Increased susceptibility to activation and increased uptake of low density lipoprotein by cholesterol-loaded macrophages. Arterioscler Thromb. 1992; 12(6): 745-53.

Olefsky JM, Glass CK. Macrophages, inflammation, and insulin resistance. Annu Rev Physiol. 2010; 72: 219-46.

O'Neill LA, Kishton RJ, Rathmell J. A guide to immunometabolism for immunologists. Nat Rev Immunol. 2016; 16(9): 553-65.

O'Neill LA, Pearce EJ. Immunometabolism governs dendritic cell and macrophage function. J Exp Med. 2016; 213: 15-23.

Oren R, Farnham AE, Saito K, Milofsky E, Karnovsky ML. Metabolic patterns in three types of phagocytizing cells. J Cell Biol. 1963; 17(3): 487-501.

Otto M. Staphylococcal biofilms. Curr Top Microbiol Immunol. 2008; 322: 207-228.

Paige LA, Mitchell MW, Krishnan KR, Kaddurah-Daouk R, Steffens DC. A preliminary metabolomics analysis of older adults with and without depression. Int J Geriatr Psychiatry. 2007; 22(5): 418-23.

Pang YY, Schwartz J, Bloomberg S, Boyd JM, Horswill AR, Nauseef WM. Methionine sulfoxide reductases protect against oxidative stress in *Staphylococcus aureus* encountering exogenous oxidants and human neutrophils. J Innate Immun. 2014; 6: 353-364.

Papathanassiu AE, Ko JH, Imprialou M, Bagnati M, Srivastava PK, Vu HA, et al. BCAT1 controls metabolic reprogramming in activated human macrophages and is associated with inflammatory diseases. Nat Commun. 2017; 8: 16040.

Pavlou S, Wang L, Xu H, Chen M. Higher phagocytic activity of thioglycollate-elicited peritoneal macrophages is related to metabolic status of the cells. J Inflamm (Lond). 2017; 14: 4.

Piao S, Cha YN, Kim C. Taurine chloramine protects RAW 264.7 macrophages against hydrogen peroxide-induced apoptosis by increasing antioxidants. J Clin Biochem Nutr. 2011; 49: 50-56.

Pláteník J, Stopka P, Vejrazka M, Stípek S. Quinolinic acid-iron(II) complexes: slow autoxidation, but enhanced hydroxyl radical production in the Fenton reaction. Free Radic Res. 2001; 34: 445-459.

Platt AM, Bain CC, Bordon Y, Sester DP, Mowat AM. An independent subset of TLR expressing CCR2-dependent macrophages promotes colonic inflammation. J Immunol. 2010; 184: 6843-6854.

Posnett J, Franks PJ. The burden of chronic wounds in the UK. Nurs Times. 2008; 104(3): 44-5.

Pragman AA, Ji Y, Schlievert PM. Repression of *Staphylococcus aureus* SrrAB using inducible antisense *srrA* alters growth and virulence factor transcript levels. Biochemistry. 2007; 46: 314-321.

Pragman AA, Yarwood JM, Tripp TJ, Schlievert PM. Characterization of virulence factor regulation by SrrAB, a two-component system in *Staphylococcus aureus*. J Bacteriol. 2004; 186: 2430-2438.

Qiu F, Cai G, Jaki BU, Lankin DC, Franzblau SG, Pauli GF. Quantitative purity-activity relationships of natural products: the case of anti-tuberculosis active triterpenes from *Oplopanax horridus*. J Nat Prod. 2013; 76(3): 413-9.

Quintin J, Saeed S, Martens JHA, Giamarellos-Bourboulis EJ, Ifrim DC, Logie C, et al. *Candida albicans* infection affords protection against reinfection via functional reprogramming of monocytes. Cell Host Microbe. 2012; 12: 223-232.

Rahal JJ. Novel antibiotic combinations against infections with almost completely resistant *Pseudomonas aeruginosa* and *Acinetobacter* species. Clin Infect Dis. 2006; 43(Supplement_2): S95-S99.

Ramm Sander P, Peer M, Grandl M, Bogdahn U, Schmitz G, Robert Kalbitzer H. NMR spectroscopy of macrophages loaded with native, oxidized or enzymatically degraded lipoproteins. PLoS One. 2013; 8: e56360.

Ray PD, Huang BW, Tsuji Y. Reactive oxygen species (ROS) homeostasis and redox regulation in cellular signaling. Cell Signal. 2012; 24: 981-990.

Richardson AR, Dunman PM, Fang FC. The nitrosative stressresponse of *Staphylococcus aureus* is required for resistance to innate immunity. Mol Microbiol. 2006; 61: 927-939.

Richardson AR, Libby SJ, Fang FC. A nitric oxide-inducible lactate dehydrogenase enables *Staphylococcus aureus* to resist innate immunity. Science. 2008; 319: 1672-1676.

Richter K, Mathes V, Fronius M, Althaus M, Hecker A, Krasteva-Christ G, et al. Phosphocholine – an agonist of metabotropic but not of ionotropic functions of α9-containing nicotinic acetylcholine receptors. Sci Rep. 2016; 6: 28660.

Roberts CA, Al-Tameemi HM, Mashruwala AA, Rosario-Cruz Z, Chauhan U, Sause WE, et al. The Suf iron-sulfur cluster biosynthetic system is essential in *Staphylococcus aureus*, and decreased Suf function results in global metabolic defects and reduced survival in human neutrophils. Infect Immun. 2017; 85: e00100-17.

Rocca-Serra P, Salek RM, Arita M, Correa E, Dayalan S, Gonzalez-Beltran A, et al. Data standards can boost metabolomics research, and if there is a will, there is a way. Metabolomics. 2016; 12: 14.

Rodríguez-Prados JC, Través PG, Cuenca J, Rico D, Aragonés J, Martín-Sanz P, et al. Substrate fate in activated macrophages: a comparison between innate, classic, and alternative activation. J Immunol. 2010; 185: 605-614.

Rosario-Cruz Z, Boyd JM. Physiological roles of bacillithiol in intracellular metal processing. Curr Genet. 2016; 62: 59-65.

Rőszer T. Understanding the mysterious M2 macrophage through activation markers and effector mechanisms. Mediators Inflamm. 2015; 2015: 816460.

Ruiz-Cabello J, Cohen JS. Phospholipid metabolites as indicators of cancer cell function. NMR Biomed. 1992; 5(5): 226-33.

Ryan DG, O'Neill LAJ. Krebs cycle rewired for macrophage and dendritic cell effector functions. FEBS Lett. 2017; 591: 2992-3006.

Saeed S, Quintin J, Kerstens HH, Rao NA, Aghajanirefah A, Matarese F, et al. Epigenetic programming of monocyte-to-macrophage differentiation and trained innate immunity. Science. 2014; 345: 1251086.

Said-Salim B, Mathema B, Kreiswirth BN. Community-acquiredmethicillin-resistant *Staphylococcus aureus*: an emerging pathogen. Infect Control Hosp Epidemiol. 2003; 24: 451-455.

Sandusky P, Raftery D. Use of selective TOCSY NMR experiments for quantifying minor components in complex mixtures: application to the metabonomics of amino acids in honey. Anal Chem. 2005; 77(8): 2455-63.

Santas J, Almajano MP, Carbó R. Antimicrobial and antioxidant activity of crude onion (*Allium cepa*, L.) extracts. Int J Food Sci Technol. 2010; 45: 403-409.

Saric J, Li JV, Wang Y, Keiser J, Veselkov K, Dirnhofer S, et al. Panorganismal metabolic response modeling of an experimental *Echinostoma caproni* infection in the mouse. J Proteome Res. 2009; 8(8): 3899-3911.

Sävman K, Heyes MP, Svedin P, Karlsson A. Microglia/macrophage-derived inflammatory mediators galectin-3 and quinolinic acid are elevated in cerebrospinal fluid from newborn infants after birth asphyxia. Transl Stroke Res. 2013; 4: 228-235.

Scalbert A, Brennan L, Fiehn O, Hankemeier T, Kristal BS, van Ommen B, et al. Mass-spectrometry-based metabolomics: limitations and recommendations for future progress with particular focus on nutrition research. Metabolomics. 2009; 5(4): 435-458.

Scalbert A, Brennan L, Manach C, Andres-Lacueva C, Dragsted LO, Draper J, et al. The food metabolome: a window over dietary exposure. Am J Clin Nutr. 2014; 99(6): 1286-308.

Schmidt C. Metabolomics takes its place as latest up-and-coming "omic" science. J Natl Cancer Inst. 2004; 96(10): 732-4.

Schmidt CW. Metabolomics: what's happening downstream of DNA. Environ Health Perspect. 2004; 112(7): A410-A415.

Sen CK. Wound healing essentials: let there be oxygen. Wound Repair Regen. 2009; 17(1): 1-18.

Sen CK, Gordillo GM, Roy S, Kirsner R, Lambert L, Hunt TK, et al. Human skin wounds: a major and snowballing threat to public health and the economy. Wound Repair Regen. 2009; 17(6): 763-71.

Serhan CN, Brain SD, Buckley CD, Gilroy DW, Haslett C, O'Neill LA, et al. Resolution of inflammation: state of the art, definitions and terms. Faseb J. 2007; 21(2): 325-32.

Serhan CN, Yang R, Martinod K, Kasuga K, Pillai PS, Porter TF, et al. Maresins: novel macrophage mediators with potent anti-inflammatory and proresolving actions. J Exp Med. 2009; 206(1): 15-23.

Shanaiah N, Desilva MA, Nagana Gowda GA, Raftery MA, Hainline BE, Raftery D. Class selection of amino acid metabolites in body fluids using chemical derivatization and their enhanced ^{13}C NMR. Proc Natl Acad Sci USA. 2007; 104(28): 11540-4.

Sharifi-Rad J, Hoseini Alfatemi SM, Sharifi Rad M, Iriti M. Antimicrobial synergic effect of allicin and silver nanoparticles on skin infection caused by methicillin-resistant *Staphylococcus aureus* spp. Ann Med Health Sci Res. 2014; 4(6): 863-8.

Sica A, Mantovani A. Macrophage plasticity and polarization: in vivo veritas. J Clin Invest. 2012; 122: 787-795.

Silhavy TJ, Kahne D, Walker S. The bacterial cell envelope. Cold Spring Harb Perspect Biol. 2010; 2(5): a000414.

Silva LS, Poschet G, Nonnenmacher Y, Becker HM, Sapcariu S, Gaupel AC, et al. Branched-chain ketoacids secreted by glioblastoma cells via MCT1 modulate macrophage phenotype. EMBO Rep. 2017; 18(12): 2172-2185.

Silveira, MG, Baumgärtner M, Rombouts FM, Abee T. Effect of adaptation to ethanol on cytoplasmic and membrane protein profiles of *Oenococcus oeni*. Appl Environ Microbiol. 2004; 70(5): 2748-2755.

Sindrilaru A, Peters T, Wieschalka S, Baican C, Baican A, Peter H, et al. An unrestrained proinflammatory M1 macrophage population induced by iron impairs wound healing in humans and mice. J Clin Invest. 2011; 121(3): 985-97.

Sindrilaru A, Scharffetter-Kochanek K. Disclosure of the culprits: macrophages-versatile regulators of wound healing. Adv Wound Care (New Rochelle). 2013; 2(7): 357-368.

Singer AJ, Clark RA. Cutaneous wound healing. N Engl J Med. 1999; 341(10): 738-46.

Singh SK, Rozycki J, Ortega J, Ishikawa T, Lo J, Steven AC, et al. Functional domains of the ClpA and ClpX molecular chaperones identified by limited proteolysis and deletion analysis. J Biol Chem. 2001; 276: 29420-29429.

Sitter B, Sonnewald U, Spraul M, Fjösne HE, Gribbestad IS. High-resolution magic angle spinning MRS of breast cancer tissue. NMR Biomed. 2002; 15(5): 327-37.

Smolinska A, Blanchet L, Buydens LM, Wijmenga SS. NMR and pattern recognition methods in metabolomics: from data acquisition to biomarker discovery: a review. Anal Chim Acta. 2012; 750: 82-97.

Snider SA, Margison KD, Ghorbani P, LeBlond ND, O'Dwyer C, Nunes JRC, et al. Choline transport links macrophage phospholipid metabolism and inflammation. J Biol Chem. 2018; 293: 11600-11611.

Spura J, Reimer LC, Wieloch P, Schreiber K, Buchinger S, Schomburg D. A method for enzyme quenching in microbial metabolome analysis successfully applied to gram-positive and gram-negative bacteria and yeast. Anal Biochem. 2009; 394: 192-201.

Sreekumar A, Poisson LM, Rajendiran TM, Khan AP, Cao Q, Yu J, et al. Metabolomic profiles delineate potential role for sarcosine in prostate cancer progression. Nature. 2009; 457(7231): 910-4.

Stephens L, Ellson C, Hawkins P. Roles of PI3Ks in leukocyte chemotaxis and phagocytosis. Curr Opin Cell Biol. 2002; 14: 203-213.

Stewart PS, Franklin MJ, Williamson KS, Folsom JP, Boegli L, James GA. Contribution of stress responses to antibiotic tolerance in *Pseudomonas aeruginosa* biofilms. Antimicrob Agents Chemother. 2015; 59(7): 3838-3847.

Stock AM, Robinson VL, Goudreau PN. Two-component signal transduction. Annu Rev Biochem. 2000; 69: 183-215.

Strisower EH, Kohler GD, Chaikoff IL. Incorporation of acetate carbon into glucose by liver slices from normal and alloxan-diabetic rats. J Biol Chem. 1952; 198(1): 115-26.

Suzuki CK, Suda K, Wang N, Schatz G. Requirement for the yeast gene LON in intramitochondrial proteolysis and maintenance of respiration. Science. 1994; 264: 891.

Tan H, Wang N, Li S, Hong M, Wang X, Feng Y. The reactive oxygen species in macrophage polarization: reflecting its dual role in progression and treatment of human diseases. Oxid Med Cell Longev. 2016; 2016: 2795090.

Tannahill GM, Curtis AM, Adamik J, Palsson-McDermott EM, McGettrick AF, Goel G, et al. Succinate is an inflammatory signal that induces IL-1β through HIF-1α. Nature. 2013; 496: 238-242.

Tarnuzzer RW, Schultz GS. Biochemical analysis of acute and chronic wound environments. Wound Repair Regen. 1996; 4(3): 321-5.

Tavakoli S, Short JD, Downs K, Nguyen HN, Lai Y, Zhang W, et al. Differential regulation of macrophage glucose metabolism by macrophage colony-stimulating factor and granulocyte-macrophage colony-stimulating factor: implications for ^{18}F FDG PET imaging of vessel wall inflammation. Radiology. 2017; 283: 87-97.

Tedesco S, De Majo F, Kim J, Trenti A, Trevisi L, Paolo Fadini G, et al. Convenience versus biological significance: are PMA-differentiated THP-1 cells a reliable substitute for blood-derived macrophages when studying *in vitro* polarization? Front Pharmacol. 2018; 9: 71.

Tenover FC, McDougal LK, Goering RV, Killgore G, Projan SJ, Patel JB, et al. Characterization of a strain of community-associated methicillin-resistant *Staphylococcus aureus* widely disseminated in the United States. J Clin Microbiol. 2006; 44: 108-118.

The review on antimicrobial resistance, chaired by Jim O'Neill. Tackling drug-resistant infections globally: final report and recommendations. 2016.

Thomas AC, Mattila JT. "Of mice and men": arginine metabolism in macrophages. Front Immunol. 2014; 5: 479.

Throup JP, Zappacosta F, Lunsford RD, Annan RS, Carr SA, Lonsdale JT, et al. The srhSR gene pair from *Staphylococcus aureus*: genomic and proteomic approaches to the identification and characterization of gene function. Biochemistry. 2001; 40: 10392-10401.

Tong SY, Davis JS, Eichenberger E, Holland TL, Fowler VG, Jr. *Staphylococcus aureus* infections: epidemiology, pathophysiology, clinical manifestations, and management. Clin Microbiol Rev. 2015; 28: 603-661.

Torella JP, Chait R, Kishony R. Optimal drug synergy in antimicrobial treatments. PLoS Comput Biol. 2010; 6(6): e1000796.

Tsao S, Yin M. *In vitro* activity of garlic oil and four diallyl sulphides against antibiotic-resistant *Psuedomonas aeruginosa* and *Klebsiella pneumoniae*. J Antimicrob Chemother. 2001; 47(5): 665-670.

Tsao S, Yin M. *In-vitro* antimicrobial activity of four diallyl disulphides occurring naturally in garlic and Chinese leek oil. J Med Microbiol. 2001; 50(7): 646-9.

Van den Bossche J, Baardman J, de Winther, MP. Metabolic characterization of polarized M1 and M2 bone marrow-derived macrophages using real-time extracellular flux analysis. J Vis Exp. 2015; 105: e53424.

van der Greef J, Martin S, Juhasz P, Adourian A, Plasterer T, Verheji ER, et al. The art and practice of systems biology in medicine: mapping patterns of relationships. J Proteome Res. 2007; 6(4): 1540-59.

van Dijl JM, Kutejova E, Suda K, Perecko D, Schatz G, Suzuki CK. The ATPase and protease domains of yeast mitochondrial Lon: roles in proteolysis and respiration-dependent growth. Proc Natl Acad Sci U S A. 1998; 95: 10584-10589.

van Furth R, Cohn ZA. The origin and kinetics of mononuclear phagocytes. J Exp Med. 1968; 128(3): 415-35.

Vandeputte OM, Kiendrebeogo M, Rasamiravaka T, Stévigny C, Duez P, Rajaonson S, et al. The flavanone naringenin reduces the production of quorum sensing-controlled virulence factors in *Pseudomonas aeruginosa* PAO1. Microbiology. 2011; 157(Pt 7): 2120-32.

Vander Heiden MG, Cantley LC, Thompson CB. Understanding the Warburg effect: the metabolic requirements of cell proliferation. Science. 2009; 324: 1029-1033.

Vannella KM, Wynn TA. Mechanisms of organ injury and repair by macrophages. Annu Rev Physiol. 2017; 79: 593-617.

Vasavi HS, Arun AB, Rekha PD. Anti-quorum sensing activity of flavonoid-rich fraction from *Centella asiatica* L. against *Pseudomonas aeruginosa* PAO1. J Microb Immunol Infect. 2016; 49(1): 8-15.

Vats D, Mukundan L, Odegaard JI, Zhang L, Smith KL, Morel CR, et al. Oxidative metabolism and PGC-1β attenuate macrophage-mediated inflammation. Cell Metab. 2006; 4: 13-24.

Vinaixa M, Schymanski EL, Neumann S, Navarro M, Salek RM, Yanes O. Mass spectral databases for LC/MS- and GC/MS-based metabolomics: state of the field and future prospects. Trends Analyt Chem. 2016; 78: 23-35.

Vitko NP, Grosser MR, Khatri D, Lance TR, Richardson AR. Expanded glucose import capability affords *Staphylococcus aureus* optimized glycolytic flux during infection. mBio. 2016; 7: e00296-16.

Vogelberg KH, Konig M. Hypoxia of diabetic feet with abnormal arterial blood flow. Clin Investig. 1993; 71: 466-470.

Wagner H, Ulrich-Merzenich G. Synergy research: approaching a new generation of phytopharmaceuticals. Phytomedicine. 2009; 16(2-3): 97-110.

Wallace HJ, Stacey MC. Levels of tumor necrosis factor-α (TNF-α) and soluble TNF receptors in chronic venous leg ulcers—correlations to healing status. J Invest Dermatol. 1998; 110(3): 292-6.

Wang C, Kong H, Guan Y, Yang J, Gu J, Yang S, et al. Plasma phospholipid metabolic profiling and biomarkers of type 2 diabetes mellitus based on high-performance liquid chromatography/electrospray mass spectrometry and multivariate statistical analysis. Anal Chem. 2005; 77(13): 4108-16.

Wang Y, Utzinger J, Saric J, Li JV, Burckhardt J, Dirnhofer S, et al. Global metabolic responses of mice to *Trypanosoma brucei brucei* infection. Proc Natl Acad Sci USA. 2008; 105(16): 6127-32.

Warburg O. On the origin of cancer cells. Science. 1956; 123: 309-314.

Warburg O, Wind F, Negelein E. The metabolism of tumors in the body. J Gen Physiol. 1927; 8: 519-530.

Watkins F, Pendry B, Corcoran O, Sanchez-Medina A. Anglo-Saxon pharmacopoeia revisited: a potential treasure in drug discovery. Drug Discov Today. 2011; 16(23-24): 1069-1075.

Weaver AJ, Peters TR, Tripet B, Van Vuren A, Rakesh, Lee RE, et al. Exposure of methicillin-resistant *Staphylococcus aureus* to low levels of the antibacterial THAM-3ΦG generates a small colony drug-resistant phenotype. Sci Rep. 2018; 8: 9850.

Wei Q, Ma LZ. Biofilm matrix and its regulation in *Pseudomonas aeruginosa*. Int J Mol Sci. 2013; 14: 20983-21005.

Weigert A, Johann AM, von Knethen A, Schmidt H, Geisslinger G, Brune B. Apoptotic cells promote macrophage survival by releasing the antiapoptotic mediator sphingosine-1-phosphate. Blood. 2006; 108(5): 1635-42.

Weinman EO, Strisower EH, Chaikoff IL. Conversion of fatty acids to carbohydrate; application of isotopes to this problem and role of the Krebs cycle as a synthetic pathway. Physiol Rev. 1957; 37(2): 252-72.

Weljie AM, Newton J, Mercier P, Carlson E, Slupsky CM. Targeted profiling: quantitative analysis of ^{1}H NMR metabolomics data. Anal Chem. 2006; 78(13): 4430-4442.

Wilde AD, Snyder DJ, Putnam NE, Valentino MD, Hammer ND, Lonergan ZR, et al. Bacterial hypoxic responses revealed as critical determinants of the host-pathogen outcome by TnSeq analysis of *Staphylococcus aureus* invasive infection. PLoS Pathog. 2015; 11: e1005341.

Williamson DA, Lim A, Thomas MG, Baker MG, Roberts SA, Fraser JD, et al. Incidence, trends and demographics of *Staphylococcus aureus* infections in Auckland, New Zealand, 2001-2011. BMC Infect Dis. 2013; 13: 569.

Wishart D. Applications of metabolomics in drug discovery and development. Drugs R D. 2008; 9(5): 307-322.

Wishart DS. Quantitative metabolomics using NMR. Trends Analyt Chem. 2008; 27: 228-237.

Wishart DS, Jewison T, Guo AC, Wilson M, Knox C, Liu Y, et al. HMDB 3.0--the human metabolome database in 2013. Nucleic Acids Res. 2013; 41(Database issue): D801-7.

Wojdasiewicz P, Poniatowski LA, Szukiewicz D. The role of inflammatory and anti-inflammatory cytokines in pathogenesis of osteoarthritis. Mediators Inflamm. 2014; 2014: 561459.

Wolf S, Schmidt S, Müller-Hannemann M, Neumann S. *In silico* fragmentation for computer assisted identification of metabolite mass spectra. BMC Bioinformatics. 2010; 11: 148.

Woollard KJ, Geissmann F. Monocytes in atherosclerosis: subsets and functions. Nat Rev Cardiol. 2010; 7: 77-86.

Wu X, Santos RR, Fink-Gremmels J. Analyzing the antibacterial effects of food ingredients: model experiments with allicin and garlic extracts on biofilm formation and viability of *Staphylococcus epidermidis*. Food Sci Nutr. 2015; 3(2): 158-168.

Wu X, Yu H, Ba Z, Chen J, Sun H, Han B. Sampling methods for NMR-based metabolomics of *Staphylococcus aureus*. Biotechnol J. 2010; 5(1): 75-84.

Wu Y, Williams EG, Dubuis S, Mottis A, Jovaisaite V, Houten SM, et al. Multilayered genetic and omics dissection of mitochondrial activity in a mouse reference population. Cell. 2014; 158(6): 1415-1430.

Wysocki AB, Staiano-Coico L, Grinnell F. Wound fluid from chronic leg ulcers contains elevated levels of metalloproteinases MMP-2 and MMP-9. J Invest Dermatol. 1993; 101(1): 64-8.

Xi Y, de Ropp JS, Viant MR, Woodruff DL, Yu P. Automated screening for metabolites in complex mixtures using 2D COSY NMR spectroscopy. Metabolomics. 2006; 2(4): 221-233.

Xia J, Wishart DS. Metabolomic data processing, analysis, and interpretation using MetaboAnalyst. Curr Protoc Bioinformatics. 2011; 34: 14.10.1-14.10.48.

Xia J, Wishart DS. Using MetaboAnalyst 3.0 for comprehensive metabolomics data analysis. Curr Protoc Bioinformatics. 2016; 55: 14.10.1-14.10.91.

Xia J, Wishart DS. Web-based inference of biological patterns, functions and pathways from metabolomic data using MetaboAnalyst. Nat Protoc. 2011; 6: 743-760.

Xu J, et al. Divergent signals and cytoskeletal assemblies regulate self-organizing polarity in neutrophils. Cell. 2003; 114: 201-214.

Yarwood JM, McCormick JK, Schlievert PM. Identification of a novel two-component regulatory system that acts in global regulation of virulence factors of *Staphylococcus aureus*. J Bacteriol. 2001; 183: 1113-1123.

Yuan K, Kong H, Guan Y, Yang J, Xu G. A GC-based metabonomics investigation of type 2 diabetes by organic acids metabolic profile. J Chromatogr B Analyt Technol Biomed Life Sci. 2007; 850(1-2): 236-40.

Zafar U, Johnson LB, Hanna M, Riederer K, Sharma M, Fakih MG, et al. Prevalence of nasal colonization among patients with community-associated methicillin-resistant *Staphylococcus aureus* infection and their household contacts. Infect Control Hosp Epidemiol. 2007; 28: 966-969.

Zhang A, Sun H, Xu H, Qiu S, Wang X. Cell metabolomics. OMICS. 2013; 17(10): 495-501.

Zhang B, Powers R. Analysis of bacterial biofilms using NMR-based metabolomics. Future Med Chem. 2012; 4(10): 1273-1306.

Zhang L, Wang CC. Inflammatory response of macrophages in infection. Hepatobiliary Pancreat Dis Int. 2014; 13(2): 138-52.

Zhang S, Kim CC, Batra S, McKerrow JH, Loke P. Delineation of diverse macrophage activation programs in response to intracellular parasites and cytokines. PLoS Negl Trop Dis. 2010; 4: e648.

Zhao G, Hochwalt PC, Usui ML, Underwood RA, Singh PK, James GA, et al. Delayed wound healing in diabetic (db/db) mice with *Pseudomonas aeruginosa* biofilm challenge: a model for the study of chronic wounds. Wound Repair Regen. 2010; 18(5): 467-77.

Zhao R, Liang H, Clarke E, Jackson C, Xue M. Inflammation in chronic wounds. Int J Mol Sci. 2016; 17(12): 2085.

Zhou M, Zhang Y, Ardans JA, Wahl LM. Interferon-γ differentially regulates monocyte matrix metalloproteinase-1 and -9 through tumor necrosis factor-α and caspase 8. J Biol Chem. 2003; 278(46): 45406-13.